Regenerative medicine applications in paediatric urology: barriers and solutions

Miss Anna Rebecca Radford

Submitted in accordance with the requirements for the award of PhD

Department of Biology

University of York, Hull York Medical School,

July 2015

Abstract:

Tissue engineering and regenerative medicine offers opportunities to introduce new techniques into paediatric urology practice.

In this thesis, two experimental approaches were used. The initial approach considered improvements to the concept of composite cystoplasty; where high pressure in end-stage disease bladders is alleviated by augmentation using bowel smooth muscle lined by an autologous in vitro-grown bladder epithelium. Secondly, a porcine bladder acellular matrix (PABM) was tested as a free graft in a surgical model as proof of principle for its use in hypospadias repair.

Immunohistochemical characterisation of neuropathic bladders was performed. A disease-model was created in order to mimic the disease phenotype using propagated normal urothelial cells and tissue *in vitro*. Trans-epithelial electrical resistance was used to measure barrier function in differentiated urothelium. Immunocytochemistry, immunoblotting and RTPCR was utilised to identify any mechanistic pathways leading to heritable changes in phenotype.

Assessment of human neuropathic bladder biopsies demonstrated significant labelling of a hypoxia-related transcription factor. *In vitro* hypoxia significantly reduced the proliferation and differentiation capacity of urothelial cells. The proliferative capacity recovered upon switching to normoxia, however, the differentiation-associated compromise persisted. Repressive epigenetic marks were found to alter location and abundance in the compromised urothelium. These marks were targeted using an

epigenetic-modifying agent, which significantly recovered the differentiated urothelial phenotype. Importantly this was replicated in urothelium from diseased bladders.

Integration of the PABM was superior to Pelvicol™. A subpopulation of $CD45^-CD163^+$ cells was identified, which were believed to be important in biomaterial remodelling.

It is proposed that hypoxia results in persistent heritable compromise in differentiated urothelium. The urothelial phenotype is recoverable by the application of an epigenetic modifying agent. By using an integrated approach both the epigenetic – modifying agent and PABM may provide strategies to improve the efficacy of autologous tissue engineering approaches in paediatric and adult urology.

Regenerative medicine applications in paediatric urology: barriers and solutions

Contents

Table of Figures

Regenerative medicine applications in paediatric urology: barriers and solutions

Regenerative medicine applications in paediatric urology: barriers and solutions

Regenerative medicine applications in paediatric urology: barriers and solutions

Regenerative medicine applications in paediatric urology: barriers and solutions

Tables:

Preface

'The more subtle and inquisitive doctors speak about nature and claim to derive their principles from it, while the more accomplished investigators of nature generally end by a study of the principles of medicine'.

Aristotle, De Respiratione (480b 26ff.)

'Science and opinion are two different things; science is the father of knowledge but opinion breeds ignorance'.

The Canon, Hippocratic Writings, Medicine p69, translated. J Chadwick, W.N. Mann. Penguin Classics. ISBN 0-14-044451-3

"If a scientist is not befuddled by what they're looking at, then they're not a research scientist."

Neil DeGrasse Tyson (American Astrophysicist)

Acknowledgements

I am particularly grateful to my supervisor, Professor Jenny Southgate, for her unerring help throughout my PhD studies. I would like to thank all members of my training committee, including Dr Roger Sturmey, whose advice and support was gratefully received.

A special thank you to my academic clinical supervisor Mr Ramnath Subramaniam, who has been instrumental in the collection of paediatric specimens, porcine acellular-matrix work and who has believed in me throughout my career in Yorkshire and further afield.

I am extremely grateful to the European Society for Pediatric Urology for their funding and continued support throughout this project.

I would like to thank all members of the Jack Birch Unit for their guidance and laughter. Fellow members of the table of cynics…I now know I am not alone. To Carl Fishwick thank you for trying to explain that it is alright not to know, particularly when it comes to epigenetics…because no one knows yet. To the Yin and the Yang of JBU Simon Baker and Jennifer Hinley, without whom I would have been lost…literally on many occasion, I say thank you for your help and friendship.

Finally, to my family both South and North, who have supported me throughout the last three years. To my partner Andy, who took no nonsense and Olly (the crazy spaniel) both of whom knew that what I needed every now and again was a walk, a hug and without whom this work would have not been completed

Author Declaration

'I confirm that this work is original and that if any passage(s) or diagram(s) have been copied from academic papers, books the internet or any other sources that these are clearly identified by the use of quotation marks and the reference(s) is fully cited. I certify that, other than where indicated, this is my own work and does not breach the regulations of HYMS, the University of Hull or the University of York regarding plagiarism or academic conduct in examinations. I have read the HYMS Code of Practice on Academic Misconduct, and state that this piece of work is my own and does not contain unacknowledged work from other sources. I confirm that any patient information obtained to produce this piece of work has been appropriately anonymised'.

1 Introduction

1.1 Morphology of the normal urothelium

Urothelium is the highly specialized transitional epithelium that lines the urinary tract from renal pelvis to urethra. It has two embryological origins: the ureters and renal pelvis derive from the mesoderm, whereas the urethra and bladder derived from the endoderm. Urothelium is multi-layered into basal, intermediate to superficial cell zones, based on morphology and phenotype (*Fig.1-1)*.

1.2 Superficial, "umbrella" cells and barrier function.

Umbrella cells are a single layer of highly differentiated and polarised cells that have distinct apical membrane delineated by tight junctions (Acharya et al., 2004). The morphology of these cells is generally cuboidal; but this is dependent on the filling state of the bladder, with the same cells becoming flattened in a full bladder state. Umbrella cells have specialised features enabling them to contribute to the urinary barrier, which in health, is maintained throughout the bladder cycle stages of filling, storage and voiding. This barrier has to withstand significant osmotic gradients; human urine osmolality, for example, can be 2-4 times higher than that in the blood creating osmotic pressures of 3800-15200 mmHg (Yu and Hill, 2011). To achieve this barrier the urothelium expresses tight junction proteins paracellularly and uroplakins transcellularly.

Superficial layer: large, flattened/binucleate, "umbrella cells".

Intermediate layer: large, polygonal cells.

Basal layer: small, cuboidal cells.

50μm
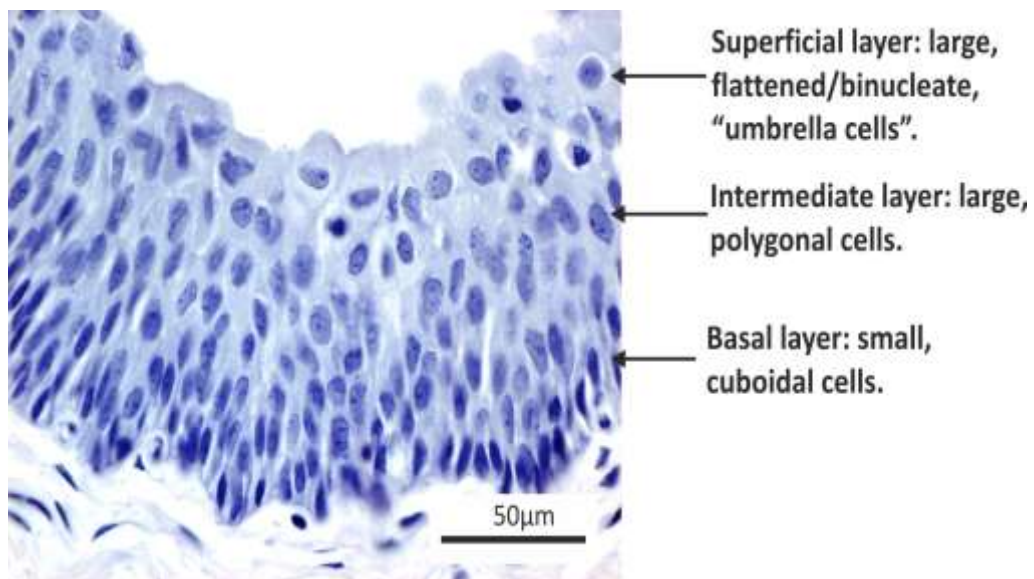
Figure 1-1: Normal human ureteric urothelium

Basal cells interact with the basement membrane via the α6β4-integrin complex (Southgate et al., 1995). In addition to basal cells, occasional superficial and intermediate cells are connected to the basement membrane via pedicles (Jost et al., 1989). The urothelium is therefore frequently described in the literature as being pseudostratified, thus all cells are attached to the basement membrane. However this has been the source of controversy with some groups questioning the presence of such connections (Khandelwal et al., 2009), (Wu et al., 2009) and considering it as a true stratified epithelium. A lack of consensus creates a challenge when attempting to recreate and validate a replacement urothelium through tissue engineering approaches.

Regenerative medicine applications in paediatric urology: barriers and solutions

1.2.1 The asymmetric unit membrane

The asymmetric unit membrane (AUM) (Southgate et al., 1999b) is a specific feature of superficial cells and along with cytokeratins (CK) is used to characterise differentiation of the urothelial layers (***Table 1-1***). The AUM is located at the apical membrane of urothelial cells. It consists of a scalloped layer of plaques connected by hinge regions. These AUM plaques are comprised of five transmembrane glycoproteins known as the uroplakins (UPKs). UPKs 1a, 1b (members of the tetraspanin superfamily) and 2, 3a and 3b (unrelated single transmembrane proteins) (Sun et al., 1996) dimerise and are assembled in regular hexagonal subunits to form these. Published evidence suggests that dimerising occurs between specific UPKs only: UPK1a with UPK2 and UP1B with UPK3a/UPK3b (Hu et al., 2001, Deng et al., 2002).

The AUM and constituent uroplakins are extremely important in the protective, barrier function of the urothelium. Hu *et al* (Hu et al., 2001) described the UPK3a-deficient mouse bladder urothelium as featuring "abnormally small urothelial plaques", which were "leaky" to water and urea and associated with a phenotype similar to vesicoureteric reflux, which resulted in hydronephrosis and renal dysfunction.   In human urothelium UPK1a and UPK2 expression is highly urothelium-specific and limited to the superficial cells of the urothelium (Lobban et al., 1998). UPK3a is primarily expressed by superficial urothelial cells (Olsburgh et al., 2003). UPK1b is found in the intermediate and superficial layers of the urothelium and has also been identified in other tissues (Lobban et al., 1998, Olsburgh et al., 2003).

1.2.2   Cytokeratins

Cell cytokeratin (CK) profiles are widely used to classify epithelia. Cytokeratins are subunits of intermediate filaments which provide structural support in epithelial and mesothelial cells. Small, acidic type I cytokeratins pair with type II, large, basic cytokeratins and polymerise to form coiled-coiled heterodimers which assemble into to filament bundles that anchor at desmosomes (reviewed by Coulombe, 1993). Twenty different cytokeratin isotypes have been identified and these are expressed in a tissue-specific manner, reflecting cell structure and differentiation state (Cooper *et al,* 1985). In man, the urothelium expresses cytokeratins characteristic of simple (CK7, CK8, CK19, CK19 and CK20) and stratified epithelia (CK13, CK17, CK5 and CK4). In normal urothelium, CK7, CK 18 and CK 19 are expressed throughout the urothelium, whilst CK17 and CK 5 are basally expressed. CK13 is present in basal and intermediate cells layers and CK8 and CK20 are found in superficial cells only (reviewed by Southgate *et al.,* 1999b).

Table 1-1: Urothelial cytokeratin expression (Southgate et al., 1999b).

	Basal	Intermediate	Superficial
CK5	+	-	-
CK7	+	+	+
CK8	+	+	+
CK13	+	+	-
CK17	+	-	-
CK18	+	+	++
CK19	+	+	+
CK20	-	-	+

1.2.3 Tight junctions

Superficial cells develop tight junctions to prevent the paracellular diffusion of urine across the urothelium. The tight junctions between the superficial cells block transepithelial ion flux enabling the urothelium to maintain barrier polarity and transepithelial resistance. The latter has been modelled in both animals (Lavelle et al., 2000, Lavelle et al., 1998, Apodaca et al., 2003, Hu et al., 2000) and humans (Cross et al., 2005) and is reported to be functional at $> 500\Omega.cm^2$.

Tight junctions modulate paracellular transport under the regulation of a group of proteins called the claudin family (Angelow et al., 2008). The claudin family has 24 members which are generally 20-25kDa; consist of four transmembrane loops and two extracellular loops. Individual claudins can interact with other claudins and zona occludens-1 (ZO-1). Claudins 3, 4, 5 and 7 have been found to be expressed in human ureteric urothelium with specific distribution patterns (Varley et al., 2006), (***Table 1-2)***. Alterations in the urothelium and umbrella cell related tight junctions have been proposed to contribute to bladder conditions, for example, interstitial cystitis (Zhang et al., 2005), however the mechanisms behind this remain unclear.

Table 1-2: Distribution of claudins within human urothelium(Southgate et al., 1999b)

Claudin	Cell layer	Location
3	Superficial cells	Tight junction
4	All layers	Intercellular borders
5	Umbrella cells	Basolateral
7	Intermediate/basal	Heterogenous

1.3 Urothelial turnover and renewal

Normal urothelium exhibits low constitutive rates of proliferation with mitotic indices of less than 1% reported (Marceau, 1990). However, in response to injury the urothelium undergoes rapid proliferation (Baskin et al., 1997), a response that is likely to have evolved to maintain its function as a urinary barrier (Southgate et al., 1999a). It has been shown that an autocrine epithelial growth factor receptor (EGFR) loop exists in NHU cells *in vitro,* which may be implicated as the driver for the injury-related proliferation through signalling pathways downstream of epidermal growth factor receptor EGFR (Varley et al., 2005).

Each self-renewing tissue has its own mechanism for cell turnover and renewal. In enteric epithelium dividing cells located in the crypts of Lieberkühn produce progeny which migrate upwards to the villi in a progressively differentiated and non-proliferative state (Tomlinson and Bodmer, 1995).

An important feature of the urothelium is its high regenerative capacity. Thus, although the urothelium is regarded as a "stable" or mitotically quiescent tissue with an extremely slow rate of cell turnover estimated to be as long as one year (Hainau and Dombernowsky, 1974), it is able to undergo rapid proliferation in response to acute injury. Lavelle and colleagues performed a controlled study of selective urothelial damage in rats, which showed that recovery of transcellular and paracellular components of the urinary barrier occurred within 72 hours, with the intermediate cells undergoing rapid maturation to form differentiated umbrella cells (Lavelle J. et al., 2002).

The urothelium, in the mouse model, is initially identified when the bladder begins to form at the anterior aspect of the urogenital sinus. The sequence of development is thought to originate from keratin-5 expressing basal cells, which give rise to intermediate and superficial cells through a Hedgehog/Wnt feedback mechanism (Shin et al., 2011). In this work, as a consequence of bacterial injury, basal cell expression of Shh increased Wnt protein expression at the stomal level; which resulted in proliferation. As a result of this response urothelial function appeared to be restored, reducing the risk of further injury.

However the human renewal mechanism for the urothelium has yet to be verified and recent fate-mapping studies suggest that intermediate and superficial cells arise from different lineages than the keratin-5 expressing basal cells (Gandhi et al., 2013) with an important role for retinoic acid suggested by other work (Mauney et al., 2010). Mitosis has been observed in basal, intermediate and superficial layers of the urothelium following injury, demonstrating that even cells labelled "terminally differentiated" retain their proliferative potential (Scriven et al., 1997).

1.3.1 Urothelial stem cells

The definition of a stem cell includes the capacity to self-renew in an undifferentiated state. Relating to investigations of urothelial regeneration and differentiation, the interest in urothelial stem cells has emerged. A database has been collated for potential stem cell markers within the urothelium (Pascal et al., 2007); however no equivocal marker has yet to be reported.

Given the documented tendency for stem cells to reside in "protected" areas, such as enteric crypts, it has been suggested that pluripotent cells reside in the basal cell layer of the urothelium (Kurzrock et al., 2008). In this model the intermediate cells are a population of transit amplifying cells, which then differentiate to form the superficial, umbrella cells. This theory was supported by work which demonstrated localised, bromo-deoxyuridine, label retaining cells within the basal layer of rat bladder urothelium (Kurzrock et al., 2008). However, contradictory findings have been reported in another study, with no clear evidence of preferential basal cell location demonstrated (Zhang et al., 2012).

1.4 Urothelial cells *in vitro*

Many techniques and culture methods are described for the successful propagation of normal human urothelial (NHU) cell cultures from surgical specimens (Reznikoff et al., 1987, Southgate et al., 1994, Hutton et al., 1993, Dubeau and Jones, 1987). NHU cells cultured in keratinocyte serum-free medium (KSFM) containing bovine pituitary extract (BPE), human recombinant epidermal growth factor (EGF), low calcium (0.09 mM) and supplemented with cholera toxin have been well characterised in terms of morphology and proliferative behaviour.(Southgate et al., 1994). Cholera toxin is shown to improve initial plating efficiency of urothelial cells in primary culture (Southgate et al 1994).

This culture method results in urothelial cells that rapidly proliferate, until cells become contact inhibited at confluence. It has therefore been indicated that this system produces a "wound response" phenotype (Southgate et al., 1994, Southgate et al., 1995). Keratinocyte and fibroblast cell cultures have also been noted to exhibit a

similar phenotype (Iyer et al., 1998, Coulombe, 1997). In wounded keratinocytes CK16, along with CK6, are up regulated as a marker of epidermal hyperproliferation. This response is also observed in NHU cells *in vitro* (Paladini et al., 1996, Bernot et al., 2002). Other observations seen *in vivo* in wounded keratinocytes (Toda et al., 1987) that are replicated in NHU cultures include fibronectin and associated receptor α5β1 integrin, a finding that is not replicated *in* vivo in urothelium.

The ability for NHU cells to migrate and reduced adherence to the basement membrane also supports the parallel drawn with "wound response" (**See 1.3**). Cell-to-cell adhesion is also different in NHU cultures, in part due to lower levels of E-cadherin expression at the intracellular borders. This process can be ameliorated by increasing the calcium concentration in the medium (Southgate et al., 1994). The growth of NHU cells *in vitro* has been shown to be mediated through an EGF autocrine feedback loop. NHU cell cultures undergo replicative senescence, which is associated with the accumulation of p16^{INK4A} (Ben-Porath and Weinberg, 2005). It has been suggested that cells in culture are subjected to high levels of oxidative stress (Dumont et al., 2000) and may undergo accelerated senescence.

1.4.1 Differentiation of urothelial cells *in vitro*

Cultured NHU cells also retain the ability to differentiate. However, unlike keratinocytes, differentiation is not spontaneous but achieved by exogenous stimuli (Cross et al., 2005, Varley and Southgate, 2008, Varley et al., 2004). Two methods have been described for inducing differentiation and the expression of differentiation-associated markers by NHU cells *in vitro*: pharmacological (Varley and Southgate, 2008) and biomimetic (Cross et al., 2005).

Regenerative medicine applications in paediatric urology: barriers and solutions

Cross (Cross et al., 2005) described the reproducible acquisition of a differentiated phenotype by NHU cells that had been cultured in medium supplemented with 5% bovine serum and physiological levels of calcium (2mM). The resulting phenotype closely models that found *in vivo* in relation to barrier function with low diffusion permeability. Stratification but not differentiation is achieved by the application of physiological calcium. The addition of 5% bovine serum is associated with the expression of the following tight junction associated proteins claudins 1 and 4, occludin and ZO-1.

Unlike the pharmacological method, NHU cells differentiated using the biomimetic model allow assessment of barrier function. This is achieved by measuring transepithelial electrical resistance (TEER) using an ohmmeter, a practice that can be used to measure the potential difference across any epithelial sheet (Cheek et al., 1989, Watts et al., 2005). As highlighted in 1.2.2 the urothelium has a particularly high TEER of >2500 $\Omega.cm^2$ (Hu et al., 2001).

1.5 Neuropathic bladder and associated features

1.5.1 What is a neuropathic bladder?

Neurogenic bladder dysfunction may complicate a variety of neurological conditions. Congenital anomalies, such as spina bifida, affect 0.3-4.5/1000 live births (de Jong et al., 2008), 40% of these children will have vesico-ureteric reflux (VUR) by the age of 5 and 61% young adults will suffer with incontinence (Verhoef et al., 2005). However

Regenerative medicine applications in paediatric urology: barriers and solutions

adult patients with conditions including multiple sclerosis (33-52%) (Araki et al., 2003), Parkinson's disease

(45-93%) (Yeo et al., 2012), stroke (15%) and spinal cord injury (70-84%) (Araki et al., 2003) will develop symptoms of neuropathic bladder as a secondary manifestation of the primary disease. Hinman's syndrome is a well-recognised condition primarily affecting young girls (Hinman, 1986). Although Hinman's syndrome has no neuropathic aetiology children can present with a clinical picture, including complications, similar to neuropathic cases and is therefore termed "non-neuropathic neuropathic bladder". .

Neuropathic bladders and non-neuropathic neuropathic bladders can either be seen as "safe", whereby the pressure experienced within them are low, usually due to an ineffective sphincter resulting in incontinence or "at risk". In the latter group a working sphincter, although preventing urinary leakage, can result in urinary retention and resulting back pressure of urine towards the kidneys. Prior to this the bladder may initially distend, lose compliance, become scarred, form diverticulum (in an effort to reduce pressure) until the system cannot cope leading to renal damage. The resulting pathology is known as end stage bladder disease.

1.5.2 End stage bladder disease

A number of diseases of the urinary bladder culminate in end-stage disease characterised by small contracted bladders that create high pressure systems with consequences for kidney function (Rasouly and Lu, 2013). These conditions, which include both neuropathic and non-neuropathic neuropathic conditions, have a poorly defined pathological pathway. Urothelial cells isolated from diseased bladders have

Regenerative medicine applications in paediatric urology: barriers and solutions

been shown to have a compromised proliferative and differentiated phenotype *in vitro* (Subramaniam et al., 2011), but as the urothelium is not implicated in the primary pathogenesis the reasons for this are unknown.

End-stage bladder disease is likely to represent the common end point of multiple pathological processes such as infection, inflammation and hypoxia; each of these insults contributing to varying degrees dependent on the individual case. In addition it is likely that the pathological pathways activated by these processes will have an element of cross activation and therefore common outcome. Focusing on how these individual pathological factors result in the small contracted bladders seen clinically may help develop a deeper understanding of the pathophysiology involved.

1.5.2.1   Current management of end-stage bladder disease#

The principle of reconstructive surgery in end-stage bladder disease is to improve drainage and increase capacity (augmentation). The overall aim is reduction in urinary tract infections (UTIs), improved continence and importantly reduced bladder pressures and subsequent damage to the upper urinary tract. Various visceral segments have been used in bladder augmentation surgery including stomach (gastrocystoplasty), small intestine

(ileocystoplasty) and large intestine (colocystoplasty). In the UK ileocystoplasty is the most commonly performed procedure (reviewed by Thomas, 1997). Complications secondary to implantation of the ileal epithelium being located in the bladder have been reported and include spontaneous perforation (Bauer et al., 1992), mucus production (Gough, 2001), bladder calcluli (Kisku et al., 2015), metabolic disturbances (Fontaine et al., 2000) and malignancy (reviewed by Austen and Kalble, 2004).

These issues are in part due to the different function the epithelial linings perform in the bladder and the bowel. The bladder is designed to be waterproof and the bowel absorptive. A tissue-engineering concept, "composite-cystoplasty" has been proposed whereby the epithelial lining of a segment of vascularised small intestine is removed and replaced with an autologous *in vitro* propagated bladder epithelial lining (Turner et al., 2011). This has been demonstrated successfully in a large animal model; however issues have arisen in propagating sufficient, differentiated human urothelium harvested from diseased bladders (Subramaniam et al., 2011).

During the above study three samples in eight lacked urothelial differentiation associated expression of UPK3a and CK20. Only four cultures were expanded in culture with all four demonstrating reduced proliferaion potential and a compromised ability to form a barrier urothelium compared to controls.

1.5.3 Inflammation and hypoxia

Inflammation is part of the process by which injured tissues respond to insult. If the inflammatory process persists in the absence of the initial cause, the inflammation becomes self-perpetuating. Unregulated inflammation of the bladder can result from primary insults that include: infection, environmental irritants, autoimmune reaction, or persistent activation of pro-inflammatory signals. It is abnormal, does not benefit the organism, and is the main pathological process in some diseases, including those that impact on human health, such as inflammatory bowel disease and demyelinating polyneuropathy. Such chronic inflammation may play a role in end-stage bladder disease (Saban et al., 2003).

Regenerative medicine applications in paediatric urology: barriers and solutions

Chronic inflammation may lead to a hypoxic microenvironment or vice-versa (reviewed Taylor, 2008), partly due to the inflammatory process consuming oxygen (Karhausen et al., 2005), thus increasing demand. In addition, the blood supply to the bladder may be impaired by other factors including conglomeration of inflammatory cells migrating to the site and cytokine-mediated vasoconstriction (Sitkovsky and Lukashev, 2005), which effectively reduce oxygen supply. Equally in some primarily non-inflammatory conditions associated with bladder outlet obstruction, for example in benign prostatic hypertrophy (BPH) (Koritsiadis et al., 2008) , high intra-vesical pressure can result in hypoxia within the bladder tissue, again by reducing perfusion of the tissue and thus oxygen supply. Hypoxia has also been shown to invoke an inflammatory response (reviewed Eltzschig and Carmeliet, 2011).

1.5.4 Hypoxia inducible factors

Hypoxia inducible factors (HIFs) are a transcription factor family instrumental in mediating the adaptive response to hypoxia in cells. HIF activation causes changes in the expression of genes responsible for angiogenesis, glucose metabolism, cell survival and microenvironment remodelling (Semenza, 2001). HIFs are heterodimeric, consisting of a constitutively-expressed HIF1β subunit (also known as aryl hydrocarbon receptor nuclear translocator [ARNT]) and one of three oxygen-sensitive alpha (α) subunits 1 α, 2α or 3α (Wang et al., 1995).

During normoxia HIF1β levels remain constant but HIFα subunits are degraded in the cytoplasm by the hydroxylation-ubiquitination-proteosomal system (HUPS) (Liang et al., 2006). Hydroxylation occurs at 2 prolyl residues (P402 and P564) in the oxygen-

Regenerative medicine applications in paediatric urology: barriers and solutions

dependent degradation domain (ODD) of HIFα mediated by prolyl hydroxylase enzymes PHD1, PHD2, PHD3 as part of the HUPS process (Jaakkola et al., 2001). This hydroxylation process enables HIFα to be recognised by Von Hippel Lindau (VHL) protein, a substrate for ubiquitination. The final step is for the ubiquitinated HIFα to be degraded by the 26S proteosomal subunit.

Also important for the stabilisation of HIFα during normoxia is the transactivation potential (TAP), which is determined by interactions between HIFα and the co-activator p300/CBP (Sang et al., 2002) and controlled by Factor Inhibiting HIF-1 (FIH). FIH is an oxygen-dependent asparagine hydroxylase which modifies HIFα and affects the hydrophobic interaction with p300/CBP (Lando et al., 2002). HIFα possesses an N-terminal and a C-terminal transactivation domain (NAD/CAD). The major transactivation activity occurs at CAD mediated through hydrophobic and charge mediated interaction with the CH1 domain of p300/CBP (Sang et al., 2002). Both HUPS and TAP processes involve hydroxylation, which is reliant on the availability of cofactors such as ferrous ions (Ivan et al., 2001), ascorbic acid (Gao et al., 2007) and co-substrates such as 2-oxoglutarate (Ivan et al., 2001).

In hypoxic conditions PHD activity is reduced and heterodimerisation of HIF can occur (McDonough et al., 2006). This permits interaction at hypoxic response elements (HREs), containing the core recognition sequence 5'- RCGTG-3' (Semenza et al., 1996) within the nucleus, leading to the induction of target genes up regulated under hypoxia. Other transcriptional activity is generally inhibited (Johnson et al., 2008). Epigenetic factors are reported to be instrumental in the hypoxic response (Watson et al., 2010).

1.5.5 Hypoxia and fibrosis

Physiologically the basement membrane of healthy urothelium has a low turnover rate, similar to the overlying urothelium and is thought to be derived from both epithelial and stromal cells (Deen and Ball, 1994). The basement membrane is predominantly composed of collagen IV and laminin with traces of collagens I, III and VII, tenascin and fibronectin. Located below the basal lamina and sitting on the lamina propria, is a muscle layer known as the muscularis mucosa. The bladder lamina propria is a loose matrix, rich in collagen IV and containing stromal cells, nerves, blood and lymphatic vessels. Very few lymphocytes or other leukocytes are found in normal, uninflamed bladder (Jost et al., 1989, Cresswell et al., 2001).

A common feature of end-stage, inflammatory entities is fibrosis where functional tissue is replaced by an accumulation of extracellular matrix resulting in scar formation. This is especially important in end stage bladder disease whereby the bladder is small and fibrotic and results in a low capacity, non-compliant organ that creates a high pressure system prone to reflux and damage to the kidneys. HIF-1 has been implicated formation of fibrosis. This is due to the persistent presence of HIF1α and its' downstream targets TGF-β (Lokmic et al., 2012) and lysyl oxidase (LOX) (Guadall et al., 2011), the latter being noted in the development of tubulointerstitial fibrosis in a murine model of ureteric obstruction (Higgins et al., 2007).

1.6 The Epigenome

The epigenome is an additional layer of control over gene expression, which is now being considered as an important "interface between genome and environment" (Bell and Beck, 2010). Epigenetics refers to modifications in gene expression controlled by heritable, but potentially reversible changes in DNA methylation and chromatin structure without alteration in the DNA sequence (Reviewed by (Momparler, 2003)) Transcriptional regulation can be altered epigenetically via various mechanisms including DNA methylation/ demethylation and histone acetylation/deacetylation.

1.6.1 Epigenetics and disease

It is becoming increasingly recognised that the epigenetic landscape, acquired during normal development, acts to define tissue-specific patterns of gene expression and may be disrupted during pathogenesis, with negative consequences for cell and tissue function. Eukaryotic cells switch their gene expression pattern to maintain a cellular homeostasis when faced with adverse conditions, such as infection, chronic inflammation and hypoxia (reviewed by (Adcock et al., 2005). These changes in gene expression are associated with changes in the chromatin structure (Johnson et al., 2008) and are believed to occur as early as *in utero* (Zaina et al., 2005a, Zaina et al., 2005b). Barker in 2002 (Barker, 2002) postulated that this may result in fetal programming that can persist into adulthood contributing to the lifetime risk of developing conditions such as cardiovascular disease.

Altered epigenetic modification has been implicated in many diseases processes including: chronic obstructed pulmonary disease (Adcock et al., 2005); cardiovascular

disease (Backs and Olson, 2006), neurodegenerative disorders (Graff et al., 2012); chronic/progressive kidney disease (Dwivedi et al., 2011) and cancer (Seligson et al., 2009). It is reported in the literature that hypoxia result in epigenetic modifications (Pollard et al., 2008) including: reduced global acetylation and increased methylation at H3K9 and H3K4me3 (Zhou et al., 2010). Zhou et al also report an overall decrease in transcription levels of JARID1A a Jumonji demethylase (Zhou et al., 2010). The Jumonji family of histone demethylases are Fe^{2+} and α-ketoglutarate dependent oxygenases, which are critical components of the transcriptional chromatin complex. Beyer (2008) (Beyer et al., 2008) demonstrated that HIF-1α bound to and activated JMJD1A and JMJD2B expression; resulting in elevated levels of mRNA and protein. JMJD1A has been implicated in the expression of pluripotency markers in murine ES cells (Loh et al., 2006).

1.6.2 Epigenetic modifying therapies and hypoxia

In cancer therapy epigenetic modifying agents have been used to target HIF1α because of its role in both tumour cell survival and chemo-radiotherapy resistance (Schwartz et al., 2010). One family of drugs investigated have been the histone deacetylase inhibitors (HDACi); the role of such substances has been extensively reported in the treatment of malignant disease (Kim et al., 2011). It is thought that HDACi, such as trichostatin A (TSA), destabilises HIF1α by affecting the transactivation potential and the interaction between p300/CBP (Fath et al., 2006) and thus potentially preventing the transcription of downstream targets such as vascular endothelial growth factor (VEGF) to prevent angiogenesis.

HDACi have also been indicated in the treatment of benign diseases, particularly those with an underlying fibrotic process (Adcock et al., 2005, Dwivedi et al., 2011). Treatment of fibrotic, neuropathic, smooth muscle bladder cells with the epigenetic modifying drugs TSA and valproic acid has been piloted in paediatric urology (Hodges et al., 2010). The study specifically reported on the reversal of abnormal collagen III deposition by smooth muscle cells, which may have an impact on fibrosis (Hodges et al., 2010) but these initial results, although promising are tentative and further results are pending.

2   Materials and Methods

2.1   General

Practical work was carried out at the Jack Birch Unit for Molecular Carcinogenesis, Department of Biology, University of York. All animal surgery was carried out at the University of Leeds. Human tissue biopsies were taken at Leeds General Infirmary or St. James's University Hospital.

2.1.1   Commercial suppliers

Manufacturers and suppliers are listed in the text with full names and addresses listed in Appendix I.

2.1.2   Stock solutions

References to H_2O in this thesis refer to double-distilled water subsequently purified by reverse-osmosis in a Purelab Ultra Purite system (Elga Veolia), to a resistivity of 18.2Ω.

All stock solutions were prepared in H_2O and from using analytical grade chemicals or of tissue culture grade depending on their intended use. All reagents were obtained

from Sigma-Aldrich, unless otherwise stated. The recipes for stock solutions are listed in Appendix II. Heat-stable solutions were sterilised by autoclaving at 121 °C for 20 minutes. Filter sterilisation of other solutions was carried out using "Acrodisc" 0.2 μM filter (Pall Corporation).

2.1.3 Glassware

Glassware was autoclaved at 121 °C (1 bar) for 20 minutes and dried in a hot air oven (60 °C). Glass Pasteur pipettes (Fisher Scientific) were autoclaved in metal pipette cans (Jencons). Polytetrafluoroethylene (PTFE) coated multispot slides (Hendley-Essex Ltd) were wiped with 70 % ethanol and autoclaved before use in tissue culture.

2.1.4 Plasticware

Disposable micro-pipette tips (Starlab) were sterilised by autoclaving and then oven dried. Other plasticware was supplied sterile and included TipOne® repeat dispenser tips (Starlab) for use with Eppendorf multi-dispensing pipette (Sigma Aldrich), fine tip and maxi-tip "Pastettes" (Axygen ®, Corning), graduated serological pipettes , 5 ml "bijoux" containers (Sterilin), 25 ml "universal" containers (Sterilin), 50 ml polypropylene centrifuge tubes (Falcon, Corning®), quadriPERM dishes (Heraeus, Fisher), cryovials (Nunc™, Thermo-Scientific), microcentrifuge tubes (Starstedt).

Urothelial cell lines were maintained as adherent cultures in Primaria™ dishes (Corning®), which are vacuum-gas and plasma-treated to promote attachment and growth of primary cells. Cells were maintained in 25 cm^2 and 75 cm^2 Primaria™ flasks

Regenerative medicine applications in paediatric urology: barriers and solutions

and 3.5 cm and 6 cm Primaria™ dishes and 96- and 6-well Primaria™ multi-well plates, cell culture inserts 3µm pore size (Falcon, Corning®), six-well plates (Costar®, Sigma-Aldrich), Thin-Cert™ (pore-size 0.4 µm) cell culture inserts (Greiner Bio-One).

2.1.5 Dissection instruments

Dissection instruments were autoclaved at 121 °C (1 bar) for 20 minutes and oven-dried prior to use. Soiled instruments were decontaminated by fifteen minutes sonication in an ultrasonic bath containing a 1:40 solution of Ultraclean M2 formula (Ultrawave) and then rinsed with deionised water (DW) and dried. Hinged instruments were lubricated with Instol™ spray (Seward Thackray) prior to sealing in autoclave pouches. The instruments were autoclaved as described in section 2.1.3 and dried prior to reuse.

2.2 Reagents

2.2.1 Antibodies

Details of the antibodies used in this study including specificity, source and concentration used for immunocytochemistry (IF), immunohistochemistry (IHC), and/or immunoblotting (IB) are given in *Tables 2-1 to 2-3*. Antibodies were supplied by Sigma, Novacastra, Serotec, Progen, Invitrogen/Zymed, Enzo Life Sciences, Chemicon, BD Biosciences, Diagenode, Abcam, Thermo Fisher Scientific and R&D

Systems (R&D). Primary antibodies were titrated against known positive cells or tissues and negative/irrelevant samples to establish optimal concentrations for use and were stored at –80 °C. Once thawed, aliquots of primary antibodies were stored at 4 °C in TBS pH 7.6, 0.1% NaN_3 ± 0.1% BSA (Appendix II).

2.2.2 Enzymes, epigenetic modifiers and other reagents

Compounds were reconstituted according to manufacturers guidelines. Optimisation was performed to determine a suitable concentration for *in vitro* cell culture and ensure low cytotoxicity with maximum functional action. All details are provided in *Table 2-4*

Regenerative medicine applications in paediatric urology: barriers and solutions

Table 2-1 Primary mouse antibodies

Antigen	Antibody/Clone	Production	Supplier	Dilution/ Application *
CK13	1C7 (Human)	Monoclonal	Abnova	1:500 (IHC-CA/Tryp)
CK14	LL002	Monoclonal	Serotec	1:500 (IHC CA/Tryp)
CK7	OV-TL12/30	Monoclonal	Novocastra	1:400 (IHC-CA) 1:40 (IF)
CK20	CK20.8	Monoclonal	Novocastra	1:200 (IHC Tryp)
UPK3a	AU1	Monoclonal	Progen	1:200 (IHC CA)
ZO-1	ZO-1-1A12	Polyclonal	Zymed	1:40 (IF) 1:500 (IB)
Ki-67	MM1	Monoclonal	Novocastra	1:100 (IHC CA)
HIF-1α	Hα111A	Monoclonal	Enzo Life Sciences	1:300 (IHC CA)
H3K9Me2	ab1220	Monoclonal	Abcam	1:1000 (IB)
P63	A4A SC-28431	Monoclonal	Santa Cruz	1:1000 (IHC CA)
NGFR	7F10 NCL-NGFR	Monoclonal	Novocastra	1:100 (CSA)
CD45 (Anti-pig)	K252-1E4	Monoclonal	Serotec	1:150 (IHC)
CD163	2A10/11	Monoclonal	Serotec	1:200 (IHC)
SMA	1A4	Monoclonal	Sigma	1:4000 (IHC)
CD107a	AE9/11	Monoclonal	Serotec	
β-actin	AC15	Monoclonal	Sigma	1:250000 (IB)

- **IHC**-immunohistochemistry**, CA** – citric acid**, Tryp** – Trypsin**, CSA** – catalysed signal amplification (further details see section **2.10.2**)

- **IB** – immunoblotting by western blot (further details see section **2.11.6**)

- **IF** – immunocytochemistry by fluorescence (further details see section **2.10.1**)

    ***all antigen retrieval performed in microwave except for CK20 (Tryp without CA). Zinc-fixed sections did not require this**.

Regenerative medicine applications in paediatric urology: barriers and solutions

Table 2-2: Primary rabbit antibodies

Antigen	Antibody/Clone	Production	Supplier	Dilution/ Application*
CK5	ab5312	Polyclonal	Abcam	1:200 (IHC CA)
H3K9Me2	C15410060 (pAb060-050)	Polyclonal	Diagenode	1:(IF)
Laminin	Lam89	Polyclonal	Sigma	1:10000 (IHC Tryp)
Occludin	71-500	Polyclonal	Zymed	1:100 (IF), (IHC-CA)
ZO-1 α+	ZO-1 α+ isoform	Polyclonal	Cambridge Bioscience	1:100 (IB)
VEGF	RB-9031-P	Polyclonal	Thermo-scientific	1:50 (IHC CA)
Occludin	71-1500	Polyclonal	Zymed	1:100 (IF) 1:100 (IHC-CA)

- **IHC-**immunohistochemistry**, CA –** citric acid**, Tryp –** Trypsin (further details see section **2.10.2**)
- **IB –** immunoblotting by western blot (further details see section **2.11.6**)
- **IF –** immunocytochemistry by fluorescence (further details see section **2.10.1**)

  *all antigen retrieval performed in microwave except for Laminin (Tryp without CA).

Regenerative medicine applications in paediatric urology: barriers and solutions

Table 2-3: Secondary antibodies

Antibody (clone)	Host	Production	Conjugate	Supplier	Dilution/ Application
Anti-rabbit IgG	Goat	Polyclonal	AlexaFluor® 488	Invitrogen™	IF (1:500)
Anti-mouse IgG	Goat	Polyclonal	AlexaFluor® 594	Invitrogen™	IF (1:700)
Anti-rabbit IgG	Goat	Polyclonal	Biotin	Dako	IHC (1:600)
Anti-mouse IgG	Rabbit	Polyclonal	Biotin	Dako	IHC (1:200)
Anti-rabbit IgG (611-131-122)	Goat	Polyclonal	AlexaFluor® 680	Rockland	IB (1:10000)
Anti-mouse IgG (A10038)	Donkey	Polyclonal	AlexaFluor® 700	Molecular probes	IB (1:10000)

- **IHC**-immunohistochemistry (further details see section 2.10.2)
- **IB** – immunoblotting by western blot (further details see section 2.11.6)
- **IF** – immunocytochemistry by fluorescence (further details see section 2.10.1)

Table 2-4: Substances, targets and reagent preparation

Name	Target	Supplier	Catalogue No.	Vehicle/concentration
Trichostatin A (TSA)	HDAC inhibitor	Enzo	BML-GR309	DMSO
UNC0646	G9a/GLP methylase inhibitor	Tocris	4342	KSFMc
Deoxyribonuclease I	Hydrolyses double/single stranded DNA	Sigma	D7291	≥ 5 mg/ml in glycerol & 20 mM sodium acetate (Appendix II)
Ribonuclease A	Hydrolyses RNA	Sigma	R6513	100 mg/ 89.5 ml sterile H_2O = 100 U/ml

2.3 Statistics

Statistical tests were performed using Instat™ software v.3.and GraphPad Prism®v. 6.05. P-values less than 0.05 were considered statistically significant. Confidence intervals were assumed to 95%.

Student's T-tests and one-way ANOVAs were performed on parametric data. Data was tested for normality using the Kolmogorov-Smirnov test and for equal variances using the method of Bartlett. Tukey multiple comparison ANOVA was performed when several datasets were being compared with each other. Welch correction was applied if standard deviations between datasets varied. Differences between non-parametric data were subjected to Kruskal Wallis one-way analysis of variance. Linear regression with a "runs" post-test, to determine deviation from linearity, was performed to assess for correlation between sets of numerical data.

Regenerative medicine applications in paediatric urology: barriers and solutions

2.4 Cell Culture

2.4.1 General cell culture practice

Cell culture work was carried out in class II laminar flow cabinets (Medical Air Technologies Ltd.) using strict aseptic technique. Surfaces were cleaned before and after use with 70 % (v/v) ethanol. Waste cells and media were aspirated by vacuum into a Buchner flask containing 10 % (w/v) Virkon (Fisher) for decontamination. Cultures were maintained in Steri-cult Hepa-filtered incubators (Forma Scientific) at 37 °C in a humidified atmosphere of either 5 % CO_{2in} air for cells cultured in Keratinocyte serum-free medium (KSFM) unless otherwise stated. Culture media were purchased from Invitrogen, and all cell culture reagents were tissue culture grade and purchased from Sigma, unless otherwise stated. All centrifugation steps were performed in a "Sigma" centrifuge (Philip Harris) at 400 g for five minutes, unless stated otherwise.

2.4.2 Collection of tissue for primary urothelial cell culture

Human tissue samples of bladder, ureter and renal pelvis were provided by the patients and surgeons at Leeds General Infirmary and St James's University Hospital, Leeds. Specimens were obtained with informed consent from the patients or parents with assent obtained where appropriate. Paediatric tissues required a new project application to be made, which was approved by application to Leeds East Research Ethics Committee (REC 12/YH/0507) and was made via the Integrated Research Application System (IRAS) website https://www.myresearchproject.org.uk/Signin.asp (IRAS project number: 102795).

At this time all details of the study were submitted along with parental and age-appropriate patient information sheets, consent and assent forms. The author was interviewed by the ethics committee after which time a number of modifications, relating to style and age-appropriateness, to the text of communications to parents and patients were suggested. Once amendments were made the application was accepted. The final documentation is provided in Appendix 3. In addition the project was approved by the Biology Ethics Committee, University of York.

Specimens were collected in "Transport medium" consisting of Hank's balanced salt solution (HBSS) buffered with 10 mM HEPES, pH 7.6 and containing 20 KIU/ml aprotinin ("Trasylol", Bayer) and stored at 4 °C before processing.   Antibiotics were not added to human tissue that would be used for primary culture to prevent molecular alterations in phenotype.

2.4.3 Isolation and culture of primary human urothelial cells

Primary urothelial cell cultures were established as described by Southgate *et al.* (1994, 2004). Individuals trained to the appropriate levels within the Jack Birch Unit performed primary human urothelial cell isolation as follows. Tissue was transferred in a sterile petri dish and excess fat and stromal tissue dissected off. A small sample of each specimen was taken for routine histology. This was fixed in 10% (v/v) formalin in PBSc (section **2.8.1**).

Remaining tissue was cut into pieces of 1 cm^2 and incubated overnight at 4°C in "Stripper" medium of modified HBSS (Ca^{2+} and Mg^{2+} free) buffered with 10 mM HEPES pH 7.6 and supplemented with 20 KIU/ml aprotinin and 0.1% (w/v) EDTA. Sheets of

urothelial cells were gently separated from the stroma using forceps, collected by centrifugation and incubated for 20 minutes in 2 ml collagenase type IV (200 U/ml, see Appendix II) at 37°C. Cell sheets were disaggregated using a plastic "Pastette," cells counted, collected by centrifugation and seeded at a minimum density of 10^4 cells/cm^2, in KSFM containing supplements provided by the supplier of 5 ng/ml recombinant epidermal growth factor (rEGF), 50 μg/ml bovine pituitary extract (BPE) and further supplemented with 30 ng/ml cholera toxin. Supplemented KSFM is referred to as KSFM complete (KSFMc).

2.4.4 Subculture of urothelial cell lines

Normal Human Urothelial (NHU) cells from patients were described as cell lines; however after initial subculture these were "finite" cell lines which eventually undergo culture senescence. NHU cell cultures were passaged upon just reaching confluence by incubating cell monolayers in 0.1 % (w/v) EDTA in PBS for five minutes at 37 °C and detaching cells with a minimum volume of modified HBSS containing 0.25 % (w/v) trypsin and 0.02 % (w/v) EDTA. . Cells were harvested in KSFMc containing 20 mg/ml soybean trypsin inhibitor (Sigma) and centrifuged. Cells were routinely reseeded at a split ratio of between 1:3 and 1:6 and discarded after reaching passage 5 unless otherwise stated. Twenty finite cell lines from independent donors were used for the studies reported here (***Table 2.5***).

2.4.5 Cell enumeration

Cells were seeded into 6 well plates at a density of 5 x10^4 cells / cm^2, with six technical repeats. Cultures were medium-changed and sub-cultured frequently to avoid

nutrient depletion or contact inhibition becoming a confounding factor. If the experiment required cells to be cultured in different conditions then cultures were continued until one of the groups had reached 80% confluence to ensure cultures were maintained in exponential growth phase. Cell counts were performed using an "Improved Neubauer" haemocytometer (Hawksley) filled with a single cell suspension. Cells were counted in four grids, each containing a volume of 0.0001 ml. The mean concentration of cells per ml was then calculated. After cell enumeration cells were reseeded at 0.6×10^{4} cells / cm^{2} and the process repeated.

Table 2-5: Origins of NHU cell lines

Number	Tissue	Donor Age	Donor sex	Pathology
Y1689	Ureter	52	M	Unknown
Y931	Bladder	85	M	Unknown
Y879	Bladder	Paediatric	Unknown	Unknown
Y1356	Ureter	63	M	Donor
Y1270	Ureter	76	F	Renal Ca
Y1387	Ureter	25	F	Donor
Y1276	Ureter	21	F	Pyeloplasty
Y1173	Bladder	11	F	Neuropathic
Y1036	Bladder	11	M	Neuropathic
Y1042	Bladder	13	F	Neuropathic
Y1559	Ureter	46	M	Nephrectomy
Y1661	Ureter	45	F	Pyeloplasty
Y1501	Ureter	46	M	Donor
Y1431	Ureter	34	M	Donor
Y1483	Ureter	44	M	Donor
Y1594	Ureter	39	F	Donor
Y1596	Ureter	70	F	Nephrectomy
Y1461	Ureter	39	M	Donor
Y1332	Ureter	52	F	Nephrectomy
Y1376	Bladder	30	F	Normal
Y1359	Ureter	46	M	Nephrectomy

2.4.6 Cryopreservation

Cells were harvested (section **2.4.3**), counted, collected by centrifugation and resuspended at $1x10^6$ cells/ml in ice-cold culture medium containing 10 % FBS and 10 % dimethylsulphoxide. One millilitre volumes of cell suspension were aliquoted into cryovials (Greiner) and transferred to an isopropanol freezing bath (Nalgene) at -70 °C to cool at a rate of approximately 1 °C per minute. The following day, vials were transferred to a liquid nitrogen cryogenic freezer (-196 °C) for storage. Cells were recovered by rapid thawing of vials in a 37 °C water bath followed by centrifugation in 10 ml pre-warmed culture medium. The cells were resuspended in the appropriate growth medium and plated at the required density. Culture medium was replaced the day after seeding to remove any dead cells.

2.4.7 Testing for *Mycoplasma spp*. Infection

Cells lines and primary cultures were routinely monitored for infection with *Mycoplasma spp.* using the DNA-intercalating fluorochrome bis-benzimide (Hoechst 33258, Molecular Probes). Cells were seeded on multi-well glass slides and left to attach overnight. Slides were washed in PBS and fixed for 30 seconds in a 1:1 mixture of methanol and acetone. DNA was stained by incubating the cells for five minutes in 1 μg/ml Hoechst 33258 dye in PBS. Slides were washed in PBS; air dried, mounted in Solovei's Antifade Mountant (Appendix II) and viewed under epifluorescence illumination with selected emission/excitation filters using an Olympus BX60 Microscope (Olympus). Slides were screened for the presence of *Mycoplasma spp.*, as determined by the presence of extra-nuclear DNA.

2.5 Cell analysis by imaging

2.5.1 Microscopy

Routine cell observations were made under phase contrast microscopy using an inverted Nikon Diaphot photomicroscope equipped with x2.5, x4 and x20 objectives or an Evos XL Core transmitted light (brightfield/ phase) cell imaging system (Life Technologies).

2.5.2 Photography

Brightfield black and white images of cells were captured using digital images taken using one of two methods. Firstly images were captured using a Nikon Coolpix 4500 camera and stored on compact flash scan disc photocards (Nikon) and subsequently downloaded onto a PC. Evos XL Core images were captured using the integrated imaging software and stored on a flash drive for transfer onto a PC.

2.5.3 Image analysis

Photographic measurements were performed and scale bars added to photomicrographs using Image Pro Plus software (Media Cybernetics).

2.6 Urothelial cell differentiation

Normal Human Urothelial (NHU) cells were differentiated using the published biomimetic model of cytodifferentiation (Cross et al., 2005) by using adult bovine serum (ABS) and increasing exogenous calcium concentration to a physiological level.

Upon reaching confluence medium was changed to KSFMc containing 5 % adult bovine serum (ABS) for a total of 5 days, also called "pre-treatment". At day four cells could be harvested and reseeded, at a density of 1 x 10^6 cells/ml, into more plasticware or ThinCert ™ inserts for electrophysiology studies. Should harvesting be performed cells remained in the KSFMc and 5 % ABS medium for 1 day, 5 days in total.

At this point medium was changed to KSFMc, 5 % ABS and a total exogenous calcium concentration of 2 mM. This was achieved by the addition of 180 µL 1M $CaCl_2$ to every 100 ml medium, given the KSFMc and 5 % ABS already contained 0.2 mM/ 100 ml of calcium. Medium was changed every 72 hours until the termination date.

2.6.1 Measurement of barrier function using Trans-epithelial electrical resistance (TEER)

After four days of KSFMc and 5 % ABS cells were passaged and seeded at a concentration of 8.84 x 10^5 cells/cm^2 into ThinCert™cell culture insert wells in a volume of 400µL and an outer well containing 1.5ml medium. The cells were allowed to attach

for 24 h prior to the medium being exchanged for KSFMc with 5 % ABS containing 2 mM calcium. In addition at the point of the calcium-containing medium being utilised, other treatments could be added.

TEER measurements were taken daily and performed prior to any planned medium change. An EVOM electrode (World Precision Instruments WPI) was placed in 10 ml of Cidex Plus Disinfecting solution (WPI) for 15 minutes, followed by 2 x 8 ml changes of KSFMc, 5 % ABS, 2 mM calcium for five minutes to allow equilibration and removal of excess disinfectant. Cells to be analysed were removed from the incubator during the final 5 minutes to also equilibrate to ambient conditions.   The electrode was plugged into an Ohmmeter (WPI) and TEER read across the insert and outer well. The final TEER was taken to be at the point where a stable reading was obtained. TEERs were measured regularly up to the time point at which barrier resistance was stable over 2 days.

2.6.2 Scratch-wounding and barrier recovery

Once a stable barrier had been established a TEER reading was taken. After this was obtained a horizontal trans-well scratch was created using a 0-10 μl micropipette tip in at least one well. A second TEER reading was taken to show initial post-wounding values and this was repeated every 2-6 hours until barrier recovery had returned to at least pre-wounding levels or demonstrated no evidence of further recovery for > 2 days. Prior to all readings disinfection and equilibration was performed as set out in section **2.6.1**.

2.6.3 Hypoxic cell culture system

Hypoxic cell culture conditions were achieved in an RS Biotech Mini Galaxy A CO_2 Incubator, in which N_2 was used to achieve the hypoxic environment by displacement (*Figure 2-1*) using controlled parameters for CO_2 (5 %) and O_2 (2 %). A humidified atmosphere at 37 °C was maintained.

Regenerative medicine applications in paediatric urology: barriers and solutions
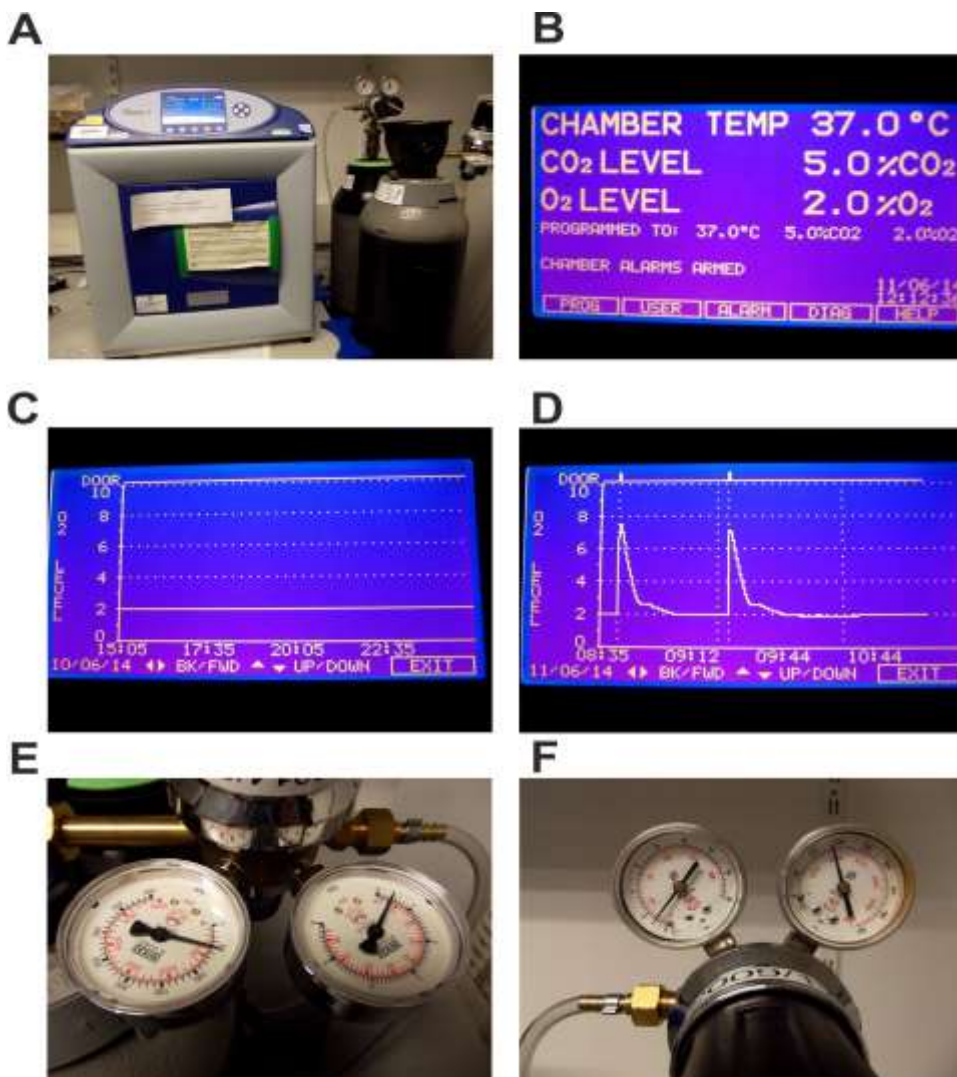
Figure 2-1: Hypoxic incubator set-up

A: Overall configuration of hypoxic incubator with carbon dioxide and nitrogen supplies attached

B: Incubator settings: temperature (37 °C), carbon dioxide level (5 %) and oxygen level (2 %)

C: Steady state oxygen levels (2 % O2) with incubator door closed

D: Oxygen level fluctuation on incubator door opening and closing twice for treatment change

E: Carbon dioxide settings 0.35 bar

F: Nitrogen setting 1 bar = 14.5 psi via High-efficiency particulate air (HEPA) filter

2.7 Organ culture

Healthy ureteric tissue (**Table 2-6**) samples were detubularised to create a flat sheet and areas of 5 mm^2 were dissected. Some sections were fixed for 24 hours in 10 % formalin prior to being stored in 70 % ethanol for histological analysis (native tissue). The other sections were maintained, urothelium side up, on cell culture semi-permeable membrane inserts (3 μm pore-size) (BD Falcon) within six-well plates at 37 ˚C, 10 % CO_2 and 90 % humidity (**Figure 2-2**).

Table 2-6: Origins of organ culture samples

Number	Tissue	Donor Age	Donor sex	Pathology
Y1598	Ureter	49	F	Nephrectomy benign disease
Y1657	Ureter	30	F	Renal transplant donor
Y1713	Ureter	74	F	Renal transplant donor

The blocks of tissue were maintained submerged with DMEM: RPMI medium at a ratio 1:1 supplemented with 5% FBS AND 1% L-glutamine. Once the appropriate experimental time point had been reached samples of tissue were removed from culture and fixed in 10% formalin and processed, in the same way as the native tissue into paraffin wax for histology (section **2.8.1**).
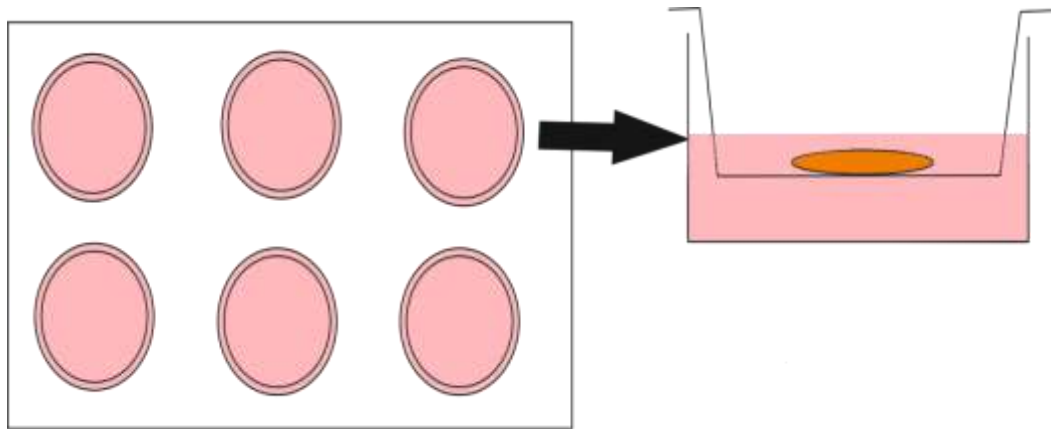
Figure 2-2: Organ culture set-up

Cell culture inserts were placed in 6 well plates. Tissue sample maintained submerged with urothelium uppermost.

2.8 Histology

Thirty two independent donor tissues were used for the studies reported here, which included samples from neuropathic bladders, "control" donors some of which had other diseases of the urinary tract (**Tables 2-7 to 2-9**).

2.8.1 Sample dehydration and embedding

Samples were removed from transport medium and fixed in 10% formalin in PBS for 24-48 hours; after fixation, samples were stored in 70% ethanol. Dehydration prior to

embedding was achieved by sequential incubation in 70 % ethanol, three baths of absolute ethanol, one bath of isopropanol and three baths of xylene for ten minutes in each. Specimens were then embedded in paraffin wax by placement in four changes of paraffin wax at 60 °C. Tissue was immersed in each wax bath for ten minutes, orientated on a hot plate heated to 55 °C and set in wax by transfer to a cold plate chilled to -12 °C. Five micrometre sections were cut using a Leica RM2135 microtome and collected, via a water bath, onto 'Superfrost Plus' slides (VWR). After air drying, sections were melted on a hot plate at 40 °C for several hours and stored at ambient temperature.

2.8.2 Haematoxylin and eosin (H&E) staining

H&E staining of paraffin wax-embedded sections was used to assess the integrity of tissue specimens from which human urothelial cells were isolated. To stain the tissue, sections were de-waxed in two changes of xylene for ten minutes and two changes of xylene for one minute. Sections were rehydrated in three changes of absolute ethanol for one minute, followed by one minute in 70 % (v/v) ethanol and one minute in running tap water. Sections were stained with haematoxylin (Appendix II) for three minutes, followed by one minute incubation in water and one minute incubation in Scott's tap water (Appendix II). Sections were counterstained with eosin for one minute, rinsed in running tap water and dehydrated by one minute incubations in graded alcohols, including one bath of 70 % ethanol, three of absolute ethanol and two of xylene. Stained sections were mounted in DPX (Sigma).

Table 2-7: Origin of donor neuropathic tissue:

Number	Tissue	Donor Age	Donor sex	Pathology	Pressure of system	rUTI* Y/N
Y777	Bladder	11	F	Neuropathic	Unknown	Unknown
Y969	*Bladder*	5	M	Neuropathic	Unknown	Unknown
Y1000	Bladder	17	F	Spina Bifida	Low	Y
Y1025b	Bladder	10	F	Tethered cord	Low	Unknown
Y1081	Bladder	10	M	Spina bifida	High	Unknown
Y1042	Bladder	11	M	Spina Bifida	High	Y
Y1295	Bladder	11	F	Spina Bifida	High	Y
Y1079	Bladder	13	F	Spina Bifida	High	N
Y1173	Bladder	11	F	Spina Bifida	High	N
Y1103	*Bladder*	10	F	*Non-neuropathic neuropathic*	High	Y
Y1107	*Bladder*	12	M	*Neuropathic*	Borderline	Unknown
Y1122	Bladder	15	M	Neuropathic	High	Y
Y1180	Bladder	10	F	Neuropathic	High	Unknown
Y1427	Bladder	11	M	Neuropathic	Unknown	N
Y1462	Bladder	9	M	Neuropathic	Unknown	Unknown
Y1535	Bladder	15	M	Neuropathic	Unknown	Y
Y1585	Bladder	2	F	Neuropathic	Unknown	Unknown
Y1036	Bladder	15	F	Neuropathic	High	Y

* rUTI recurrent urinary tract infections

Table 2-8: Origin of donor control tissue:

Number	Tissue	Donor Age	Donor sex	Pathology
Y836B	*Bladder*	10	M	VUR
Y952	*Ureter*	Paediatric	Unknown	Nephrectomy*
Y1186	*Bladder -*	79	M	BPH
Y1216	*Ureter*	56	M	Nephrectomy*
Y1278B	*Ureter*	69	F	Nephrectomy*
Y1272B	*Bladder*	4	F	VUR
Y1299a	*Ureter*	64	M	Donor ureter#
Y1303	*Bladder*	12	M	VUJO
Y1328	*Bladder*	12	F	Re-implant
Y1200	Renal pelvis	17	M	PUJO
Y789b	Bladder	83	M	UC

* Benign pathology

donor ureter removed at time of renal transplantation

Regenerative medicine applications in paediatric urology: barriers and solutions

Table 2-9: Origin of post-augmentation native bladder tissue

Number	Tissue	Donor Age	Donor sex	Pathology	System Pressure
E1	*Bladder*	61	Unknown	Post-augment, urge/stress incontinence, detrusor instability	Low
E2	*Bladder*	59	Unknown	Post-augment urge incontinence, detrusor instability	Low
E4	*Bladder*	67	Unknown	Post-augment, urge incontinence	Low
E8	*Bladder*	44	Unknown	Post-augment, urge incontinence	Low

2.9 Histological analysis

2.9.1 Imaging techniques: Microscopy

Routine observations were made under brightfield conditions using an Olympus BX60 microscope, equipped with x4, x10, x20 x40 and x60.Brightfield images were captured using 35 mm Olympus U-TVO 5XC-2 digital camera and Image-Pro Plus software (Media Cybernetics).

2.9.1.1   Microscopy Image analysis

Photographic measurements were performed and scale bars added to photomicrographs using Image Pro Plus software.

2.9.2 Slide scanner

To permit further quantifiable results some slides were scanned using **a** Zeiss AxioScan.Z1 slide scanner. Images were stored in the format of a Carl Zeiss Image (CZI) file.

2.9.2.1   HistoQuest (TissueGnostics) image analysis software

CZI files were transferred to the HistoQuest software (TissueGnostics). A detailed, illustrated flow scheme of the image analysis process is described on next page:

1) Regions of interest (ROI) were created (dashed lines) in all scanned images to ensure only urothelium would be analysed (**Figure 2-3***)*.
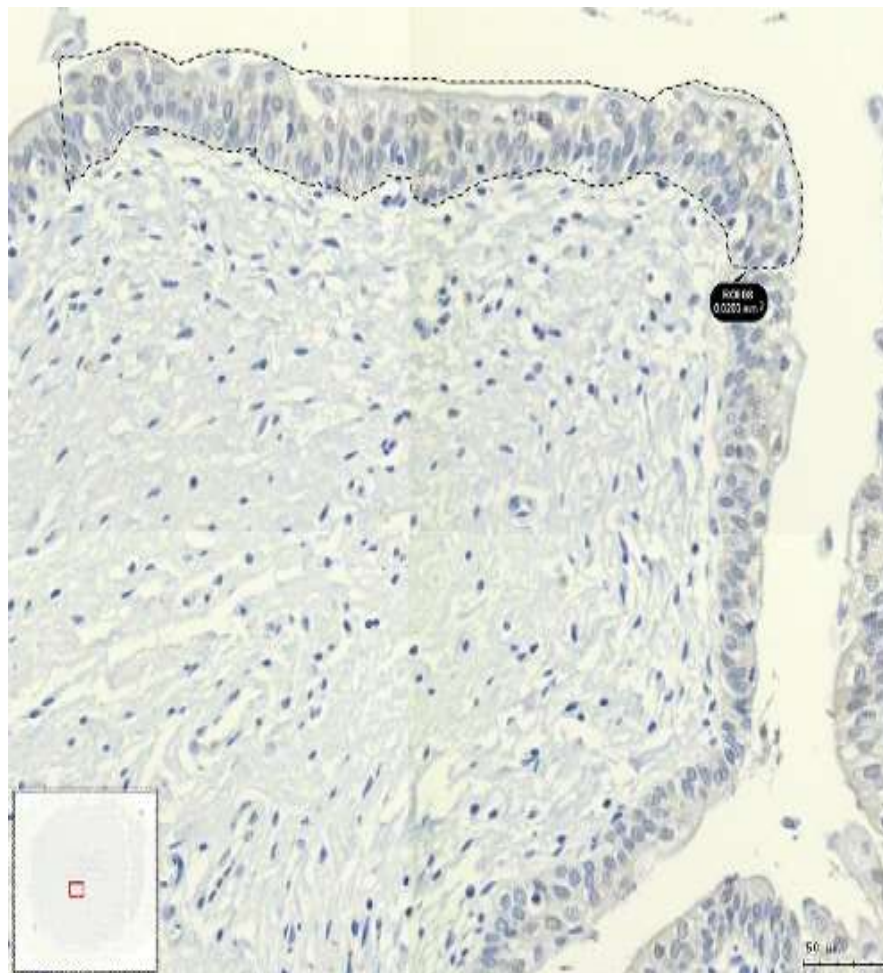
Figure 2-3: Example of manual selection of urothelium to create a "region of interest" (ROI).

*S*ample Y1299a is illustrated here with the ROI shown within the dashed lines. For ease the urothelium was subdivided into several ROI for analysis by HistoQuest software, which collated data from all ROI to perform analysis for the complete urothelium**.**

2) Colour shades were picked manually for DAB and haematoxylin counterstaining using the software "colour-picking" function.

3) All nuclei were identified using nuclear size and area as discriminators. These were manually checked to ensure all nuclei had been recognised, nuclei had not been subdivided and no non-nuclear structures were included in the analysis (*Figure 2-4*). Background thresholds were also manually derived.
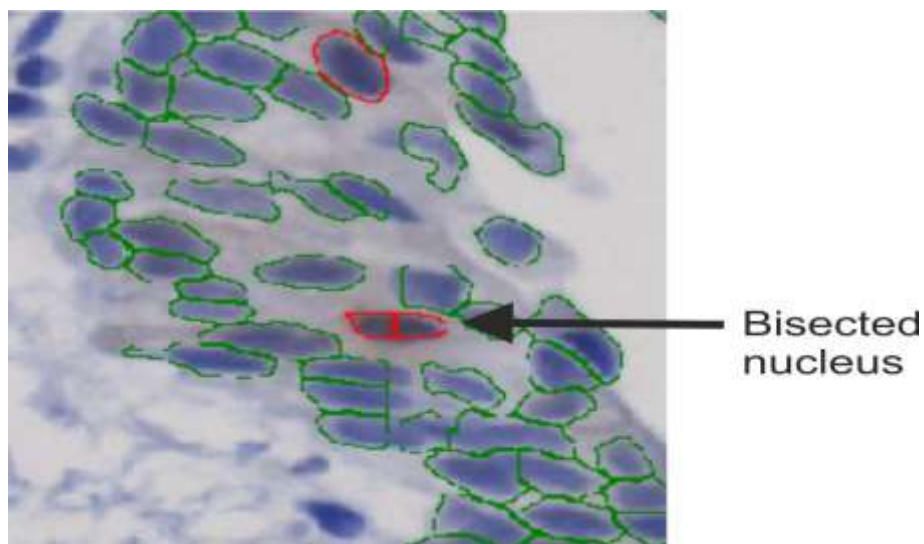
Figure 2-4: Manual correction of analysis.

Example of subdivided nuclei (arrowed), this was easily corrected using manual editing tool within HistoQuest software preventing the single nucleus being analysed as two nuclei.

4) After manual correction all nuclei samples were analysed for DAB staining intensity based on the nuclear segmentation mask function within the software.

5) Histograms and scatterplots of Haematoxylin v DAB staining for all nuclei within each sample were generated by the software using the validated automated algorithm function (**Figure 2-5**).
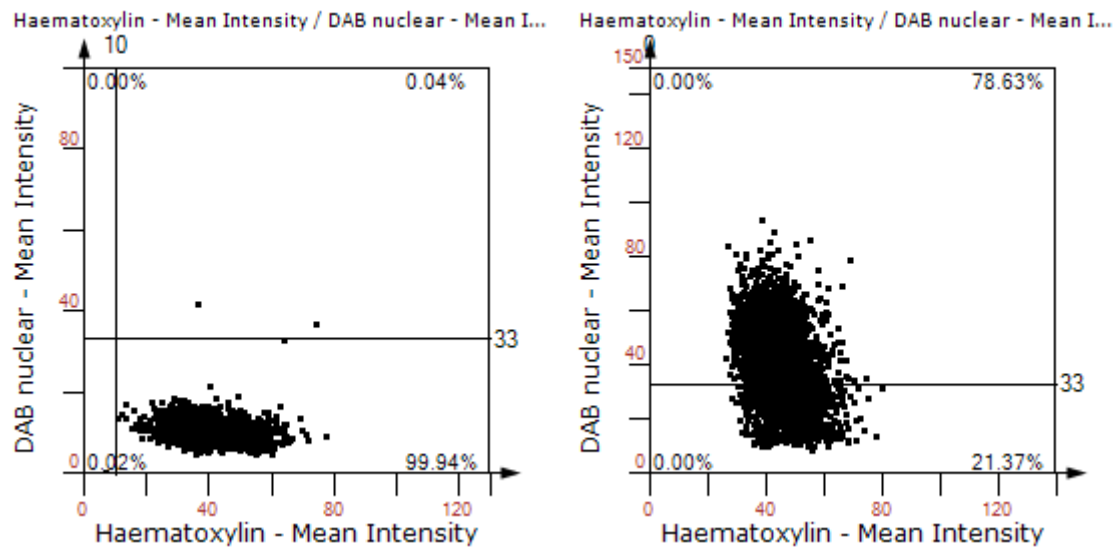
Figure 2-5: Examples of scatterplots from different bladders.

An antigen of interest, located within the nuclei in this example, was labelled using immunohistochemical techniques and visualised using DAB staining. The mean intensity of this staining varied depending on the abundancy of the antigen. Using mean haematoxylin as a control stain HistoQuest software plotted the mean haematoxylin intensity against mean DAB intensity per nuclei. The resulting scatterplots can be used to visualise all cells within a sample, homogeneity of the cells within a sample and identify aberrant results.

6) Raw data was then exported into Microsoft Excel and Instat software for statistical analysis.

2.10 Immunochemical Analysis

All steps were performed at ambient temperature unless otherwise stated.

2.10.1 Indirect immunofluorescence labelling of cultured cells

2.10.1.1 Slide preparation

NHU cells were seeded onto sterilised Polytetrafluoroethylene (PTFE) coated 12-well multispot slides (Hendley Ltd) placed in Heraeus boxes. Fifty µl drops, at a concentration of 2×10^4 cells/ml (proliferation studies) or 1×10^6 cells/ml onto 12 well glass slides during the differentiation process 24 hours prior to the application of medium containing calcium. Cells were left to attach at 37 °C for six hours after which slides were flooded with 5 ml of medium and left to grow at 37 °C for the duration of the experiment with medium changes every 72 hours. Cells were washed in PBS and fixed for 30 seconds in a 1:1 mixture of methanol acetone at various times after seeding/treatment, air-dried and then wrapped in cling film and stored at -20 °C in boxes containing silica gel.

2.10.1.2 Immunolabelling

Frozen slides were thawed and a grease pen was used to provide a barrier around individual wells to prevent spill-over of one antibody into surrounding wells. Primary antibodies were diluted in Tris buffered saline (TBS) containing 0.1 % (w/v) BSA and 0.1 % (w/v) sodium azide and 20 µl of primary antibody added to each well, except for the negative control which had 20 µl of diluent only applied.

Slides were incubated overnight at 4 °C in a humidified atmosphere. After this period, unbound antibody was removed by pipetting, again to prevent contamination between wells, followed by three five minute washes in PBS. Cells were then fixed in methanol: acetone (1:1) for 30 seconds and air dried.

The appropriate secondary antibody for the primary was incubated with the cells, including the negative control, in the dark for 30 minutes. The slides were washed three times for five minutes with PBS containing 0.25% (v/v) Tween 20. Slides were then incubated with PBS containing 0.1 µg/ml Hoechst 33258 for 5 minutes and washed twice with PBS containing 0.25% (v/v) Tween 20 and finally rinsed in H_2O and air-dried. Slides were mounted in antifade mountant (Appendix II) and sealed with nail varnish. Slides were visualised under epifluorescence illumination using an Olympus BX60.

2.10.2 Immunoperoxidase labelling

2.10.2.1 Section preparation

Tissue was embedded in paraffin wax and sectioned as described in section **2.8.1.**
Sections were dewaxed and rehydrated in xylene and ethanol as for H&E. Endogenous peroxidase activity in human tissue sections and organ cultures was blocked with 3 % hydrogen peroxide for ten minutes, this was not necessary for zinc-fixed porcine tissue. Tissue was then washed for ten minutes in running tap water. All experimental work where localisation or intensity of immunoperoxidase labelling would be compared from one sample to another or more then all labelling would be performed during one single experimental run. All experiments had a negative control (no

primary antibody but secondary), positive controls (tissue known to label positively for the antigen in question). All antibodies were optimised prior to experimental use in terms of antigen retrieval technique and dilution.
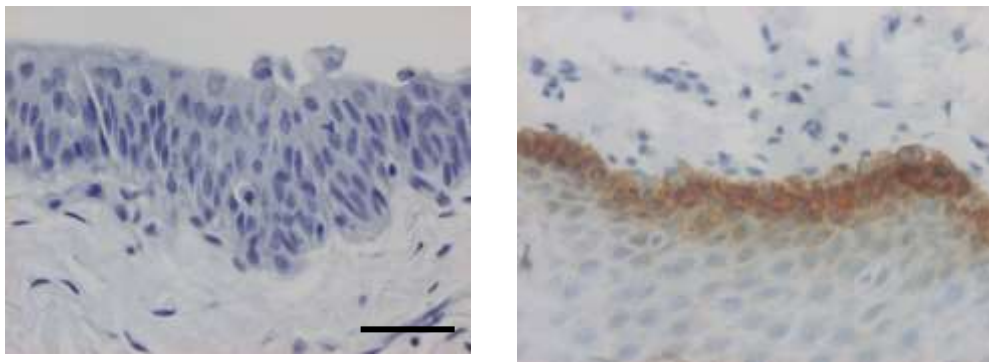
Figure 2-6: Examples of both negative and positive controls for immunohistochemistry

Image on the left was a standard negative control performed for all immuno-histochemical experiments. The right hand image was a positive control for CK14, using buccal mucosa a tissue known to express CK14, which is generally absent in healthy urothelium. The positive control ensures that the epitope of interest is labelled and that there are no false negatives.

2.10.2.2 Antigen binding

Antigen retrieval was performed using various methods, which had been optimised for each antibody. These included:

1) Microwaving sections in 10 mM citric acid pH 6.0 (Appendix II), for three minutes, after which, sections were cooled on ice

2) Incubation of slides for 10 minutes in 0.1 % (w/v) trypsin solution at 37 $^{\circ}$C in a water bath. One gram of trypsin was fully dissolved in 100mls of pre-warmed CaCl$_2$ (pH 6.0) (Appendix II).

3) Incubation of slides for 10 minutes in 0.1 % (w/v) trypsin solution at 37 $^{\circ}$C in a water bath. One gram of trypsin was fully dissolved in 100 mls of pre-warmed CaCl$_2$ (pH 6.0) (Appendix II).

4) Trypsinisation was performed, as per method 2 for 1 minute only, followed by slides being washed in distilled water and placed in citric acid buffer and microwaved for 13 minutes, as per method 1.

Slides were placed in Shandon Sequenza ® units using Shandon coverplates™ and washed in TBS. Endogenous avidin binding sites were blocked by adding 100 μl avidin (Dako Inc.) for ten minutes, washing twice in TBS, adding 100 μl of biotin (Dako Inc.) for ten minutes and performing two further TBS washes.

Non-specific antibody binding was blocked by applying 100 μl of a 1:10 (v/v) dilution of rabbit serum in TBS for five minutes. The primary antibody was diluted in TBS and added to the sections without the removal of serum. Sections were incubated in primary antibody at 4 °C overnight. Primary antibodies were removed by three washes in TBS and biotinylated rabbit anti-mouse IgG diluted in TBS added to the sections for 30 minutes at ambient. Sections were washed three times to remove unbound secondary antibody.

2.10.2.3 Antibody detection

The streptavidin-biotin-horseradish peroxidase complex (Vector Laboratories) was prepared according to the manufacturer's instructions 30 minutes prior to use and 100μl was added to each slide followed by 30 minute incubation. Unbound complex was removed by two washes in TBS and one wash in H_2O. Sigma Fast DAB (diaminobenzidine) tablets were placed in 5 ml H_2O and vortexed thoroughly to dissolve and 200 μl was applied to each section. After 15 minutes incubation, sections were washed twice in $H_2O$and placed in a staining rack. Sections were counterstained in haematoxylin for ten seconds and placed under running tap water for one minute. Sections were dehydrated by incubation for one minute in each of one bath of 70 % ethanol, three changes of absolute ethanol, and two changes of xylene before being placed in Histoclear™ (Thermo-Fisher)and immediately mounted in DPX. Initial assessments of labelled specimens were observed under brightfield conditions using an Olympus BX60 microscope, equipped with x10, x20, x40 and x60 objectives.

2.10.2.4 : ImmPRESS™ Excell Immunolabelling

The ImmPRESS™ Excel Amplified Staining Kit (Vector) amplified staining and reduced background when labelling for NGFR. The system used a polymerised reporter enzyme staining system. The protocol for labelling using ImmPRESS™ did vary from that used for biotinylated immunoperoxidase labelling detailed in **2.10.2.2** and **2.10.2.3.** Slides were dewaxed, blocked with hydrogen peroxide (3 %) and antigen retrieval performed as per **2.10.2.2.** Slides were placed in Shandon Sequenza ® units using Shandon coverplates™ and washed in TBST. 100 μL normal horse serum (2.5 %) was applied to each slide and incubated for 20 minutes at ambient temperature followed by 100 μL primary antibody (concentration determined by optimisation) left overnight at 4 °C.

Three washes with TBST was performed to remove the primary antibody followed by 100 µL of a proprietary ready-to-use amplifier antibody. This was incubated on each slide for 15 minutes at ambient temperature and removed by two TBST washes. The kit also contained ready-to-use ImmPRESS™ Excel polymer reagent of which 100 µL was applied to each slide for 30 minutes and removed with one was of TBST and a subsequent was with H_2O. DAB staining was achieved by applying 100 µL of a 1:1 combination of ImmPACT™ DAB reagents 1 & 2 to the slides for 5 minutes prior to rinsing with H_2O. Slides were then counterstained in haematoxylin, dehydrated and mounted as in section **2.10.2.3.**

2.11 Immunoblotting

2.11.1 Protein Extraction

Whole cell lysates were prepared from cells *in situ*, under non-reducing conditions using 2x SDS lysis buffer (Appendix II), which contained 0.2% 1M Dithiothreitol (DTT) and Protease Inhibitor Cocktail (PIC) at a final dilution of 1:500 (Sigma-Aldrich). Culture medium was removed from cultures which were subsequently rinsed twice with ice-cold PBS.   The volume of lysis buffer varied from $50 - 200$ µl according to the cell culture area and density due to be lysed. Once the buffer had been applied adherent cells were scraped using a sterile 25 cm cell scraper into a 1.5 ml microfuge tube on ice. Lysates were sonicated 25 Watts (W) on ice using an ultrasonic probe processor (Jencons Scientific Ltd.) for two ten second bursts with a ten second interval in between. After sonication cell lysates were incubated on ice for 30 minutes. Lysates were then micro-centrifuged (Hettich Mikro 200R – SLS) at 14 000 revolutions per minute (rpm) for 30 minutes at 4 °C and the supernatants aliquoted into 500 µL microfuge tubes and stored at -20 °C. Samples were discarded after a

 single use and not freeze/thawed.

2.11.2 Protein Quantification

Total protein concentration of each sample was measured using a variant of the Bradford colorimetric method. Cell lysates were diluted 1:12.5 with H_2O. Bovine serum albumin (BSA supplied at 2mg/ml by Thermo Fisher) was diluted in H_2O. to 1000, 750, 500, 250, 125 and 25 µg/mL to provide standards for protein concentration. Two hundred microlitres of Coomassie Plus™ (Thermo Fisher) protein assay reagent was added to 10 µl duplicates of either cell lysates or BSA standards in a 96 well plate (Corning) to produce a standard curve from which the protein concentration of the cell lysate was estimated. Absorbance was read on a Multiskan Ascent plate reader (Thermo-Scientific) at 480 and 630 nM wavelengths. The BSA samples produced a standard curve against which the protein concentration of cell lysates could be determined.

2.11.3 Preparation of protein lysates:

Using the quantification method described above the volume of lysate required to provide 20 µg of protein was taken and lithium dodecyl sulfate (LDS) sample buffer (x4) (Life Technologies) and reducing agent (x10) were added both to a final concentration of 1x. The lysate which required the largest total volume (A) did not require further dilution. The other samples to be used within a set were diluted to the volume of (A) by the addition of water. Samples were boiled for 10 minutes at 70°C.

2.11.4 SDS polyacrylamide gel electrophoresis (PAGE)

Novex® apparatus (Life Technologies) was used to perform PAGE electrophoresis. All running buffers were used at a dilution of x1 with H_2O and placed in the inner and outer chambers. Precast gels were selected based on the target protein size.

Precast 3-8% (w/v) Tris-acetate (TA) NuPAGE® gels (Life Technologies) were used to separate proteins of a molecular weight between 500 and 40 kDa with Tris-acetate running buffer. Proteins of between 200 and 14 kDa were separated using precast Bis-Tris (4-12% w/v) NuPAGE® gels (Life Technologies) with either MOPS or MES running buffers. NuPAGE® electrophoresis gels (Life Technologies) were loaded with cell lysates. Five microliters of All-blue protein standard ladder (BioRad) was loaded into one well of each gel. Antioxidant (200 µl) (Life Technologies) was added directly to the inner chamber. Empty wells were loaded with 4xLDS sample buffer of an equal volume to that of the prepared cell lysates. Electrophoresis was performed using a power pack at gel-specific settings: 200V for 45 – 65 minutes (Bis-Tris gels) and TA gels at 150v for 45-60 minutes or until the dye front and reached the bottom of the gel.

2.11.5 Protein transfer

On completion of electrophoresis, resolved proteins were blotted onto an Immobilin-FL polyvinylidene difluoride (PDVF) transfer membrane (Millipore). PDVF membranes were briefly dipped in 100 % methanol prior to being rinsed in deionised water for two minutes. The membranes, blotting pads and filer paper were soaked in transfer buffer (Appendix II). The gel was removed from the gel cassette and placed on a transfer buffer soaked piece of filter paper; the membrane was then placed on the other side of the gel, followed by another buffer-soaked piece of filter paper. This gel "sandwich" was then placed onto two transfer buffer soaked blotting pads assembled within the cathode section of an Invitrogen XCell II™ blot module.

Air bubbles were removed by rolling a Universal tube over the gel membrane sandwich, followed by two further buffer-soaked blotting pads. The anode section of the blot module was then placed to close the unit and placed into the gel tank.

Transfer buffer was placed within the inner chamber and H_2O in the outer chamber. Protein transfer was carried out using a power pack set at 30 V for 180 minutes.

Transfer was assessed by reversibly staining for protein with 5-10 ml Ponceau Red (1x) (Appendix II). Ponceau red was removed with 2-3 deionised water washes. The membrane was stored in TBS at 4^oC until labelled (Appendix II).

2.11.6 Antigen binding

All work was performed on a shaking platform at ambient temperature unless otherwise stated. To minimise non-specific binding, the membrane was blocked in 1:1 mixture of Odyssey® blocking buffer (Licor Biosciences) and TBS for one hour. Primary antibodies were diluted in a 1:1 mixture of Odyssey blocking buffer and TBS –Tween 20 (Appendix II). Once added to the membrane primary antibodies were left overnight on an orbital shaker at 4 °C. The primary antibody was removed by rinsing the membrane in TBS-tween 20 four times for five minutes. Anti-mouse IgG (alexa680) or anti-rabbit RDye 1800 (Odyssey® LI-COR Biosciences) secondary antibody was diluted in blocking solution and TBS –Tween 20, added to the membrane and incubated on an orbital shaker, for one hour at ambient temperature and covered. Secondary antibody was washed away with four washes of TBS-Tween 20 for five minutes duration. A secondary only control was included in order to assess the level of background signal and a lysate, known to contain the primary antibody target, was included as a positive control.

Immunolabelled proteins were visualised by enhanced chemiluminescence (ECL). The membrane was placed onto the scanning surface of an Odyssey Infrared Imager 9120 or into an Odyssey SA scanner (LI-COR Biosciences). A solid-state diode excited

infrared fluorochromes at 680 nM and 780nM and emissions detected with a silicon avalanche photodiode detector. Images were correctly orientated, excess cropped and densitometry analysis performed using IS Lite software (LI-COR Biosciences). Images were exported as JPEGS.

2.11.7 Stripping of PDVF membrane

If required the PDVF membrane was stripped of prior labelling with a Western blot recycling kit (Autogen Bioclear). Stripper solution was diluted 1:10 with H_2O. Eight millilitres of solution was added to the membrane and placed on a shaking platform for 15 – 30 minutes. After this time the membrane was rinsed with TBS for 2 x 5 minutes and the membrane rescanned to ensure complete removal of the previous antibodies.

2.12 Molecular biology

For all RNA work, solutions and 1.5 ml Eppendorf tubes were incubated overnight with 0.1% (v/v) diethyl pyrocarbonate (DEPC) at ambient temperature to inhibit RNAase activity. DEPC was destroyed by autoclaving prior to use. RNAase-free "Rainin" filter tips (Anachem) and RNAase-free microfuge tubes (Ambion®) were also used. All work surfaces and equipment were wiped down with RNAase ZAP ®wipes (Ambion®).

2.12.1 RNA extraction

All RNA extraction work, apart from the final pellet drying phase, was performed in a chemical safety cabinet. Urothelial cells, contained within each well of a 6-well plate, were solubilised *in situ* by the addition of 1 mL TRIzol®reagent (Ambion®). If urothelial cells were cultured in Greiner ThinCert™ (Greiner Bio-One) inserts then 2-3 samples, exposed to the same experimental conditions, were serially solubilised using a total of 1 ml TRIzol®. The cell lysate was collected using sterile plastic scrapers (Greiner Bio-

One) into 1.5 ml RNAase- free microfuge tubes (Ambion®) vortexed and stored at −80°C. Lysates were thawed on ice and 0.2 ml chloroform per ml of TRIzol® reagent was added, the tubes were shaken vigorously for 15 seconds and placed on ice for five minutes. Lysates were centrifuged at 11 500 rpm for 15 minutes at 4 °C in Hettich Mikro 200R refrigerated centrifuge (SLS). The upper aqueous phase, containing the RNA, was carefully transferred to a new RNAase free microfuge tube. The RNA was precipitated by adding 0.5 ml of isopropanol, mixing well and incubating at ambient temperature for ten minutes. The RNA pellet was then collected by centrifugation at 11 500 rpm for twenty minutes at 4 °C.

The supernatant was removed gently and the pellet was washed in 75 % (v/v) ethanol, vortexed and centrifuged at 9000 rpm for 5 minutes at 4 °C. The ethanol wash and centrifugation was repeated once. The pellet was dried and subsequently dissolved in 30 µL DEPC deionised water.

2.12.2 DNA-ase treatment

DNA contaminating the newly harvested RNA was digested using DNA Free™ kit (Ambion®). RNA samples were transferred into 500 µL RNase free microfuge tubes along with DNase (10x) 1 buffer (3.3 µL/ 30 µL) and 1 µL DNase enzyme (2 U/ µL). The solution was mixed by pipetting and placed in a heat block at 37 °C for 30 minutes. The DNase enzyme was inactivated by the addition of 3.3 µL of 'DNase Inactivation Reagent' to the microfuge tube. Vortexing every 30 seconds the resulting mixture was incubated in total for two minutes at ambient temperature. Centrifugation at ambient temperature followed at 10 000 rpm for 90 seconds. This permitted the DNA-free RNA, in the form of the supernatant, to be removed. The purified RNA was placed, along with 1 µL (40 U/ µL) RNAse-OUT ™ (Ambion®) into a new 500 µL RNase free microfuge tube and stored at −80 °C.

2.12.3 Quantification of nucleic acids

RNA was quantified by UV spectrophotometry (NanoDrop ™ Thermo Scientific) using the knowledge that absorbance of an aqueous solution containing 40 µg/ ml single-stranded RNA at 260 nm is 1.0 and pure preparation of RNA have an OD_{260}/OD_{280} ratio of 2.0.

2.12.4 cDNA synthesis using Random Hexamers

Complementary DNA (cDNA) was synthesised using second strand synthesis by reverse transcriptase and random hexamers. Firstly 1 µg purified RNA was combined with 1 µL random hexamers and the total volume made up to 12 µL with nuclease –free water. This mixture was then incubated, using a heat block set to 65 °C for ten minutes; this promoted the hexamers to anneal to the RNA. The sample was then placed on ice. Using the Superscript Synthesis Kit (Life Techologies) the following reagents were combined to form a "master mix", which would be then added to each sample: First Strand buffer (x5) 4 µL, 0.1 M DTT 2 µL and 1 Ml dNTP mix. Once combined the complete solution would be incubated at 25 °C for 2 minutes.

To ensure that DNA contamination would not affect the results two of each sample were prepared. One containing 1 µL Superscript II reverse transcriptase (RT+) and the other 1 µL nuclease –free water (RT-). Following the formation of both RT+ and RT – samples all underwent a further incubation at 25 °C but for 10 minutes. This was followed by a 50 minute reverse transcription process at 42 °C. A final incubation at 70 °C for 15 minutes ensured that the transcriptase was inactivated. Samples of cDNA were then ready for use.

2.12.5 Reverse transcriptase polymerase chain reaction (RT-PCR)

PCR was performed in a T100 thermal cycler (BioRad) using the GoTaq ®G2 polymerase reagent kit (Promega). PCR reactions were performed with a total volume of 20 μL / sample using the manufacturers recommended recipe (**Table 2-10).**

PCR reaction mixes were heated to 95 °C for 5 minutes in order to denature the DNA. This was followed by a further 30 seconds at 95 °C, 30 seconds of annealing at 50 – 65°C and an extension period of 1 minute/kb DNA at 72 °C. This was repeated to give a total of 25 – 35 cycles. The number of cycles and annealing temperature was determined during optimisation for each primer set. A final extension phase at 72 °C for 10 minutes completed the reaction that was then cooled and stored at 4 °C.

Table 2-10: Constituent reagents for PCR reaction

8.5 μL nuclease-free water	Promega	19 μL
4 μL GoTaq buffer	Promega	
0.4 μL dNTPs	Life Technologies	
2 μL $MgCl_2$	Promega	
2 μL Forward Primer (10mM)	MWG Eurofins	
2 μL Reverse Primer (10 mM)	MWG Eurofins	
0.1 μL GoTaq polymerase	Promega	
1 μL cDNA OR 1 μL Genomic DNA OR 1 μL nuclease-free water		

2.12.6 Gel electrophoresis

Isolated DNA was visualised under UV light after separation by gel electrophoresis. Electrophoresis grade agarose was boiled in 1 x tri-borate EDTA (TBE buffer Appendix II) and cooled to 50°C before adding 1/10000 (v/v) SYBR-Safe® (Life Technologies) which fluoresces under UV light when it combines with dsDNA. Gels were cast and allowed to set with combs in-situ to form wells. Hyperladder IV or other appropriate marker for the size of the product to be obtained (New England Biolabs®) were electrophoresed on gel submerged in 1 x TBE at 5V/cm, for the required amount of time to resolve the bands. Gel images were captured digitally using a Gene Genius Gel Imaging System (Syngene) with GeneSnap software.

2.12.7 Primer Design and Optimisation

Primers were designed against target regions using the National Center for Biotechnology Information (NCBI) primer-BLAST tool http://www.ncbi.nlm.nih.gov/tools/primer-blast/. Primers of 20 base pairs in length were designed with an optimal melting temperature of 60 °C and G: C ratio of 50 %. Primers were subjected to gradient PCR in the presence of template human genomic DNA (Roche, Sigma). Smaller primer sizes were electrophoresed through a higher percentage agarose gel (3-4 %) compared to larger products. The number of cycles was set according to abundancy of product and in order to differentiate potential differences between two or more samples.

Table 2-11: PCR primers

Target	NCBI Accession No.	Sequence	Product size (bp)	Optimum annealing temperature (cycles)
28S	NR_003287	F:AGCCGACTTAGAACTGGTGC R:GGCAGAAATCACATCGCGTC	102	62.1 ^{o}C 28 cycles
EHMT1 G9a/ GLP	NM_024757	F:GTGTGAAAACCGAGCTGCTG R:CAGCAGAGAAACAGGCAGGT	170	65°C 30 cycles
HIF-1α	NM_181054	F: TTTCCTCAGTCGACACAGCC R: GCAGGGTCAGCACTACTTCG	686	64° C 24 cycles
LDHA	NM_005566.3 NM00116541-4.1	F: TCTTGACCTACGTGGCTTGG R:CCAGCCTTTCCCCCATTAGG	110	62.1 ^{o}C 26 cycles
VEGF	NM_0010253 70 NM_003376.3	F: CCATCCAATCGAGACCCTGG R:TATGTGCTGGCCTTGGTGAG	794	28 cycles
ZO-1*	NM_003257 NM_175610	F: CTGATCATTCCAGGCACTC R: GAGCTACGTTGGTCAGTTC	1092	55°C 30 cycles
ZO-1α+*	NM_003257	F: CTCTCAACAGAAAGCAGAAG R: CTCTTAGCATTATGTGAGCTG	209	62.1^{o}C, 24 cycles

F = forward primer

R = reverse primer

* Supplied by Sigma not MWG Eurofins

Regenerative medicine applications in paediatric urology: barriers and solutions

2.13 Porcine Native Tissue Samples

:

2.13.1 Sample collection

Whole porcine bladders were obtained from a local abattoir (Traves & Son Ltd) during the slaughter process. Bladders were removed from the animal at the time of death and placed into an autoclaved 1 L tub containing sterile transport medium (Southgate et al., 1994) (Hank's balanced salt solution (HBSS, Gibco®), containing 20 kallikrein-inhibiting units/ml of Aprotonin (Trasylol®, Nordic Pharma), 10 mM HEPES pH 7.6 (Gibco®), 1 µg/ml Amphotericin B (Fungizone®Gibco®), 100 U/ml penicillin and 100 µg/ml streptomycin (Penicillin-Streptomycin, Gibco®). Bladder tissues were returned to the laboratory and processed immediately.

Penile and peri-urethral tissues were collected from large white hybrid male pigs undergoing planned Schedule 1 killing and obtained from Spen Farm, University of Leeds. Peri-urethral and penile tissues were placed immediately into 10 % formalin in PBS for 72 hours and then transferred to 70 % EtOH.

2.13.2 Bladder decellularisation

This process has been developed by the Jack Birch Unit in York and patented (WO2007110634A2) and has been described by Bolland *et al* (Bolland and Southgate, 2008). All work was carried out aseptically in a class II safety cabinet unless otherwise

stated. Solutions (see Appendix II) and equipment were prepared and autoclaved at 121 °C (1 bar) for 20 minutes. SDS (Pierce), BSA (Pierce), DNase, RNase and Trasylol® (Nordic Pharma) were heat sensitive and therefore were added to the appropriate buffer on the day of use after filter sterilisation.

Once delivered to the laboratory the bladder was removed from the transport medium and placed into a petri dish. Wash buffer was used to remove residual transport medium. Using sterile scissors and forceps excess fat and connective tissue was removed. The urethra was shortened to approximately 3 cm when required and the ureters trimmed to 0.5 cm length extra-vesically.

In a wide-mouthed sterile container > 1 L the intact bladder was filled with hypotonic buffer (Appendix II) using a sterile funnel inserted into the urethra. During this process the bladder is held upright using Spencer-Wells forceps. Once completely full, avoiding air bubbles, two Spencer-Wells forceps were used to cross-clamp across the bladder neck. The external surface of the bladder was also immersed in hypotonic buffer and left for 24 hours at 4 °C.

Removal of the buffer was performed by removing the forceps from the neck of the bladder and placing one of them at the base to tip the bladder upside-down and allow the buffer to drain from the bladder neck and urethral stump. Waste buffer was collected into a beaker and then discarded down a standard sink and flushed with tap water.

The bladder was filled again, as per the hypotonic buffer, but with hypotonic buffer containing 0.1 % SDS and placed on a shaker for 24 hours at ambient temperature.

Once again this was removed and discarded down the laboratory sink and replaced with wash buffer (without EDTA) for 24 hours at 37 °C on an orbital shaker. Once the wash buffer has been removed in the standard way nuclease solution (Appendix II) was placed within the bladders for 24 hours at 37 °C but with gentle agitation only. The nuclease solution was then replaced by wash buffer and EDTA (Appendix II) for 24 hours at 37 °C without agitation. Upon removal the bladders were incubated with hypertonic buffer (Appendix II) for a further 24 hours followed by a final wash stage with wash buffer and EDTA at 37 °C for 24 hours.

From this point forwards the bladder was treated as a sterile entity and was incubated with 0.1 % (v/v) peracetic acid solution (39 %) in PBS (pH 7.2) for three hours. After sterilisation the bladder was dissected out into a flattened sheet with removal of the bladder neck. The sheet was washed with sterile PBS for three, one hour intervals, followed by a fourth 24 hour PBS wash. The material was stored in sterile containers at 4 °C until batch tested to confirm successful decellularisation.

2.13.3 Quality control of decellularisation process

To confirm decellularisation and removal of DNA standard histology and immunocytochemistry techniques were employed. The sections of PABM were aseptically sub-divided into four rectangles with 0.5 cm x 0.5 cm sections removed at each corner (*Figure 2-7*),. This provided nine identifiable samples to fix and embed in paraffin wax ready to section (see **section 2.8**)

The 5 μm explant sections were placed on 'Superfrost Plus' slides (VWR) and analysed using immunohistology by H&E staining (section **2.8.2**) and immunocytochemistry using Hoechst 33258 staining (slides was dewaxed and then protocol followed as per section **2.10.1**), to exclude the presence of any cellular or DNA. Once decellularisation had confirmed the PABM was ready to be implanted. An example of H&E and Hoechst 33258 stained PABM section compared to a cellularised pig bladder is shown in ***Figure 2-8***).
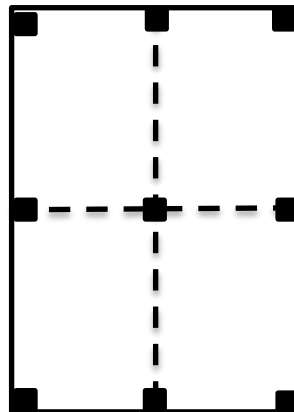
Figure 2-7

Diagram of PABM sections for quality control

PABM was cut into four with 0.5 cm^2 sections taken from each corner to confirm decellularisation was complete. Each section was numbered for traceability.

Regenerative medicine applications in paediatric urology: barriers and solutions
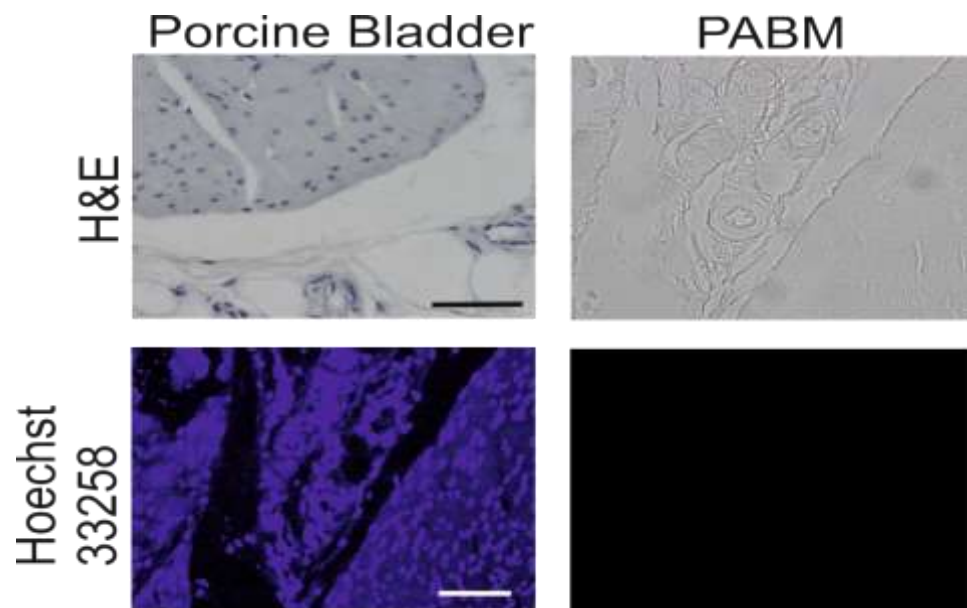
Figure 2-8: Assessment of complete decellularisation of PABM by H&E and Hoechst 33258 staining: Native porcine bladder tissue demonstrated blue nuclei and DNA upon both H&E and Hoechst 33258 staining. This was absent in the decellularised porcine acellular bladder matrix material.

2.13.4 Experimental animals

2.13.4.1 Animal husbandry

Large White Hybrid (LWH) male pigs of approximately 15 – 20 kg weight were purchased from a local farm and transported to an animal surgical facility for at least seven days quarantine. Numbered ear tags were used to aid individual identification.

The animals were inspected for signs of disease by a vet and the facility's technical staff and they were housed together in pens, with appropriate clean bedding. Assessment of the animals was performed at least twice a day. The animals were

weighed every two weeks and feeding regime altered accordingly. Ready-made food was available up to twice a day, with the amount varying according to weight gain and behaviour. Access to water was unlimited.

2.13.5 Surgical procedure

2.13.5.1 Surgical instruments

Contents of surgical instrument packs were discussed with the University vet, prior to the first procedures. The standard contents are shown in **Table 2-12.** All packs once complete were autoclaved at 121°C for 20 minutes. After use the instruments were cleaned, checked, repacked and re-autoclaved ready for re-use.

Table 2-12 Standard contents of surgical pack

Instruments			Quantity
Clips	Small	Mosquito straight/ curved	2
	Large	Straight	2
Needle Holder	Small	Crile Wood	1
Forceps	Toothed	DeBakey /Gillies	2
Scissors	Straight/Small	Sharp/Mayo	1
	Straight/Curved/Large	Mayo	1
Retractors	Langenbeck		2

2.13.5.2 General anaesthesia

Food but not water was withheld for 18 hours prior to surgery. Initial sedation was performed using intramuscular Hypnovel (0.3 mg/kg) (Roche) and Stresnil (1.2 mg/kg) (Elanco). The animal was left for 20-30 minutes in a quiet and calm environment before transportation to the anaesthetic room on a trolley. Induction of anaesthesia was achieved by utilising a snout mask containing an isoflurane-soaked. Isoflurane 2.5 % in oxygen was then used for maintenance of anaesthesia and delivered via the snout mask attached to an anaesthetic machine. The electrocardiogram, pulse, blood pressure and oxygen saturation of the animal was continuously monitored during the surgical procedure. Eyes were protected using Lacri-lube® (Allergan-Actavis).

An over-the-needle intravenous cannula (22 G) was introduced into an ear vein and secured with Micropore ™ (3M). The animal was given AmoxyPen LA (MSD Animal Health) (15 mg/kg) and Rimadyl (Zoetis) (2 mg/kg), a non-steroidal anti-inflammatory agent

2.13.5.3 Positioning for surgery

The anaesthetised animal was place supine on the operating table, which had been he broken longitudinally to prevent inadvertent rolling. Skin on the lower abdomen was shaved. A plate electrode (Conmed) was placed onto shaved flank skin and attached to the diathermy machine. The animal's skin was prepared with Chlorhexidine solution (Vetasept-Animal Care). The animal was draped using 307 x 254cm StreriDrapes with incise pouch (3M). The monopolar diathermy pen (Ambu) was attached to the diathermy machine.

2.13.5.4 Asepsis:

Surgeons scrubbed in an adjacent scrub room using Chlorhexidine wash (Hibiscrub® Molnlycke). Sterile, disposable surgical gowns (3M) were worn along with supersensitive surgical gloves (Biogel®Molnlycke), caps (Barrier® Molnlycke) and masks (LiteOne® Halyard Health).

2.13.5.5 Surgical Basics:

A 5cm midline incision was made, approximately 5cm from the preputial sac, caudally. using a size 15 disposable scalpel (Swann Morton). The peri-urethral tissues were opened using blunt dissection. Bleeding was stopped, when necessary using monopolar diathermy.

2.13.5.6 Post-operative care:

At skin closure 3ml of 0.5 % Marcaine local anaesthetic was infiltrated locally. In addition Vetergesic (0.3 mg), an opioid analgesic was administered to provide post-operative pain relief. The animal was transferred from the operating table to trolley and then to a pen with fresh bedding and sawdust. The animal was allowed to recover in a quiet environment in isolation until up on all four limbs and drinking water. Once this was achieved the animal was placed in a pen with another animal and food made available.

2.13.6 Schedule 1

The process of euthanasia began with sedation of the animal using Hypnovel and Stresnil (**section 2.13.5.2**). An ear vein was cannulated and barbiturate was administered intravenously to overdose.

3. Potential role of hypoxia in end-stage bladder disease

3.1. Background

The air that is inhaled by most animals and sea-dwelling mammals is composed of 20-21 % (v/v) oxygen, however this is not a true reflection of the oxygen saturation experienced *in vivo*. The most common measurement of oxygen levels within the human body used in medicine is percentage oxygen saturation; that is the fraction of oxygenated haemoglobin relative to total haemoglobin expressed as a percentage. Arterial blood carries 12 % oxygen into capillary beds in order to perfuse organs and tissues with varying oxygen demand. Therefore the actual percentage of oxygen saturation within the body will vary significantly depending on location and function from the brain (0.5 %-7 %) (Panchision, 2009), liver (4-7.5 %) (Shiyan et al., 2014, Jung et al., 2012) and kidneys (1.33 – 9.6 %) (Guelen et al., 2008, Muller and Strutz, 1995).

The normal urinary bladder experiences variation in perfusion and hence oxygenation throughout the filling and voiding of the micturition cycle. It is thought that compression of intramural vasculature, during filling, results in intermittent hypoxia. Marsumoto *et al* (Matsumoto et al., 2003) demonstrated this cyclical pattern using a rabbit model and were also able to show that bladder muscle and mucosa maintained a percentage oxygen saturation of at least 3.35 % oxygen. However the literature with

regard to normal oxygen levels within the bladder is limited. In a porcine model of the effects of hypoxia on the bladder the authors allude to this lack of consensus

(Greenland et al., 2000) and report their results to concur with the 2.5-5.5 % oxygen quoted in the literature for smooth muscle as a whole (Sheridan et al., 1990).

Hypoxia-inducible factors have been utilised as markers of hypoxic pathway activation in both benign and malignant human disease; including bladder outlet obstruction (Koritsiadis et al., 2008). Stephany *et al* have recently published evidence that hypoxia-dependent pathways were upregulated in a murine model of chronic, intermittent bladder over-distension (Stephany et al., 2013). Quantitative RT-PCR data from this work reported a 2.6 fold increase in HIF-1α transcript and of markers downstream relating to fibrosis and inflammation: arylhydrocarbon receptor nuclear translocator 2 (ARNT2); connective tissue growth factor (CTGF); glutathione peroxidase-1 (GPX1); hemoxygenase 1 (HMOX1); collagen 1 alpha 1 and interleukin-6 (IL-6). However the longest time-point of the study was only 5 days, with once daily bladder distension for 90 minutes; this would not have been a sound physiological model and may have been a reflection of an acute phase response.

Greenland (Greenland et al., 2000), using a porcine model, maintained partial bladder outlet obstruction for a total of 12 weeks. The results of this longer study suggested that chronic bladder outlet obstruction led to the detrusor experiencing both a reduction in blood flow and increased hypoxia. The authors concluded that these physiological changes may lead to the "functional and structural" changes characteristic of obstructed bladders.

End-stage bladder disease is frequently associated with an obstructed system and results in a small, fibrotic bladder of limited capacity with an increased risk of upper urinary tract damage (Rasouly and Lu, 2013). In Chapter 1 the potential components of the pathological pathway were discussed in detail, along with the candidate role of

hypoxia as a common contributing factor. Cell culture systems generally utilise atmospheric conditions of 19-21 % oxygen supplemented with carbon dioxide (CO_2) gas (to control pH via carbonate buffer within the culture medium). In addition the culture system maintains a controlled saturated humidity, (95 %) and temperature. Published work in the 1970s began to question conventional culture techniques and reported improved plating efficiencies and lifespan of cells grown in lower oxygen tensions (Richter et al., 1972, Packer and Fuehr, 1977).

Richter reported that neoplastic cells also grew better in low oxygen tensions (Richter et al., 1972) and others have established similar improvements using commonly used cancer cell lines such as K562 (Danet et al., 2001), MCF7 and A549 (Simiantonaki et al., 2008). This has clinical relevance, as human solid tumours can become poorly perfused, particularly in the central core, which is hypoxic and contains necrotic cells. Such changes within the tumour microenvironment activate hypoxia-related pathways and promote angiogenesis (Kondo et al., 2008), metabolic adaptation (Kondo et al., 2008), cell proliferation and survival (Koong et al., 2000). As a consequence there is promotion of tumour growth, invasion and metastasis. This hypoxic tumour phenotype is also important in terms of chemo- and radio-resistance and therefore research into tumour biology and therapeutics frequently use *in vitro* models of hypoxia.

Various methods for recreating hypoxia exist; including the use of incubators to create a hypoxic environment, use of chemical hypoxic mimetics (e.g. deferroxamine

mesylate, DFO) (Chen et al., 2010), 3-D tissue constructs (Tausendschon et al., 2015) and more sophisticated proprietary integrated incubator/manipulation systems. The purpose of any *in vitro* model is to mimic the particular conditions found *in vivo*. Knowledge of normal physiological parameters is therefore required in order to establish an appropriate target percentage oxygen saturation or physioxia (Chen et al., 2010, Erez et al., 2003) and in some systems is poorly understood. These latter issues surrounding the normal physiological oxygen tensions are particularly pertinent to the bladder, which as an organ has varying perfusion and oxygen tensions depending on where in the filling and voiding cycle a measurement is taken.

3.2. Aims

- To test the hypothesis that hypoxia plays a role in end-stage bladder disease in children using the presence of the hypoxia-related marker HIF-1α by Immunohistochemical analysis of diseased bladders.

- To evaluate the acute and potentially heritable effect of hypoxia on human urothelium using an *in vitro* approach evaluating both markers of proliferation, differentiation and barrier function.

3.3. Experimental Approach

3.3.1. To test the hypothesis that hypoxia plays a role in end-stage bladder disease in children.

As introduced in this chapter, hypoxia has been associated with both malignancy and outlet obstruction in adult human bladder disease. Bladder samples from patients with urothelial carcinoma and bladder outlet obstruction were utilised as controls (list and description of all samples provided in *Tables 2.6 – 2.8,* (Chapter 2). Immunohisto-chemical studies were performed to seek objective evidence for the activation of hypoxiarelated pathways in relation to the status of the urothelial compartment.

Four samples taken from native post-enterocytoplasty bladders (at the time of surveillance cystoscopy for malignancy) were included in the HIF-1α dataset. These samples enabled subjective comparison to be made between bladders that had been augmented and those that had not. Urodynamic studies and clinical notes, where available, were reviewed to assess whether the bladder and upper tracts were under abnormally high pressures (Neveus et al., 2006).

Primary antibodies were selected to proteins considered to be hallmarks of urothelial phenotype and function, including squamous and proliferative phenotypes (CK14 and Ki67, respectively). Labelling for HIF1α was performed on all samples in a single run;

should hypoxia-related pathways be active then a nuclear localisation would be expected (as discussed in Chapter 1).

To permit image analysis, slides of HIF1α labelled sections were scanned on a Zeiss AxioScan.Z1 slide scanner**.** HistoQuest (TissueGnostics) image analysis software was used to determine the intensity of nuclear DAB staining for each specimen using the method described in section **2.9.2**. This raw data enabled both descriptive and non-parametric statistical analysis to be performed. A comparison of nuclear DAB staining in the urothelium of end-stage bladder disease versus control specimens was performed by applying an unpaired t-test with Welch correction using a commercial software package (Instat™ V3).

Table 3-1 : Origin and pathology of samples used including unique identification number used in the laboratory

Sample No.	Sample Type	Bladder Pressure	Sample No.	Sample Type	Bladder Pressure
Y789b	Bladder – UC	Not known	Y777	Neuropathic bladder (paed)	Not known
Y836B	Bladder – VUR (paed)	Not known	Y969	Neuropathic bladder (paed)	Not known
Y952	Ureter (paed)	Not known	Y1000	Neuropathic bladder (paed)	High
Y1186	Bladder - TURP (adult)	Clinically BOO	Y1025 b	Neuropathic bladder (paed)	Low
Y1216	Ureter (adult)	Not known	Y1042	Neuropathic bladder (paed)	High
Y1278B	Ureter (adult)	Not known	Y1079	Neuropathic bladder (paed)	High
Y1272B	Bladder - VUR (paed)	Not known	Y1103	Neuropathic bladder (paed)	High
Y1299a	Ureter (adult)	Not known	Y1107	Non- neuro neuropathic	Borderline
Y1303	Bladder VUJO (paed)	Not known	Y1122	Neuropathic bladder(paed)	High
Y1328	Bladder (paed)	Not known	Y1173	Neuropathic bladder(paed)	High
			Y1180	Neuropathic bladder(paed)	High
E1	Post-augment (adult)	Detrusor instability	Y1427	Neuropathic bladder(paed)	Borderline
E2	Post-augment (adult)	Detrusor instability	Y1462	Neuropathic bladder(paed)	Low
E4	Post-augment (adult)	Not known	Y1535	Neuropathic bladder(paed)	Not known
E8	Post-augment (adult)	Not known	Y1585	Neuropathic bladder(paed)	Not known

3.3.2. To evaluate the acute and potentially heritable effect of hypoxia on human urothelium using an *in vitro* approach.

3.3.2.1 Impact on proliferation

The direct effects of hypoxia were investigated on the proliferation potential of NHU cell lines established from three independent donors and maintained in parallel normoxic (21 % O_2) or hypoxic (2 % O_2) conditions. Other than for medium changes, microscopy and sub-culture the cultures remained in normoxic or hypoxic conditions throughout the experiment.

Biomass assays that rely upon metabolic activity to provide a proxy for population size are affected by hypoxic conditions and were therefore not a suitable method of evaluating population growth. Therefore culture health was assessed using serial phase contrast microscopy images throughout culture and cell counts were taken at sub-culture to evaluate total cell number. Every well in a six-well plate was assessed to provide six technical replicates.

At P3 sub-culture, some cultures that had previously been exposed to hypoxia were transferred to normoxic conditions for two sub-cultures; this was to assess for heritable changes in proliferation (see flow scheme A); these cultures were described as "pre-exposed".
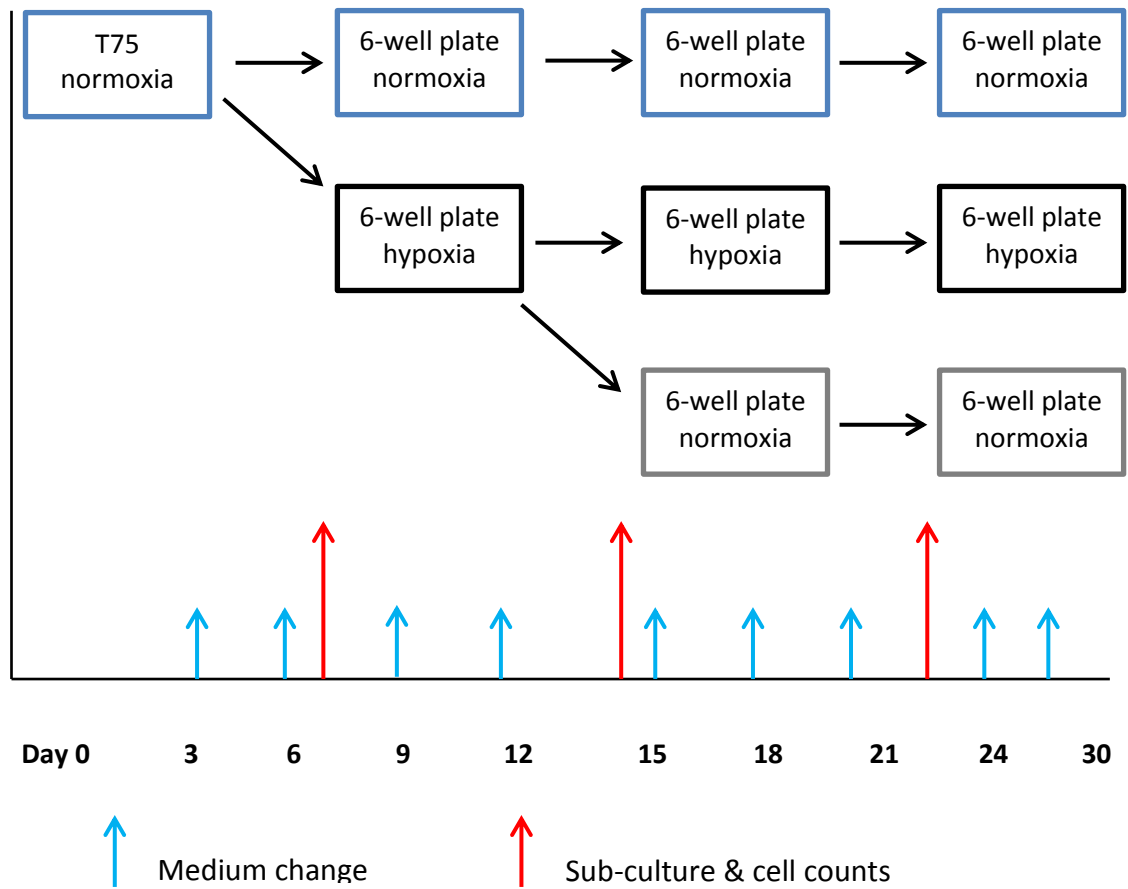
Figure 3-1: Flow-scheme A

Experimental plan for proliferation studies providing details of time scales for hypoxia (black boxes) /normoxia (blue boxes) and pre-exposed (grey boxes). Medium changes (blue arrows) and subculture time points and cell counts (red arrows) are also shown.

3.3.2.2 Impact on differentiation

To evaluate the direct effects of hypoxia on the capacity of cultures to differentiate and form a tight barrier, TEER was measured. For four biological replicates (independent cell lines), each treatment condition had 3 - 5 technical replicates, with a total of 16 measurements.

In order to assess for heritable changes in barrier formation, half of the cultures exposed to hypoxic conditions for one subculture were subsequently transferred to a normoxic growth environment. The biomimetic differentiation protocol was commenced a total of 17 days after removal from the hypoxic environment (see flow scheme B); this group was labelled "pre-exposed." In one cell line, once stable barriers had been recorded for > 48 h scratch wounding was performed in three technical replicates to assess for barrier recovery in normoxia, hypoxia and pre-exposed to hypoxia conditions.

Protein lysates and RNA were harvested from the cell culture inserts for each condition for further analysis of transcript and protein expression. In addition parallel cultures on multiwall glass slides were removed from culture medium and fixed using methanol:acetone (Appendix II). Immunocytochemistry was performed to assess markers of differentiation and barrier formation.
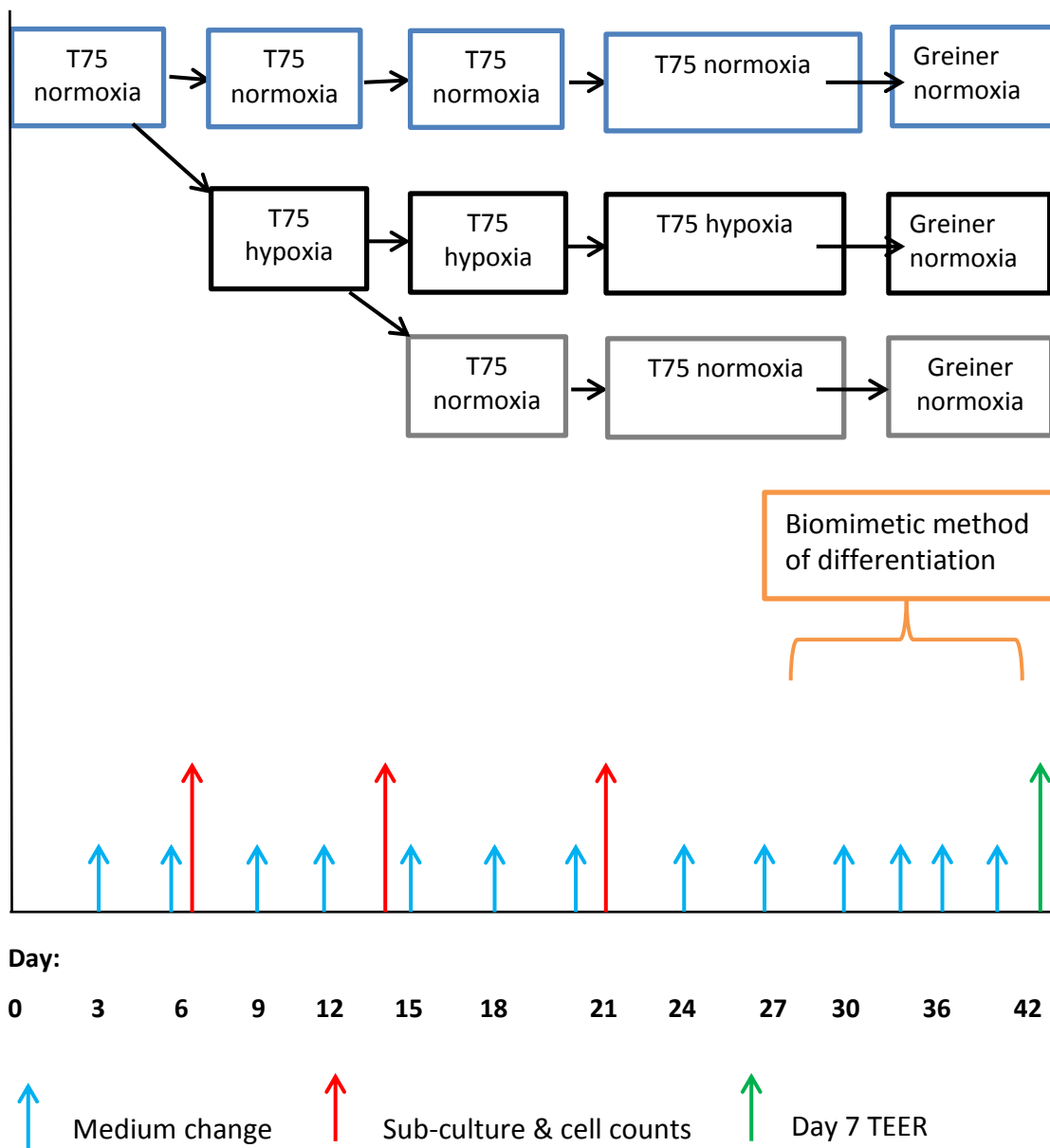
Figure 3-2: Flow-scheme B.

*Experimental plan for differentiation studies providing details of time scales for hypoxia (black squares)/normoxia (blue boxes) and pre-exposed (grey boxes). T75 = 75 cm^2 treated cell culture flasks. Greiner = Thin-Cert™ (pore-size 0.4 µm/ surface area 3.36 cm^2) cell culture inserts (Greiner Bio-One) utilised for barrier studies. Medium changes (blue arrows), subculture time points and cell counts (red arrows) and final TEER reading/scratch wounding (green arrow) are indicated and occurred between days 42 - 45. The orange box refers to the biomimetic method of urothelial differentiation (**Section 2.6**)*

3.3.2.3 Characterisation of organ cultures of urinary tract tissue acutely and pre-exposed to hypoxia.

Three ureteric tissue donor samples were utilised. All were maintained in submerged organ culture conditions in six-well plates, as set out in **section 2.7**. Maintenance in normoxic, hypoxic or pre-exposed conditions from day 6 on flow scheme B was performed. After 21 days (pre-exposed organ cultures had been in normoxic conditions for 14 days at this timepoint) the samples of tissue were removed from culture and fixed in 10% formalin and processed into paraffin wax for immunohistology.

3.4   Results

Immunolabelling for evidence of hypoxia

Nuclear labelling of HIF-1α in neuropathic bladder samples, particularly those from high pressure systems, appeared to be more prominent than both tissue and age-similar controls (***Fig 3.3***). There was also a subjective increase in HIF-1α within the nuclei of a benign prostatic hypertrophy sample (Y1186).

Analysis of nuclear HIF-1α labelling within the urothelium involved the identification of all nuclei within the urothelium of labelled samples (***Table 3.2***). The mean number of nuclei analysed per sample was as follows: control bladders n = 1906.56, neuropathic bladders n = 1471.21, postenterocystoplasty native bladders n = 723.25.

Analysis of nuclear labelling provided a semi-quantitative assessment of HIF-1α protein expression. This indicated that the median intensity and interquartile ranges of HIF-1α nuclear labelling in the 15 neuropathic bladder samples (overall median = 60.21, IQR = 42.37 – 95.05) was greater than all control samples (overall median = 26.04, IQR = 11.66 – 33.98) and the four post-enterocystoplasty specimens (overall median 33.42 IQR=.26.08 – 37.00), (***Fig.3.4***).

Statistical analysis comparing the mean nuclear label intensity in normal and neuropathic samples was performed using the Welch- corrected t-test (***Fig. 3.5***). This indicated an extremely significant difference between groups (*p value <0.0001*).
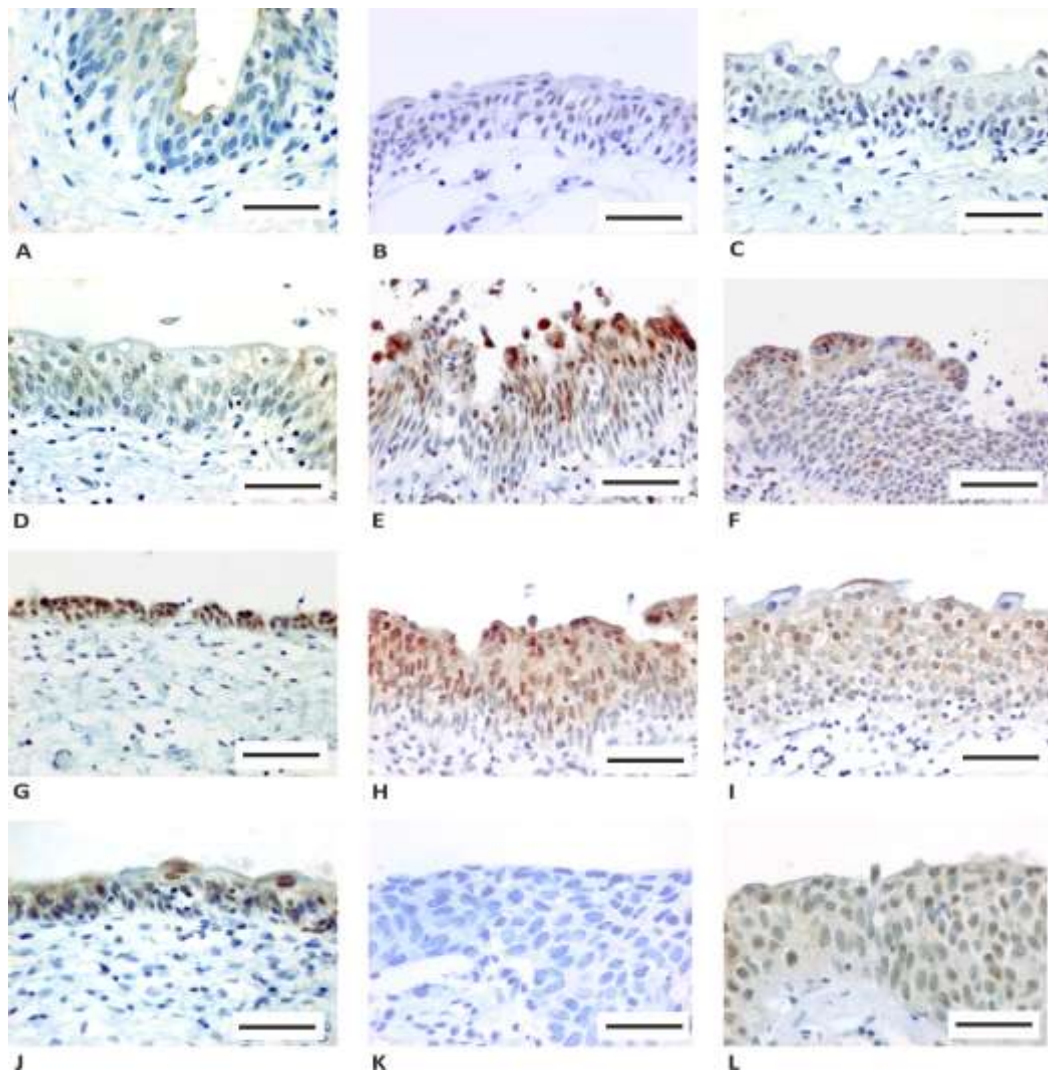
Figure 3-3: Immunoperoxidase labelling of HIF-1α on a range of human bladder and ureteric specimens

A: Y1278 Normal ureter

B: Y1186 Bladder (BPH with BOO)

C: Y1272 Bladder (VUJO)

D: Y1299a Normal ureter

E: Y1122 Neuropathic bladder

F: Y1000 Neuropathic bladder

G: Y1103 Neuropathic bladder

H: Y1079 Neuropathic bladder

I: Y1042 Neuropathic bladder

J: Y1173 Neuropathic bladder

K: Y789b Urothelial carcinoma (-ve control) *L: Y789b Urothelial carcinoma*

Scale bar = 50μm

Table 3-2: Number of nuclei analysed per sample (n) and sample type.

Sample No.	Sample Type	No. of nuclei	Sample No.	Sample Type	No. of nuclei
Y836B	Bladder – Vesico-uretric reflux (VUR), (paed)	1036	Y777	Neuropathic bladder (paed)	353
Y952	Ureter (paed)	1087	Y969	Neuropathic bladder (paed)	1713
Y1186	Bladder –Benign prostatic hypertrophy (BPH) bladder outlet obstruction (BOO), (adult)	2578	Y1000	Neuropathic bladder (paed)	2058
Y1216	Ureter (adult)	835	Y1025b	Neuropathic bladder (paed)	237
Y1278B	Ureter (adult)	1410	Y1042	Neuropathic bladder (paed)	1078
Y1272B	Bladder - VUR (paed)	2100	Y1079	Neuropathic bladder (paed)	3200
Y1299a	Ureter (adult)	2298	Y1103	Neuropathic bladder (paed)	1546
Y1303	Bladder Vesico-ureteric junction obstruction (VUJO), (paed)	4913	Y1107	Neuropathic bladder (paed)	960
Y1328	Bladder VUJO (paed)	965	Y1122	Neuropathic bladder(paed)	755
			Y1173	Neuropathic bladder(paed)	404
E1	Post-augment (adult)	192	Y1180	Neuropathic bladder(paed)	1229
E2	Post-augment (adult),	1192	Y1427	Neuropathic bladder(paed)	100
E4	Post-augment (adult),	496	Y1462	Neuropathic bladder(paed)	1557
E8	Post-augment (adult),	1013	Y1535	Neuropathic bladder(paed)	2478
			Y1585	Neuropathic bladder(paed)	566

3.1.1.1   Image analysis
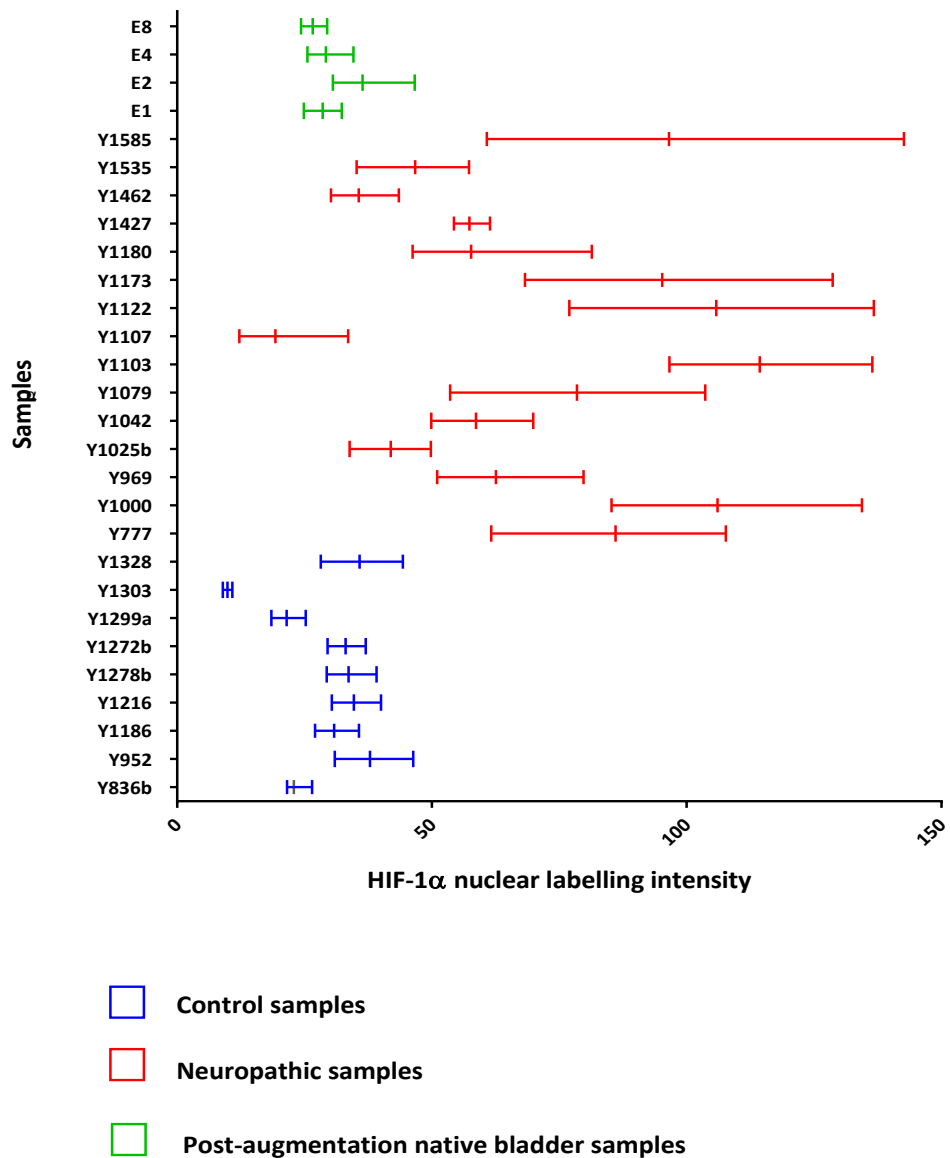
Figure 3-4: Line chart of median and interquartile range of nuclear HIF-1α (DAB intensity) in individual human control, neuropathic and post-augmentation samples.

*Transverse lines represent interquartile range with the median represented by the vertical line within. Control samples are shown in blue, neuropathic in red and post-augmentation in green. Total nuclei analysed per sample are detailed in **Table 3.2**.*
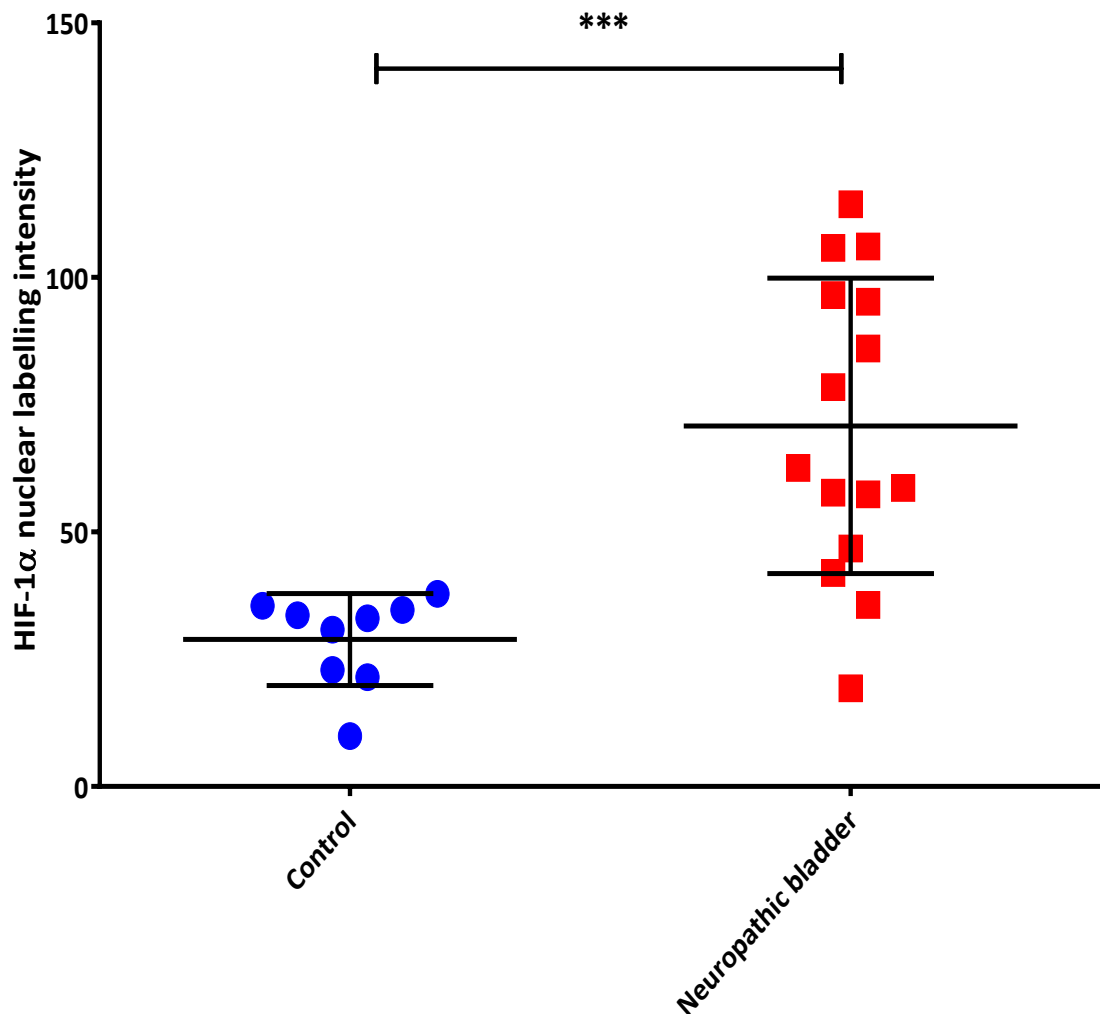
Figure 3-5: Comparison of mean nuclear HIF-1α labelling intensity between control and neuropathic samples.

Each data point represents the mean nuclear labelling intensity for HIF-1α within the urothelium for each sample. The solid horizontal line represents the mean of the group as a whole and the error bars = s.d. Comparison was made between the mean nuclear DAB intensity of the urothelium in 9 control samples and 15 neuropathic bladders. Using an unpaired t-test with Welch correction, there was an extremely significant difference found p<0.0001.

Of the 15 neuropathic samples only 11 had traceable, routine retrospective clinical information regarding urodynamic studies (**Table 3.3**); 3 patients had low pressure systems and 8 had high detrusor pressures recorded. Histology samples taken from the four patients with the lowest recordable detrusor pressures were found to have the lowest intensity of labelling for HIF-1α within the neuropathic samples group (**Fig. 3.4**).

Both initial and maximum detrusor pressures recorded at urodynamic assessment when plotted against HIF-1α labelling intensity produced an upward trendline (**Fig. 3.6a-b**). Linear regression was used to test the null hypothesis that there was no correlation between either initial or maximal detrusor pressure and DAB staining for HIF-1α labelling intensity. All 11 datasets were analysed, with no missing events. $r^2 = 0.60$, *p= 0.005* for maximum detrusor pressure (PDetMax) and $r^2 = 0.37$, *p= 0.046* for initial/opening detrusor pressure (PDetInitial). Both datasets passed the post-test for deviation from linearity. Based on the linear regression for correlation results the null hypothesis was rejected as there was a significant association found between both opening and maximum detrusor pressure and HIF-1α labelling intensity (*p ≤ 0.05)*.

Table 3-3: Detrusor pressures known for neuropathic samples

Opening detrusor pressures was taken at the start of urinary flow. A pressure > 10 would suggest an abnormally high opening pressure for all ages. High pressure systems were identified as systems where both opening and maximum detrusor pressures were high or an obstructive urodynamic trace was seen with detrusor pressure rising and poor flow. Although initially for adults (Abrams, 1999), and modified for children the ICS nomogram was used to guide subdivision of the systems based on pressure (Neveus et al., 2006). Using this guide opening pressures >10 cmH_2O and maximum detrusor presures >40 cmH_2O are seen to represent high pressure systems.

	Opening Detrusor Pressure: PDet Initial (cmH2O)	Maximum Detrusor Pressure: PDetMax (cm H2O)	System Pressure
Y1000	54	294	High
Y1025b	2	29	Low
Y1042	53	99	High
Y1079	56	137	High
Y1103	39	165	High
Y1107	6	57	Low
Y1122	25	134	High
Y1180	46	172	High
Y1173	89	190	High
Y1427	9	81	High
Y1462	6	17	Low
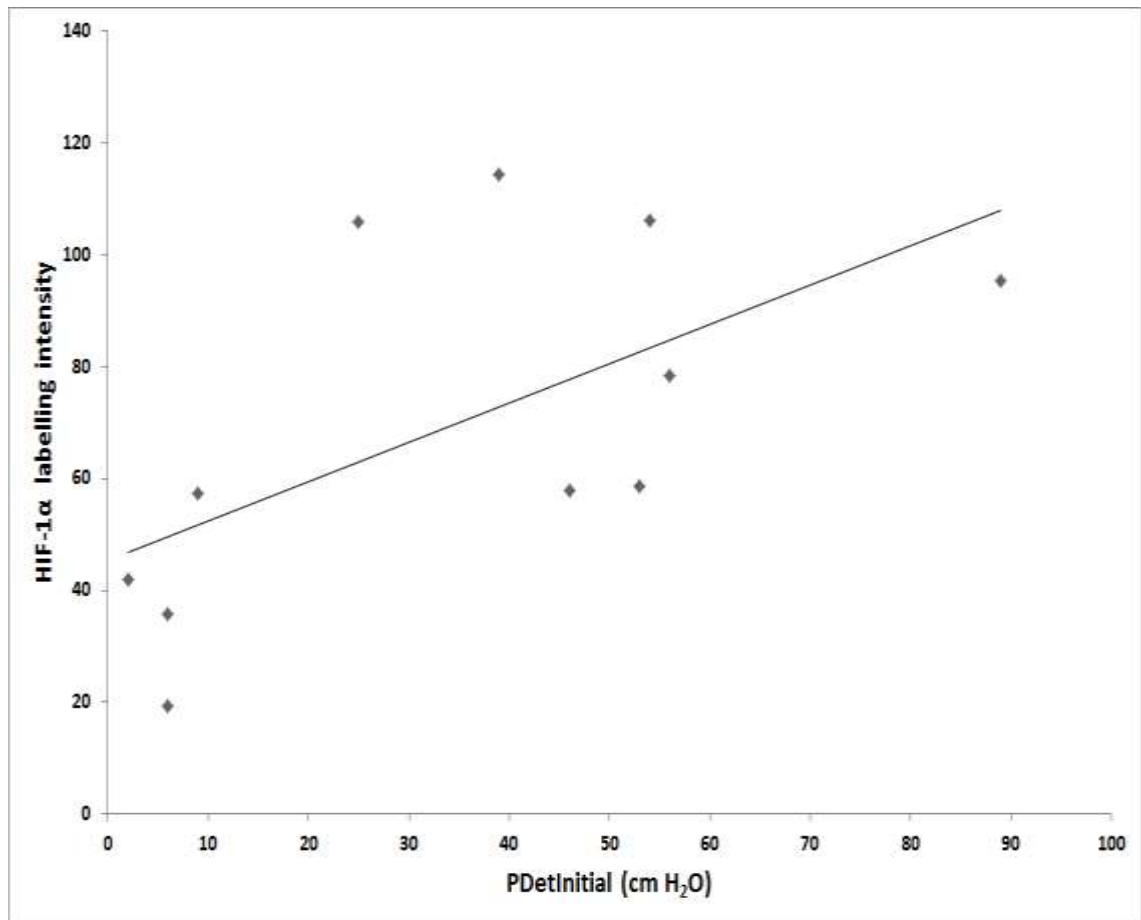
Figure 3-6a: Scatterplot of initial (opening) detrusor pressure against HIF-1α labelling intensity.

Opening detrusor pressure was determined by urodynamic data available from patient notes (n=11). A linear trend line was calculated using Microsoft Excel®. Linear regression with post-test was performed: R^2= 0.37, p=0.046.
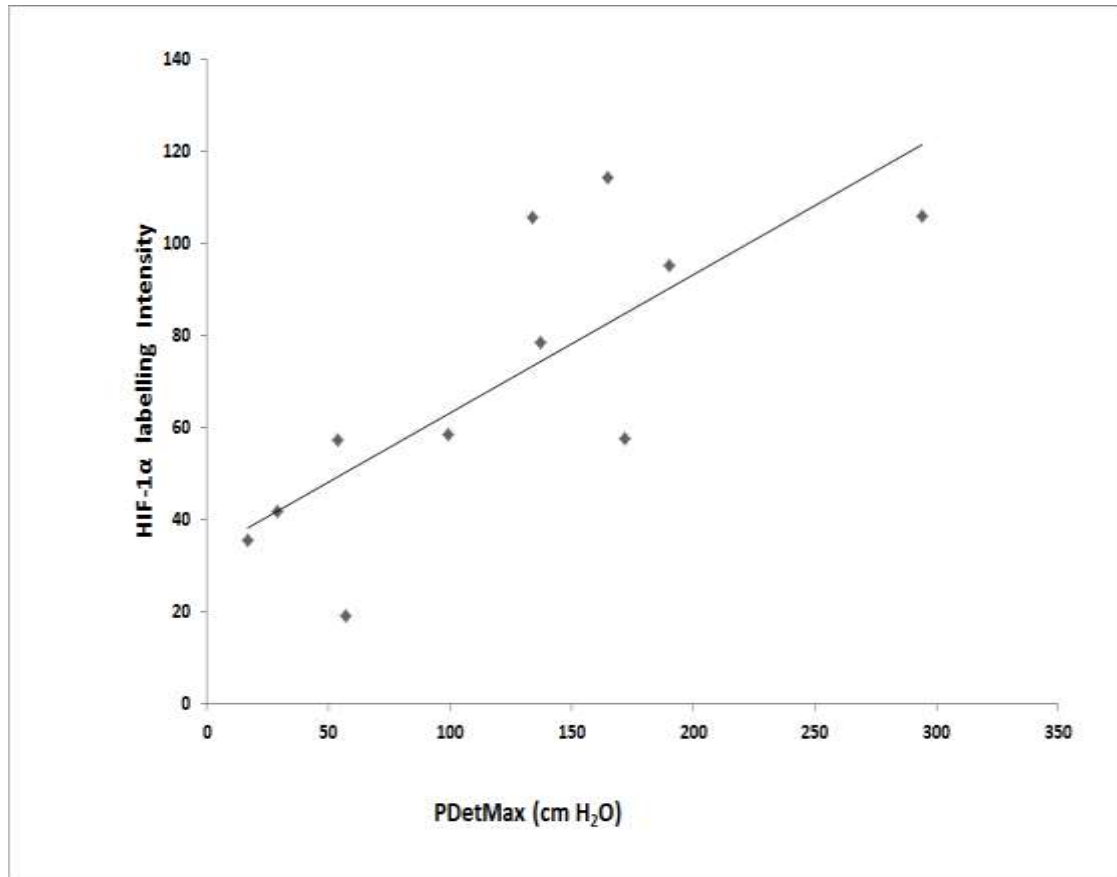
Figure 3-6b: Scatterplot of maximum detrusor pressure against HIF-1α labelling intensity.

Maximum detrusor pressure was determined by urodynamic data available from patient notes (n=11). A linear trend line was calculated using Microsoft Excel®. Linear regression with post-test for correlation was performed. R^2= 0.60, p=0.005

3.1.2 Impact of acute and prior exposure to hypoxia on proliferation

Mean cell number was consistently lower across all three biological replicates (***Figs. 3.7A-C)*** in NHU cells cultured in hypoxic conditions compared to normal oxygen tensions. By the fourth subculture of Y1431, Y1483 and Y1512 cell lines, the mean (s.d.) cell number in the normoxia cultures was 13.2 x 10^4 (2.79), 17.76 x 10^4 (4.25) and 13.46 x 10^4 (3.46) respectively. These figures can be compared to the mean cell number achieved in the same three cell lines in hypoxic conditions which were: 5.22 x 10^4 (0.33), 5.34x 10^4 (0.14) and 3.39 x 10^4 (1.49), respectively.

The reduction in cell number was supported further by micrographs taken at day 3, 5, and 7 post sub-culture (***Fig. 3.8***). Although population sizes were smaller in the 2% oxygen group there were no changes in morphology noted suggestive of loss by apoptosis or other forms of cell death. Some individual cells within the population did exhibit a larger morphology with loss of cell membrane definition as highlighted in the expanded image **A.** Although not formally tested, this indicated a reduction in cell proliferation rather than attrition due to cell loss.

When the data across the three biological replicates was pooled and normalised statistical analysis could be performed, which suggested a significant difference in the mean cell numbers between cells cultured in normoxia and to those maintained in hypoxia. This was true across all subcultures *p*-values ranging from *<0.01 to < 0.001* (***Fig. 3.9a***).

Cells transferred from the hypoxic incubator to normoxic conditions after sub-culture two had a mean cell number consistently similar to normoxic controls in all cell lines

116

Further support was shown by microscopy (***Fig. 3.8***) taken in the week prior to subculture 4; there being more cells evident in the pre-exposed cultures compared to hypoxia maintained comparators. Looking at the three cell lines individually (Y1431, Y1483 and Y1512) at sub-culture four only those cultures switched from hypoxia to normoxia resulted in a mean total cell number (s.d.) of; 14.42×10^4 (3.52), 15.4×10^4 (3.18), 13.38×10^4 (3.1) respectively compared to those achieved in cultures maintained in normoxia; 13.2×10^4 (2.79), 17.76×10^4 (4.25) and 13.46×10^4 (3.46) (***Figs. 3.7A-C)***.

These results suggested that the total cell number increased following removal from hypoxia with little disparity between the pre-exposed cultures and those that had been maintained in normoxia throughout. When these results were normalised across cell lines and analysed together there was no significant difference throughout subcultures three and four between cell number in the controls (normoxia) and those switched from hypoxia to normoxia (pre-exposed) (***Figs. 3.9A)***.

However, when the pre-exposed cultures are compared to cultures maintained in hypoxia there was an improvement and significant difference in cell number with every subculture. The significance of this difference between these two conditions, shown by ANOVA analysis was: *p<0.001* at sub-cultures three and four (***Figs. 3.9A)***. This was also evident in all three cell lines when analysed independently (***Figs 3.7A-C***) with all three demonstrating total cell number to be greater than hypoxia at subcultures three and four.

Looking at normalised values across all three cell lines achieved over all subcultures (***Figs. 3.9A)*** what was also evident was that any compromise or improvement, proportional to normoxia controls, was stable in both hypoxia and pre-exposed

populations. When subculture three and four values were normalised as a single group (***Figs. 3.9B)*** statistical analysis was more robust. The results further supported a significant difference between both normoxia and pre-exposed populations compared to hypoxia with regard to cell number (*p =<0.001).* Therefore once hypoxia exposed NHU cells are transferred to normoxia there was an apparent return to a proliferative capacity similar to that of cultures maintained in normoxia throughout.
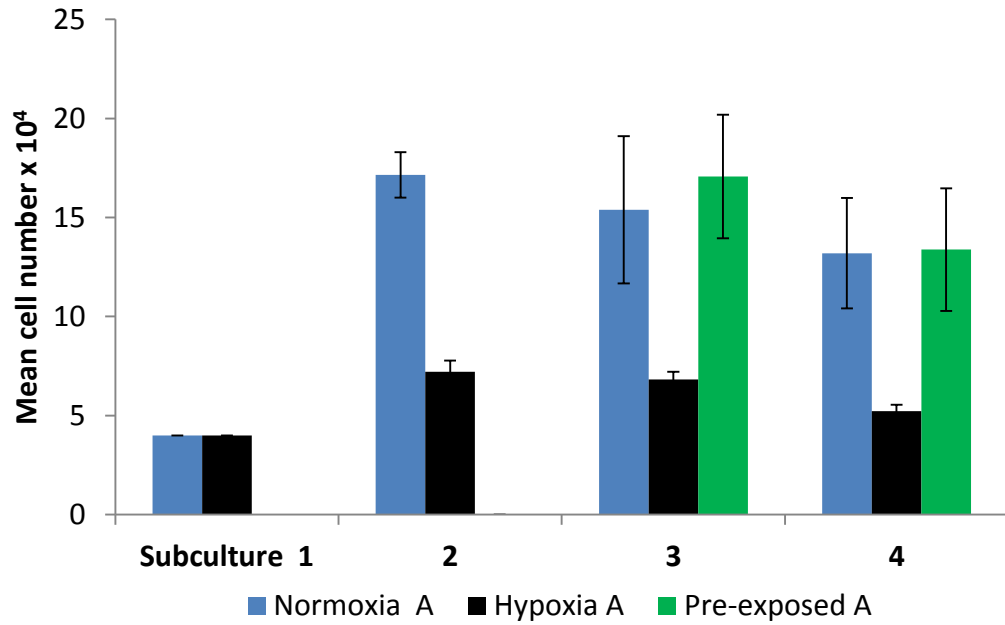
Figure 3-7A
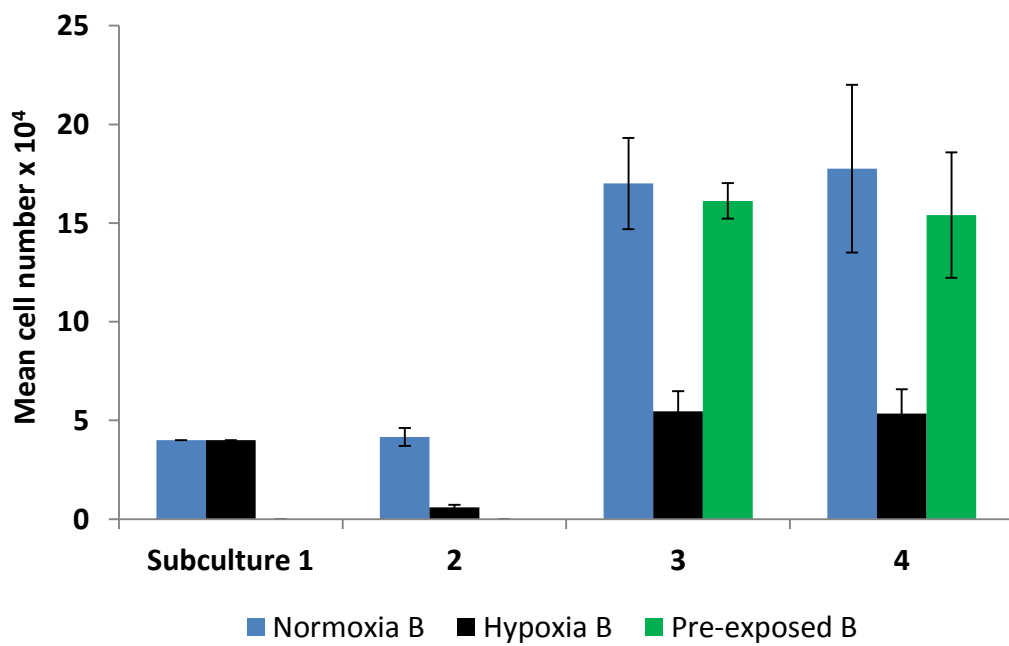
Figure 3-7B

Figure 3.7C
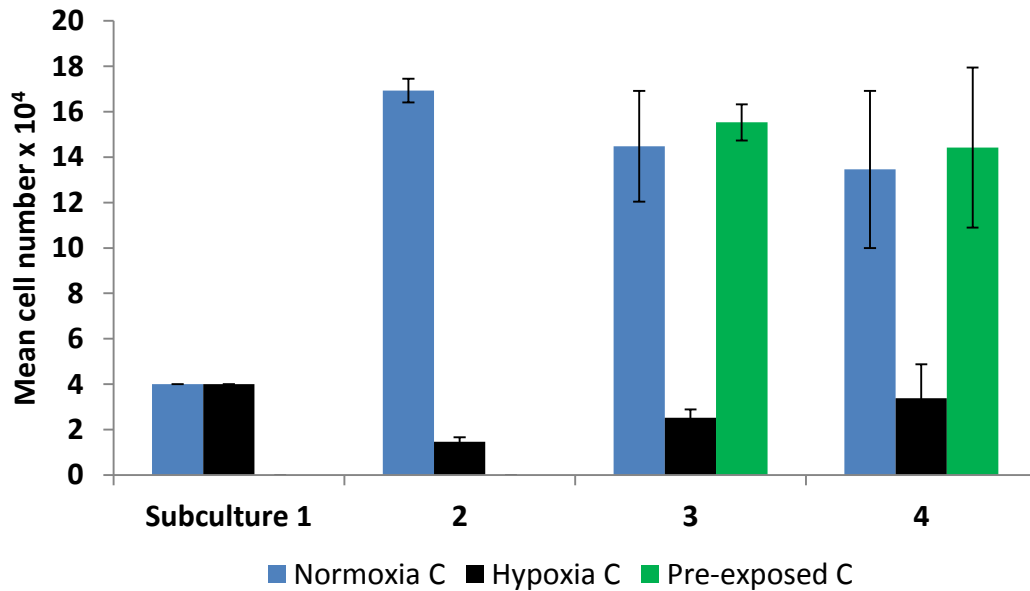
Figure 3-7A-C.: Mean cell number in three independent cell lines in different conditions:

All cell lines were initially seeded at a density of 2x 10^4cells/ml (2 ml = 4 x 10^4 cells) and at subsequent subcultures. A = Y1431, B = Y1483 and C = Y1512. In each cell line there were 6 technical replicates for each condition (normoxia, hypoxia and pre-exposed). Mean cell number at each subculture, in A-C, represents the mean of the 6 technical repeats. Error bars (s.d.) are shown. Once one well of any of the conditions reached confluence all wells for all conditions were counted enabling direct comparison of cell numbers at that given time. All wells were reseeded at 2x 10^4cells/ml (2 ml = 4 x 10^4 cells). Pre-exposed cells were taken from the hypoxia population (therefore mean cell number was equal to that for hypoxia at subcultures one and two) and switched from hypoxia to normoxia after subculture two. Pre-exposed cultures were seeded at 2x 10^4cells/ml (2 ml = 4 x 10^4 cells) throughout the experiment, consistent with the practice for hypoxia and normoxia populations. Cell lines A and C, both normoxic and pre-exposed populations, demonstrated a small reduction in mean cell number between subcultures two and four. In cell line A this was also the case for the hypoxic cultures but not in cell line C.
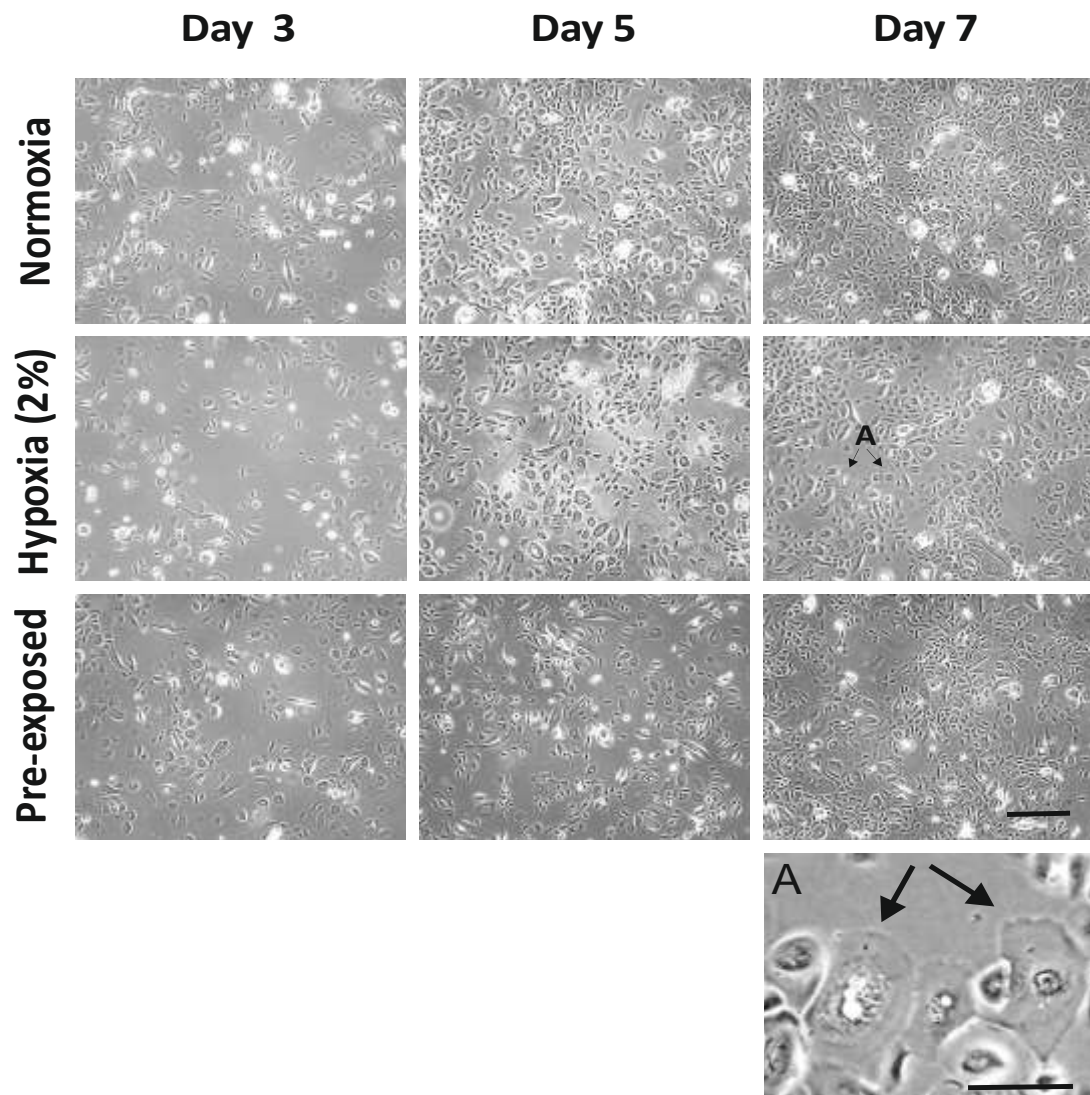
Figure 3-8: Phase contrast micrograph of a representative NHU cell line in proliferative growth phase exposed to different oxygen tensions.

Monolayers of Y1431 NHU cells were seeded at $2x10^4$ cells/ml at sub-culture three onto Primaria™ tissue culture plastic. Phase contrast microscopy images were taken on days 3, 5 and 7 post sub-culture. Cultures were expanded in KSFMc medium in normoxic (21 % O_2) or hypoxic (2 % O_2) conditions. Half of the cultures previously exposed to hypoxia were subsequently maintained in normoxia (pre-exposed). Note the altered morphology by day 7 in the hypoxic culture, with some cells exhibiting loss of distinction (shown by lack of "brightness") of the cell borders (arrowed and expanded in A). The scale bar represents 200 μm (A = 25 μm).
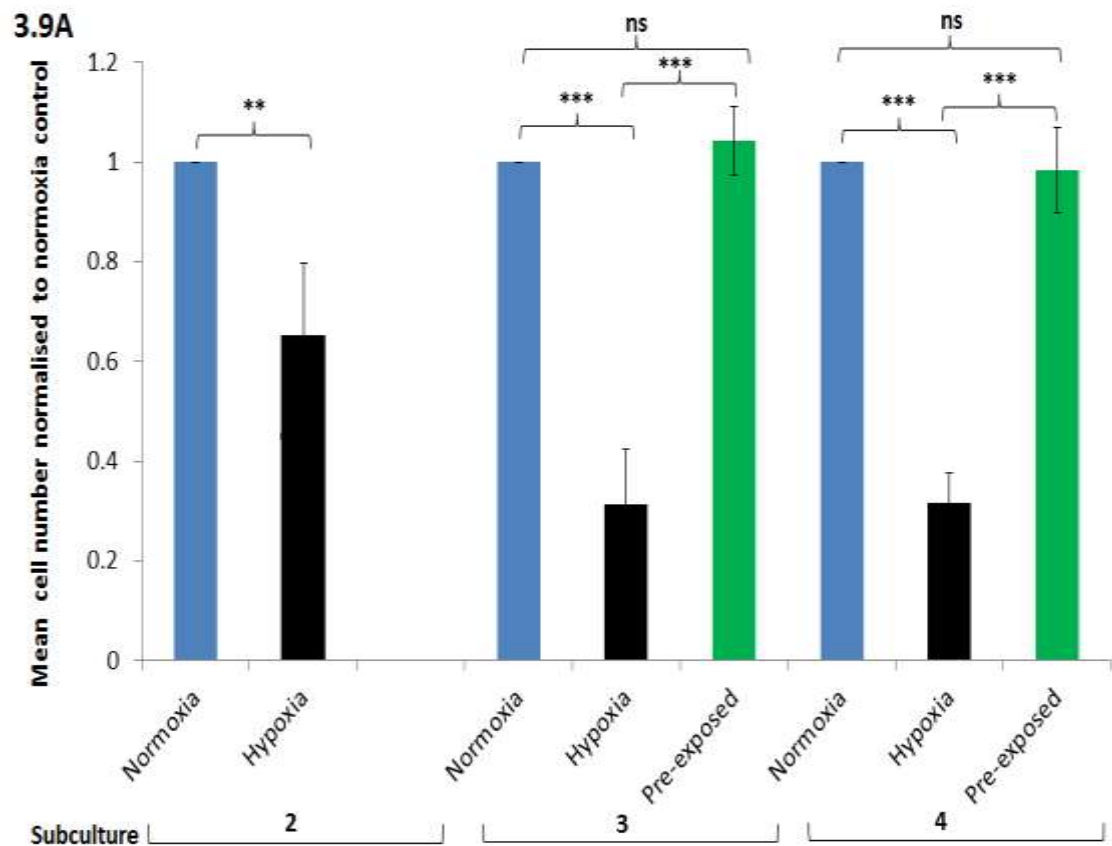
Figure 3-9A: Normalised mean cell number across sub-cultures

*The mean cell number in the normoxia control for each cell line and across all cell cultures was used as a normalising value for each cell line/ biological replicate. All data for mean cell number was then converted, using the control value to produce comparable data across all 3 cell lines for each individual subculture (n= 3). ANOVA analysis was performed with Tukey multiple comparison performed post-test (ns = not significant, ** = p<0.01, ***= p<0.001. Note the disparity between controls (normoxia) and hypoxia in terms of normalised values across all subcultures. However there was a significant improvement in the values within the pre-exposed cultures which were switched to normoxia over subcultures three and four suggesting the compromise to be reversible and sustainable. . There was no obvious variation in the results across the subcultures suggesting any compromise or improvement was proportional regardless of any culture senescence.*
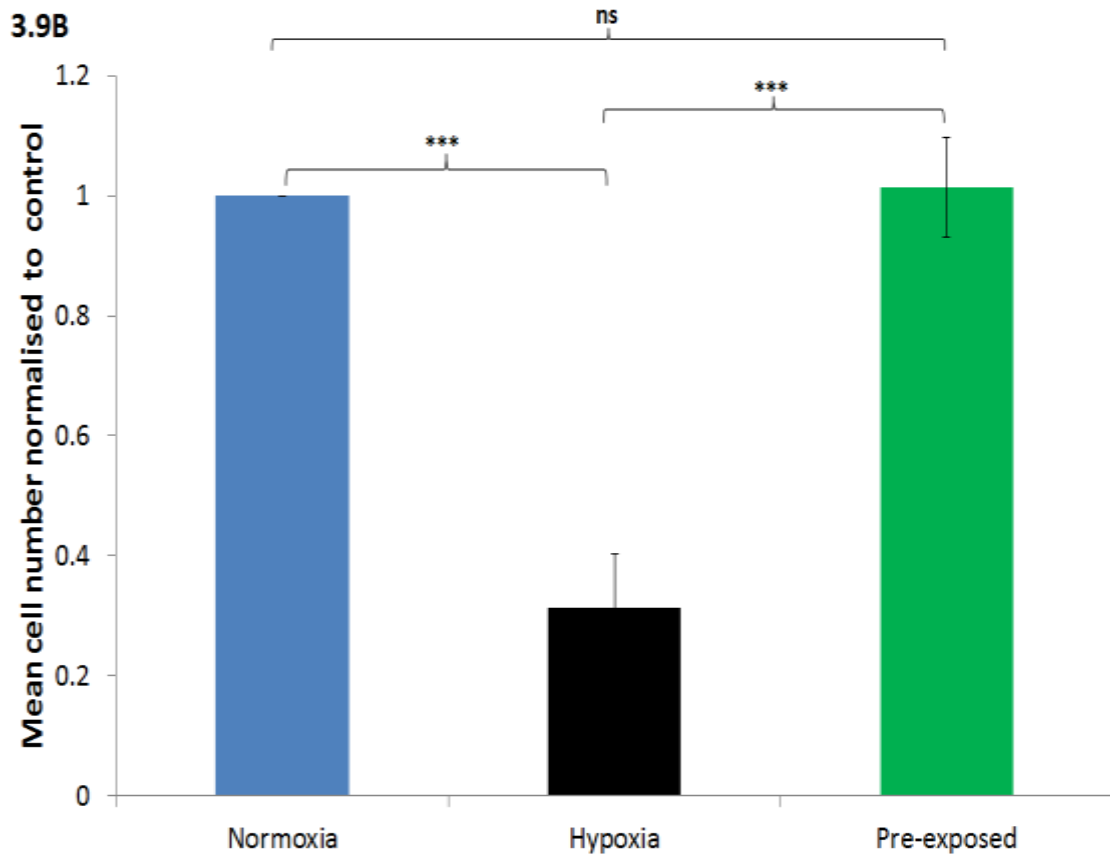
Figure 3-9b: Summary of mean normalised cell number.

*The mean cell number in the normoxia control group was used as a normalising value for each cell line/ biological replicate. All data for mean cell number was then converted, using the control value to produce comparable data across all 3 cell lines (n= 6) over subcultures three and four. The reason for this was to evaluate an equal number of values for all conditions. ANOVA analysis was performed with Tukey multiple comparison performed post-test (ns = not significant, ***= p<0.001. Note the disparity between both controls (normoxia) and pre-exposed values and hypoxia confirming that there is a significant difference between cell that are switched form hypoxia into normoxia.*

3.1.3 Impact of acute hypoxia on barrier formation and function

All four independent cell lines Y1431, Y1483, Y1512, Y1227 **(A-D** respectively**)** developed a satisfactory, stable barrier in control (normoxia) conditions by day eight. ***Fig. 3.10*** demonstrates the increase in TEER over eight days in each cell line as the urothelial barrier developed. This temporal increase in TEER was still present in three of the four cultures maintained in hypoxia; however there was a significant reduction (*p< 0.001*) in the normalised final TEER readings achieved by cultures in hypoxia compared to parallel cultures maintained in normoxia (***Fig.3.11***).

3.1.4 Effect of pre-exposure to hypoxia on barrier formation and function

NHU cultures exposed to hypoxia then subsequently sub-cultured and differentiated in normoxia developed a stable but weaker barrier than controls. This was found in all four cell lines (***Fig. 3.10***).   There was no significant difference between normalised, mean TEER values achieved in pre-exposed cultures and those maintained in hypoxic conditions (***Fig. 3.11***). There was however a significant difference in the final TEER obtained between cells maintained in normoxia and those pre-exposed to hypoxia (*p<0.01*). The difference in the normalised mean TEER however between pre-exposed versus controls was less significant compared to hypoxia versus controls (p<0.001) (***Fig. 3.11***).
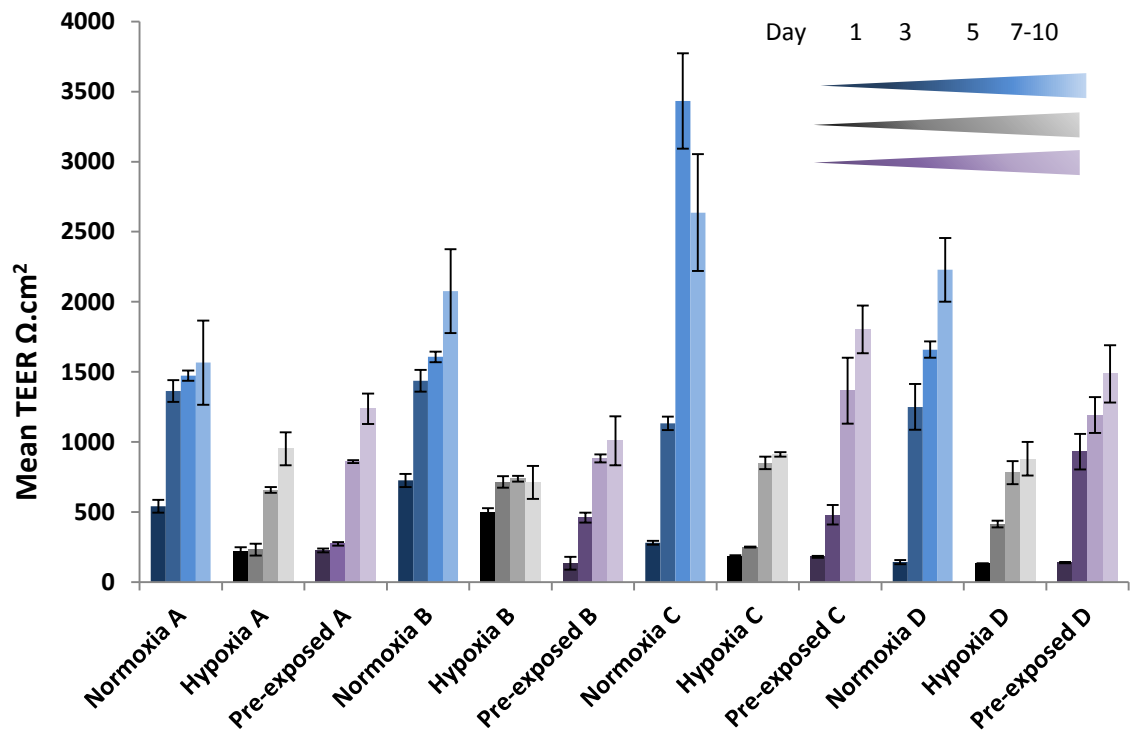
Figure 3-10: Mean TEER in four independent cell lines maintained in conditions of normoxia, hypoxia and pre-exposed to hypoxia.

Cell lines: A = Y1431 (n=3), B= Y1483 (n=3), C=Y1512 (n=5), D Y1227 (n=5). TEERs were measured over a 7- 10 day period or until the barrier had been stable for at least 48 hours
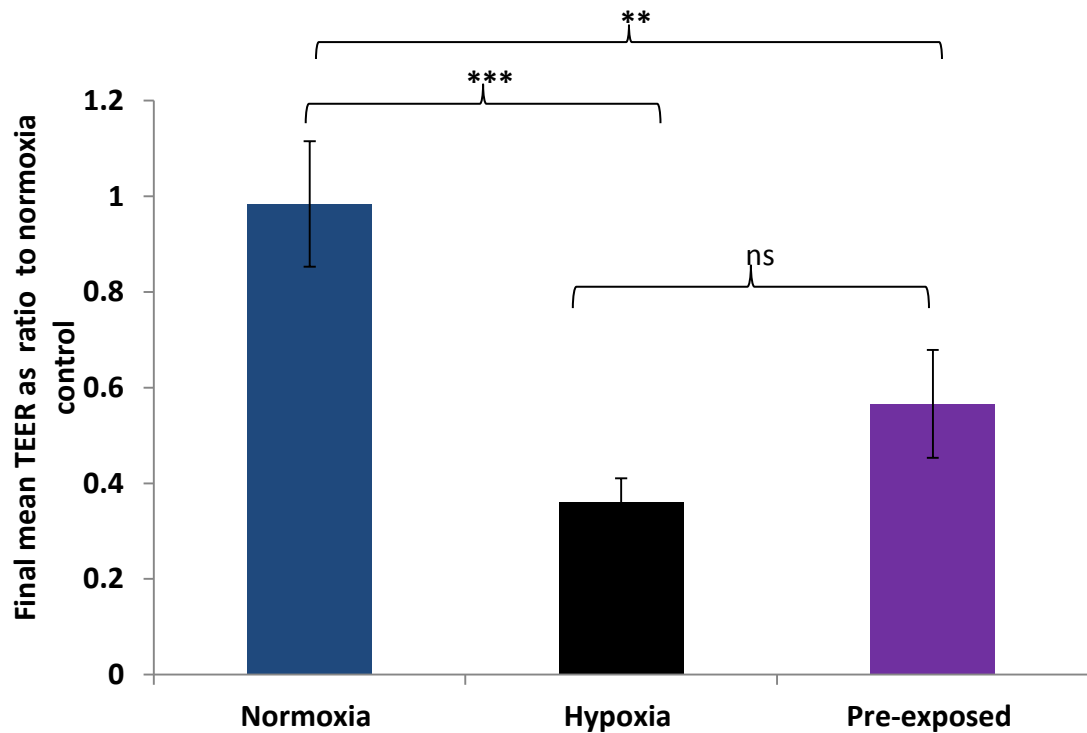
Figure 3-11: Final mean TER in hypoxia and pre-exposed cells expressed as a ratio to normoxia controls.

*The mean stable (day eight) TEER values in the normoxia controls were used as a normalising value for each cell line/ biological replicate. All data for TEER readings were then converted, using the control value to produce comparable data across all 4 cell lines. This enabled an n=16 to be analysed statistically without being affected by inter- cell line variation. The result of the ANOVA analysis with Tukey multiple comparison performed post-test is shown on the chart (ns = not significant, ** = p<0.01 ***= p<0.001.*

3.1.5 Effect of acute exposure and pre-exposure to hypoxia on barrier recovery after wounding.

No significant difference was seen between the initial TEER and the final post-wounding TEER normoxia, hypoxia and pre-exposed cultures, with all barriers recovering to pre-wounding levels. The "speed" of repair in those cultures maintained in hypoxia, or pre-exposed to hypoxia, appeared to lag behind controls for the first 24 hours (***Fig 3.12***).
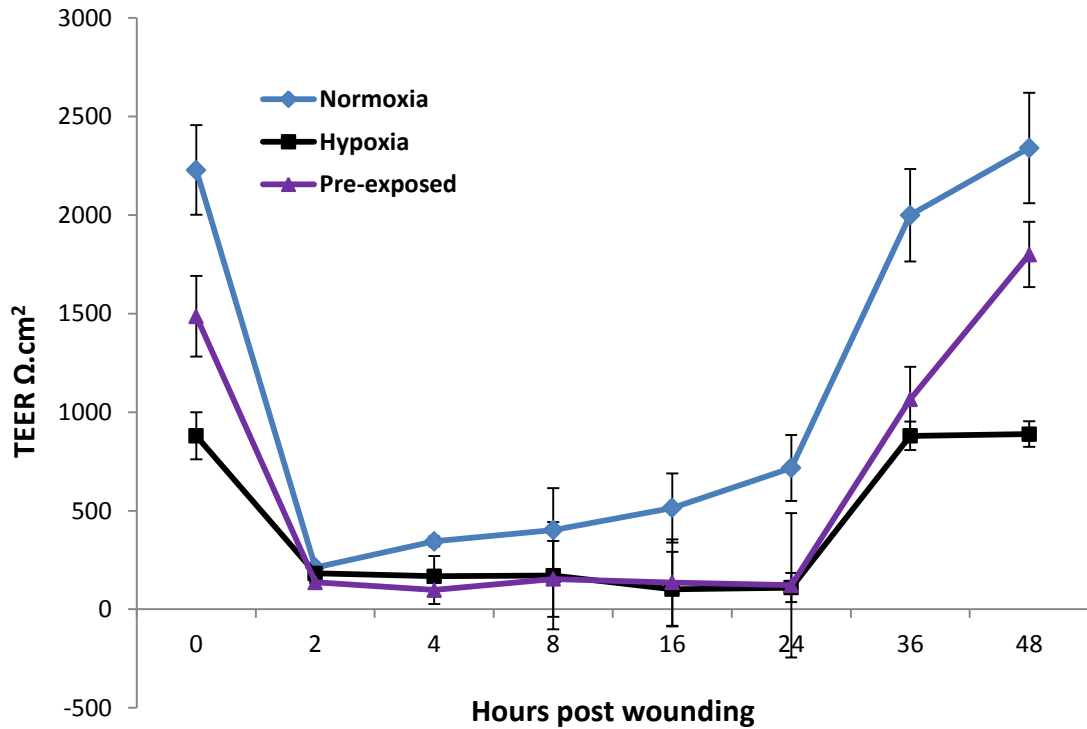
Figure 3-12:   Barrier recovery in normoxia, hypoxia and pre-exposed differentiated NHU cell line (Y1227).

TEER values were acquired regularly until a stable barrier was seen for 2 days. The TEER at this point is represented by time 0 hours on this graph. Scratch wounding of the cell sheet was then performed in 3 technical repeats. TEER readings were obtained at regular intervals until the pre-wounding TEER was achieved. Error bars represent s.d. of the mean for three replicates.

3.1.6 The effect of persistent and pre-exposure to hypoxia on expression of barrier proteins and markers of differentiation

The normal distribution of cytokeratins in healthy urothelium is tabulated in the introductory chapter in *Table 1.1* .Both immunohistochemistry (*Figs 3-13 a- d & 3-15)* and immunocytochemistry of organ cultures (*Figs 3-16a- c)* were used to assess the impact of hypoxia on urothelial health and phenotype. After 21 days of exposure to hypoxia in organ culture in organ culture a loss of most of the urothelium, with some sparing of the basal layer was seen (*Figs 3-13 a- d & 3-15)*. The urothelium in the pre-exposed samples (*Figs 3-13 a*) also demonstrated an incomplete loss of urothelium, seen as urothelial "thinning". Sparing of the basal layer in both hypoxia and pre-exposed t hypoxia samples was demonstrated by persistence of the basal markers CK5 and NGFR (*Figs 3-13b).*

CK13 expression was retained in all three conditions, but was more sporadic within the basal and intermediate layers within the hypoxia and pre-exposed samples (*Figs 3-13 a*). CK14 was generally more prevalent within the organ culture system compared to the *in situ* control. This was similar to that found with immunohistochemistry of CK13 and CK14 in human neuropathic samples (*Fig. 3-14*) (see also Appendix III).

Associated with persistent and pre-exposure to hypoxia there was a loss of superficial and intermediate cells and markers of terminal differentiation including UPK3A and CK20 (*Fig.3.13c).* Laminin was associated with the basement membrane which appeared intact (*Fig. 3.13 c)*.

Of interest, within organ cultures, Ki67 and Cyclin D3 were found to be located within the superficial cells in normoxia. This distribution was lost in the hypoxia and pre-exposed cultures, with a complete absence of both Ki67 and Cyclin D3 (*Fig. 3-13 d)*. In the normoxia controls, P63 was found within the basal and intermediate nuclei of the urothelium with complete absence in the superficial cells, consistent with normal distribution within the urothelium (*Fig. 3-13 c)*. There was almost a complete loss of P63 in both the hypoxia and pre-exposed cultures.

In all organ cultures, including normoxia and *in situ* controls, nuclear staining for HIF-1α was found to be present (*Fig. 3-13 d)*. Histoquest™ analysis of nuclear intensity of HIF-1α labelling (DAB intensity) demonstrated an increase in nuclear HIF-1α activity within the organ culture model compared to native tissue (*Fig. 3-15)*. Within the organ culture system itself, cultures maintained in normoxia had a median DAB intensity of 39.99 (interquartile range (IQR) 35.2 – 47.18) compared to those maintained in hypoxia with a median of 51.11 (IQR 43.52 – 58.98). Those cultures that had been exposed to hypoxia and were then placed in normoxia had a median nuclear labelling higher than controls but lower than those cultures maintained hypoxia 57.52 (IQR 42.52 – 77.11).

The persistently greater nuclear HIF1α expression, despite removal of the hypoxic challenge, suggested either ongoing cellular stress or epigenetic modification resulting in the promotion of HIF-1α translocation into the nucleus despite the absence of a hypoxic stimulus.
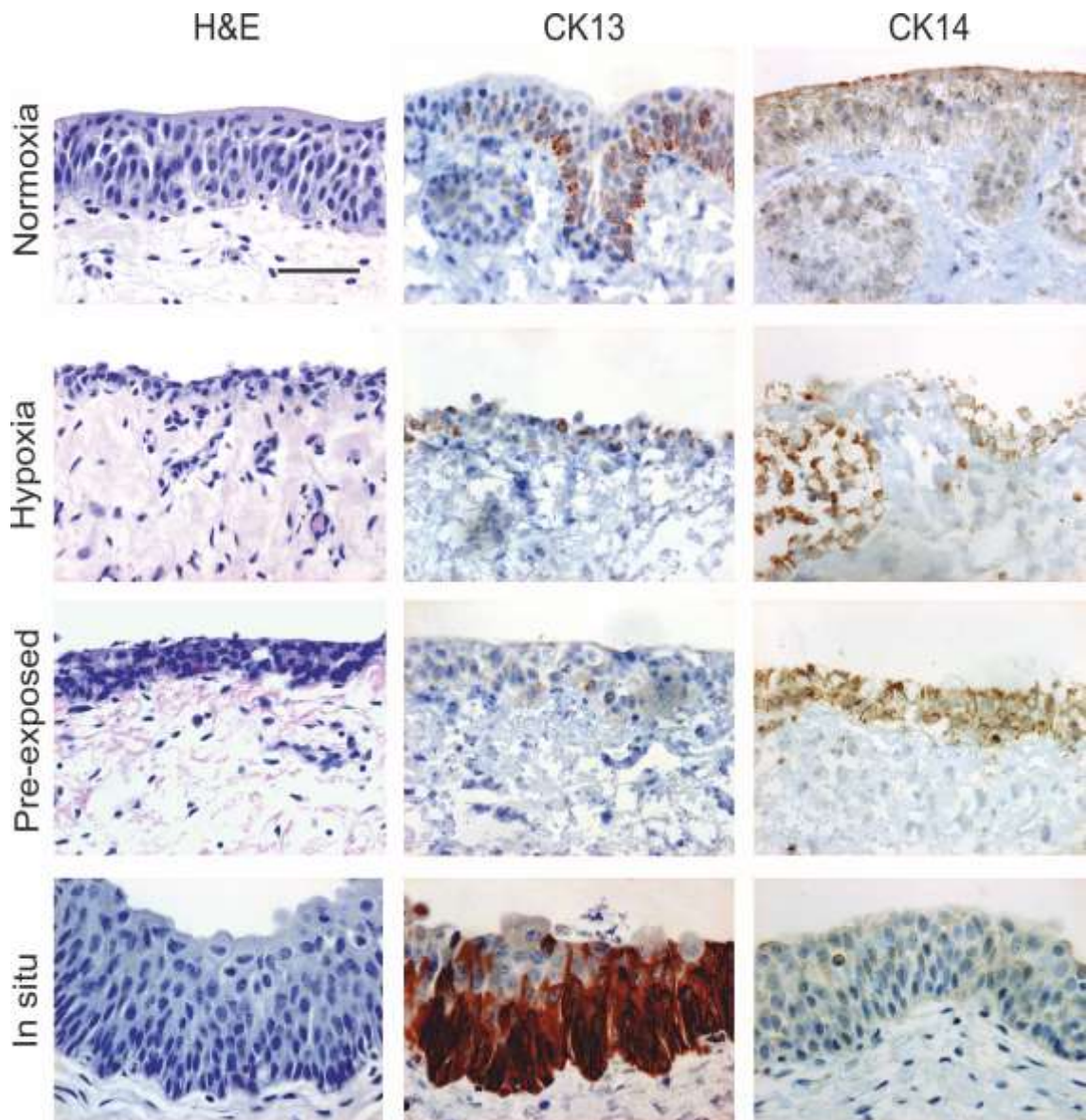
Figure 3-13a: H&E staining and immunoperoxidase labelling of cytokeratins 13 and 14 in organ culture specimens and matched in situ ureter for comparison

Evident in all images of organ cultures maintained or pre-exposed to hypoxia for 21 days there was loss +/- thinning of the urothelium. CK13 was reduced in the organ culture system, even in normoxia but remained within the basal/intermediate layers as opposed to CK14 labelling, which appeared to be more prominent in organ culture. Scale bar = 50 µm.Y1593 shown.
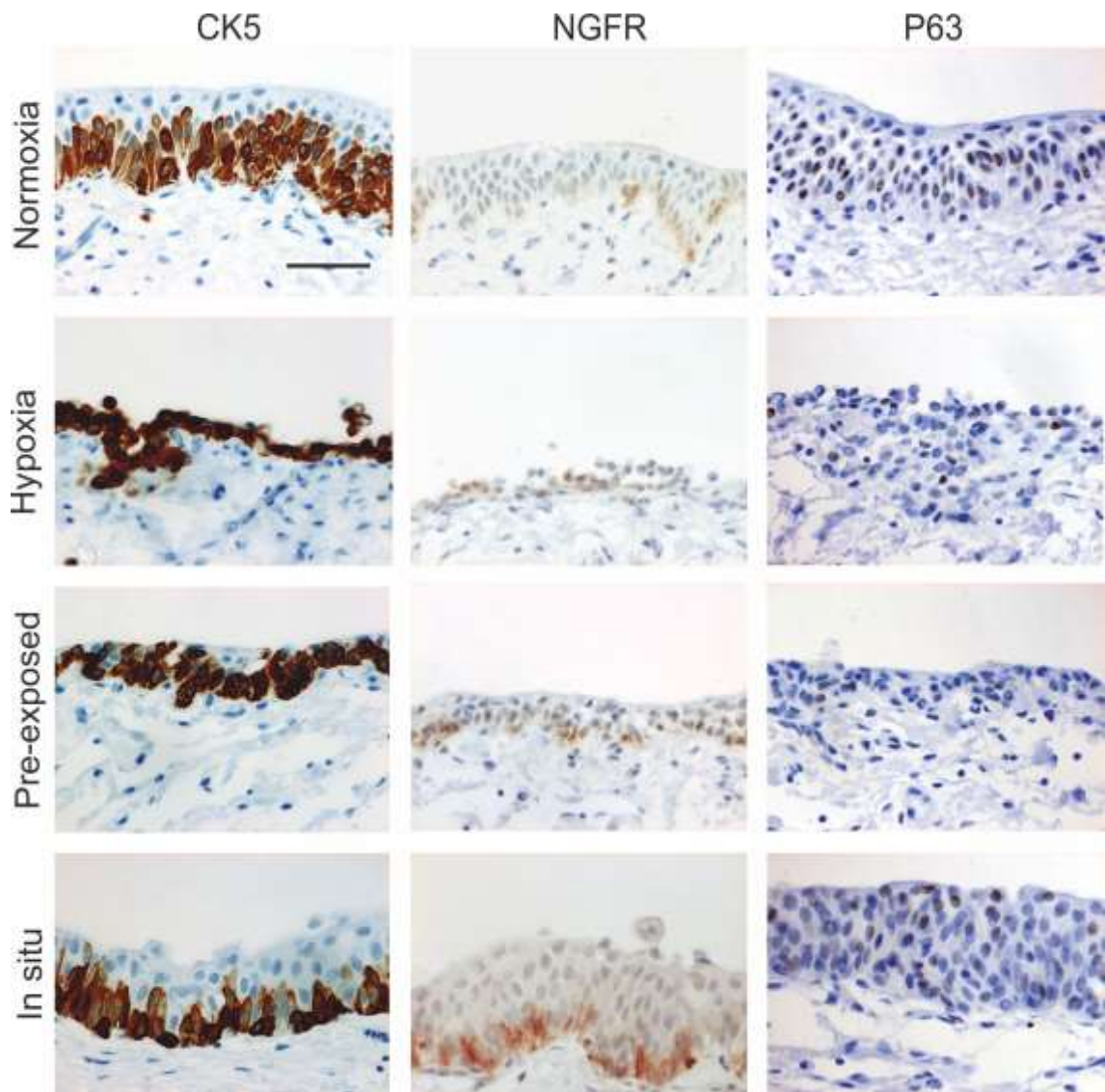
Figure 3-13b: Immunoperoxidase labelling of basal markers: CK5 and NGFR and stem-cell associated P63 markers in organ culture specimens and matching in situ ureter for comparison.

Both CK5 and NGFR were located within the basal cells of all organ cultures. P63 expression was reduced in the hypoxia and pre-exposed cultures. Scale bar = 50 μm. Y1593 shown. Sections were in organ culture for a total of 21 days.
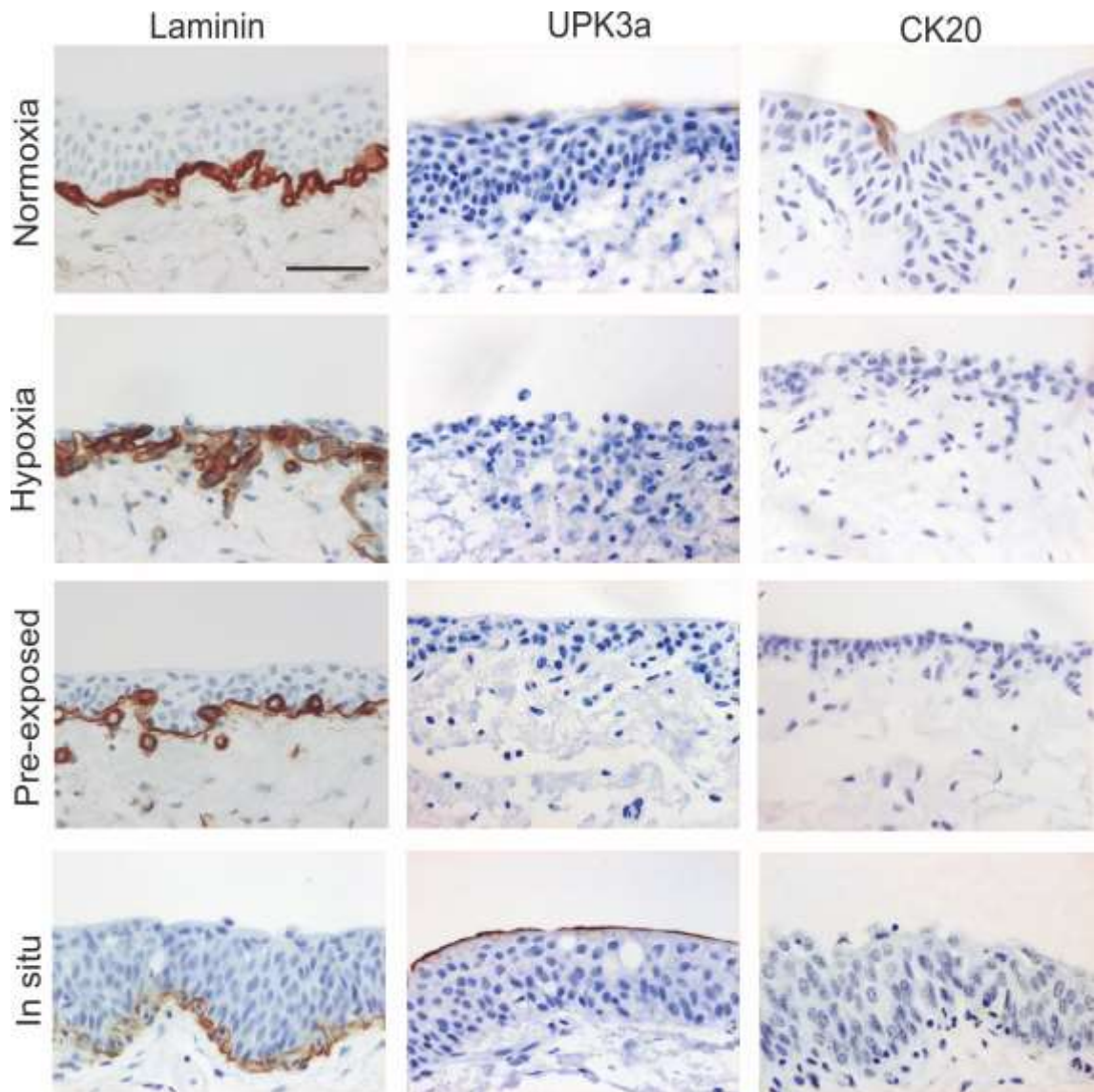
Figure 3-13c: Immunoperoxidase labelling of superficial urothelial cell markers (UPK3a and CK20) and basement membrane-associated laminin in organ culture specimens and matched in situ ureter for comparison.

Laminin defined the basement membrane. Uroplakin 3A (in-situ and normoxia) expression and CK20 (normoxia) was seen and noted to be absent in the hypoxia and pre-exposed cultures. Scale bar = 50 μm. Y1593 shown. Total time in organ culture 21 days.
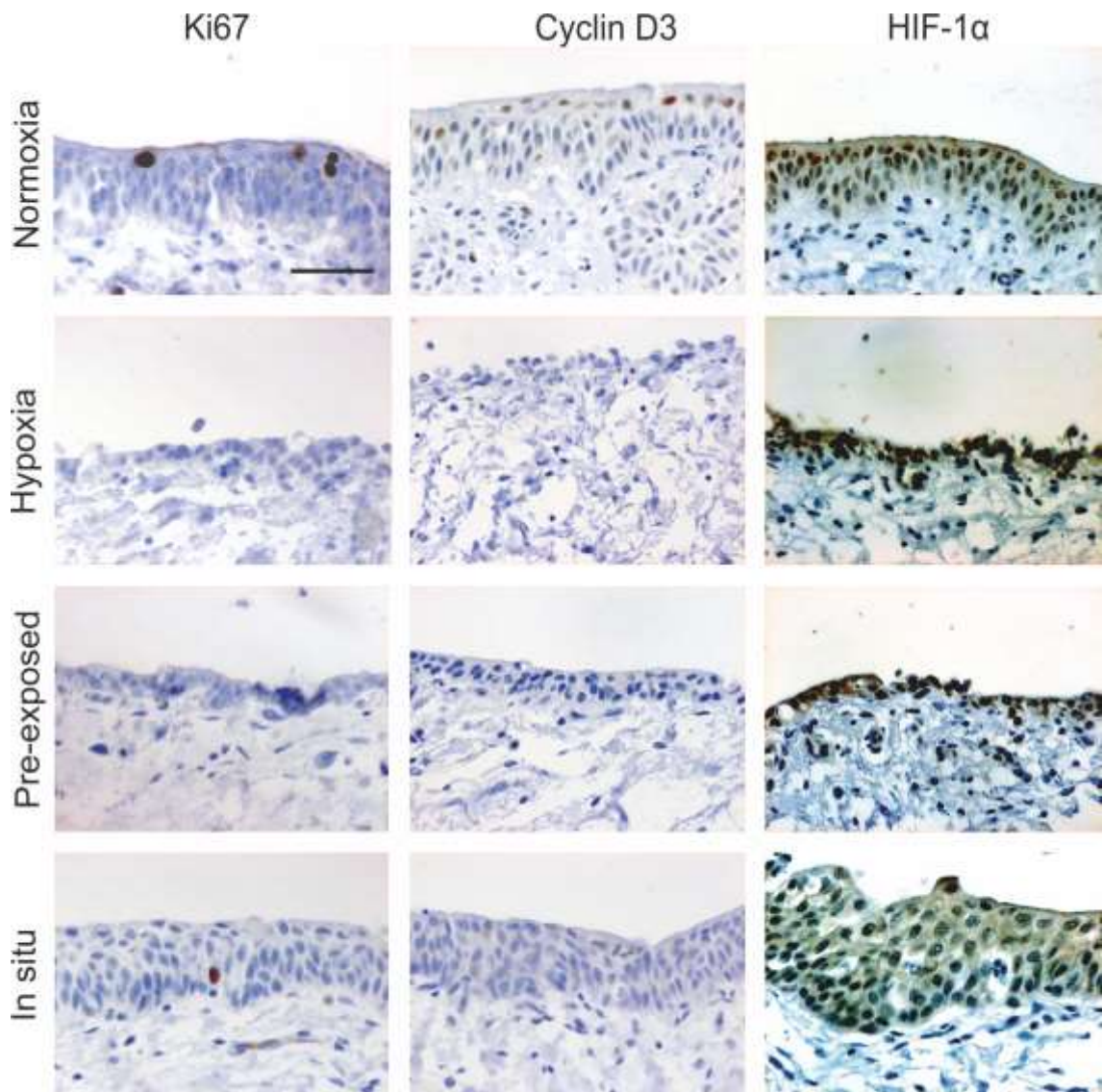
Figure 3-.13d: Immunoperoxidase labelling of Ki67, Cyclin D3 and HIF-1α in organ culture specimens and matching in situ ureter for comparison.

Ki67 and Cyclin D3 were located within superficial cells in normoxia maintained organ cultures but were absent in hypoxia and pre-exposed samples. Ki67 was located basally in the in situ ureter. HIF-1α was present in all organ cultures, subjectively more than the in situ control. Intensive DAB staining of the nuclei in the hypoxia and pre-exposed urothelium was noted. Scale bar = 50 μm. Y1593 shown. Total time in organ culture 21 days.
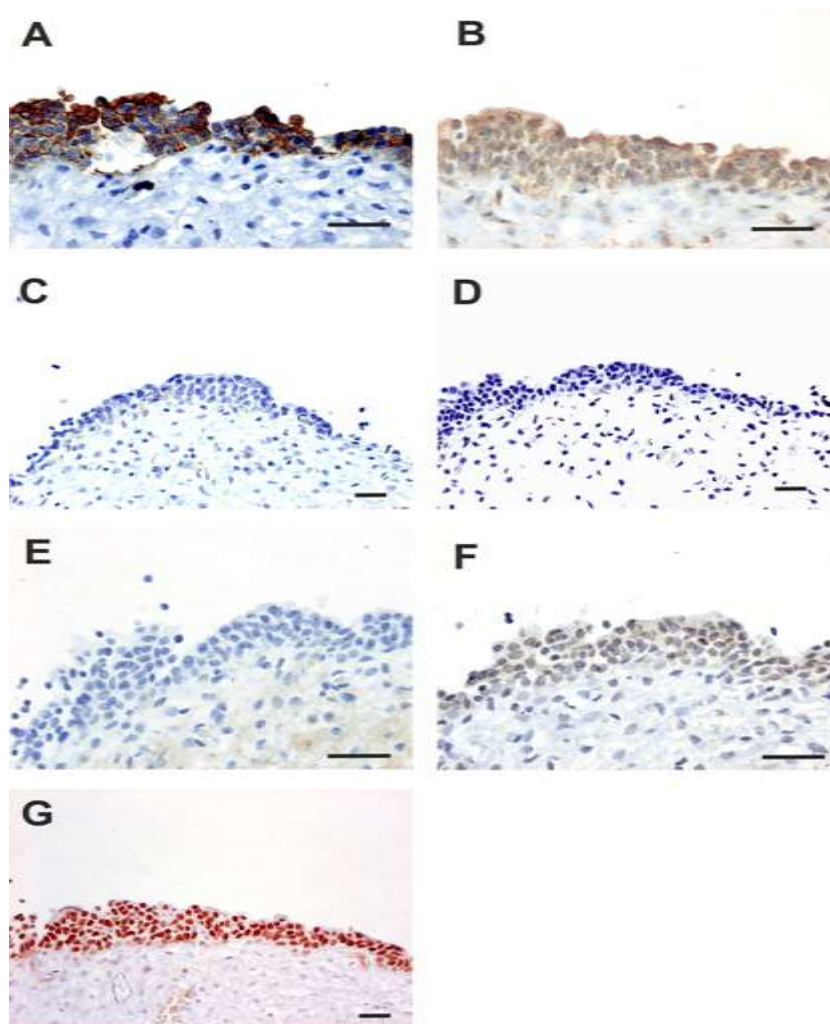
Figure 3-14: Immunohistochemical evaluation of a neuropathic bladder specimen

*Sections from embedded human neuropathic bladders were evaluated using immunohistochemistry labelling for **A** - CK13, **B**-CK14, **C**- UPK3a D- CK20 **E** – Ki67 **F**-Cyclin-D3 and **G** – P63.   There were similarities between the expression of some markers in neuropathic bladders and organ cultures maintained or pre-exposed to hypoxia. CK13 and CK14 were present however UPK3a and CK20 were lost with loss of a superficial layer. Lack of cells superficial to p63 labelling, which was present in **G** also suggested the absence of a superficial layer. Scale bar = 50 µm. Y969 shown.*
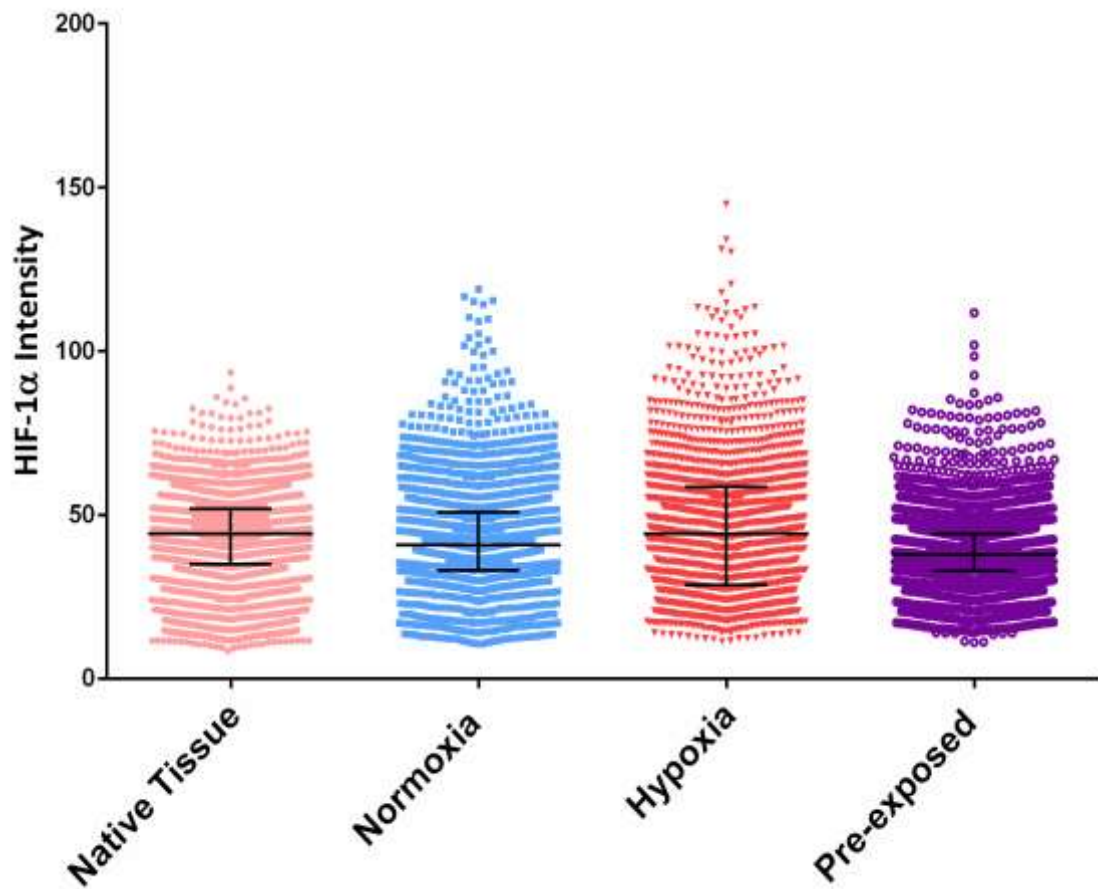
Figure 3-15: Intensity of nuclear HIF-1α labelling in organ culture urothelium maintained in normoxia, hypoxia and pre-exposed to hypoxia.

Comparison was made between the median intensity of nuclear labelling for HIF-1α (DAB staining) of all nuclei of the urothelium within all organ culture (OC) conditions and native tissue that had not been exposed to organ culture. Total time in organ culture was 21 days. Each datum point represents a single urothelial nucleus, from a single donor (Y1689) across three organ culture sections. Native tissue n = 2736, normoxia OC, n = 10264, hypoxia n= 1812, pre-exposed n=3036. The IQR is shown within the black range bars and the median the black horizontal line. Chart for other organ culture donor, Y1593 can be found in Appendix III.
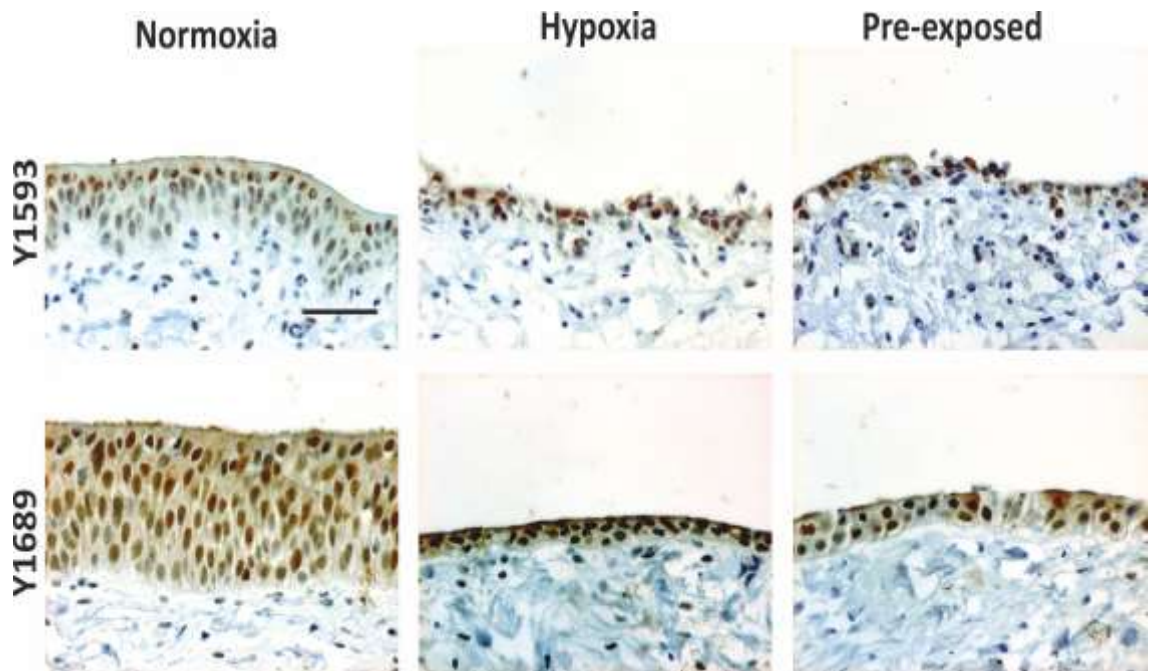
Figure 3-16: HIF-1 α labelling in organ cultures

Two independent donors were set up in organ cultures for 21 days. Pre-exposed sections were removed from hypoxia after day seven and switched to normoxia. Three sections per condition per donor were maintained. It can be seen the loss of urothelium in those sections maintained or pre-exposed to hypoxia.

3.1.7 The effect of persistent and pre-exposure to hypoxia on ZO-1 expression in differentiated urothelium

Immunocytochemistry of ZO-1 (***Figure 3.17a-c)*** in three cell lines demonstrated an apparent reduction in ZO-1 fluorescence in both differentiated NHU cells maintained in hypoxia and pre-exposed to hypoxia when compared to normoxia controls. The cell membrane presence of ZO-1 in the compromised cultures appeared less defined with variation of "thickness" of expression and gaps present in some images (arrowed), suggesting more variation in ZO-1.

3.1.8 The effect of persistent and pre-exposure to hypoxia on H3K9Me2 in differentiated urothelium

Immunocytochemistry of H3K9Me2 appeared to indicate a change in localisation of H3K9Me2 from a global expression within the nucleus in normoxia to a more "ringlike" appearance when cells were either cultured in hypoxia or pre-exposed to hypoxia, suggesting a switch to localisation at the nuclear lamina (***Figure 3.18)***.
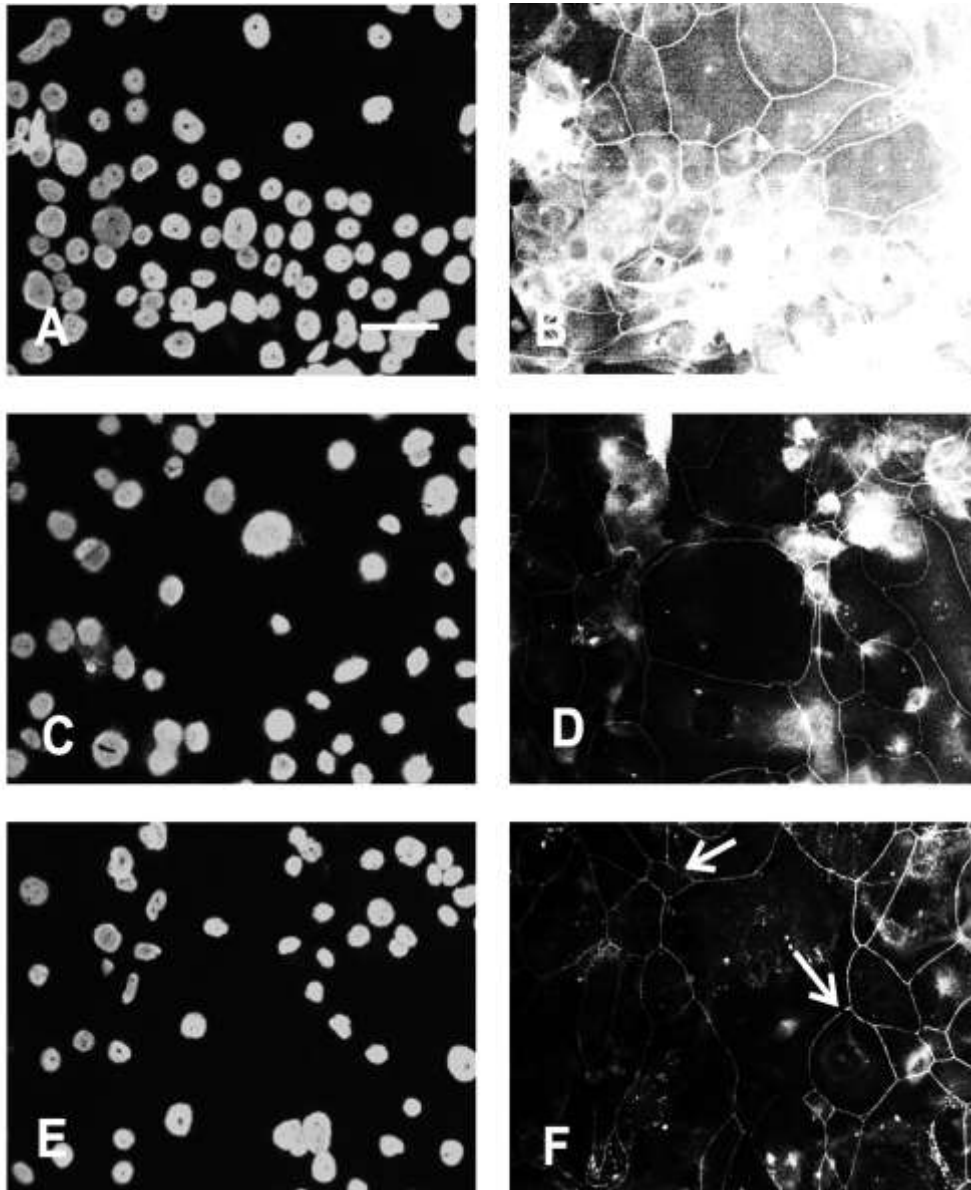
Figure 3-17a: ZO-1 labelling in differentiated NHU cells exposed to normoxia and acute exposure or pre-exposure to hypoxia.

Y1227 cell line is illustrated here. Images for ZO-1 labelling were taken at equal exposure (1/1.1s) (B, D and F) with Hoechst 33342 staining to identify nuclei (A, C and E). A –B were cells cultured and differentiated in normoxia, C- D cells were cultured in hypoxia, E-F cells were pre-exposed to hypoxia and transferred to normoxia. There was reduced clarity of ZO-1 labelling in both the hypoxia and pre-exposed cultures. Gaps in the cell membrane labelling for ZO-1 are arrowed in the pre-exposed image. Scale bar 50µm
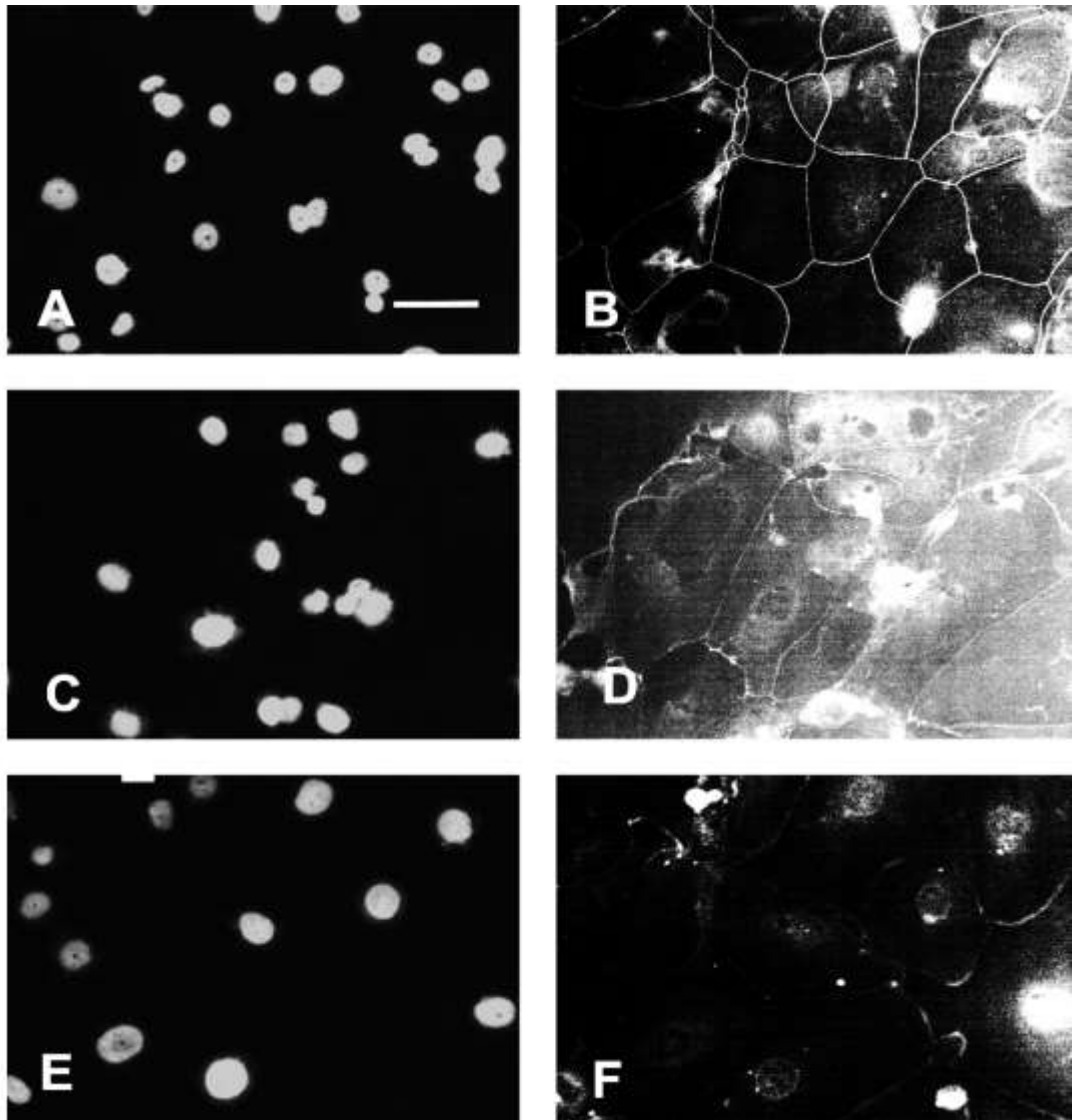
Figure 3-17b: ZO-1 labelling in differentiated NHU cells exposed to normoxia and acute exposure or pre-exposure to hypoxia.

Y1501 cell line is illustrated here. Images for ZO-1 labelling were taken at equal exposure (1/1.1s) (B, D and F) with Hoechst 33342 staining to identify nuclei (A, C and E). A –B were cells cultured and differentiated in normoxia, C- D cells were cultured in hypoxia, E-F cells were pre-exposed to hypoxia and transferred to normoxia. There was a reduction in the presence of ZO-1 in the cell membrane of cells cultured in hypoxia or pre-exposed to hypoxia. Scale bar 50μm
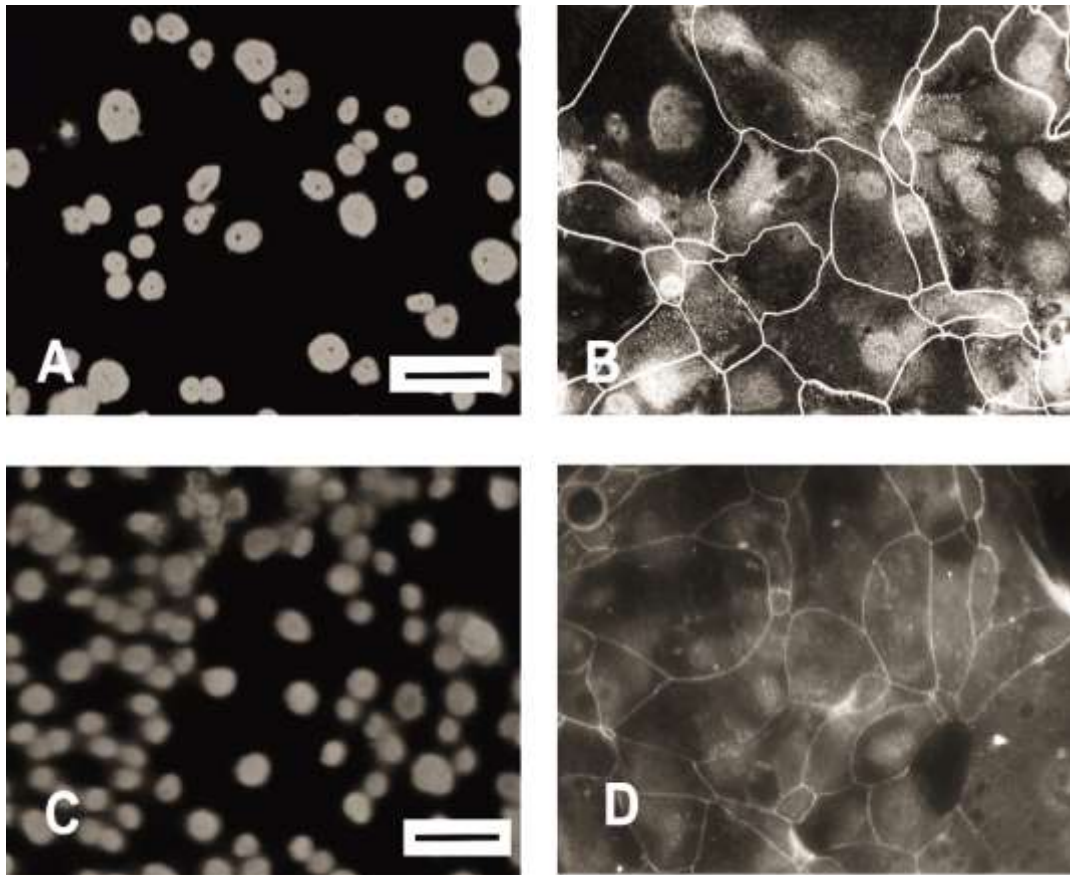
Figure 3-17c: ZO-1 labelling in differentiated NHU cells exposed to normoxia and acute exposure to hypoxia.

Y1483 cell line is illustrated here. Images for ZO-1 labelling were taken at equal exposure (1/1.1s) (B, D) Hoechst 33342 staining to identify nuclei (A, C). A –B were cells cultured and differentiated in normoxia, C- D cells were cultured in hypoxia. A lack of intensity in ZO-1 labelling is noted in the hypoxia maintained cells. Scale bar 50µm.
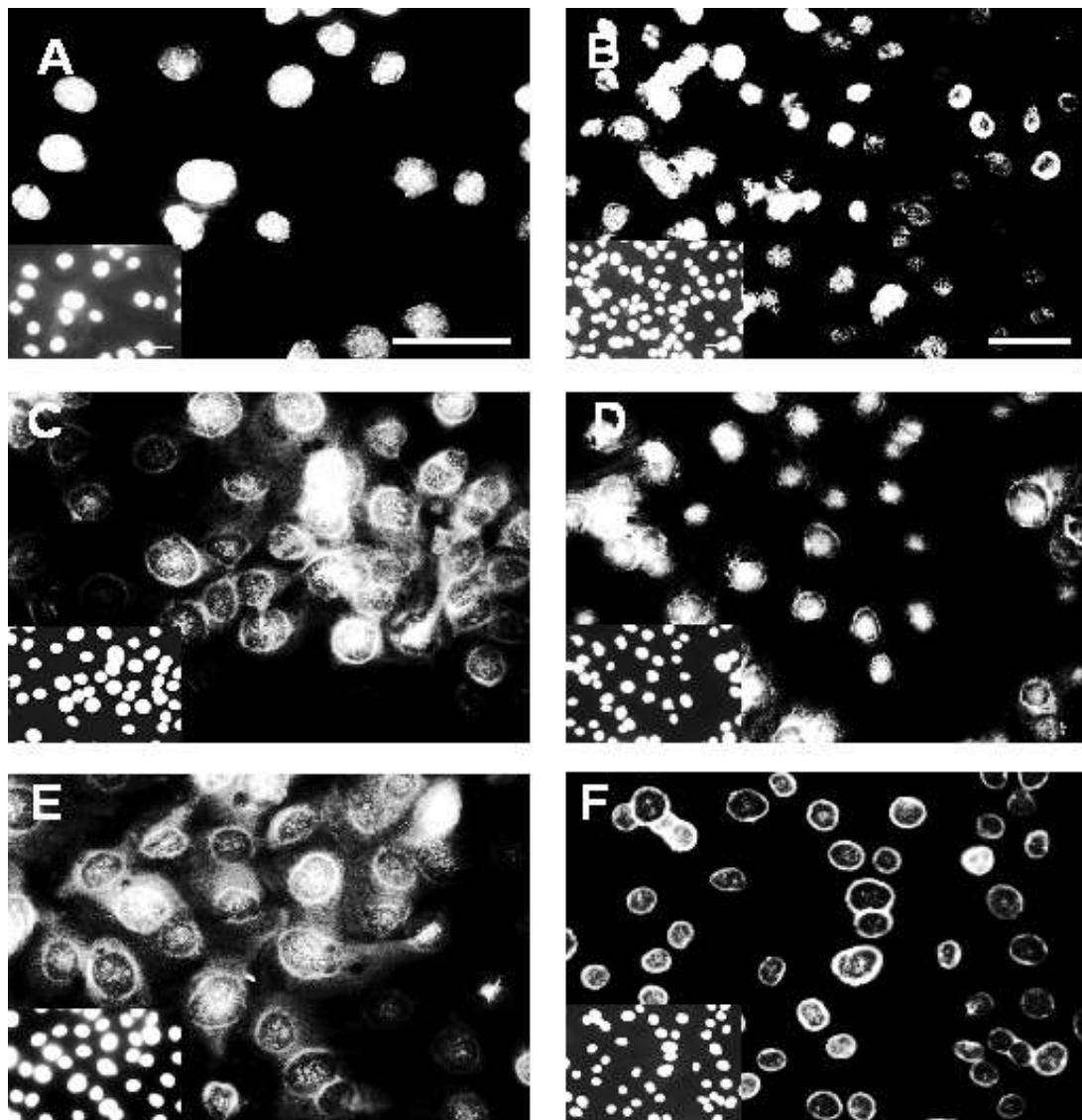
Figure 3-18: Immunocytochemistry labelling for H3K9Me2.

Differentiated NHU cells from two donors: Y1512 (A, C, E) & Y1689 (B, D, F) cultured in normoxia (A-B), hypoxia (C-D) or pre-exposed to hypoxia (E-F). Cultures were fixed, on glass slides, at the point that a stable barrier had been obtained in parallel TEER experiments. Images for H3K9Me2 labelling were taken at equal exposure for all conditions with variation between cell lines (1/1.5s and 1/1.8 respectively) with Hoechst 33342 staining for cell density (inserts). Images were taken using the x60 and x40 lens. Nuclear lamina location of labelling noted in some cases. Scale bar =50µm

3.2 Discussion

End-stage bladder disease is the result of multiple insults upon the entire organ, not specifically the urothelium. However prior knowledge that the urothelial cells taken from patients with end-stage bladder disease and cultured *in vitro* exhibit a compromised phenotype suggests that the urothelium is altered (Subramaniam et al., 2011). Increased levels of nuclear HIF-1α were seen both subjectively and quantitatively in the histology of end-stage bladder disease, particularly in those bladders associated with raised detrusor pressures (***Figs 3.3 – 3.6***). Based on these observations, hypoxia was used experimentally to mimic the *in vivo* insult the urothelium and evaluate any potential long-term "hangover" effects of exposure to hypoxia.

Proliferation occurred at significantly lower rates in the hypoxia-exposed cells compared to normoxic controls; this persisted through two sub-cultures (***Figs 3.7 – 3.8***). This is not necessarily surprising given the available literature supports hypoxia being a cause of cell cycle arrest (Goda et al., 2003). Micrograph images (***Fig. 3.9***) demonstrated that the majority of cells did not exhibit large, flat cell morphology, characteristic of cellular senescence. The mTOR pathway is thought to be important in the activation of cellular senescence and it has been reported that hypoxia inhibits the mTOR pathway, promoting a more quiescent culture, a state that is reversible (Brugarolas et al., 2004). Although the molecular basis was not investigated here, a reversible quiescence may well in part explain the recovery seen in cumulative cell number when cells were removed from hypoxia and subsequently cultured in normoxia (***Figs. 3.7A-C and 3.8***).

Urothelial cells isolated from end-stage diseased bladders have been reported to exhibit a reduced proliferative potential *in vitro* (Subramaniam et al., 2011), despite being removed from the pathological environment. Based on these preliminary results hypoxia alone does not appear to be a sufficient cause for this reported phenomenon. In this experimental model urothelial cells removed from a hypoxic environment retained proliferative potential. As a result when transferred to normoxia there was no significant difference between the mean cell number achieved in cultures maintained in normoxia and those pre-exposed to hypoxia. However there are many other pathological components to the adverse environment that exists within these bladders that may impact on the proliferative capacity *in vitro*; including recurrent infection and inflammation.

A compromised proliferative phenotype may also be contributed to by the loss of the urothelium, perhaps as a direct result of hypoxia, as suggested by the significantly increased presence of nuclear HIF-1α in neuropathic bladder sections *Figs 3.3 – 3.6.* The resultant loss of urothelium in neuropathic bladders may lead to reduced initial cell numbers in primary cultures derived from diseased samples. The impact of this is that there would be more population doublings needed to achieve confluence and subsequent premature cell loss due to culture senescence (Balin et al., 2002). The H&E staining and immunohistochemistry (particularly CK20, UPK3a and Cyclin D3) of organ cultures support this possibility by emphasising the loss of urothelium, particularly the superficial cells in both cultures `maintained and pre-exposed to hypoxia. Furthermore examination of the neuropathic bladder samples labelled for HIF-1α also demonstrated a "thinning" of the urothelium, with loss of both CK20 and UPK3a being a common characteristic, suggesting loss of superficial, terminally differentiated cells (*Figure 3-14* and **Appendix III**).

In the organ culture system there was loss of markers of differentiation and p63. P63 is closely associated with P53 and is vital for normal urothelial differentiation and loss of p63 is associated with high stage and poorly differentiated TCC (Koga et al., 2003) (Langner et al., 2003). The relationship between p63 and hypoxic activation of HIF-1α is not as straight forward. There are two analogues of P63 ΔNp63 and Tap63. The former is associated with increased nuclear HIF-1α activity and stem-cell like properties and the later with a reduction in HIF-1α activity. P63 has also been associated with regulation of the mTORC1 pathway in cancers; including those of childhood (Bid et al., 2014) (Amelio and Melino, 2015) and of DNA damage (Yu et al., 2013), and its loss may therefore impact upon the proliferation results.

Hypoxic conditions had an apparent detrimental impact on the ability for NHU cell lines to form a barrier upon differentiation (***Figs. 3.10 – 3.11***). The reason for this remains uncertain; however it is possible that there are multiple mechanisms responsible. Hypoxia can influence many gene targets (Semenza, 2001) and it may be that a wound response phenotype (Hong et al., 2014) predominates which may impact on success of differentiation when cells remain in hypoxic conditions.

The improvement in the mean TEER readings obtained in cultures transferred from a hypoxic environment to a normoxic one, compared to those that remained in hypoxia indicates that there is some recovery. Despite this significant compromise still exists in those cultures pre-exposed to hypoxia implying heritable processes are responsible. Such mechanisms may include epigenetic processes which would result in the persistent compromise of barrier structure and function seen in the pre-exposed cultures, even though the cells had been removed from the hypoxic environment (***Figs. 3.10 – 3.11***). As the mean TEER values for pre-exposed cultures did not recover to levels comparable to the normoxic controls a degree of inherited change is supported by this work.

The apparent relationship by immunocytochemistry between H3K9Me2 and hypoxia reflects other work in the literature (Kosakai et al., 1992). The change in localisation of H3K9Me2 to the nuclear lamina has been associated with areas of low gene expression called lamina associated domains (LADs) (Guelen et al., 2008). Two methylases that are instrumental in the mono- and dimethylation of histone three lysine nine (H3K9) are G9a and G9a-like protein (GLP), the latter sharing 80% sequence homology with the former. Huang et al (Huang et al., 2010) have published their findings on the impact of a mouse ESC G9a knockout) model on gene expression They concluded that in the knockout phenotype 167 genes were upregulated, with 119 genes overlapping with differentiated neural precursor cells; genes upregulated included members of the aquaporin, cytokeratin and GATA families – no genes were found to be repressed.

To conclude: experimentally induced hypoxia resulted in compromised proliferation and differentiation capacity in NHU cells. The proliferative compromise was alleviated by returning to normoxia. Urothelial cells that were proliferated in hypoxia and later differentiated in normoxia did demonstrate some improvement in barrier structure and function but there was a residual, significant reduction in barrier resistance achieved with associated poor ZO-1 expression on immunocytochemistry (*Fig 3.17a-b*) and altered H3K9Me2 localisation (*Fig 3.18*).The H3K9Me2 observation offers a potential epigenetic mechanism involving demethylation of H3K9 by G9a and G9a-like protein (GLP), or by another epigenetic mechanism. With the addition of a methylase inhibitor, dimethylation of H3K9 would be reduced and potentially ameliorate the persistent compromise of the differentiated urothelial phenotype.

The next chapter aims to investigate, within the constraints of the *in*-vitro model, the use of epigenetic modifying agents. If rejuvenation of the diseased cells is possible and a functional barrier can be obtained *in vitro*, this may have significant implications for autologous tissue engineering strategies for the urinary tract in the future.

4 Application of epigenetic modifying agents to urothelium compromised by hypoxia or neuropathy.

4.1 Background

As discussed in section **1.5.2** cultured NHU cells, taken from diseased bladders, are reported to have a compromised phenotype, despite being removed from the environment of the diseased bladder (Subramaniam et al., 2011). Results from Chapter Three suggest that exposure to hypoxia impacted upon both the *in vitro* proliferating and differentiated urothelial phenotype The compromised differentiated phenotype persisted, like those of urothelial cells taken from diseased bladders, despite being removed from the hypoxic environment; thus indicating a potential epigenetic mechanism. This was further supported by immunocytochemistry which demonstrated a switch from homogeneous nuclear expression to a more defined nuclear lamina localisation of the dimethylation mark H3K9Me2.

G9a (EHMT2) and G9a-like protein/GLP (EHMT1) are ubiquitously expressed euchromatic histone lysine methylases (HKMTs) and belong to the SUV39h subgroup of Su (var) 3-9-Enhancer of *zeste* Trithorax (SET) domain-containing molecules. G9a and GLP are commonly found as a heteromeric complex and are responsible for mono- and dimethylation at histones H1 and H3 at lysines 9 and 27 in mammals (Tachibana et al., 2002, Tachibana et al., 2005). Non-histone substrates of G9a/GLP have also been identified, including p53 (Chuikov et al., 2004), however the biological impact of methylation at these sites is not yet fully understood.

A significant amount of research into the varied biological roles of G9a/GLP methylation has already reported. The majority of this work has been performed using a mouse G9a or GLP knock-out model. The importance of G9a and GLP to mouse development has been shown by virtue of the fact that both G9a and GLP knockout models lead to significant growth defects and embryonic lethality (Tachibana et al., 2002, Tachibana et al., 2005).

Dimethylation of H3K9 is found abundantly at repressive loci (Barski et al., 2007) and CpG islands (Lienert et al., 2011) predominantly at the nuclear lamina (Guelen et al., 2008). In developmental biology gene repression is broadly associated with the differentiated phenotype (Meissner et al., 2008); therefore G9a/GLP have been implicated in differentiation of several cell types including haematopoietic stem cells (Chen et al., 2012) and recently linked to the inhibition of PPARγ in adipogenesis (Wang et al., 2013). The latter is an interesting finding as PPARγ is thought to be central to the differentiation of urothelium (Varley et al., 2004).

G9a methylation of H3K9 has been shown to have a role in pathogenic T-cell responses to inflammatory bowel disease in a mouse colitis model (Antignano et al., 2014) by restricting both Th17 and Treg differentiation. Specific cytokine gene expression (IL-4, IL-5, and IL-13) has also been shown to be reduced in the G9a knockout mouse, increasing susceptibility to parasitic infection (Lehnertz et al., 2010). Other impacts on the immune system extend to B-cell function. G9a-deficient B cells have compromised proliferative capacity and ability to differentiate into plasma cells after stimulation by lipopolysaccharide (LPS) and IL-4 (Thomas et al., 2008).

Other roles for G9a/GLP in disease include: upregulation in human cancer cells with knockdown models demonstrating suppression of tumour growth, invasion (Kondo et

al., 2008) and metastasis by altering cellular adhesion (Chen et al., 2010); altered cognition and adaptive behaviour (Schaefer et al., 2009, Kleefstra et al., 2012), sub-telomeric deletion syndrome (Kleefstra et al., 2005) and cocaine-induced plasticity as a contributory mechanism for addiction (Maze et al., 2010).

Specific inhibitors for G9a and GLP have been developed. Despite initial problems with developing a significant difference between toxic and functional doses currently the more recent inhibitors have promising pharmacokinetic profiles (Liu et al., 2010). Sensori-neural hearing loss as a result of hair cell damage has been identified as potentially due to G9a/GLP increasing levels of H3K9Me2 (Yu et al., 2013). The same work also reports the benefits of using two inhibitors BIX01294 and UNC0638 on a mouse damage model with reduction in H3K9Me2 seen and cell death reduced.

In cancer therapy epigenetic modifying agents have been used to target HIF1α because of its role in both tumour cell survival and chemo-radiotherapy resistance (Schwartz et al., 2010). One family of drugs investigated have been the histone deacetylase inhibitors (HDACi); the role of such substances has been extensively reported in the treatment of malignant disease (Kim et al., 2011). It is thought that HDACi, such as trichostatin A (TSA), destabilises HIF1α by affecting the transactivation potential and the interaction between p300/CBP (Fath et al., 2006) and thus potentially preventing the transcription of downstream targets such as vascular endothelial growth factor (VEGF) to prevent angiogenesis. TSA and valproic acid (another HDACi) have been used by Atala *et al*, reportedly with some success, in an attempt to reduce aberrant collagen production by smooth muscle cells derived from neuropathic bladders (Hodges et al., 2010). Valproic acid has also been shown to improve ZO-1 expression in burn-injured gut epithelium (Costantini et al., 2009).

Chapter 4: Application of epigenetic modifying agents to urothelium compromised by hypoxia or neuropathy

Regenerative medicine applications in paediatric urology: barriers and solutions

Given the literature and the results from Chapter Three inhibition of G9a/GLP in order to reduce H3K9 dimethylation and HDAC inhibition may rejuvenate the compromised differentiated phenotype of the NHU cells that have been pre-exposed to hypoxia. Such observation may improve the outcome of autologous tissue engineering solutions for end-stage bladder disease.

4.2 Aims

- To determine the effects of epigenetic modifiers upon urothelial differentiation in cultures compromised by hypoxia or neuropathy by measuring markers of proliferation, differentiation and function.

- To assess phenotypic effects of direct application of epigenetic modifying agents to normal human urothelium using an *in vitro* approach using by measuring markers of proliferation, differentiation and function.

4.3 Experimental Approach

4.3.1 Examine the effects of epigenetic modifiers upon urothelial differentiation in cultures compromised by hypoxia or neuropathy.

Using flow scheme C, shown in *Figure.4-1*, cells from three different donors were differentiated using the ABS/Ca^{2+} model. After five days of 5 % ABS treatment, calcium was added to achieve a final concentration of 2 mM but with the addition of a non-cytotoxic dose of either Trichostatin A (TSA) or UNC0646, or a combination of both epigenetic modifying agents in 0.1% DMSO (vehicle control). This was maintained throughout the final stage of differentiation by including the treatment at every medium change.

The timing and method of application of epigenetic modifiers was chosen based on previous results and available literature. Firstly the modifying agents would need to be administered after exposure to hypoxia had taken place and the switch to normoxia had occurred. This would ensure that any direct compromise that hypoxia caused would have been ameliorated by the switch to normoxia, leaving only persistent alterations to the phenotype.

To evaluate the direct effects of epigenetic modifiers on the capacity of cultures to differentiate and form a tight barrier, TEER was measured. For each of the three biological replicates (cell lines), each treatment condition had three to five technical replicates, with a total of 11 measurements Analysis of barrier recovery after wounding as in Chapter Three was also performed.
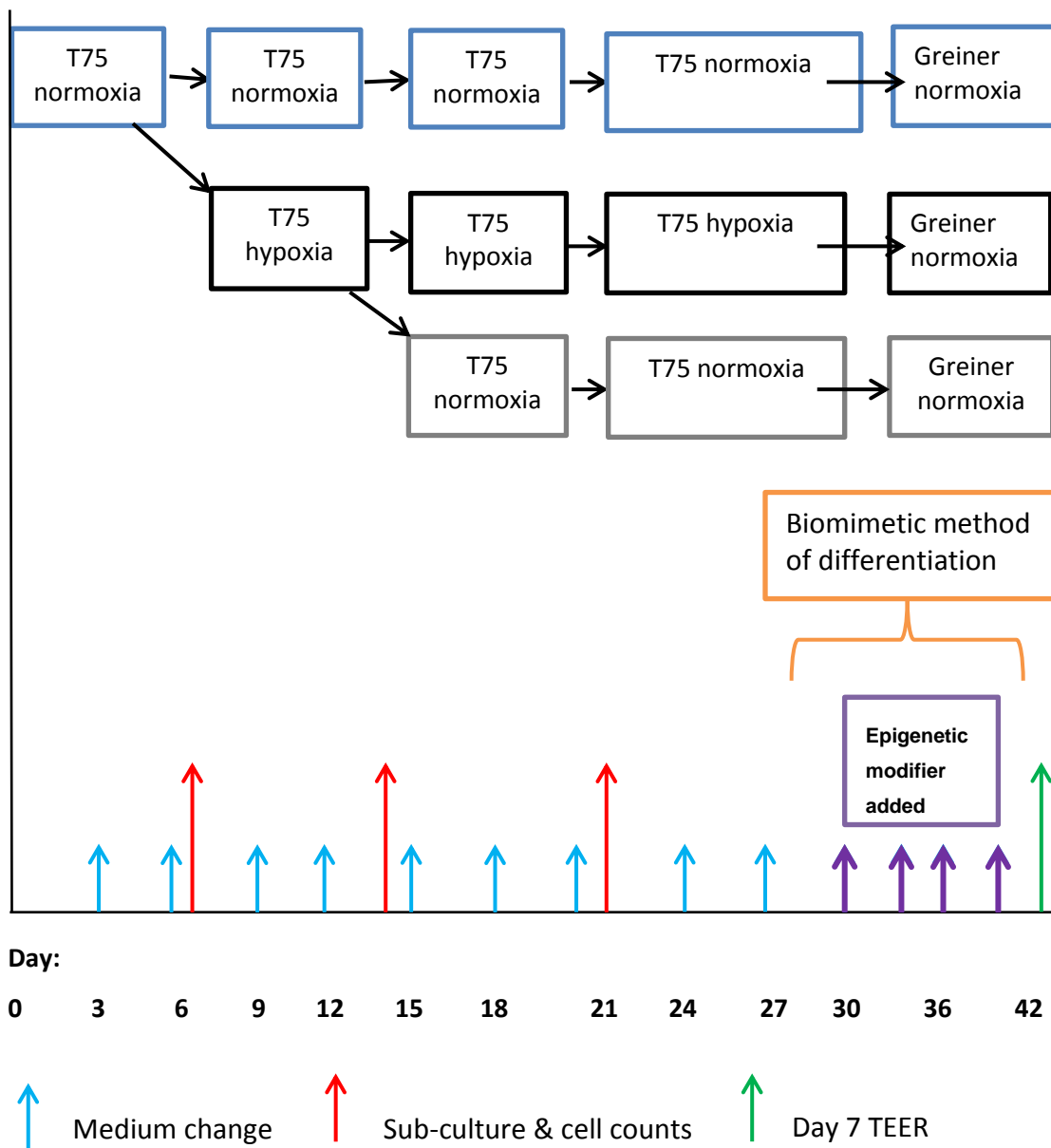
Figure 4-1: Flow scheme C - addition of epigenetic modifiers

Protein lysates and RNA were obtained from the cell culture inserts, for each of the conditions for further analysis of transcript and protein expression. The ribosomal subunit 28S was used as a housekeeping gene as a marker of equal loading. The reason for choosing 28S instead of a more conventional housekeeping gene, such as GAPDH, was that hypoxia, through hypoxia activated pathways, is reported to alter transcript abundance in commonly used genes; but not 28S (Zhong and Simons, 1999, Caradec et al., 2010b, Caradec et al., 2010a).

Immunocytochemistry was performed at the same time as that reported in Chapter 3 with control (DMSO) and treatment cultures maintained on multiwell glass slides. These slides were removed from culture medium and fixed using methanol:acetone (**section 2.10.1.1**). Immunocytochemistry was performed to assess markers of differentiation and barrier formation.

Neuropathic bladder-derived cell lines were used for validation of the experimental model. They had been pre-exposed to the environment of the diseased bladder and subsequently expanded *in vitro* and compromise to the phenotype should already be present. All neuropathic cell culture work was performed in normoxic conditions

Three cryopreserved neuropathic cell lines (sub-culture 1 or 2) were expanded in T25 flasks until confluent. Smaller area plasticware was used to reduce the number of cell divisions and inhibit culture senescence where possible. Neuropathic cultures were then sub-cultured once only into a T75 flask and differentiated along the normoxic condition pathway in *Figure.4-1*. After four days in 5 % ABS they were again sub-cultured and resuspended at a density of 1×10^6 cells/ ml of which 500 μL was seeded into Greiner Thin-CERT ™inserts. The following day calcium was added (final

concentration 2 mM) along with either UNC0646 (500 nM) or DMSO (0.1 %) and TEER monitored until a stable barrier was obtained.

4.3.2. Investigate whether epigenetic modifying agents result in phenotypic changes within the urothelium using an *in-vitro* approach.

Three ureteric tissue donor samples were detubularised to create a flat sheet and 5mm x 5mm pieces were dissected. Representative pieces were fixed in 10% formalin for histological analysis (native tissue). The other sections were maintained on cell culture inserts (Falcon ®) in normoxic, hypoxic or pre-exposed conditions (**Figure 4-2**). After 2 weeks either UNC0646 500nM or DMSO (0.1%) was added to the medium with each medium change for one week. Three replicates were created for both control and treated organ cultures in Y1593 and Y1657. In donor Y1713 pieces were created for organ culture allowing for samples to be fixed for histology on days 1, 2, 3, 5 and 7 in both the treatment and control arms but with an *n=1*. This was to permit time-point analysis of the tissue for any phenotypic changes by immunohistochemistry.
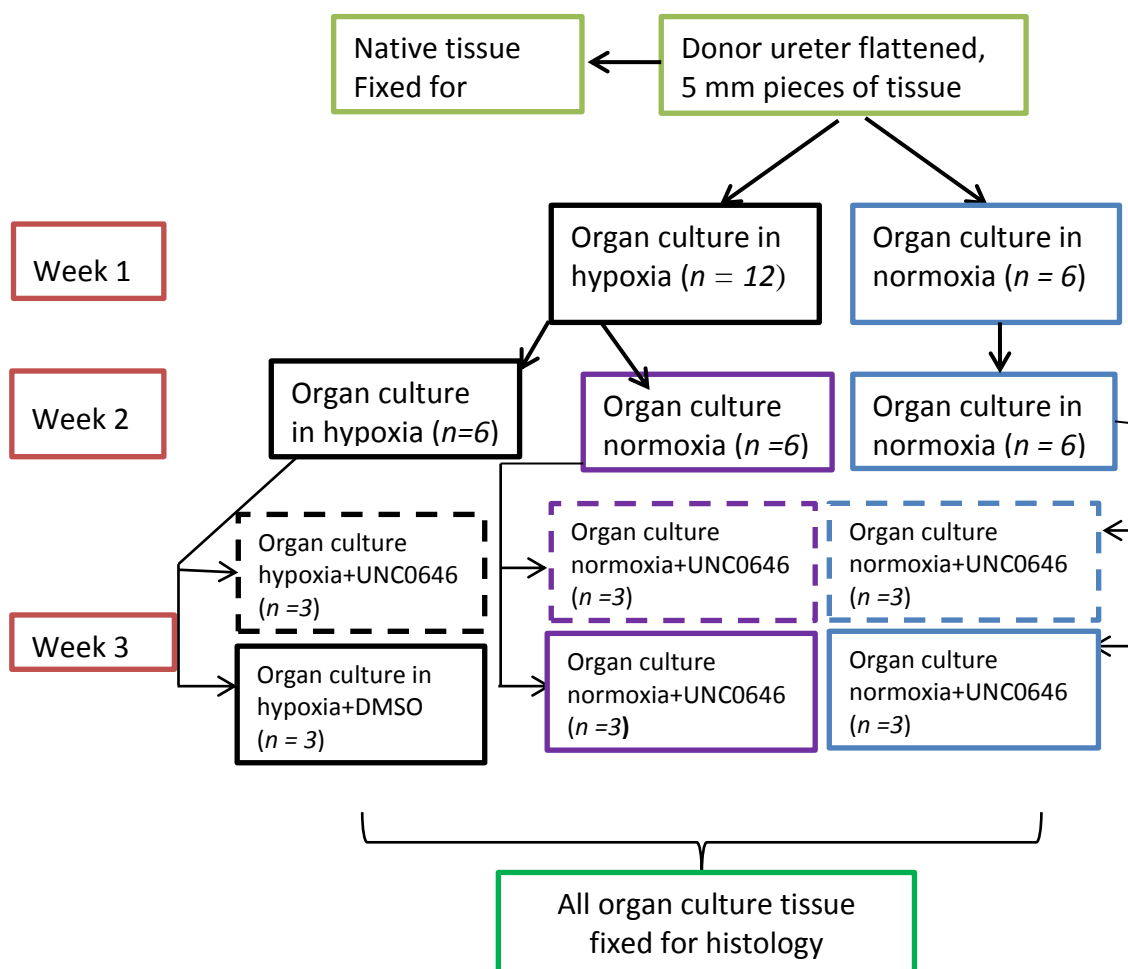
Figure 4-2: Flow-scheme D: Organ culture with epigenetic modifier treatment

Ureteric tissue samples (Y1539, Y1657 & Y1713) were detubularised and 5mm x 5mm pieces were created. Representative pieces were fixed in 10% formalin (native tissue). Organ cultures was also set up in hypoxic or pre-exposed conditions After 2 weeks (pre-exposed organ cultures had been in normoxic conditions for 7 days) either UNC0646 500nM or DMSO (0.1 %) was added at medium changes for 1 week. Y1593 and Y1657 had three technical replicates (see above). At day 7 the organ cultured tissue was removed from culture and fixed in 10 % formalin and processed into paraffin wax for histology.

Primary antibodies were selected to proteins considered to be hallmarks of urothelial phenotype and function, including squamous and proliferative phenotypes (CK14 and Ki67, respectively). Labelling for HIF1α was performed; should hypoxia-related pathways have been active then a more nuclear localisation would be expected (**section 1.5.4**)

To permit image analysis, slides of HIF1α labelled organ culture specimens were scanned on a **Zeiss AxioScan.Z1 slide scanner.** HistoQuest (TissueGnostics) image analysis software was utilised to determine the intensity of HIF-1α labelling in every urothelial nuclei in all donor sections, using the method described in section **2.9.2.1**. This raw data enabled both descriptive and non-parametric statistical analysis to be performed.

4.4 Results

4.4.1 To determine the effects of epigenetic modifiers upon urothelial differentiation in cultures compromised by hypoxia or neuropathy.

Both UNC0646 and TSA were well tolerated at the doses used, with all cell lines and conditions able to produce a stable barrier > 500 $\Omega.cm^2$ within 10 days. There was no decrease in TEER values in the treatment arms compared to the DMSO controls.

4.4.1.1 Effect of UNC0646 on barrier formation and function

In two of the three cell lines: Y1227 (***Fig. 4-3a***) and Y1512 (***Fig. 4-3c***) the addition of 500nM UNC0646 did not significantly change the mean TEER values in cultures maintained in either normoxic or hypoxic environments. Y1483 (***Fig. 4-3b***) showed a mean increase of 1823 $\Omega.cm^2$ when UNC0646 was included. However, as seen with Y1227 and Y1512, the TEER readings in the hypoxia cultures were not improved by the addition of the G9a/GLP inhibitor.

Exposure and pre-exposure to hypoxia did compromise barrier formation in all three cell lines. The compromise seen in the pre-exposure cultures was improved with the addition of UNC0646 in all three cell lines by the final TEER reading; this was not replicated in cultures maintained in hypoxic conditions (***Table 4-1***).

Table 4-1: Summary of mean final TEER readings

Cell line	Culture condition	Mean TEER/ $\Omega.cm^2$ ($\pm$s.d.) + UNC0646	Mean TEER/ $\Omega.cm^2$ ($\pm$s.d.)$-$ UNC0646
Y1227	Normoxic	2228.6 ($\pm$ 227.31)	2218 ($\pm$ 133.33)
	Hypoxic	1033.5 ($\pm$ 119.54)	879.8 ($\pm$ 73.26)
	Pre-exposed	2122.00 ($\pm$ 198.33)	1486.20 ($\pm$ 204.89)
Y1483	Normoxic	3910 ($\pm$ 299.83)	2076 ($\pm$ 679.41)
	Hypoxic	951 ($\pm$ 118.20)	711 ($\pm$ 22.76)
	Pre-exposed	3560.00 ($\pm$ 376.65)	1008.67 ($\pm$ 118.20)
Y1512	Normoxic	2636.67 ($\pm$ 416.52)	3203.33 ($\pm$ 220.66)
	Hypoxic	910.67 ($\pm$ 15.63)	1023.67 ($\pm$ 15.11)
	Pre-exposed	3513.33 ($\pm$ 487.10)	1803.33 ($\pm$ 235.02)

The ability for UNC0646 to improve barrier function in cultures pre-exposed to hypoxia was retained when the stable barrier had been wounded, illustrated in *Figure 4-4*. All barriers returned to pre-wounding levels. This included hypoxia pre-exposed populations with the recovered barrier only 12 $\Omega.cm^2$ less that the stable barrier achieved pre injury, despite the UNC0646 no longer being applied.

Analysis of normalised mean TEER values from all three cell lines permitted ANOVA with Tukey multiple comparison post-test statistical analysis to be performed. This

provided a measure of how significant the improvement in TEER values was in the UNC0646 treated group compared to the controls (***Fig. 4-5***). A very significant

difference was found between the mean TEER of normoxia vehicle controls and both the hypoxia and pre-exposed controls ($p < 0.001$). No difference was observed between the hypoxia and pre-exposed TEERs. When UNC0646 was added to pre-exposed cultures there was a significant improvement in TEER values compared to the pre-exposed controls ($p < 0.001$).

A
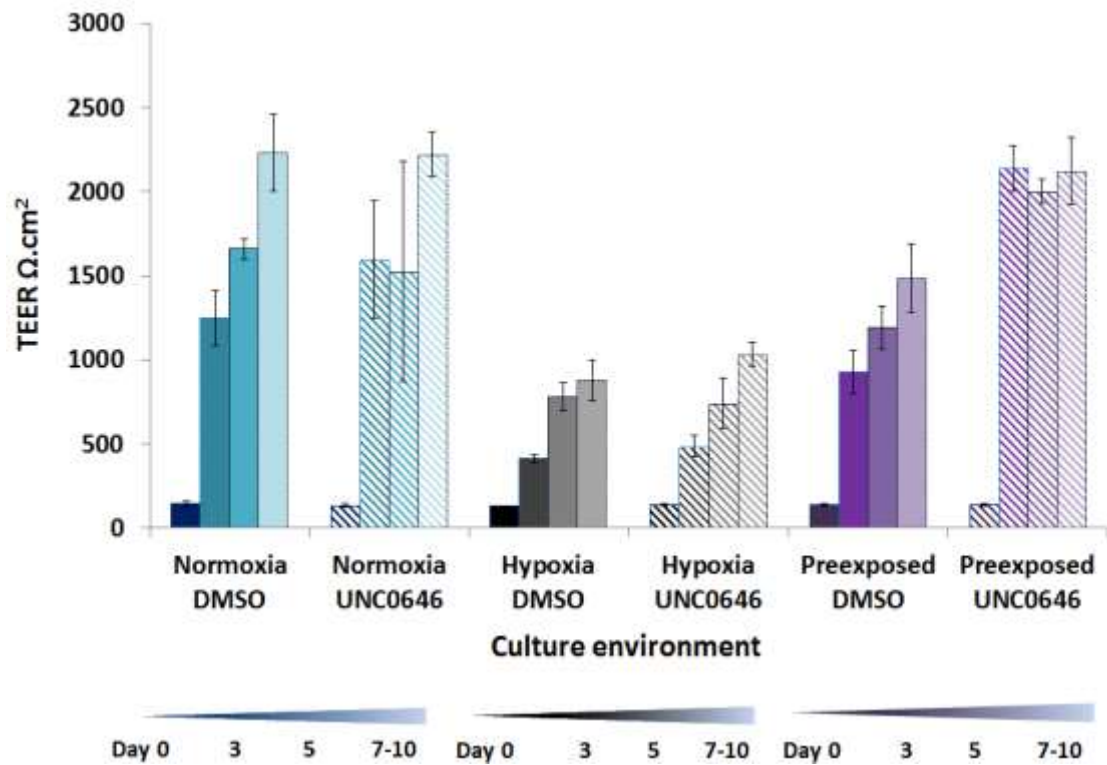
Figure 4-3A: Mean TEER obtained using the Y1227 cell line cultured in normoxia, hypoxia or pre-exposed ± 500 nM UNC0646.

TEERs were measured until the barrier had been stable for at least 48 hours. All groups had n=5. Controls are shown in solid bars, UNC0646 in lined bars and standard deviations are shown. A stable TEER in this cell line was obtained by 10, all cultures were differentiated and had TEERs measured over the same 10 days.

B
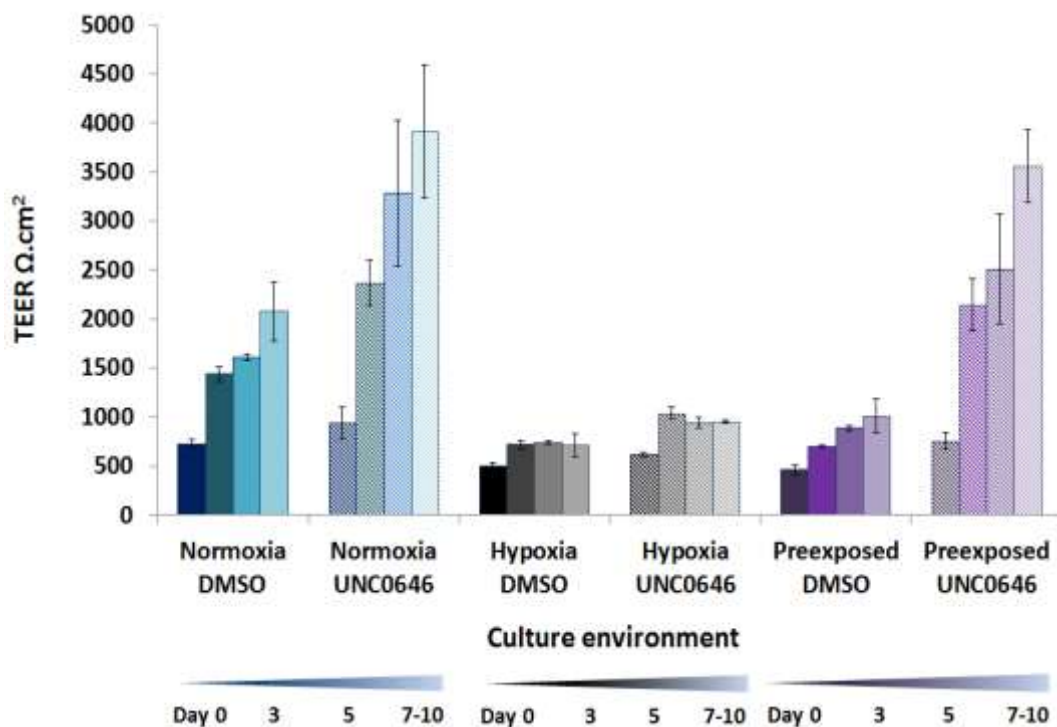
Figure 4-3B: Mean TEER obtained using Y1483 cell line cultured in normoxia, hypoxia ore pre-exposed ± 500nM UNC0646

TEERs were measured until the barrier had been stable for at least 48 hours. All groups had n= 3. Controls are shown in solid bars, UNC0646 in lined bars and standard deviations are shown. A stable TEER in this cell line was obtained by day 8, all cultures were differentiated and had TEERs measured over the same 8 days.

C
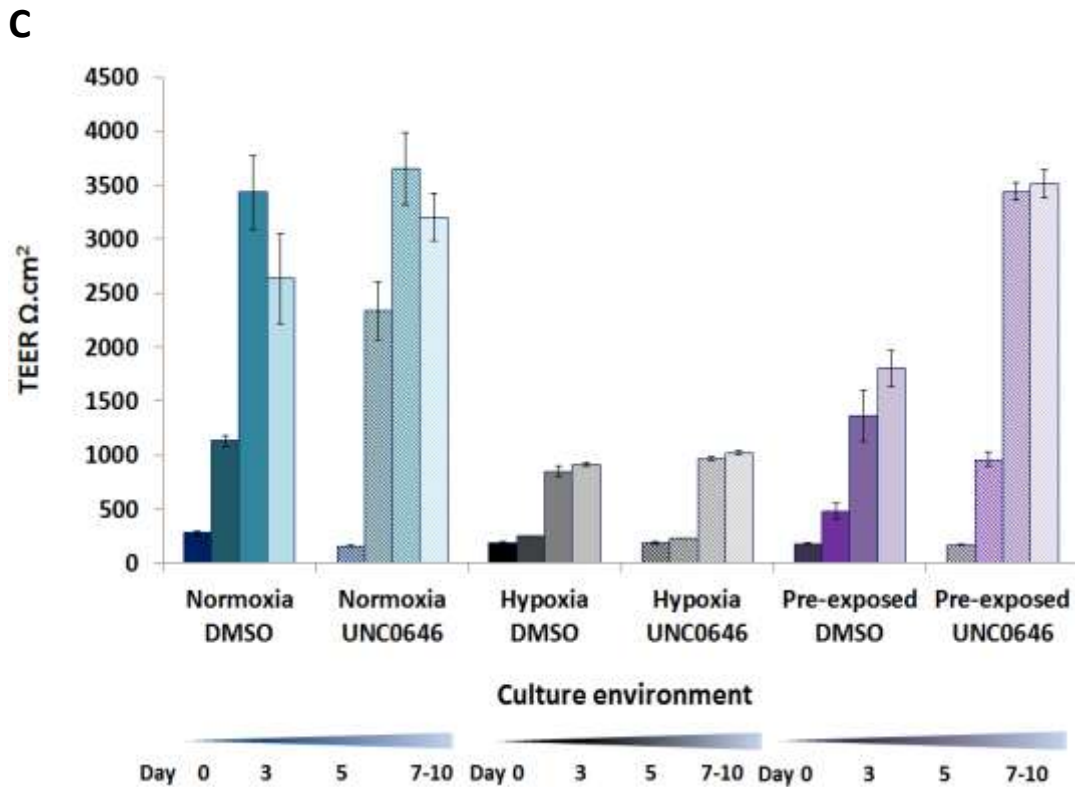
Figure 4-3C: Mean TEER obtained using Y1512 cell line cultured in normoxia, hypoxia or pre-exposed ± 500 nM UNC0646

TEERs were measured until the barrier had been stable for at least 48 hours. All groups had n=3. Controls are shown in solid bars, UNC 0646 in lined bars and standard deviations are shown. A stable TEER in this cell line was obtained by day 7, all cultures were differentiated and had TEERs measured over the same 7 days.
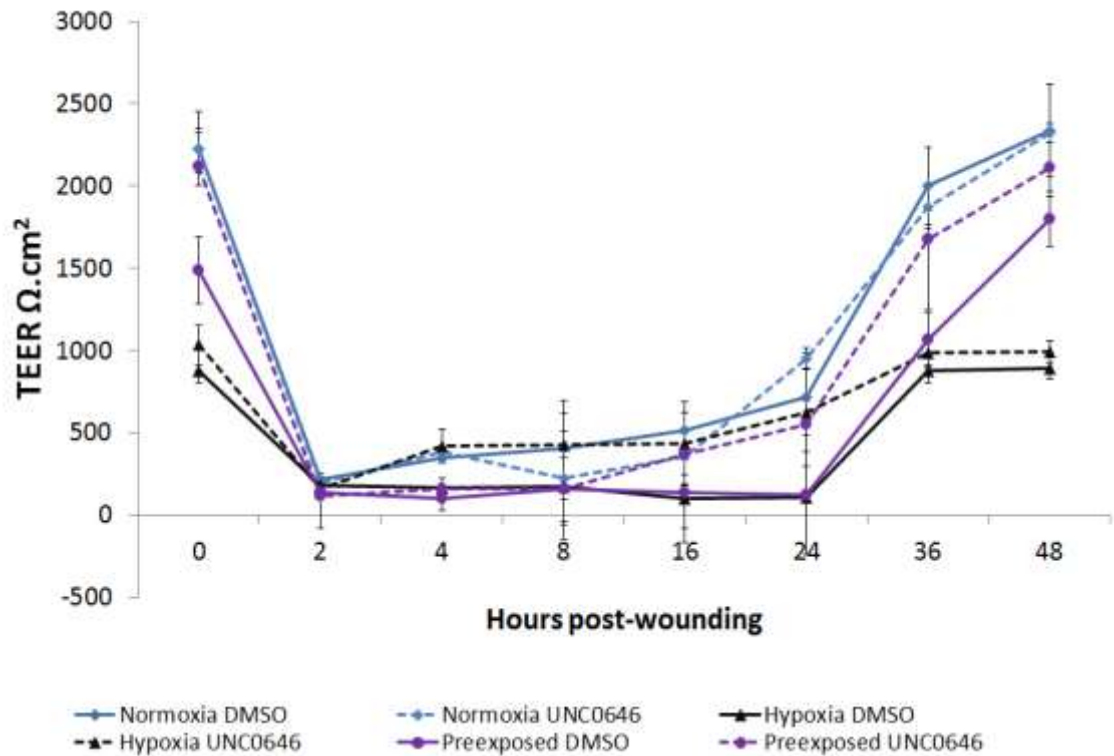
Figure 4-4: Barrier recovery after wounding off differentiated NHU cell culture (Y1227) exposed to normoxia, hypoxia and pre-exposed to hypoxia ± 500 nM UNC0646

TEER values were obtained regularly until a stable barrier was obtained for 2 days. The TEER at this point is represented by time 0 hours on this graph. Scratch wounding of the cell sheet was then performed in 3 technical repeats (n=3). TEER readings were obtained at regular intervals until a pre-wounding TEER was achieved. Error bars represent s.d. of the mean for three technical replicates.
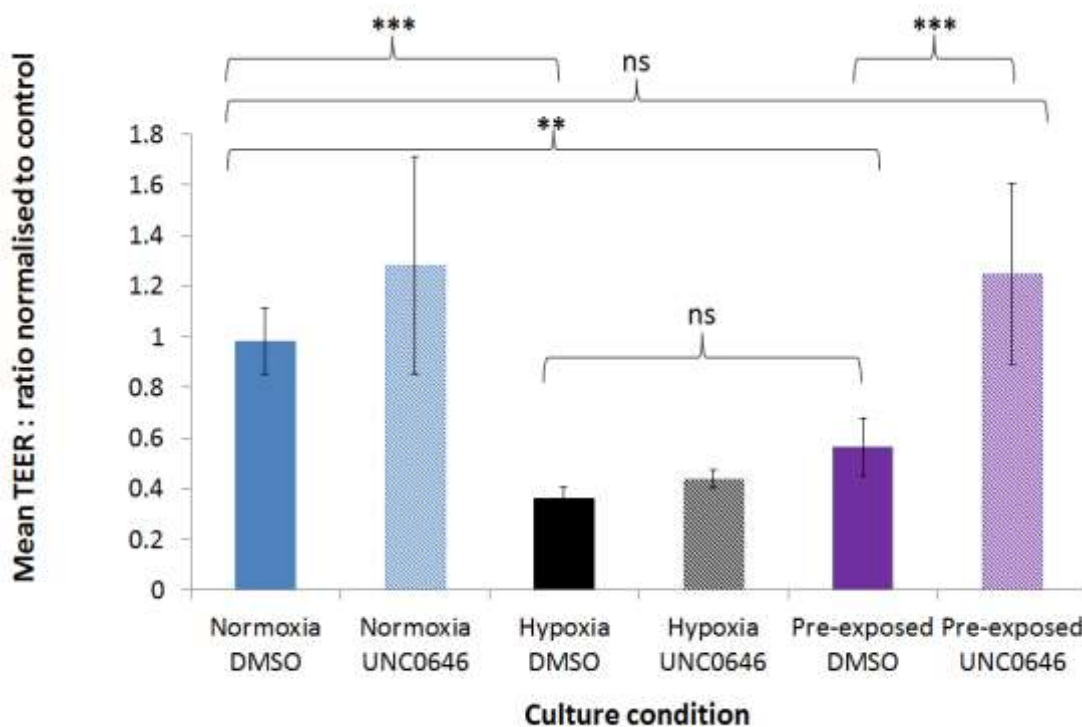
Figure 4-5: Final TEER reading for NHU cell cultures maintained in normoxic, hypoxic or switched (hypoxic to normoxic) ± the addition of UNC0646.

The mean stable TEER values in the normoxia controls were used as a normalising value for each cell line/ biological replicate. All data for TEER readings were then converted, using the control value to produce comparable data across all three cell lines; n=11. Standard deviations are shown. Normalisation enabled the data to be analysed statistically without being affected by inter- cell line variation. The result of the ANOVA analysis with Tukey multiple comparison performed post-test is shown on the chart and data Table 4a (ns = not significant, ***=p<0.001)

4.4.1.2 The effect in organ culture of UNC0646 on HIF-1α expression

Given that UNC0646 did not impact on hypoxia exposed barriers directly it was interesting to evaluate the impact of UNC0646 on nuclear HIF-1α immunohistochemical labelling in organ cultures exposed to normoxia and persistent/pre-exposure to hypoxia with and without the addition of UNC0646 (***Fig. 4-6***). A summary of Y1689 data is illustrated in ***Figure 4-7*** and a similar chart for Y1535 can be found in the Appendix IV. Both charts exhibit similar results with no marked difference in the intensity of HIF-1α labelling between normoxia, hypoxia and pre-exposed conditions. There was however a noticeable reduction in the median labelling intensity between the untreated and UNC0646 treated nuclei in all three conditions. Given the number of donors and technical replicates it was not possible to make any meaningful statistical analysis.
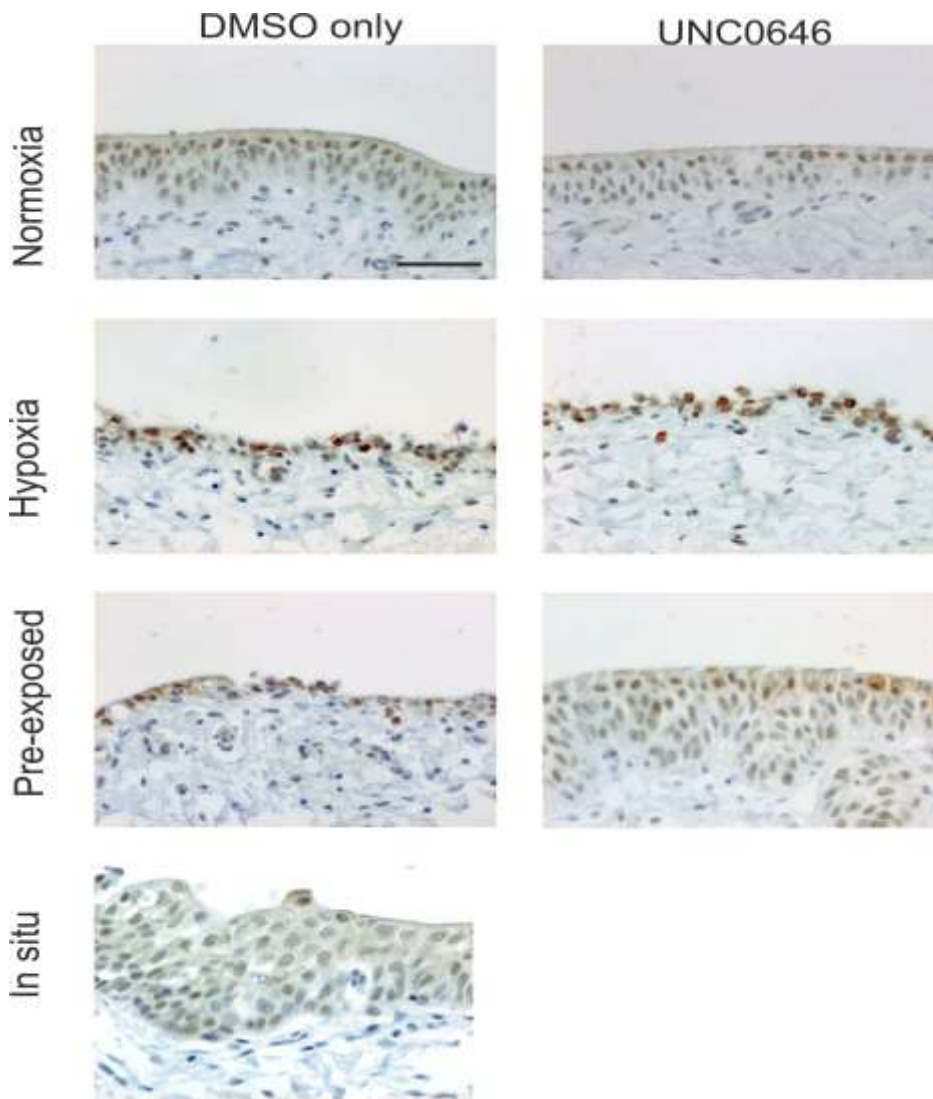
Figure 4-6: Immunoperoxidase labelling of HIF1-α in organ cultures ± UNC0646

The urothelium in organ cultures pre-exposed to hypoxia was "thinned" in appearance in comparison to normoxia controls. In both Y1593 and Y1657 the addition of UNC0646 for seven days did not alter the histological appearance in the normoxia controls but did improve the thickness and morphology of the urothelial layer in treated pre-exposed cultures by day 21. Scale bar = 50 μm
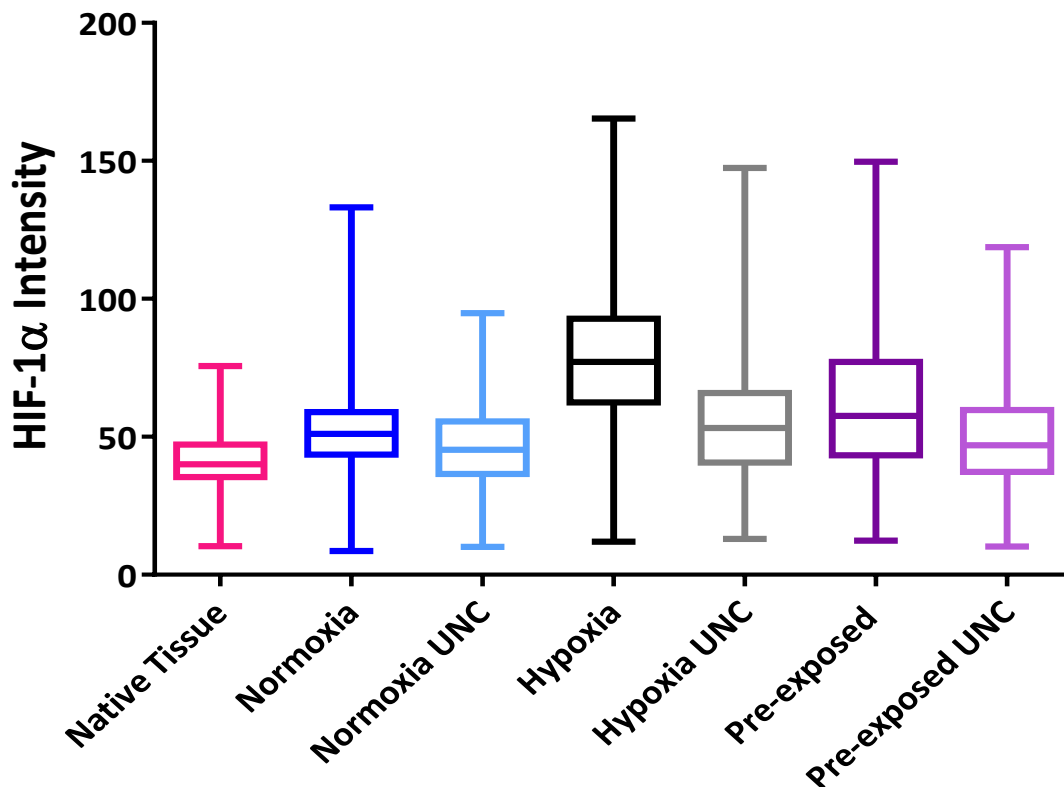
Figure 4-7: Box and whisker chart depicting nuclear HIF-1α labelling intensity in organ culture urothelium maintained in normoxia, hypoxia and pre-exposed to hypoxia ± UNC0646.

Comparison was made between the median HIF-1α intensity of urothelial nuclei within sections of all organ culture (OC) maintained in normoxia, hypoxia or pre-exposed conditions ± 500 nM UNC0646 and native tissue with three replicates per condition. All sections were maintained in organ culture for 21 days. Each datum point analysed represented a single urothelial nucleus, from a single donor (Y1689) from all three replicates. Total number of nuclei analysed was: native tissue n = 4086, normoxia n = 2121 (+ UNC0646 = 1386), hypoxia n= 1870 (+ UNC0646 = 2714), pre-exposed n=2724 (+ UNC0646 = 1137). IQR is shown within the boxes with the median represented by the horizontal line within. Whiskers illustrate the full range of labelling intensities. Box and whisker chart for Y1593 can be found in Appendix IV.

RT-PCR (*Fig. 4-8*) to assess for the presence of the HIF-1α transcript expression produced clean bands at approximately 686 base pairs. All three cultures maintained in hypoxia (H1-H3) produced negligible bands, particularly when compared to those obtained from cultures in normoxia (N1-N3). Pre-exposed samples did not produce consistent results across the three cell lines but the addition of UNC0646 did produce more prominent bands in cell line 2 (PU2) compared to the same cell line maintained or pre-exposed to hypoxia.

mRNA transcripts associated with hypoxia were investigated using RT-PCR (*Figure 4-9*). In three out of four cell lines there was an associated increase in the band intensity for lactate dehydrogenase A (LDHA) in samples harvested from hypoxia-maintained cultures compared to normoxia. Vascular endothelial growth factor (VEGFA) did not appear to demonstrate any subjective difference between normoxic and hypoxic cultures except in one cell line (Y1594).
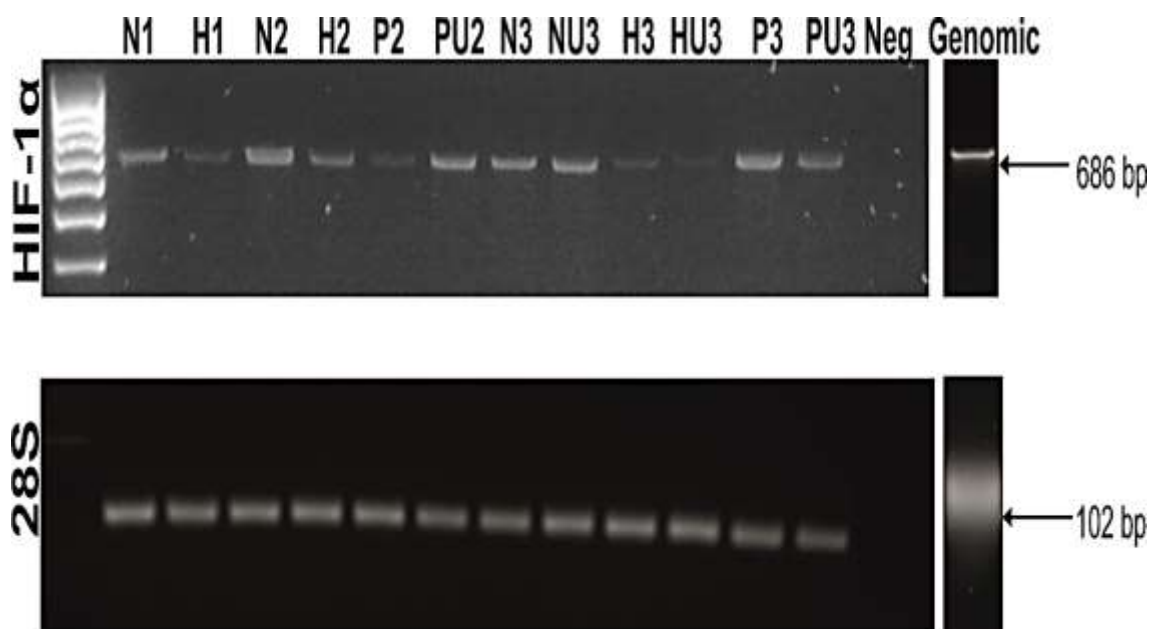
Figure 4-8: Transcript expression of HIF-1α by NHU cells cultured in vitro in different conditions ± UNC0646

RNA from three NHU cell lines Y1227, Y1594, Y1483(1-3), cultured in normoxia (N), hypoxia (H), pre-exposed (P) to hypoxia for 28 days ± the addition of UNC0646 (U) in the last seven days was screened for the presence of HIF-1α mRNA by RT-PCR. The expected size of PCR product was located at 686 base pairs (28S at 102 base pairs). Control PCR product samples are shown in which H_2O substituted template to demonstrate no contamination. Negative control reactions, with omission of reverse transcriptase (RT negatives) were included to demonstrate the absence of contaminating DNA (see Appendix IV). Positive template control (genomic) shown performed on prior HIF-1α PCR with the same samples but sub-optimised for determining variation.
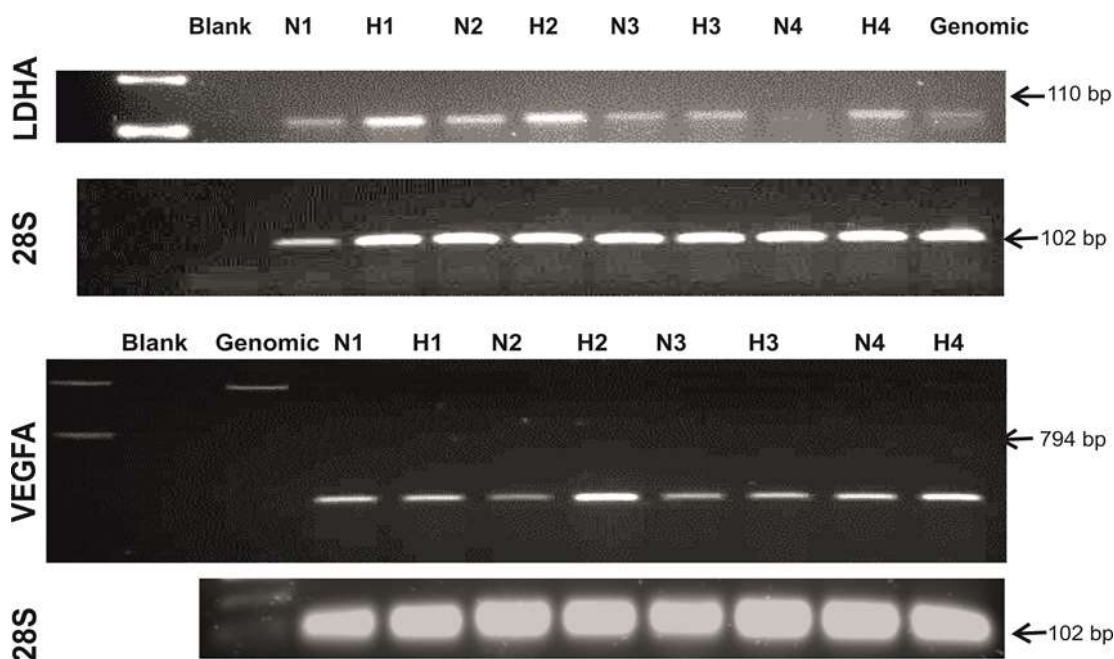
Figure 4-9: RT-PCR of hypoxia-related transcripts in four cell-lines

RNA from four differentiated NHU cell lines Y1227, Y1594, Y1483, Y1431 (1-4) cultured in normoxia (N) or hypoxia (H) for 35 days, was screened for the presence of lactate dehydrogenase A (LDHA) and vascular endothelial growth factor A (VEGFA) mRNA by RT-PCR. The expected sizes of PCR products were located at 102 base pairs and 794 respectively (28S at 102 base pairs). Blank PCR samples are shown in which H_2O substituted DNA to demonstrate no contamination. Negative control reactions, with omission of reverse transcriptase (RT negatives) were included to demonstrate the absence of contaminating DNA (see Appendix IV). Positive template control (genomic shown.)

4.4.1.3   Addition of TSA on barrier formation and function

The addition of Trichostatin A (TSA) improved barrier function in both cell lines and in all conditions however the greatest benefit was seen in the normoxia maintained cells. In Y1483 and Y1512 cultures maintained in normoxia the mean improvement of TEER values with the addition of TSA was 1377.33 and 473 $\Omega.cm^2$ respectively. In comparison Y1483 and Y1512 hypoxia pre-exposed cultures that had been treated with TSA only showed mean improvements of 122 and 286.62 $\Omega.cm^2$ respectively (***Figs. 4-10A and 4-10B***).
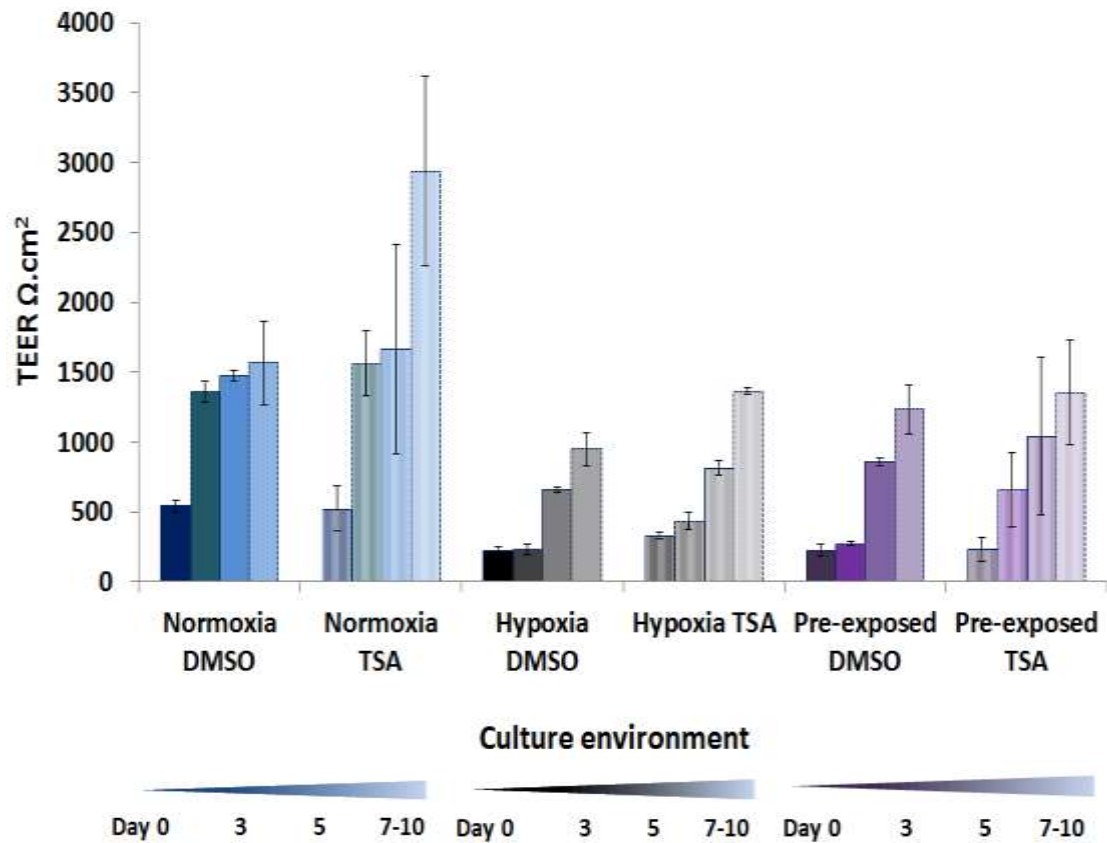
Figure 4-10A: Mean TEER obtained using Y1483 cell line cultured in normoxia, hypoxia or pre-exposed ± 5 nM TSA.

TEERs were measured until the barrier had been stable for at least 48 hours. In all conditions n=3. Controls are shown in solid bars, TSA in lined bars and standard deviations also shown.
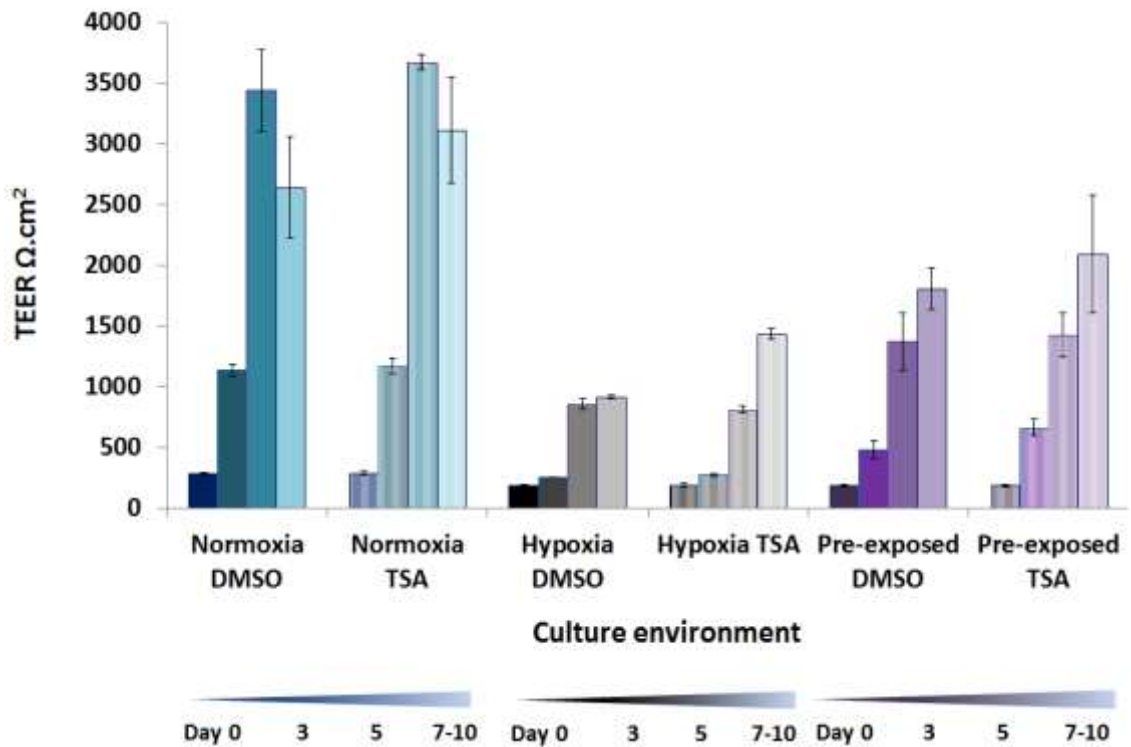
Figure 4-10B: Mean TEER obtained using Y1512 cell line cultured in normoxia, hypoxia or pre-exposed ± 5 nM TSA.

TEERs were measured until the barrier had been stable for at least 48 hours. In all groups n=3. Controls are shown in solid bars, TSA in lined bars and standard deviations are shown.

4.4.1.4 Addition of a combination of UNC0646 and TSA on barrier formation and function

A combination of 5nM TSA and 500nM UNC0646 in the Y1512 cell line resulted in an improvement in mean TEER in the hypoxic cultured group 910.67 $\Omega.cm^2$ (±15.63) to 1786.33 $\Omega.cm^2$ (±106.80). An improvement was also seen in the pre-exposed group 1366 $\Omega.cm^2$ (± 235.02) to 3660 $\Omega.cm^2$ (± 129.61) (***Fig. 4.-11***), although this appeared comparable to just the addition of UNC0646 alone. The combination of both TSA and UNC0646 was a limited study with one cell line but did not appear to bring any significant benefit over sole treatment with UNC0646.
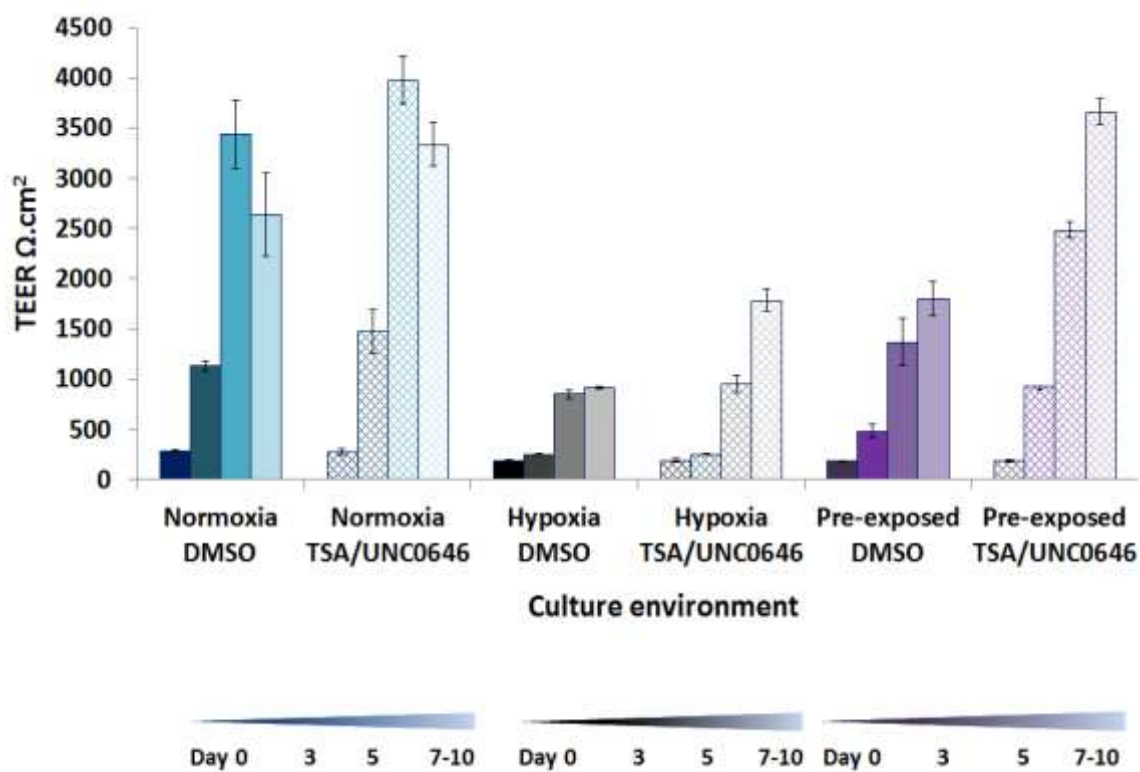
Figure 4-11: Mean TEER obtained using Y1512 cell line cultured in normoxia, hypoxia or pre-exposed ± combination of 5 nM TSA & 500 nM UNC0646

TEERs were measured until the barrier had been stable for at least 48 hours. In all

groups n=3. Controls are shown in solid bars, TSA/UNC0646 in hashed bars and

standard deviations are shown.

4.4.1.5 The effect of UNC0646 on ZO-1 expression by cultures maintained and pre-exposed to hypoxia

Immunolabelling of ZO- 1 varied between vehicle controls and with the addition of UNC0646. There was some improvement in the clarity of ZO-1 labelling at the cell membrane in the UNC0646 treated differentiated NHU cultures. This was evident in those cells maintained or pre-exposed to hypoxia (***Figures 4-12a and 4-12b***). No real difference was seen between the normoxia DMSO controls and UNC0646 treated images in either Y1227 or Y1512.

RT-PCR confirmed the presence of total ZO-1 and ZO-1α+ transcripts (***Fig. 4.-13***). Strong, visible bands for ZO-1 appeared in all three normoxia samples (N1-N3). These bands were not as evident in all three hypoxia (H1-3) or two (P2-3) pre-exposed samples. Transcript expression was subjectively higher in pre-exposed cultures that had been treated with UNC0646 (PU2 and PU3) when compared to P2-P3. ZO-1α+ transcript bands gave an opposing result with transcript expression being subjectively weaker in the cultures maintained in normoxia and stronger in those managed in or pre-exposed to hypoxia. However no quantitative detail could be determined by RTPCR.
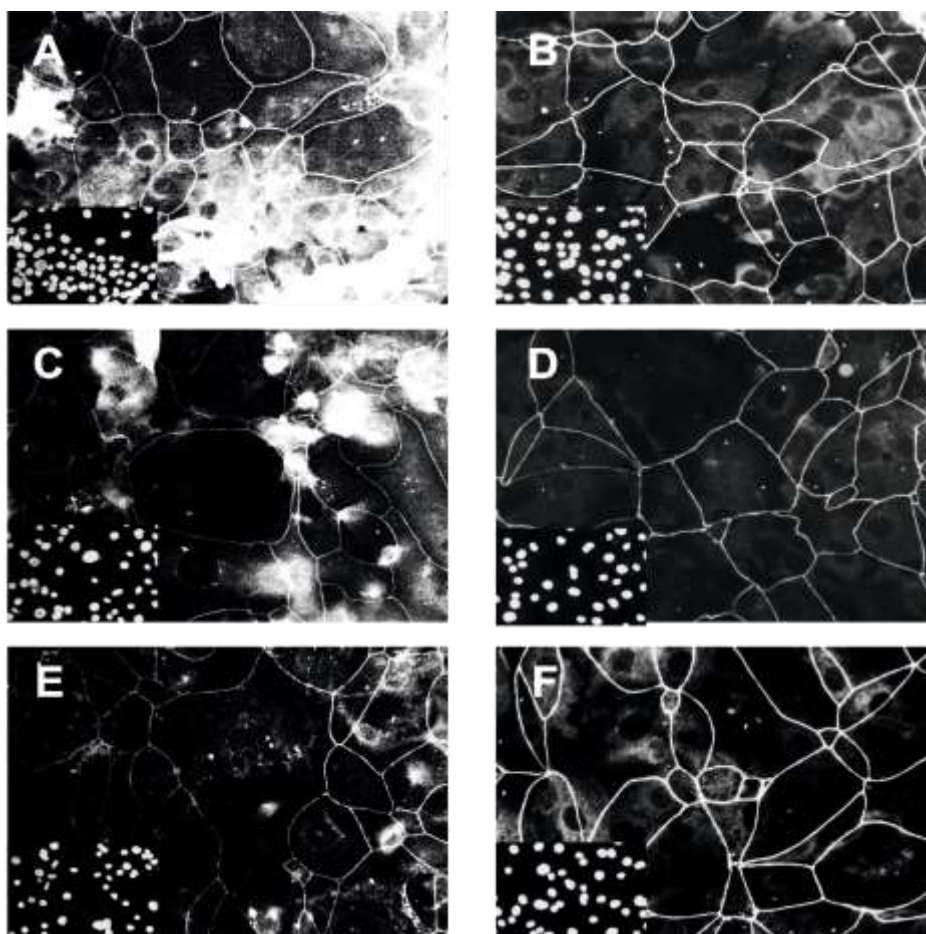
Figure 4-12a: ZO-1 labelling in NHU cells exposed acute exposure or pre-exposure to hypoxia± UNC0646

Y1227 cell line is illustrated here. Slides were fixed with methanol: acetone after a stable TEER reading had been obtained in parallel experiments. Images for ZO-1 labelling were taken at equal exposure (1/1.1s) with Hoechst 33342 staining to identify nuclei (insert). A –B were cells cultured and differentiated in normoxia, C- D cells were cultured in hypoxia, E-F cells were pre-exposed to hypoxia and transferred to normoxia. A, C and E are DMSO vehicle controls, B, D and F had 500 nM UNC0646 added to medium. There was a reduction in the presence of ZO-1 in the cell membrane of cells cultured in hypoxia or pre-exposed to hypoxia. ZO-1 labelling seemed more prominent in cultures with UNC0646 present in both hypoxia and pre-exposed cultures; this was not evident in those cultures maintained in normoxia. Scale bar 50μm.

Figure 4-12B: ZO-1 labelling in differentiated NHU cells exposed to acute exposure or pre-exposure to hypoxia± UNC0646

Y1512 cell line is illustrated here. Slides were fixed with methanol: acetone after a stable TEER reading had been obtained in parallel experiments Images for ZO-1 labelling were taken at equal exposure (1/1.1s) with Hoechst 33342 staining to identify nuclei (insert). A –B were cells cultured and differentiated in normoxia, C- D cells were cultured in hypoxia, E-F cells were pre-exposed to hypoxia and transferred to normoxia. A, C and E are DMSO vehicle controls, B, D and F had 500 nM UNC0646 added to medium. There was a reduction in the presence of ZO-1 in the cell membrane of cells cultured in hypoxia or pre-exposed to hypoxia. ZO-1 labelling seemed more prominent in cultures with UNC0646 present in both hypoxia and pre-exposed cultures; this was not evident in those cultures maintained in normoxia. Scale bar 50µm.

Figure 4-13: Transcript expression of Total ZO-1 and ZO-1α+ by NHU cells cultured in vitro in different conditions ± UNC0646.

RNA from three NHU cell lines Y1227, Y1594, Y1483 (1-3), cultured in normoxia (N), hypoxia (H), pre-exposed (P) for 21 days ± the addition of UNC0646 (U) for seven days were screened for the presence of ZO-1 mRNA by RT-PCR. Genomic RNA from human was used as a positive control (G) in the ZO-1α+. The expected size of PCR product was obtained in ZO-1 and ZO-1α+ (1092 and 209 base pairs respectively). Negative control reactions, with omission of reverse transcriptase (RT negatives) were included to demonstrate the absence of contaminating DNA (see Appendix IV).

4.4.1.6   The effect of pre-exposure to hypoxia on H3K9Me2 with the addition of UNC0646

Hypoxia-maintained and pre-exposed organ culture samples labelled intensely for H3K9Me2 throughout all nuclei within the urothelium. In the pre-exposed samples treated with UNC0646 there was a generalised shift from an intense global nuclear labelling for H3K9Me2 to a more heterogeneous pattern similar to that seen in normoxia samples and native tissue controls (*Figs. 4-14a and 4-14b*).

Immunocytochemistry of differentiated NHU cells illustrated localisation of H3K9Me2 at the nuclear lamina in cultures maintained and pre-exposed in hypoxia. The addition of UNC0646 changed the localisation of H3K9Me2, which was seen throughout the nuclei with the addition of smaller, focal patches of labelling (*Figs 4-15a & 4-15b*). In Y1713 the change in localisation of H3K9Me2 was observed by the 5th day of treatment with UNC0646 (*Figs 4-14b*). However, H3K9Me2 remained at the nuclear lamina in those NHU cultures maintained in hypoxia irrespective of the addition of UNC0646.

Immunoblotting of whole cell lysates from two donors suggested that there was an overall increase in H3K9Me2 in both the hypoxic and pre-exposed lysates compared to those maintained in normoxia or treated with UNC0646 (*Fig.4-16*). This was particularly marked in the Y1227 cell line, with a 16 fold increase in H3K9Me2 in hypoxia and 9x increase in pre-exposed cultures. This was reduced to double in the pre-exposed cultures that had been treated with UNC0646.

RT- PCR to assess for transcript expression common to G9a and GLP in three cell lines suggested an increase in the intensity of expression in hypoxia samples (H1 – H2) and

one pre-exposed sample (P3). UNC0646 did not alter the amount obtained for samples maintained in normoxia or hypoxia. There was a reduction in the intensity of the band seen in the pre-exposed sample that had been treated with UNC0646 for a week in the third cell line (Y1483) (**Fig.4.-17**).
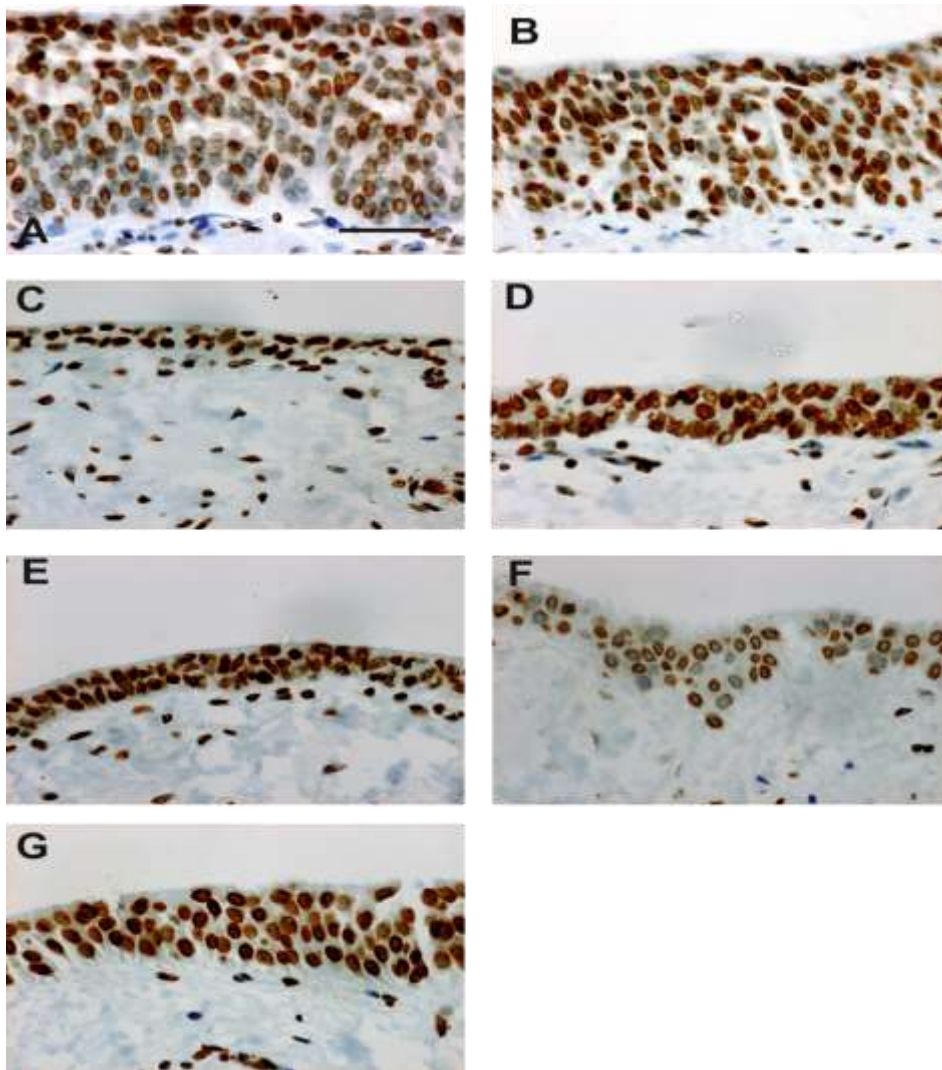
Figure 4-14a: Immunoperoxidase labelling of H3K9Me2 expression and localisation in Y1657 organ cultures pre-exposed to hypoxia ±UNC0646.

A: Normoxia, B: Normoxia +UNC0646, C: Hypoxia, D: Hypoxia + UNC0646, E: Pre-exposed, F: Pre-exposed + UNC0646 and G: In situ. All sections were maintained in organ culture for 21 days, 500 nM UNC0646 was added to culture medium in the last seven days. H3K9Me2 is heterogeneously expressed throughout the urothelium in normoxia ± UNC0646) and pre-exposed + UNC0646 (A, B & F). A more intense, uniform labelling is seen in the hypoxia ± UNC0646 and pre-exposed untreated sample (C, D & E). . Scale bar = 50 µm.
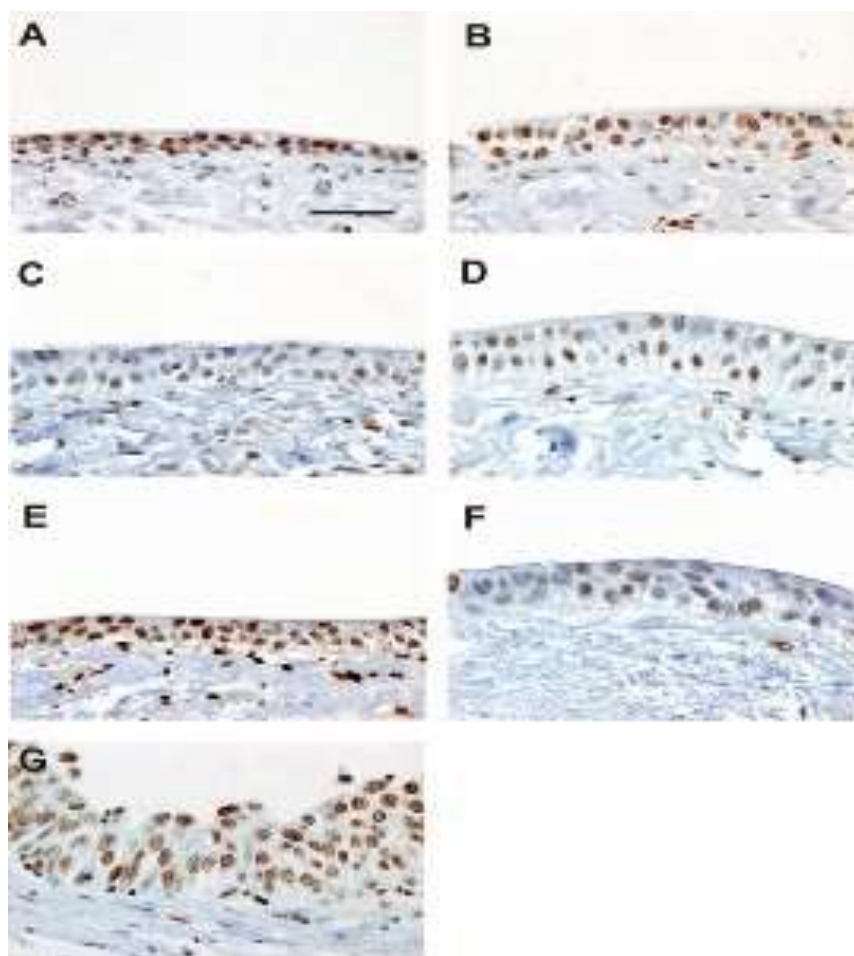
Figure 4-14b: Immunoperoxidase labelling of H3K9Me2 expression and localisation in organ cultures pre-exposed to hypoxia and treated over seven days with UNC0646.

Organ cultures (Y1713) were maintained for 21 days, the last seven days with or without treatment with 500 nM UNC0646. Formalin fixation was performed at the following time-points for immunochemical investigation. A: day 1, B: day 3, C: day 5, D: day 7, E: pre-exposed vehicle control day 7, F: normoxia no treatment day 7 G: in situ. Over the last seven days H3K9Me2 in pre-exposed organ cultures progressed from global to heterogenous expression comparable to the normoxia control (D compared to F). UNC0646 improved the thickness of the urothelium by day 7 (D compared to E). Scale bar = 50 μm
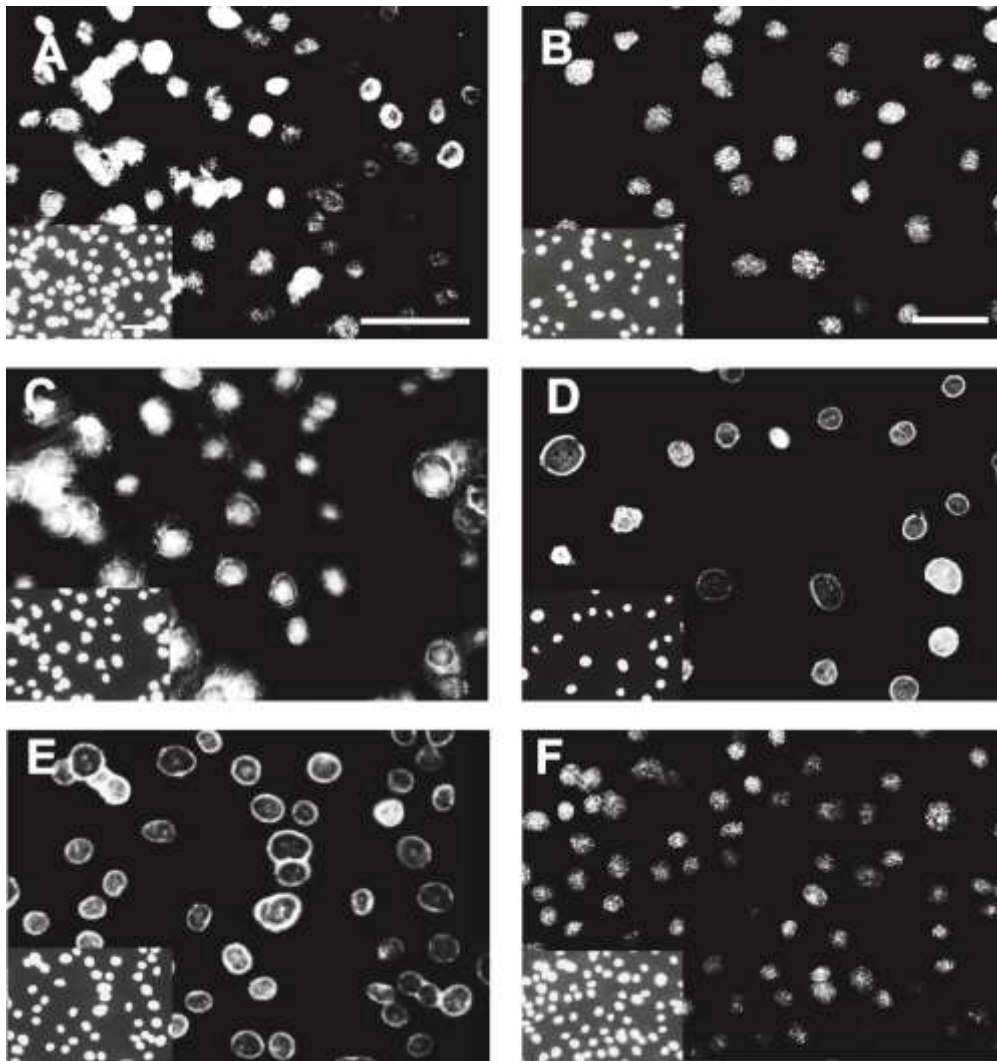
Figure 4-15A: Immunofluorescence of H3K9Me2 ± UNC0646:

Differentiated NHU cells from one donor: Y1227 cultured in normoxia (A-B), hypoxia (C-D) or pre-exposed to hypoxia (E-F). A, C & E = DMSO vehicle controls, B, D &F = 500 nM UNC0646 for seven days. Cultures were fixed, on glass slides, at the point that a stable barrier had been obtained in parallel TEER experiments. Images for H3K9Me2 labelling were taken at equal exposure for all conditions (1/1.8) with Hoechst 33342 staining for cell density (insert). Nuclear lamina localisation of labelling in hypoxia and pre-exposed cultures noted with apparent change in the latter with addition of UNC0646. Scale bar =50µm
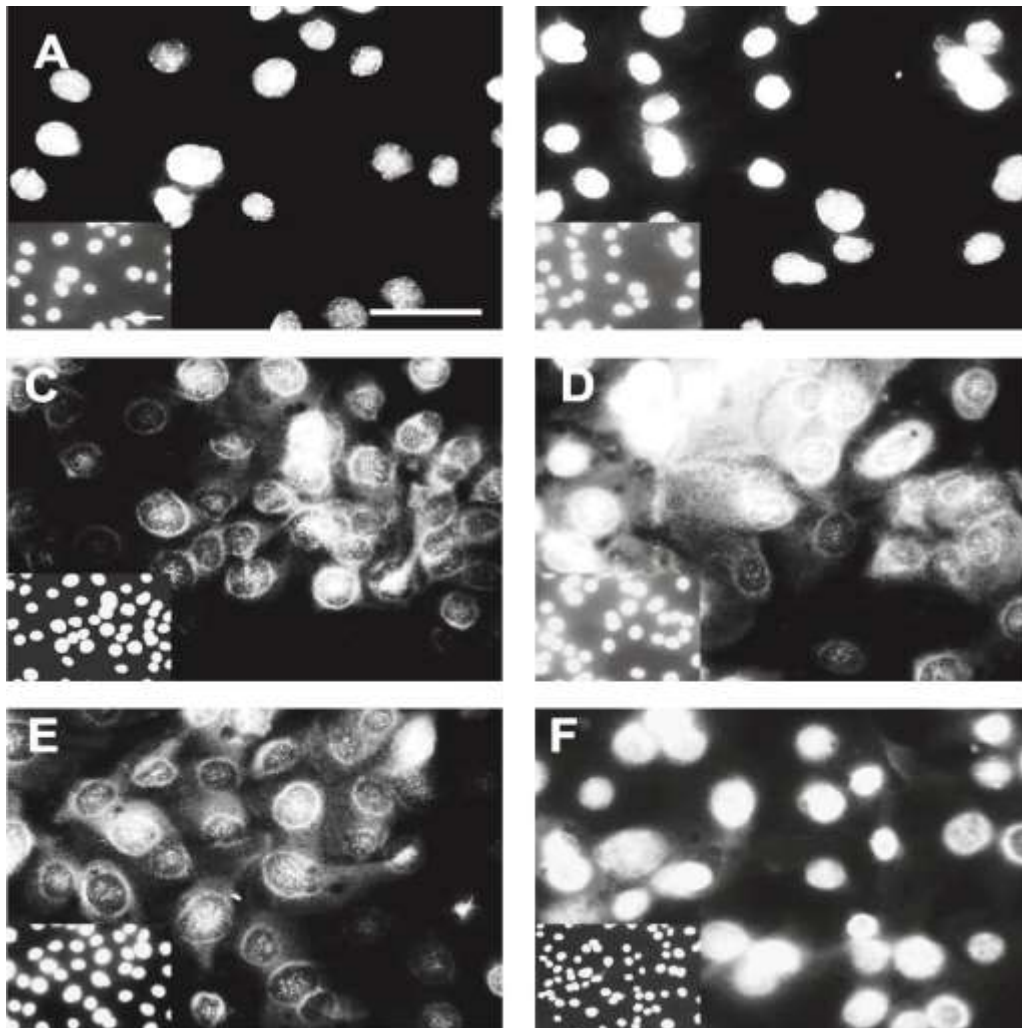
Figure 4-15b: Immunofluorescence of H3K9Me2 ± UNC0646:

Differentiated NHU cells from one donor Y1512 cultured in normoxia (A-B), hypoxia (C-D) or pre-exposed to hypoxia (E-F). A, C & E = DMSO vehicle controls, B, D &F = 500 nM UNC0646 for seven days. Cultures were fixed, on glass slides, at the point that a stable barrier had been obtained in parallel TER experiments. Images for H3K9Me2 labelling were taken at equal exposure for all conditions (1/1.5) with Hoechst 33342 staining for cell density (insert). Nuclear lamina localisation of labelling in hypoxia and pre-exposed cultures noted with apparent change in the latter with addition of UNC0646. Scale bar =50µm
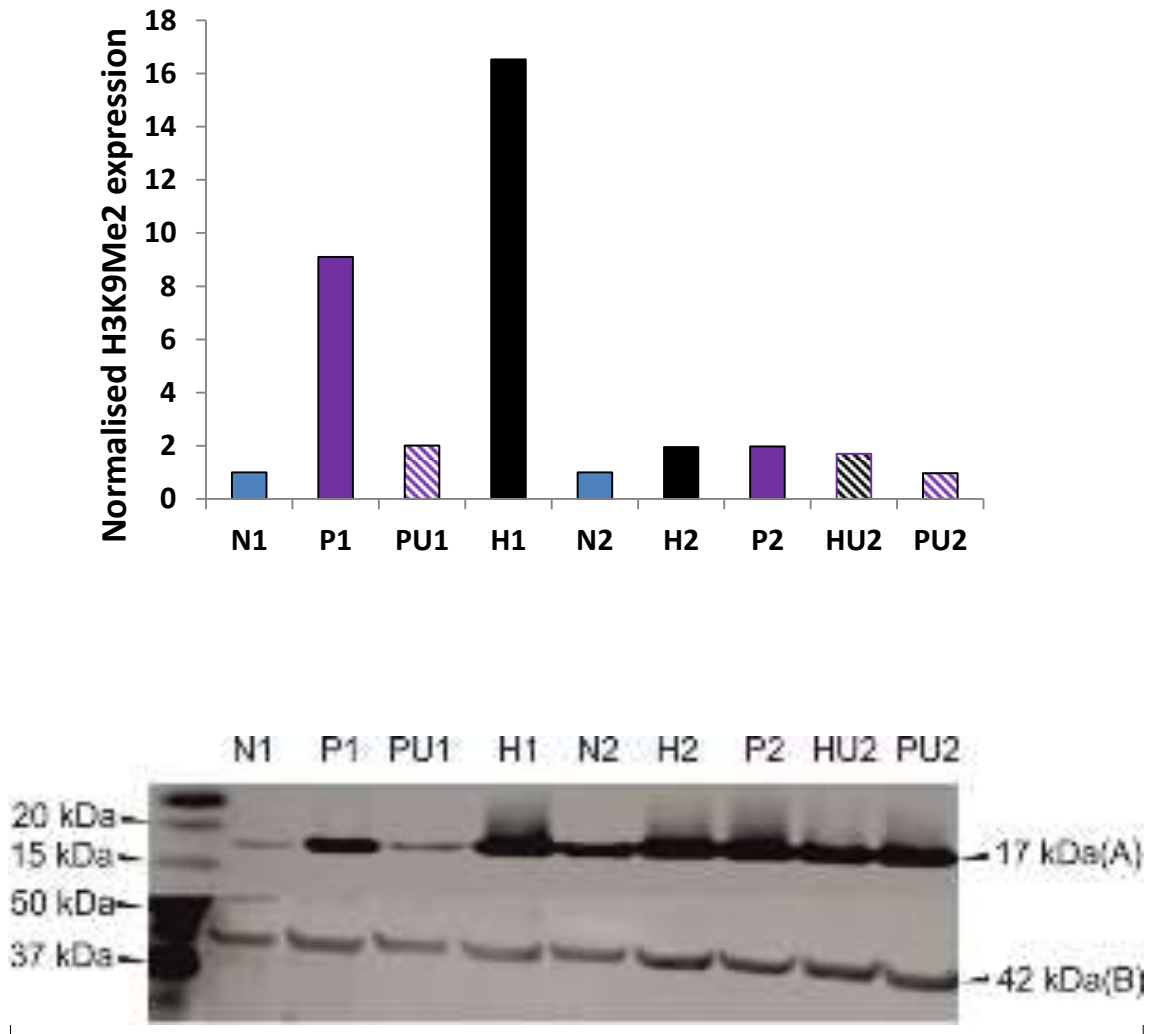
Figure 4-16: Immunoblotting for H3K9Me2. Whole cell lysates were isolated from two confluent, differentiated NHU cell line cultures (Y1227 and Y1594).

H3K9Me2 protein expression in normoxia (N), hypoxia (H), pre-exposed (P), pre-exposed + UNC0646 (PU) or hypoxia +UNC0646 (HU) lysates were determined by immunoblotting. Abcam H3K9Me2 (ab1220) mouse monoclonal antibody (17 kDa) = A. was utilised. H3K9Me2 expression was normalised to β-actin (42 kDa) (B) for each whole cell lysate and expression is illustrated in the bar chart above.
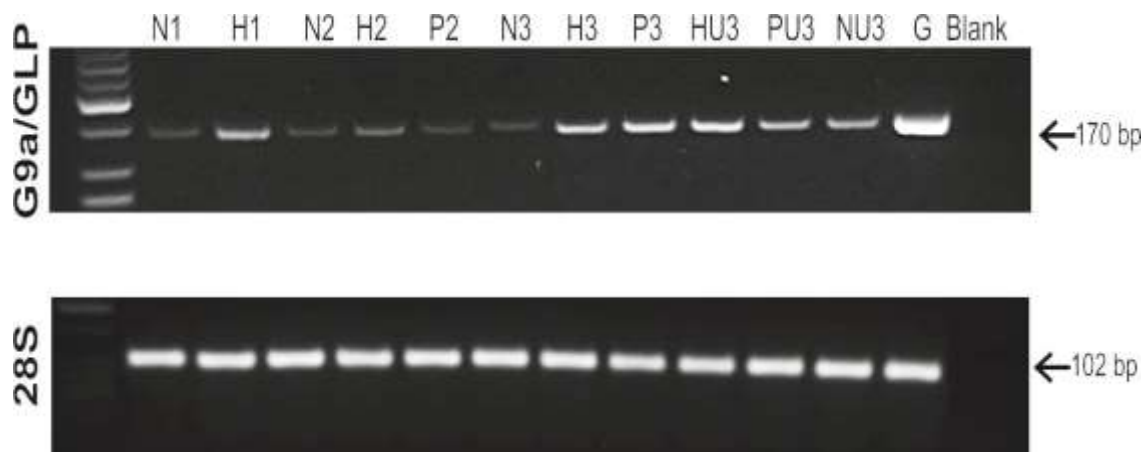
Figure 4-17: Transcript expression of G9a/GLP by NHU cells cultured in vitro in different conditions ± UNC0646

RNA from three NHU cell lines Y1512, Y1594, Y1483(1-3), cultured in normoxia (N), hypoxia (H), pre-exposed (P) ± the addition of UNC0646 (U) for seven days were screened for the presence of a mRNA transcript common to both G9a and GLP by RT-PCR.   Genomic RNA from human was used as a positive control (G). The expected size of PCR product was obtained (170 base pairs. Negative control reactions, with omission of reverse transcriptase (RT negatives) were included to demonstrate the absence of contaminating DNA (see appendix IV).

4.4.1.7   Effect of application of UNC0646 on urothelial cells from diseased bladders

As highlighted in the experimental approach precautions were taken prior to differentiation to try and encourage proliferation. Although this was moderately successful it was noted that on average one sub-culture took a mean of 10 days to complete ± 3 days as opposed to the standard for NHU of 4 – 7 days.

Despite the cell number issues with Y1042 an adequate barrier was obtained in both the control and UNC0646 paired replicates with only 75 Ωcm^2 separating the final mean TERs obtained (2060.67 *vs* 2135) (***Fig. 4-18***).

The other two cell lines from diseased bladders demonstrated that there was poor barrier development in the control samples with a mean of Y1173: 441 Ωcm^2 (range 367 – 513) and Y1036: 989 Ωcm^2 (range 928 – 1052). With the addition of UNC0646 this compromise was overcome producing barriers in both cell lines of > 1500 Ωcm^2.
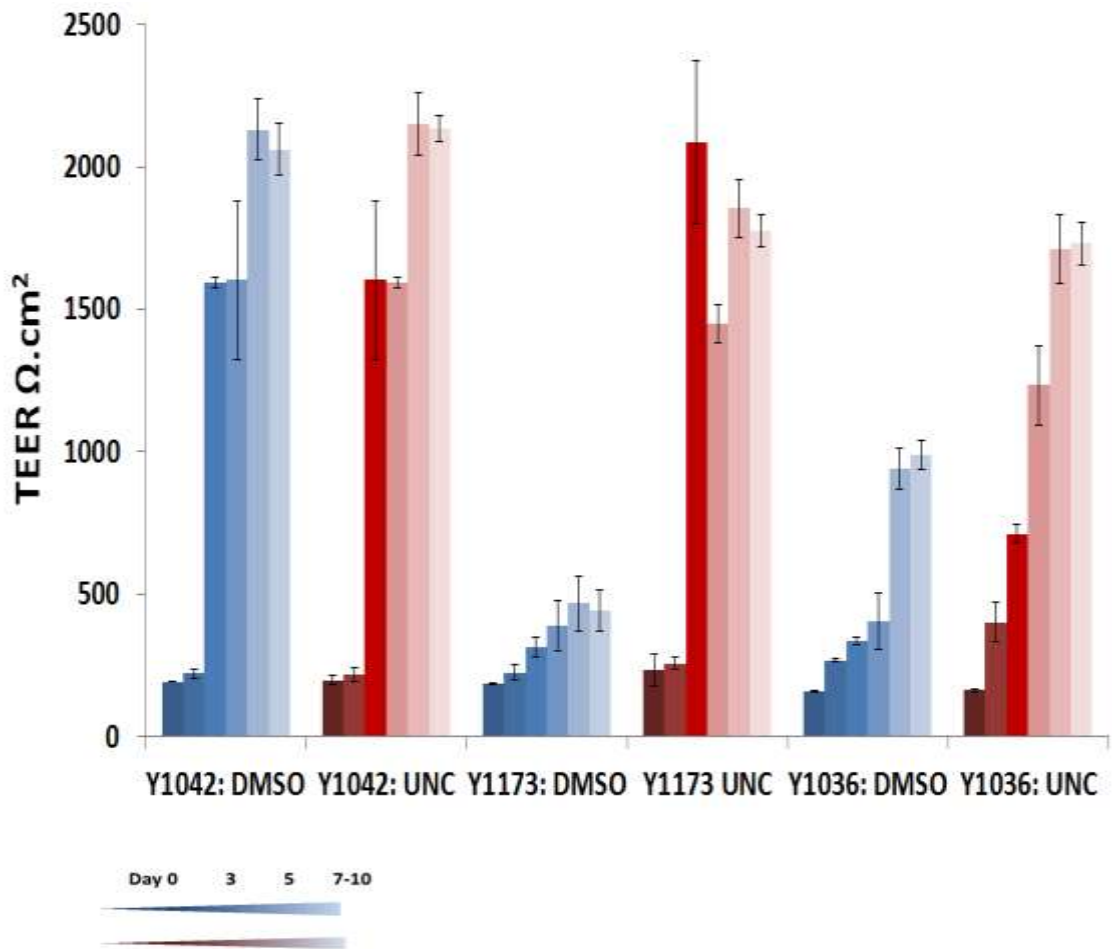
Figure 4-18: Mean TEER obtained using three neuropathic cell lines ± UNC0646

TEERs were measured until the barrier had been stable for at least 48 hours. Y1042 (n=2), Y1173 (n=3) and Y1036 (n=3). Controls are shown in solid blue bars, UNC0646 in red bars and standard deviations are also shown.

4.4.2 Investigate whether epigenetic modifying agents result in phenotypic changes within the urothelium using the *in vitro* approach.

Organ culture sections underwent H&E and immunohistological analysis to assess for markers of urothelial differentiation and proliferation. Sections from organ cultures maintained in normoxia and pre-exposed to hypoxia with and without application of UNC0646 were analysed. These were evaluated against the normal pattern of distribution as shown by matched native tissue sections (normal pattern summarised in *Figure 4-19)*. In all three donors there was preservation of all urothelial layers in the normoxia organ cultures. In the normoxia specimens treated with UNC0646 there was no perceivable alteration in the histologIcial structure or organisation of sample (Y1593 & Y1657 shown in *Fig. 4.-20*, Y1713 see Appendix IV).

As reported in Chapter Three (**section 3.4.6**) organ cultures that had been exposed to hypoxia for a week prior to spending a further 14 days in normoxia had "thinning" of intermediate and superficial cell types. Therefore the process of returning to normoxia was not sufficient for differentiation to recover. However with the treatment of pre-exposed organ cultures for seven days with 500 nM UNC0646 recovery of the urothelium was evident with good thickness of urothelium achieved (***Figure. 4.-20).***
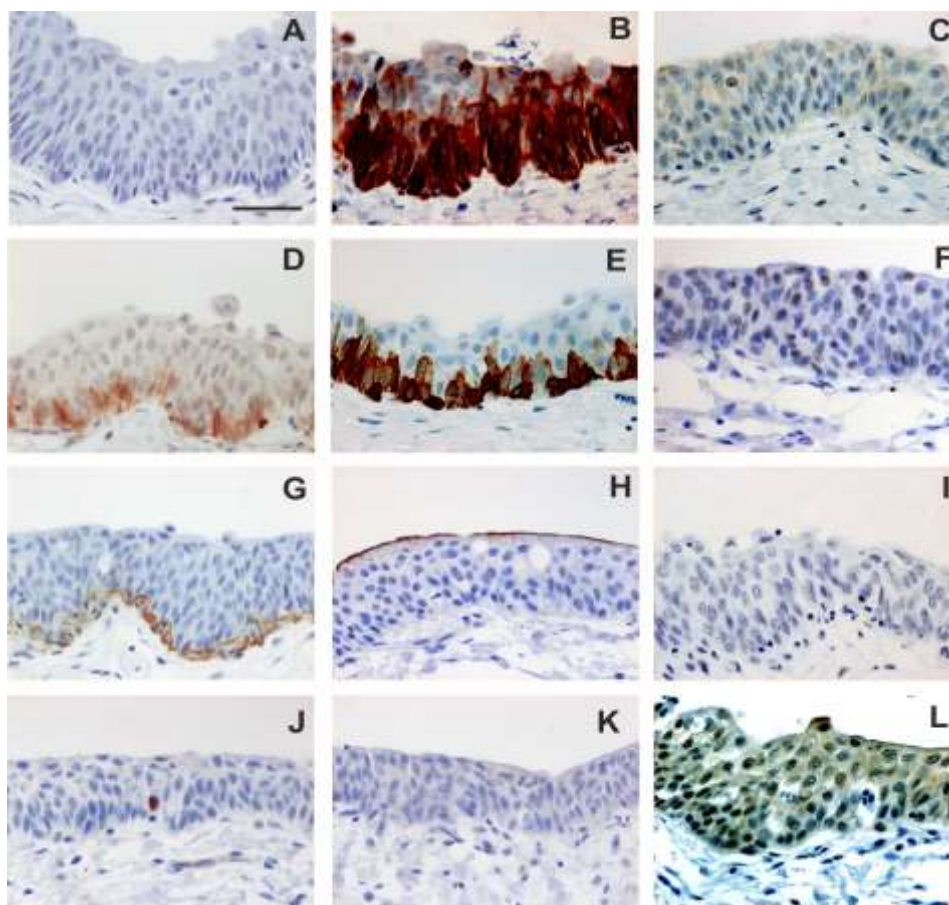
Figure 4-19: Normal localisation and expression of immunohistochemical markers in human urothelium

Sections of normal human ureter: A= H&E stain with basal, intermediate and superficial layer. B basal and intermediate intense staining of CK13, the opposite is shown in CK14 expression which is scanty (C). Basal cell markers include NGFR (D) and CK5 (E). P63 a marker of urothelial differentiation is shown in (F). Laminin is a marker that identifies the basement membrane (G). Superficially uroplakin 3A (UPK3A) is found at the apical surface (H) and CK20 is also expressed in the superficial layer but with variability between individuals (I). Markers of proliferation and cell cycle are nuclear; Ki67 is scanty in expression in the usually quiescent urothelium (J) and Cyclin D3 commonly found in the superficial to intermediate layers (K). HIF-1α is found in the cytoplasm and nuclei. Scale bar = 50μm.
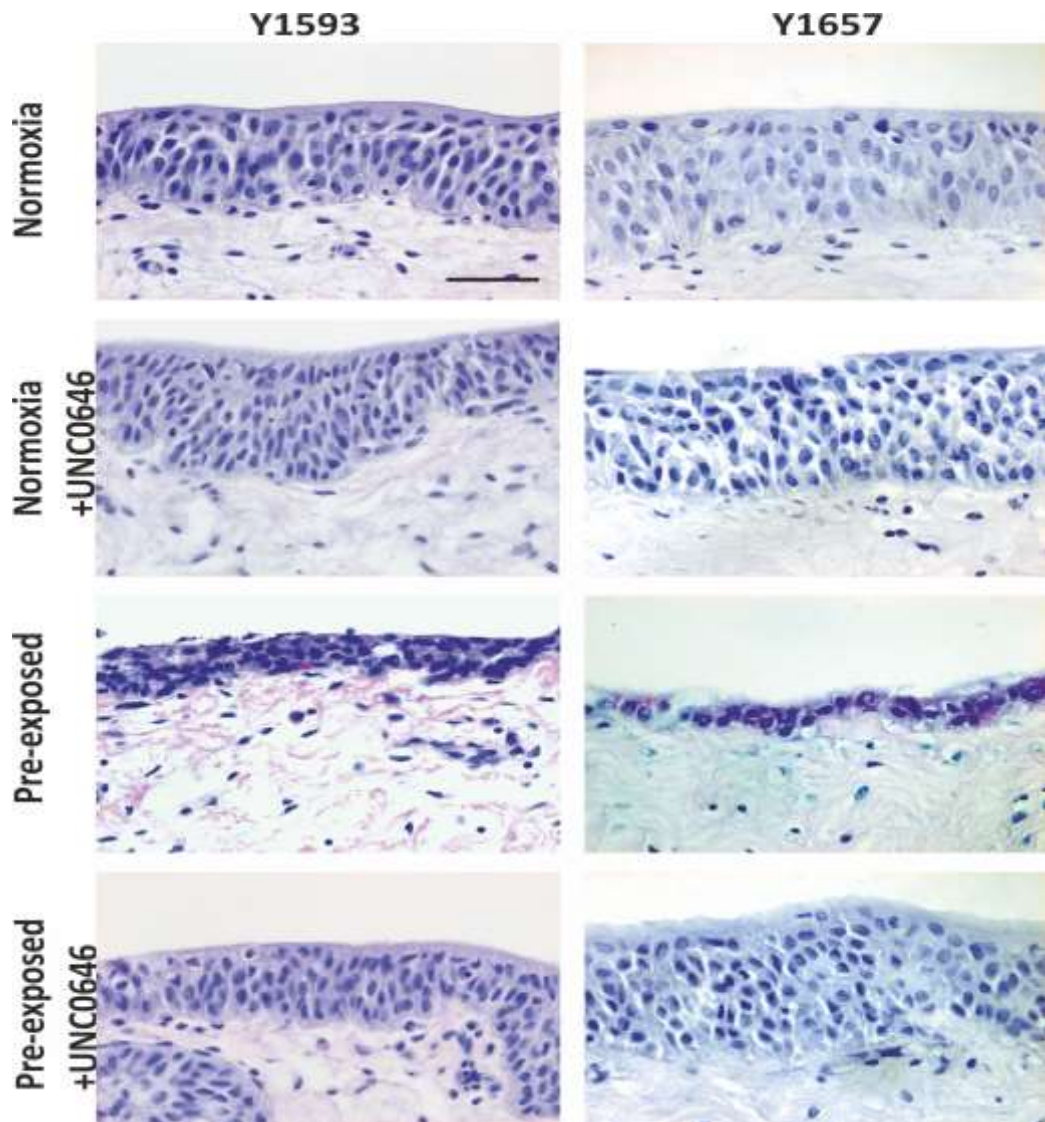
Figure 4-20: &E staining of two independent 21 day organ cultures ± UNC0646 maintained in normoxia, hypoxia or pre-exposure to hypoxia.

The urothelium in organ cultures pre-exposed to hypoxia was "thinned" in appearance in comparison to normoxia controls. In both Y1593 and Y1657 the addition of UNC0646 did not alter the histological appearance in the normoxia controls but did improve the thickness and morphology of the urothelial layer in treated pre-exposed cultures by day 21. Scale bar = 50 µm

Normal morphology and differentiation remained in organ cultures maintained in normoxia when UNC0646 was added to them. Importantly in the compromised pre-exposed cultures, the recovery in urothelial thickness after a week of UNC0646 treatment was accompanied by normal expression and distribution of basal and superficial markers. Therefore not only was there recovery in terms of cell number but also of the differentiated phenotype in the presence of UNC0646. Significantly the aberrant squamous marker, CK14, observed in normoxia, hypoxia and pre-exposed organ cultures was also abrogated by the addition of UNC0646 thereby improving the urothelial phenotype associated within the *in vitro* model. Evidence for the above was shown by immunolabelling for various markers.

Laminin, an integral part of the basement membrane, remained correctly and located in all samples (***Figure 4-21***). CK5 (***Figure 4-22)*** and NGFR ***(Figure 4-23)*** were located, as expected from the pattern seen in the *in situ* tissue, within the basal component of the urothelium. Generally this was not altered by organ culture or the addition of UNC0646. However NGFR labelling ***(Figure 4-23)*** appeared reduced in organ cultures maintained in normoxia and treated with UNC0646. However NGFR was present in all samples except in the pre-exposed control section from Y1593, which recovered with UNC0646 treatment. In both donors, CK5 and NGFR labelled sections illustrate the increased urothelial thickness in the pre-exposed samples treated with UNC0646.
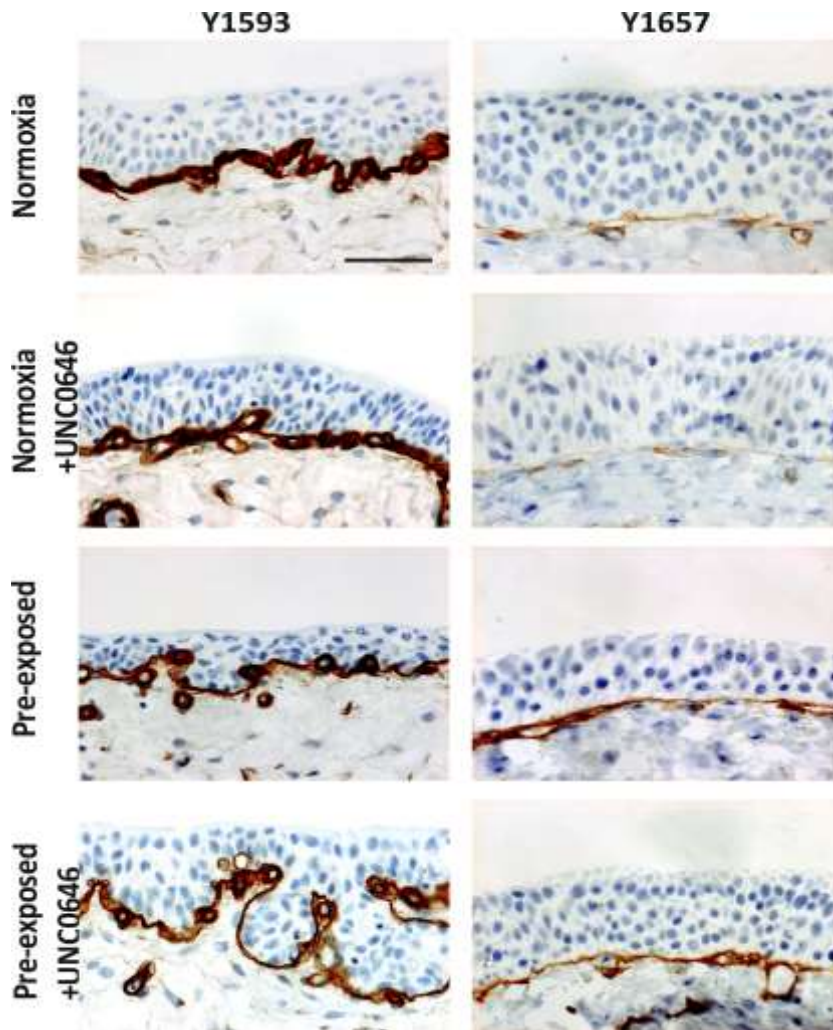
Figure 4-21: Immunoperoxidase labelling of Laminin expression and localisation in two independent 21 day organ cultures.

Laminin was located within the basement membrane (BM) of the urothelium and was present in all organ cultures including those having been treated with UNC0646 from day 14. Scale bar = 50 μm
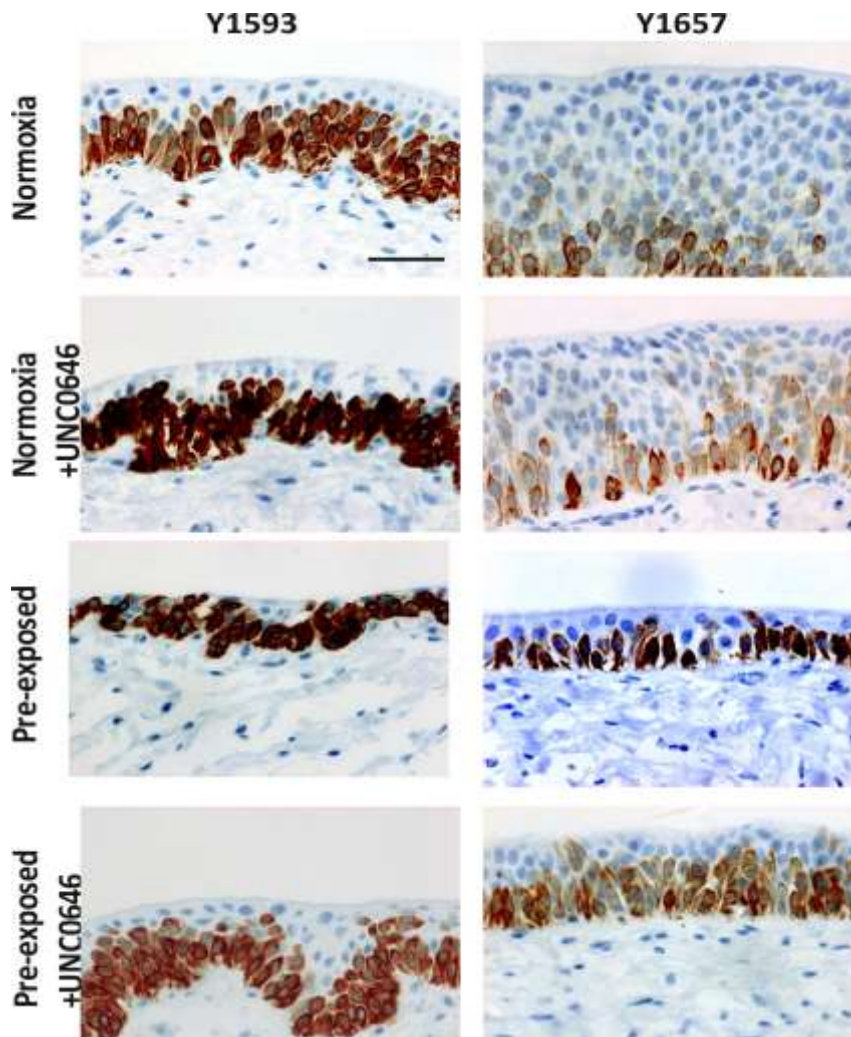
Figure 4-22: Immunoperoxidase labelling of CK5 expression and localisation in two independent 21 day organ cultures ± UNC0646.

CK5 was located within the basal cells of all organ cultures, including those that had been treated with UNC0646 from day 14, suggesting that the epigenetic modifier did not alter CK5 distribution. Scale bar = 50 μm
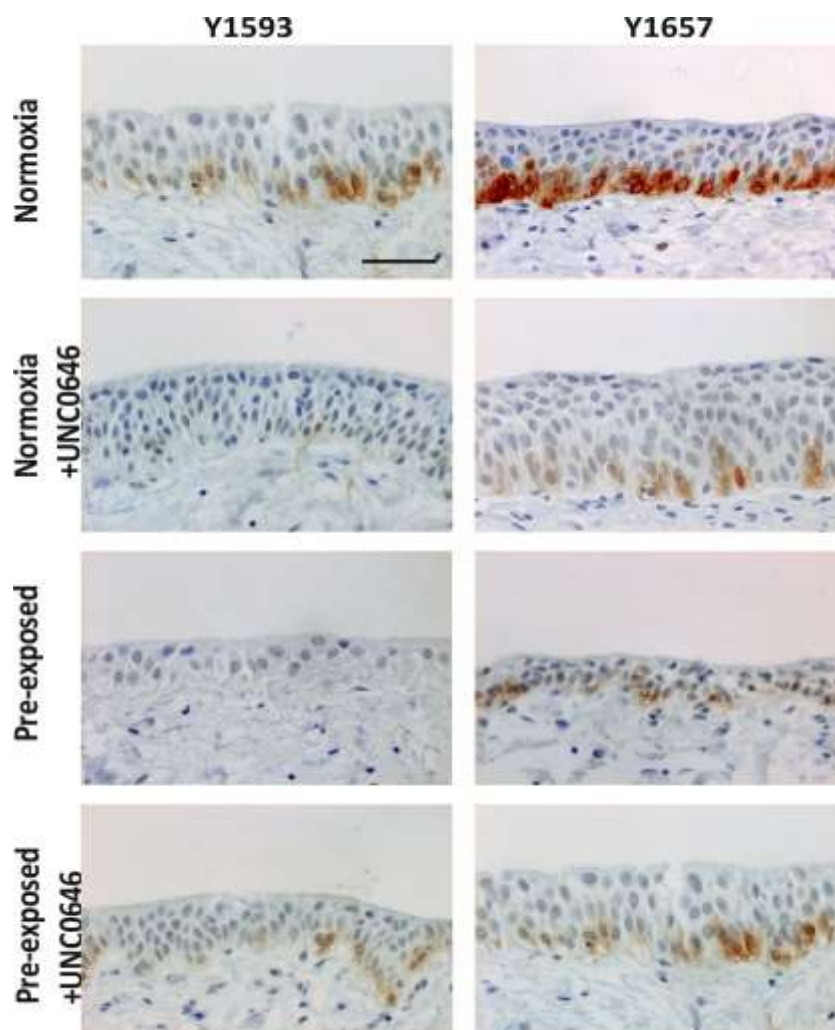
Figure 4-23: Immunoperoxidase labelling of NGFR expression and localisation in two independent 21 day organ cultures ± UNC0646

NGFR was located within the basal cells of all organ cultures, including those that had been treated with UNC0646 from day 14, suggesting that the epigenetic modifier did not negatively impact on NGFR distribution. Y1593 pre-exposed+ UNC0646 section may show some recovery in NGFR expression as opposed to the pre-exposed control. This was not replicated in the other two donors. Scale bar = 50 µm

CK13 was expressed in the basal and intermediate layers of the urothelium in most of the organ cultures, which is congruent with normal *in-situ* expression. In the pre-exposed controls there was either an absence (Y1593) or low abundance of CK13. This abrogation was improved with the addition of UNC0646, so that CK13 was present in a normal pattern of distribution, even if expression was still subjectively reduced compared to normoxia controls (***Figure 4-24***).

CK14 is not normally a feature of differentiated urothelium (***Figure 4-19***); however it would appear that organ culture results in an increase in CK14 expression, even in normoxia (***Figure 4-25***). Pre-exposed organ cultures demonstrate this more prominent labelling pattern for CK14, which is removed by the application of UNC0646.
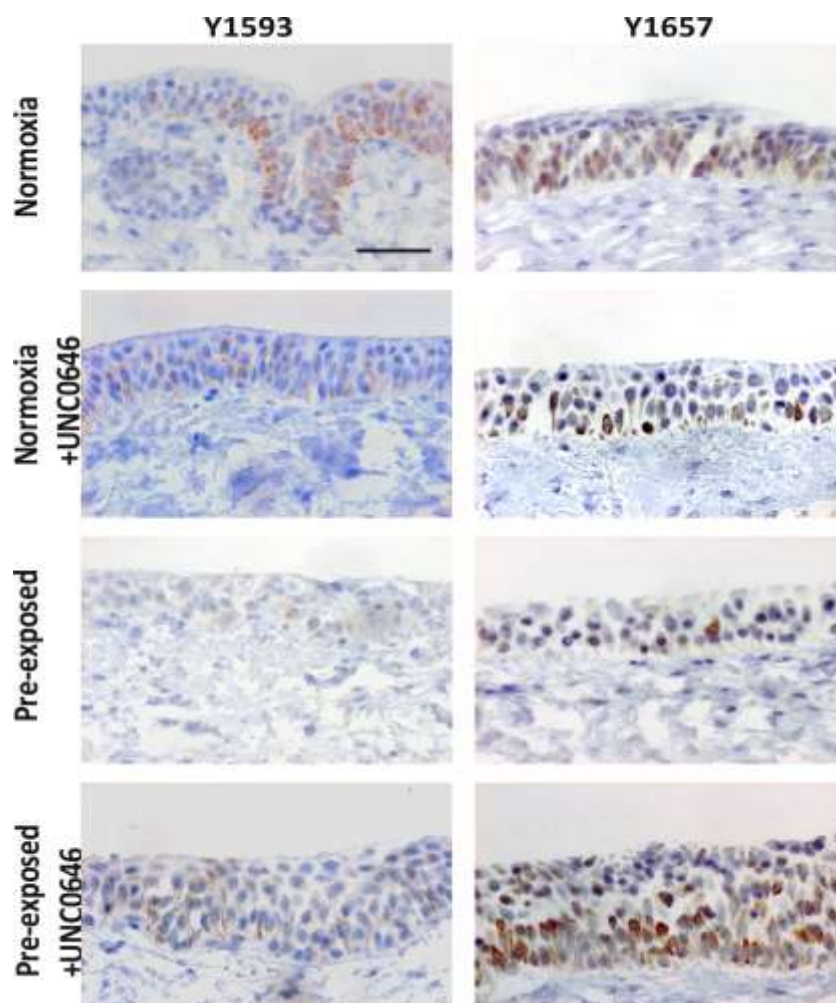
Figure 4-24: Immunoperoxidase labelling of CK13 expression and localisation in two independent 21 day organ cultures ± UNC0646.

CK13 was located within the basal and intermediate cells of all organ cultures, although with subjective reduction in the pre-exposed samples. CK13 was found in a normal distribution (basal/intermediate) in those organ cultures maintained in normoxia and treated with UNC0646 from day 14, suggesting that the epigenetic modifier did not alter CK13 distribution in controls. However the addition of UNC0646 may have improved CK13 expression in pre-exposed samples by day 21. Scale bar = 50 μm
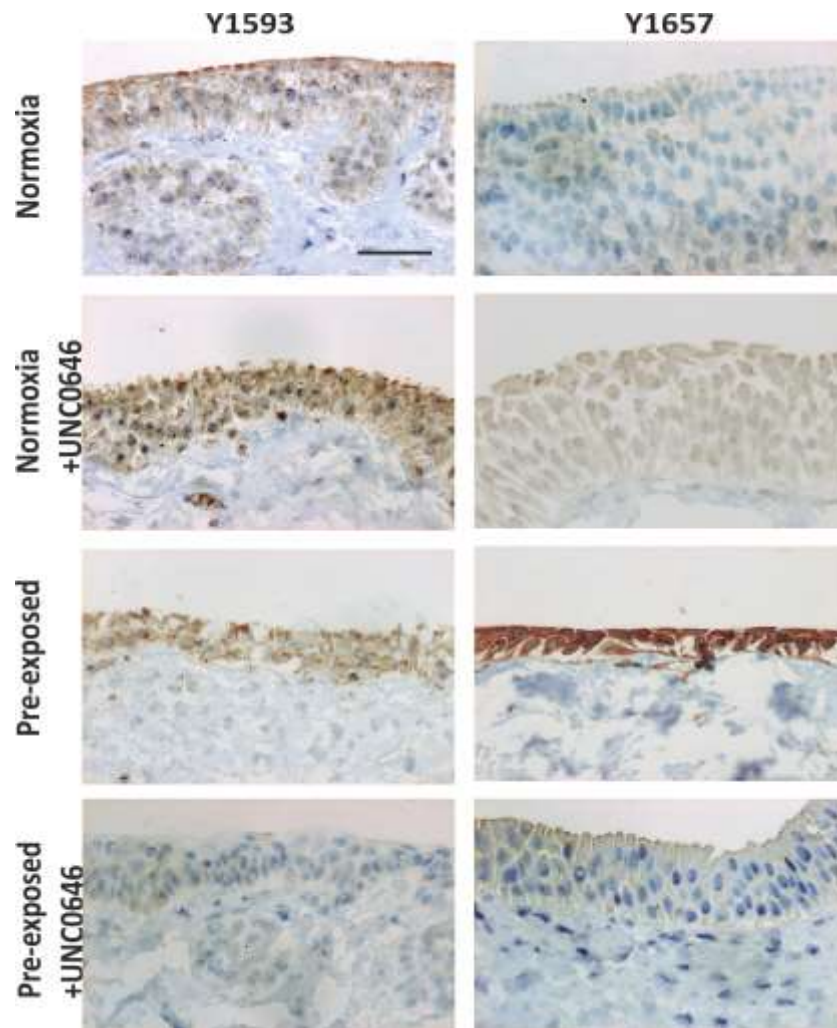
Figure 4-25**: **Immunoperoxidase labelling of CK14 expression and localisation in two independent 21 day organ cultures ± UNC0646.

CK14 was located within the urothelium of all organ cultures but was more evident in the pre-exposed untreated samples. CK14 was also seen in those normoxia maintained samples treated with UNC0646 from day 14; but in the pre-exposed treated samples there was a reduction in CK14 labelling; suggesting that the epigenetic modifier may alter CK14 expression compared to compromised controls by day 21. Scale bar = 50 μm

Superficially CK20 was evident in one of the normoxia controls and both UNC0646 treated cultures in normoxia. There was no abnormal localisation of CK20 within the urothelium in any of the organ cultures. CK20 was absent in all three pre-exposed organ cultures with UNC0646 resulting in CK20 expression in Y1593 (***Figure 4-26***).

Another superficial marker, linked with terminal differentiation, UPK3a was scantily expressed in one normoxia control and absent in the other. Both however labelled positively for UPK3a when UNC0646 had been applied to normoxia organ cultures for seven days. A similar pattern was seen in the pre-exposed cultures; the controls expressing no UPK3a but when UNC0646 was applied normal UPK3a expression was seen at the apical surface of the urothelium ***Figure 4-27***).
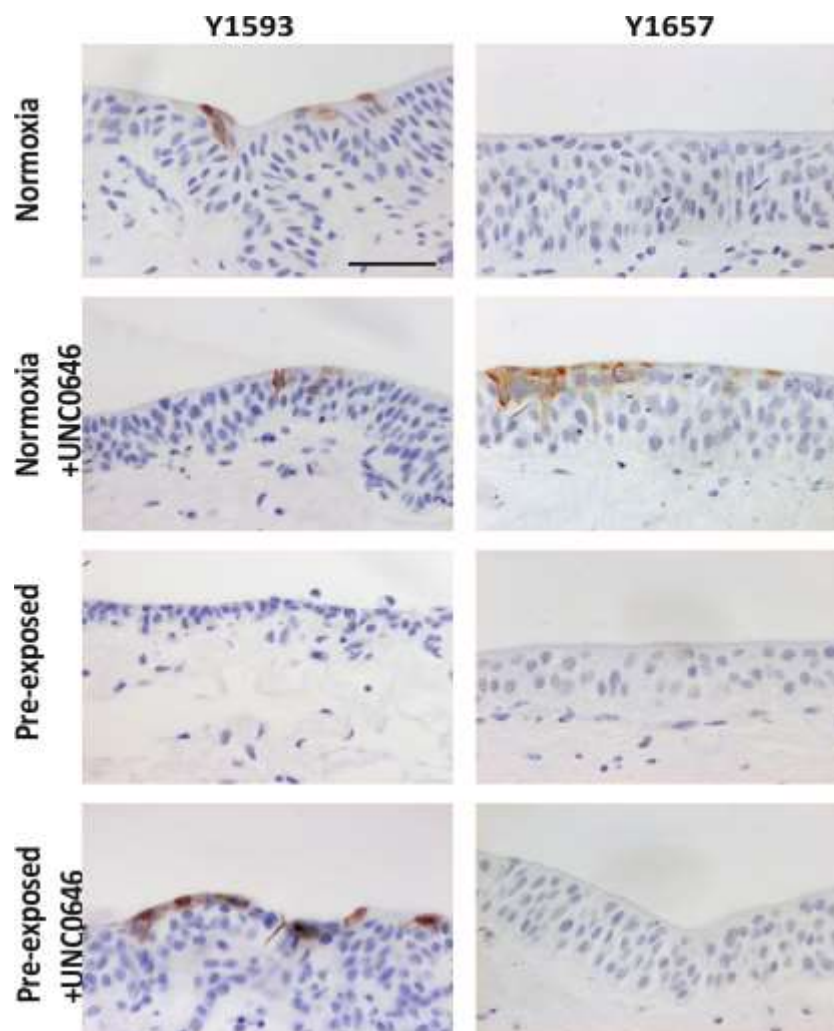
Figure 4-26: Immunoperoxidase labelling of CK20 expression and localisation in two independent 21 day organ cultures ± UNC0646

CK20 was located within the superficial cells of some of the organ cultures, including normoxia controls. CK20 was absent in the pre-exposed organ culture controls. CK20 was expressed in one pre-exposed OC treated with UNC0646 (Y1593), suggesting that the epigenetic modifier may have improved CK20 expression. The other donor (Y1657) also exhibited an increase in CK20 expression but in the normoxia sample treated with UNC0646. Scale bar = 50 μm.
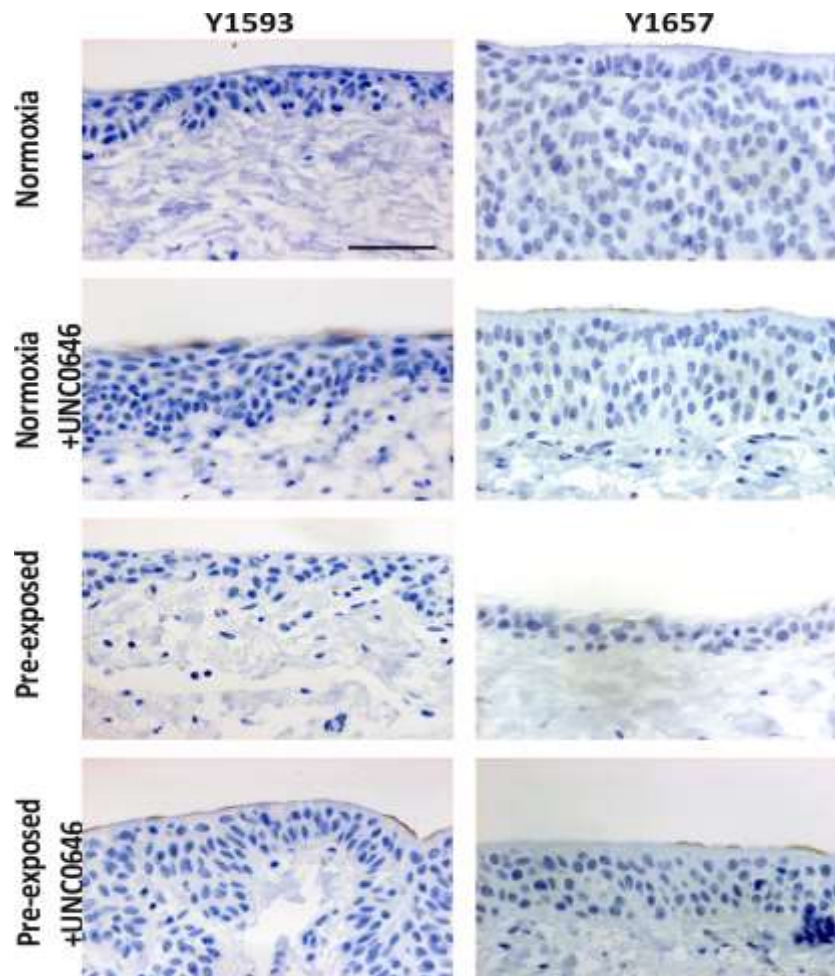
Figure 4-27: Immunoperoxidase labelling of Uroplakin-3a (UPK3a) in two independent 21 day organ cultures ± UNC0646

UPK3a was located within the superficial cells of some of the organ cultures, including one of the normoxia controls. There was absence of UPK3a in all of the pre-exposed controls. UPK3a was expressed in all pre-exposed OC treated with UNC0646, suggesting that the epigenetic modifier improved UPK3a expression in pre-exposed OC The UNC0646 treated normoxia controls also exhibited an increase in UPK3a expression. Scale bar = 50 μm

Overall expression of Cyclin D3 varied between samples (***Fig. 4-28***).   In one donor the pre-exposed untreated cultures there was no expression of Cyclin D3 with expression seen superficially with the addition of UNC0646. In the other donor, Y1657, any differences were less pronounced due to the increased labelling of Cyclin D3 throughout the urothelium. In the pre-exposed cultures, both untreated and treated with UNC0646 the location of labelling remains predominantly superficial.

Looking closely at expression of Cyclin D3 in pre-exposed samples over the seven day treatment with UNC0646 (***Fig. 4-29***) it illustrated the tendency for Cyclin-D3 expression to move superficially with time as the urothelium becomes thicker. The Cyclin- D3 expression in the pre-exposed samples without treatment remained limited by the extent of the urothelium.
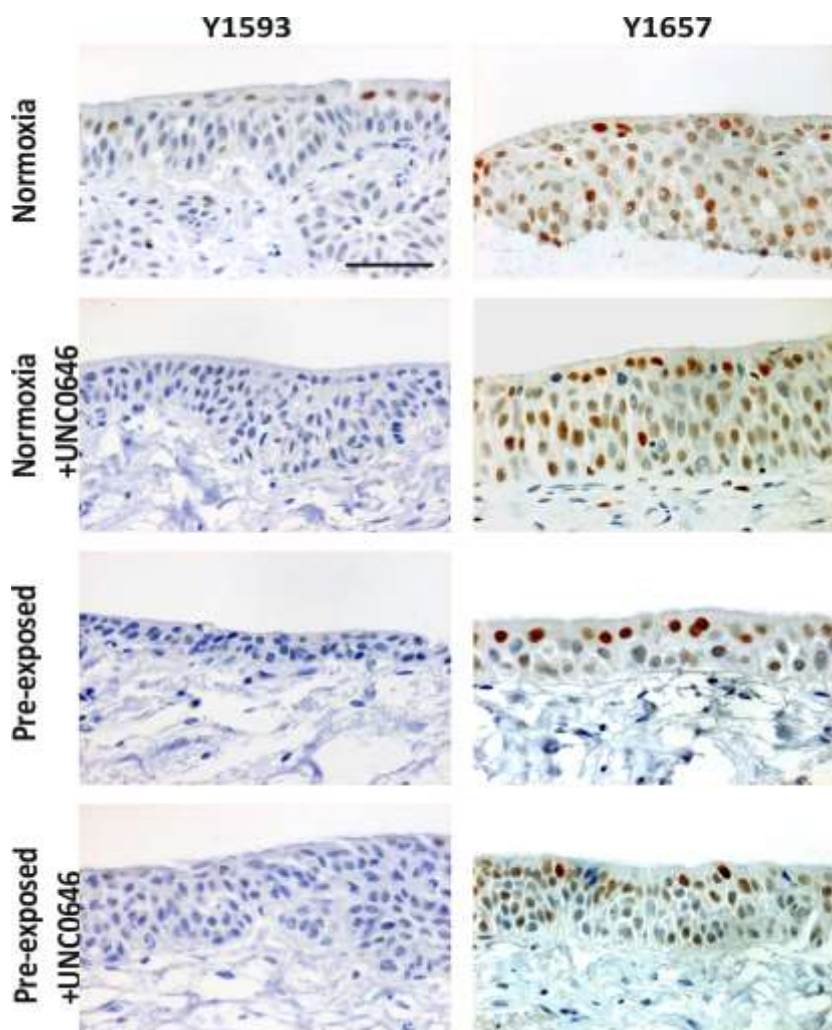
Figure 4-28: Immunoperoxidase labelling of Cyclin D3 in two independent 21 day organ cultures ± UNC0646

Cyclin D3 was located within the superficial cells in normoxia maintained organ cultures and also in the basal and intermediate layers in Y1657. UNC0646 treatment resulted in a subjective reduction in expression of Cyclin D3 in normoxia which was not replicated in Y1657. Y1593 demonstrated no Cyclin D3 labelling in the pre-exposed controls but his was present with addition of UNC0646 .Subjectively there was more labelling in the Y1657 treated pre-exposed samples, comparable to controls. In both donors the pre-exposed organ cultures treated with UNC0646 increased thickness of urothelium compared to the pre-exposed controls. Scale bar = 50 μm
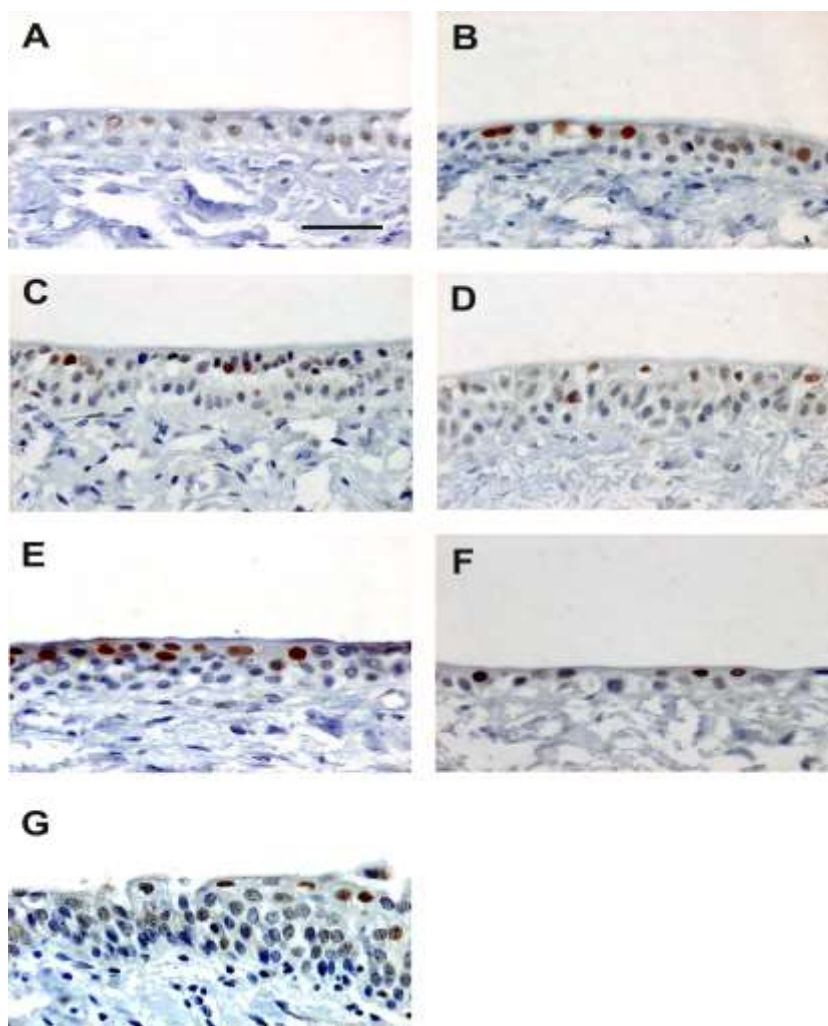
Figure 4-29: Immunoperoxidase labelling of Cyclin D3 expression during seven days treatment with UNC0646.

*Organ cultures (OC) (Y1713) pre-exposed to hypoxia and maintained in normoxia for seven days were treated for a further seven days with 500 nM UNC0646. Formalin fixation occurred at the following time-points for immunochemical investigation. **A:** Day 1, **B**: Day 2, **C**: Day 3, **D**: Day 5, **E**: Day 7, **F**: Pre-exposed no treatment Day 7, **G**: In situ. Expression of Cyclin D3 was noted superficially, with a subjective increase in intensity at all time-points compared to day 1, including day 7 in the untreated OC. Treatment with UNC0646 improved the thickness of the urothelium by day 7 (**E** compared to **F**). Scale bar = 50 μm*

Ki67was generally noted to be superficial in the organ culture system, similar to Cyclin D3. Most striking was the absence or scanty expression of Ki67 in the pre-exposed controls at day seven compared to the marked superficial labelling seen with UNC0646 treatment. A similar pattern was also seen in organ cultures maintained in normoxia when UNC0646 was added (*Fig. 4-30*) and *in-situ* (**G** in *Fig. 4-30*).

The temporal relationship between Ki67 localisation and expression throughout the treatment with UNC0646 was similar but more striking than that seen for Cyclin D3. Expression of Ki67 moved from basal to superficial over time (*Fig. 4-31*). The appearance of the pre-exposed untreated culture at day seven is almost the same at that seen at day two of the UNC0646 treated cultures (**B** & **F,** *Fig. 4-31*)
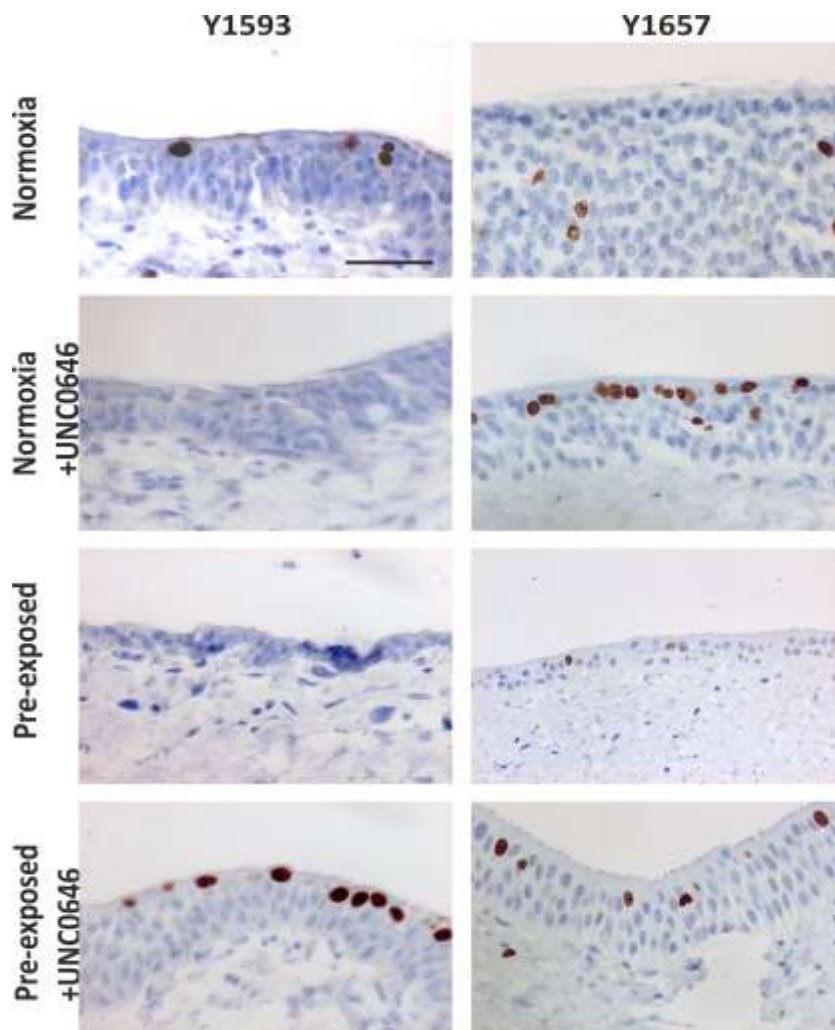
Figure 4-30: Immunoperoxidase labelling of Ki67 expression and localisation in two independent 21 day organ cultures ± UNC0646

Ki67 expression was localised predominantly in the superficial layer of the urothelium with some labelling in the intermediate region in the Y1657 normoxia control sample. Ki67 was absent in Y1593 and sparse in the Y1657 pre-exposed controls. UNC0646 treatment in the last seven days did alter localisation of Ki67 in Y1657 normoxia control to be more superficial. This was not replicated in Y1593 sample which had no Ki67 evident with the addition of UNC0646. Subjectively there was more labelling in both the treated pre-exposed samples, comparable to normoxia untreated controls. Scale bar = 50 µm
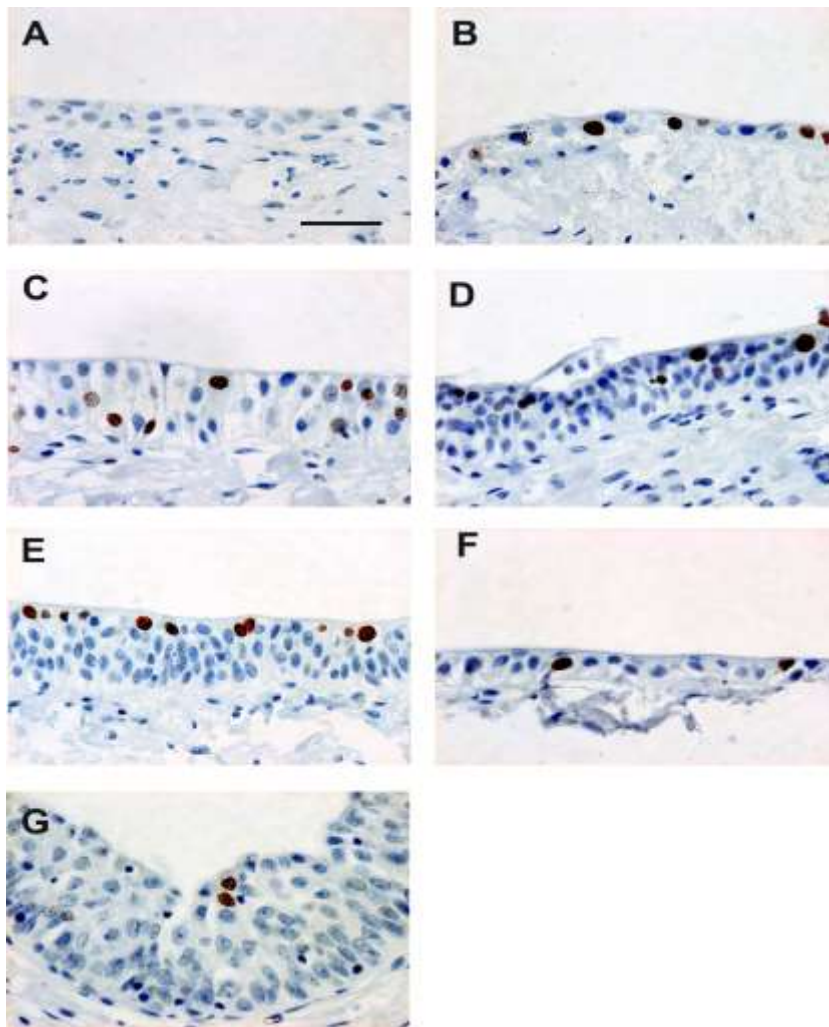
Figure 4-31: Immunoperoxidase labelling of Ki67 expression and localisation during seven days treatment with UNC0646

*Organ cultures (Y1713) were treated with 500 nM UNC0646 and formalin fixed at the following time-points for immunochemical investigation. **A**: day 1, **B**: day 2, **C**: day 3, **D**: day 5, **E**: day 7, **F**: pre-exposed no treatment day 7, **G**: In situ. Expression of Ki67 progressed from basal to superficial, with a subjective increase in intensity at all time-points compared to day 1, including day 7 in the untreated OC. Treatment as compared to no treatment improved the thickness of the urothelium by day 7 (**E** compared to **F**). Scale bar = 50 µm*

Sparing of the superficial cells was seen with p63 labelling in normoxia organ cultures treated with UNC0646, consistent with untreated controls and *in situ* expression (***Fig. 4-32***). One of the donors had loss of p63 expression in response to pre-exposure to hypoxia and the other retained basal labelling only. The addition of UNC0646 did increase the intensity and number of nuclei labelling positive for p63. The analysis of labelling over the seven days treatment with UNC0646 demonstrated that with increasing thickness of urothelium there was an associated increase in p63 expression (***Fig. 4-33***)
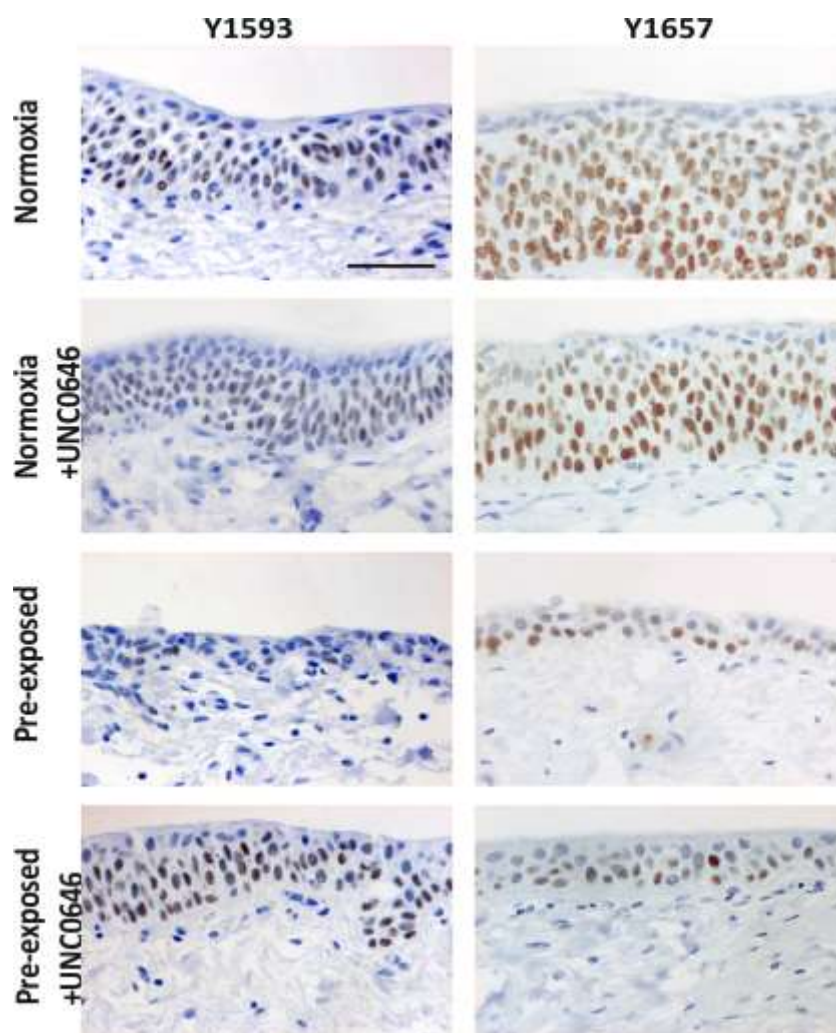
Figure 4-32: p63 expression and localisation in two independent organ cultures ± UNC0646

P63 was located within the basal and intermediate layers. This was not replicated in the Y1593 pre-exposed sample which had no p63 evident. However with the addition of UNC0646 p63 was present within the normal pattern of distribution. Subjectively there was more labelling in both the treated pre-exposed samples, comparable untreated pre-exposed sections. There was also more urothelium in the pre-exposed treated samples compared to those without treatment. Scale bar = 50 μm
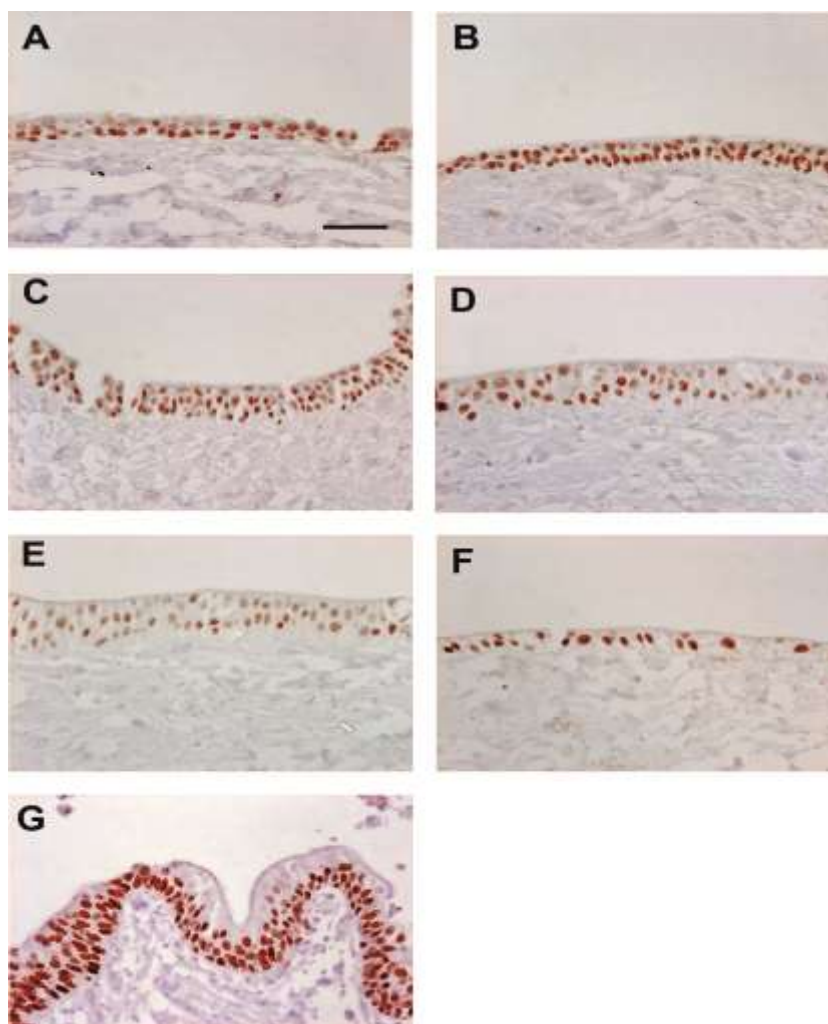
Figure 4-33: p63 expression and localisation over seven days of treatment with 500 nM UNC0646

Organ cultures (Y1713) were treated with 500 nM UNC0646 and formalin fixed at the following time-points for immunochemical investigation. A: day 1, B: day 2, C: day 3, D: day 5, E: day 7, F: pre-exposed no treatment day 7, G: In situ. Expression of p63 remained basal and intermediate. Treatment as compared to no treatment improved the thickness of the urothelium by day 7 (E compared to F). Scale bar = 50 μm

4.5 Discussion

4.5.1 Impact of epigenetic modifiers on the compromised urothelial phenotype

Initial work in this chapter focussed on the application of two different classes of epigenetic modifying agents individually and in combination to NHU cells exposed and pre-exposed to hypoxia *in vitro.* The hypothesis being tested was that the heritable compromise of urothelial cell health seen in Chapter 3 would be responsive to such manipulation. Results indicated that use of UNC0646, a specific inhibitor of histone methyl transferase enzyme G9a and its close relation GLP appeared to significantly reverse the compromised phenotype to enable barrier formation and repair (***Figs 4-3 to 4-6***).

Trichostain A is known to promote cell cycle arrest in G1 (Yoshida and Beppu, 1988) and therefore could not be applied during active proliferation, leaving only the differentiation period. Despite there being interest in the use of HDACi in epithelial injuries (Costantini et al., 2009) and synergistic actions of HMT and HDAC inhibitors (Fiskus et al., 2009) Trichostatin A did not alone have any effect on trans-epithelial resistance values acquired by two cell lines (***4.6a-b***). In addition it did not convey any advantage in combination with UNC0646 over UNC0646 alone (***Fig 4-7***). The use of DMSO as a vehicle control was important as DMSO itself has been cited in the literature as a potential epigenetic modifying agent (Iwatani et al., 2006).

There was no supporting evidence that the compromise of urothelial differentiation capacity was directly associated with HIF-1α expression. Organ cultures showed a subjective reduction in the median nuclear HIF-1α labelling intensity in all oxygen tensions upon addition of UNC0646, but this was not significant. By RTPCR there was a potential reduction in transcript levels for HIF-1α when samples had been maintained and differentiated in hypoxia. Recent literature has demonstrated that chronic unremitting hypoxia is associated with a switch from HIF-1α to HIF-2α in order to activate genes permitting adaptation to chronic hypoxia (Koh and Powis, 2012) and this could be worth checking in the hypoxia disease model. It is worth considering that the organ culture system lacks an immune component that would be active in the *in situ* situation.

The subjective increase in LDHA transcript does support HIF-1α having played a part in the ongoing processes within the hypoxia model, as it is one of the genes preferentially activated by HIF-1α than HIF -2α (Koh and Powis, 2012). Equally VEGF transcript abundance is governed predominantly by HIF-2α and there was little qualitative difference seen by RTPCR between hypoxic and normoxic cultures. It would be of interest to assess the presence of HIF-2α in urothelium in the experimental model but also in the patient derived samples and cell populations. However it could be that the mechanism of reversal of the compromised phenotype is not a direct consequence of changes in HIF-1α.

ZO-1 had been identified as being a compromised barrier component in Chapter Three *(section 3.4.7)* by immunocytochemistry. The application of UNC0646 did appear to improve the expression of ZO1 at cell margins (**Figs. 4-*11a* & *4-11b***). RTPCR did not provide any definitive support for the immunocytochemistry images seen. There was a subjective reduction in total ZO-1 band intensity in the compromised samples. ZO-1α+

transcript bands appeared more intense in the pre-exposed samples that had been treated with UNC0646 (*Figs. 4-12*). It was unclear of the significance of these results, given that they are not in keeping with initial reports describing the switch between the two isoforms of ZO-1 upon differentiation. This "switch" was first described in fetal tissue (Sheth et al., 1997) and has recently been reproduced in human urothelium (Smith et al 2014). More recent work has questioned the timing of expression of the different isoforms of ZO-1 in terms of mRNA and protein (Ciana et al., 2010) and there appears to be some uncertainty of what is "normal" in both health and disease. RtPCR is non-quantitative and more work needs to be done to elucidate the importance of ZO-1 in terms of the barrier recovery seen with the addition of UNC0646 in heritably compromised urothelium.

4.5.2   The impact of UNC0646 on H3K9Me2 in the compromised urothelial phenotype.

Histone methylation is a post-translational process (Greer and Shi, 2012) which does not act by altering chromatin structure as too small to create a change in either histone tail charge or configuration (Bannister and Kouzarides, 2011). Methylation at lysine sites on histone effects changes in gene expression by altering the affinity of the chromatin to particular proteins, such as transcription factors; this is achieved by changes in basicity and hydrophobicity (Nakayama et al., 2001). Therefore UNC0646, by inhibiting G9a/GLP appears to have reduced the repressive H3K9Me2 mark. The result is that by removal of methyl groups particular promotors of urothelial differentiation and regeneration have more attraction to transcription factors perhaps including PPARγ (Wang et al., 2013). One possibility of trying to identify which promoters are associated with the H3K9Me2 mark after exposure to hypoxia would be to use Chip-Seq analysis.

The improvement in the urothelial thickness in organ cultures achieved within just seven days of applying 500 nM UNC646 was striking. UNC0646 not only improved the thickness of urothelium but also the subjective presence of urothelial protein markers of differentiation including CK13, CK20 and UPK3a. Whether this was as a direct consequence of UNC0646 or secondary to the urothelium regenerating and then expressing markers of urothelial differentiation is uncertain at present.

The increased labelling for other markers, such as p63 and Ki67, with UNC0646 treatment is probably associated with the increase in regeneration, including active cellular division, in order to achieve the enhanced structure of the previously compromised urothelium. Important for translational studies are that none of the markers assessed had aberrant labelling with the addition of UNC0646 and tissues maintained a urothelial phenotype, including those in normoxia. Particularly notable was the reduction seen in CK14 labelling in organ cultures in the presence of UNC0646, given that CK14 is not normally expressed by the urothelium. The rapidity of the apparent recovery of pre-exposed urothelium with UNC0646 would suggest that any potential translational application would require only a short treatment – although obviously studies of long-term effects would be required.

Although UNC0646 and related G9a inhibitors do not institute well documented effects on the proliferative phenotype it is known to have a role in limiting replication of DNA damaged cells and many different cancer cell types. For this reason many histone demethylase inhibitors have been investigated for possible clinical translation predominantly for the treatment of cancer. Reported tumours of interest have including: head and neck squamous cell carcinomas (Li et al., 2014), neuroblastomas (Ke et al., 2014), lung and breast carcinomas (Chen et al., 2010, Dong et al., 2012), however the predominant area has been haematological malignancies.

The first reports of the use of a HMT inhibitor as an anti-cancer drug was reported by Spannhoff et al in 2009. In this study S-adenosylmethionine (SAM) and related analogues were found to be non-specific and therefore their use limited (Spannhoff et al., 2009). Chaetocin is a fungal mycotoxin and competitive against SAM therefore acts as a lysine methyltransferase. At low concentrations it was reported to inhibit G9a with limited "off-target" action (Greiner et al., 2005). The attraction for anti-cancer therapy is that chaetocin induces cellular oxidative stress and targets rapidly proliferating cells (Isham et al., 2007), it is thought to accomplish this by acting as a substrate for theoredoxin reductase-1 (Tibodeau et al., 2009). EZH2 inhibitors, such as 3-Deazaneplanocin A (DZNep) have also been of particular interest for cancer therapeutic works due to the role of EZH2 in cell proliferation (Glazer et al., 1986). DZNep targets EZH2 levels directly and reduces methylation at H3K27 in human acute myeloid leukaemia cells (HL-60, OCI-AML3 (Fiskus et al., 2009)). The results of this methylation inhibition was cell cycle arrest and apoptosis believed to be mediated through cell-cycle regulators p21, p27, and FBXO32 and DZNep.

A specific G9a inhibitor that targets H3K9Me2 without altering levels of mono- or trimethylation and other lysine methylation sites is BIX-01294. A mouse model has been used to assess the effect of a combination of BIX01294 and a calcium channel activator (BayK8644), which has been reported to generate induced pluripotent stem cells *in vitro* (Shi et al., 2008). BIX-01294 has also been used as a reprogramming agent in bone marrow cells to generate a cardiac competent phenotype by reduction of methylation of H3K9 (Mezentseva et al., 2013). However BIX01294 was toxic to cells at 4.1 µM compared the reported therapeutic 2.7 µM that the Shi study used (Shi et al., 2008). The problem with the poor delineation between toxic and therapeutic doses will make BIX-01294 an unattractive compound for translational studies.

Chapter 4: Application of epigenetic modifying agents to urothelium compromised by hypoxia or neuropathy

Regenerative medicine applications in paediatric urology: barriers and solutions

The UNC family of compounds are a group of potent and increasingly selective G9a and GLP inhibitors. The purpose of exploring 2, 4-diamino-6, 7-dimethoxyquinazoline structure was to overcome the narrow margin between toxicity and functional potency. UNC0224 and UNC0321, early members of the UNC family were found to inhibit other HMTases (SET7/9 and 8) (Liu et al., 2010) and have reduced potency compared to BIX-01294 (Chang et al., 2010). Work to improve the UNC family in terms of improved specificity and reduced cellular toxicity has resulted in the production of more compounds, the most recent of which was UNC0646 (Liu et al., 2010).

Excitingly in this chapter the application of UNC0646 onto urothelial cells cultured from diseased bladders, resulted in an improvement in two cell lines out of three. The third had a normal barrier in the control arm; importantly UNC0646 did not increase nor decrease the barrier in these cultures. However the vehicle controls in the other two donors, in which there was amelioration of TEER values with UNC0646, both had poor barrier formation. Although these results have shown UNC0646 to be a real prospect for urothelial regeneration not only in a disease model but also on urothelium from diseased bladders, like all histone demethylase inhibitors this is still at a very early pre-clinical stage, indeed there are currently no ongoing clinical trials with such agents, further pre-clinical work obviously needs to follow.

Using the data presented here, UNC0646 or a related compound, could improve the treatment for patients with end-stage bladder disease via two potential therapeutic modalities:

1) Harvesting of patient urothelium for expansion and differentiation *in vitro* with the application of UNC0646 at the differentiation stage and cessation of treatment prior to use of the urothelial sheet in a composite cystoplasty procedure.

2) Intravesical instillation of UNC0646 over a short treatment timeframe to try and rejuvenate diseased urothelium *in situ* after standard augmentation.

The second option would only be feasible once the bladder has been augmented and the bladder no longer experiencing raised pressures and thus ongoing hypoxia. As found in this chapter UNC0646 did not improve urothelial compromise seen in a persistently hypoxic environment.

Although one of the disease urothelium donors (Y1042) had normal barrier formation the pressure within the bladder on urodynamic tests performed on the patient was deemed high. It is important to note however that in the high pressure "cohort" the pressure was the second lowest of eight. Is it possible that there is a window of opportunity for alternative treatment in this group of patients where there is increasing pressures but *in vitro* the cells appear not to have acquired any inherited changes?

Procedures comprising of release of the detrusor muscle and associated fibrosis in order to make the bladder mucosa bulge and improve capacity exist; these are called auto-augmentation or detrusorectomy. Unfortunately results of such operations are mixed and some patients do go on to require enterocystoplasty; it is thought that this may be in part due to initial patient selection. However, could regenerative medicine offer a strategy to improve the outcome of such procedures and stop patients progressing to end-stage bladder disease and requiring augmentation; this possibility will be discussed in Chapter 5.

5 Use of decellularised scaffolds in paediatric urology

5.1 Background

Tissue engineering and regenerative medicine (TERM) offer potential strategies for managing conditions where there is an inherent lack of healthy tissue or where the presence of disease limits the use of the patient's own material. These approaches can be broadly divided into implantation of *in vitro* expanded autologous cells or use of biomaterials, such as natural acellular matrices (ACMs) or where both methods are combined in the form of cell-seeded biomaterials or ACMs. Potentially these approaches could provide improvements in the therapies offered by paediatric urologists where current surgical approaches are flawed or fail (reviewed by Garriboli et al., 2014, Wezel et al., 2011).

5.1.1 Bladder auto-augmentation

Chapter Four concluded with a brief description of the current treatment options available to patients in whom medical and minimally-invasive therapies are failing, but who still have reasonable bladder capacity and do not warrant full augmentation using a bladder substitute, such as enterocystoplasty. These options include auto-augmentation and detrusorectomy, in which the patient's own bladder is utilised in order to increase capacity, thereby reducing intra-vesical pressures (Cartwright and Snow, 1989, Chrzan et al., 2013). Both procedures have been recognised to be of most use in patients whose bladders still have some capacity but also show reduced compliance and detrusor hyperreflexia (Snow and Cartwright, 1999).

The principle of such procedures is the opening and removal of the detrusor using dissection to create a mucosal "bulge" or diverticulum and thereby increasing capacity. Because of the detrusor removal the outpouchings of mucosa are exposed and at risk of perforation (Dik et al., 2003), with some animal model work suggesting this risk to be greater in auto-augmentation compared to enterocystoplasty (Rivas et al., 1996). It is accepted that small, sub-clinical perforations or surgery itself can result in adhesions to other structures and fibrosis. Collagen infiltration into the mucosal diverticulum has been noted; this results in the bladder becoming small and fibrosed, as in end-stage bladder disease (Perovic et al., 2003). Patients who develop such complications post-detrusorectomy would require augmentation (Veenboer et al., 2013).

To reduce the risk of perforation, there has been some attempts to cover the exposed mucosa with flaps derived from a variety of autologous sources including uterus (Dapena et al., 2013), rectus muscle (Perovic et al., 2002), stomach (Close et al., 2004), small intestine (Cranidis et al., 1998), sigmoid colon (Lima et al., 2004) and peritoneum (Close et al., 2001), all of which remain on the donor organs' own vascularised pedicle. Could TERM and specifically the use of biomaterials provide alternative strategies for such procedures? Such treatments would not only prevent other organs being used as protective flaps, but also aim to stop patients entering end-stage bladder disease and requiring augmentation.

One group has reported using synthetic and natural biomaterial scaffolds in the form of polyglycolic acid (PGA) and small intestinal submucosa (SIS) in auto-augmentation (Lai et al., 2005). They used a rabbit bladder augmentation model to not only examine the difference between PGA and SIS, but also cell-seeded and unseeded scaffolds. Their findings after 6 months were that all four experimental groups maintained a urothelial lining within the created diverticulum, but only the PGA unseeded cohort

resulted in satisfactory bladder capacity and bladder wall morphology. The other groups resulted in shrinkage with poor smooth muscle cell infiltration. There was no difference between seeded and unseeded. It was concluded that PGA offered better support than SIS to the auto-augmentation (Lai et al., 2005).

SIS is derived from small bowel and is therefore not homologous to the urinary tract. In adults, the normal small intestine wall thickness is believed to be between 1-2mm (Macari and Balthazar, 2001), but normal mean bladder wall thickness is 4.78mm (Abou-Gamrah et al., 2014); this discrepancy would be even greater in a diseased bladder. A decellularised scaffold derived from the urinary bladder may provide a more suitable, homologous bladder wall substitute.

5.1.2 Hypospadias

Another urological condition that could benefit from TERM approaches is hypospadias, a common congenital problem affecting as many as 1 in 250 boys (Kraft et al., 2010). The complexity of the anomaly varies and is dependent on the position of the urethral meatus, deficiency of good quality tissue and the absence or presence of chordee. A majority of hypospadiases require surgical correction and further surgery is required in some cases. There is a huge array of surgical techniques described in the literature, which illustrates the absence of any gold standard, (reviewed by Springer et al., 2011).

Management of complex and redo hypospadias is challenging predominantly due to an inherent deficiency of good quality urethral and peri-urethral tissue (Sunay et al., 2007). Recent studies of acellular matrices being utilised to reconstruct urethras either alone or seeded with cells have been published in both animal (Li et al., 2008) and human (Fossum et al., 2007) studies with varying success

The importance of a lack of healthy tissue as a contributory factor in the development of urethral fistulae (UF) after urethroplasty was considered by Springer and Subramaniam (Springer and Subramaniam, 2012), who hypothesised that a lack of support in the peri-urethral tissues promotes turbulent flow and contributes to the development of UF and other complications. These authors utilised Pelvicol ™ as an implant to splint the peri-urethral tissue in 12 boys and reported good cosmetic and functional outcome in all, albeit that one child suffered an infection (Springer and Subramaniam, 2012).

Pelvicol™ (Bard, Covington, GA) is an acellular porcine dermal collagen matrix available "off-the-shelf" and has also been recognised as having non-homologous roles in adult urology and uro-gynaecology, being used as a sub-urethral sling (Abdel-Fattah et al., 2004), to aid colposuspension (Khan et al., 2014), enhance cystoplasty (Barrington et al., 2006) and ameliorate Peyronie's disease (Chrobok et al., 2008, Lloyd SN, 2002) amongst others. Other non-homologous-derived ACMs have also been used for the treatment of hypospadias and urethral reconstruction; including small intestine submucosa (SIS), which was been described as a "biological bridge" enabling surrounding tissues to recover (Mantovani et al., 2011). Another group found the use of SIS did not reduce the reported fistula rate and in 50 patients recorded a re-stricture rate of 20% within 6 months; these complications were felt to be related to the length of the ACM graft used in the repair (Fiala et al., 2007).

ACMs have also been used as an onlay-graft forming an integral part of the reconstructed urethra as opposed to enhancing peri-urethral tissues and such work has been extensively reported in the literature. Chen *et al* created a ventral urethral defect in 10 male rabbit urethras and performed a urethral repair using homologous acellular porcine bladder submucosa (Chen et al., 1999). After 6 months there was limited fibrosis and good integration reported. A further study assessed the role of

acellular cadaveric human bladder matrix in the treatment of 28 patients presenting with urethral stricture. These patients were followed for a mean of 37 months. Twenty four patients were recounted to have had a good outcome, one had developed a self-resolving sub-coronal fistula and four patients had an anastomotic calibre change on urethrography (El-Kassaby et al., 2003).

Complete reconstruction of the urethra has also been attempted using autologous bladder-derived urothelial cell sheets seeded onto acellular dermis matrices. These constructs have been used as onlay-grafts to construct a neo-urethra. One group reported a case series of six boys, with severe hypospadias with a median follow-up of 7.25 years. The complication rate was similar to that reported in the literature with 2/6 developing stricture and a further 2/6 resulting in fistula formation with all 4 requiring intervention (Fossum et al., 2012). One major issue with such studies is the lack of a robust control arm. Such a design would require age and disease severity matching and require comparison between standard surgical technique, ACM alone and cell-seeded ACM. Given the small number of cases in individual centres a multi-centre approach would be required.

5.1.3 Choice of Biomaterial

Decellularised cadaveric bladder and SIS matrices are non-cross-linked ACMs, whereas Pelvicol ™ aka. Permacol™ is a cross-linked matrix. Non-cross-linked materials are reported to have a superior profile in terms of host tissue integration and cellular ingrowth with neovascularisation (Butler et al., 2010, Macleod et al., 2005). However, some long-term animal models are beginning to demonstrate variation in results. A rodent study (de Castro Bras et al., 2010) demonstrated no difference between Permacol™ and SIS at 12 months, whereas differences were noted at earlier time

points. The same study was unable to find evidence of encapsulation of the

Permacol™, which had been identified in other work (Valentin et al., 2006).

Nevertheless when considering findings from rodent models the potential disparities

between the animal and the human situation must be respected. The mechanical

strength of non-crosslinked ACMs have been thought to be inferior to chemically

cross-linked alternatives, such as Pelvicol™, however some long term animal studies

are also beginning to question this finding (Mestak et al., 2014).

5.2 Aims

Porcine acellular bladder matrix (PABM) is a non-crosslinked scaffold that has been developed from full thickness porcine bladders (Bolland et al., 2007). The PABM was shown to be biocompatible to cells in vitro (Bolland et al., 2007) and as part of the patent filing was shown to be biocompatible in transgenic mice lacking the α-gal epitope responsible for hyperacute rejection of xenogeneic material in humans (WO2007110634A2). The strong, but compliant properties of the PABM suggested that it may be a suitable biomaterial for homologous use in the urinary tract, such as in hypospadias repair, or as a free graft to support bladder augmentation.

The aim was to develop a large experimental model equivalent to anatomical size to children, in which to test surgical compatibility and examine the potential use of PABM in paediatric urology. The following experimental objectives were investigated:

- To determine the cellular integration properties of PABM when surgically implanted in vivo as a free onlay graft in a peri-urethral position

- To compare the integration of non-crosslinked PABM with that of a commercially-available crosslinked decellularised dermal matrix (Pelvicol ™)

5.3 Experimental Approach

A large surgical model was required to test surgical compatibility and provide an adequate model in terms of anatomical size, in comparison to children. A porcine model was chosen for this purpose with the male animals weighing on average 16.59 kg ± 1.25. Mr Ramnath Subramaniam provided surgical operative expertise with previous porcine surgical model work (Turner et al., 2011), which abrogated the learning curve for the surgical procedure. He also provided experience of implantation and handling of Pelvicol™ (Subramaniam et al., 2011). From an immunological perspective porcine models are superior to many others due to similarities in the macrophage populations (Kapetanovic et al., 2012).

5.3.1 The Porcine Model

Twelve large white hybrid (LWH) pigs were used in the experimental study; six animals were implanted with Pelvicol ™ and six with PABM. These were divided into two groups of six with three pigs having PABM and the other Pelvicol™ implanted into the peri-urethral tissues approximately five months apart (*Figure 5-1*). This was to limit any inherent bias that may have ensued by implanting either only Pelvicol ™ or PABM first, thereby improving the surgical procedure used for the second batch of six. Schedule 1 was performed three-months post-operatively as this was felt to be an appropriate time to evaluate integration (section **2.13.6**). During the Pelvicol ™ clinical study children were followed-up at six months to assess outcome and at that juncture there was felt to be no clinical evidence that the Pelvicol ™ graft had not been integrated. Three months was chosen to ensure that there would be some persistent material within the explanted tissue to help investigate any ongoing remodelling process.

Peri-urethral tissue from a control pig that had not been operated upon was also acquired for comparison from the same breed, age and weight as the study pigs. All tissues were fixed in either 10% formalin or zinc salt fixative (see Appendix II), processed and embedded into paraffin wax, before sectioning and analysis by histology and immunohistology.

All work was carried out in accordance with the Animal (Scientific Procedures) Act 1986 under project licence (PPL70/7930) and personal licence (PIL 70/25844). Refer to section **2.13.4** for more details of anaesthesia, general animal husbandry and peri-operative care.

During the surgical implantation of the grafts, the peri-urethral plane was opened. The graft itself was secured with eight dissolvable Vicryl™ (polyglactin 910; Ethicon) sutures, similar to the surgical procedure reported (Springer and Subramaniam, 2012) in urethrocutaneous fistula (UF) treatment. At the time of operation the two Prolene® (polypropylene; Ethicon) non-dissolvable "marker" sutures were placed at either end of the opened superficial fascia to the graft, this was to enable localisation of the implant site. The rest of the superficial fascia and subcutaneous fat (where necessary) was closed using Vicryl™ interrupted sutures. Skin closure was achieved using Vicryl™ or Monocryl® in a continuous closure. Two further Prolene® sutures were placed as external markers of the closure to enable successful location of the site at three-months be that the persistence of the suture of scarring at the suture site. A schema for the procedure is shown in *Figures 5-2* and *5-3.*

An operation note was completed for each pig (Appendix V) and attached to their individual care plans. Weight gain was plotted over the three-month period to assess for any long-term complications. All animals were monitored and evaluated at least twice/day by myself, Dr Syed Khawar Abbas as the named veterinary surgeon (NVS) or

animal welfare officers working for the University of Leeds. For more details of general animal husbandry and care see section **2.13.4**
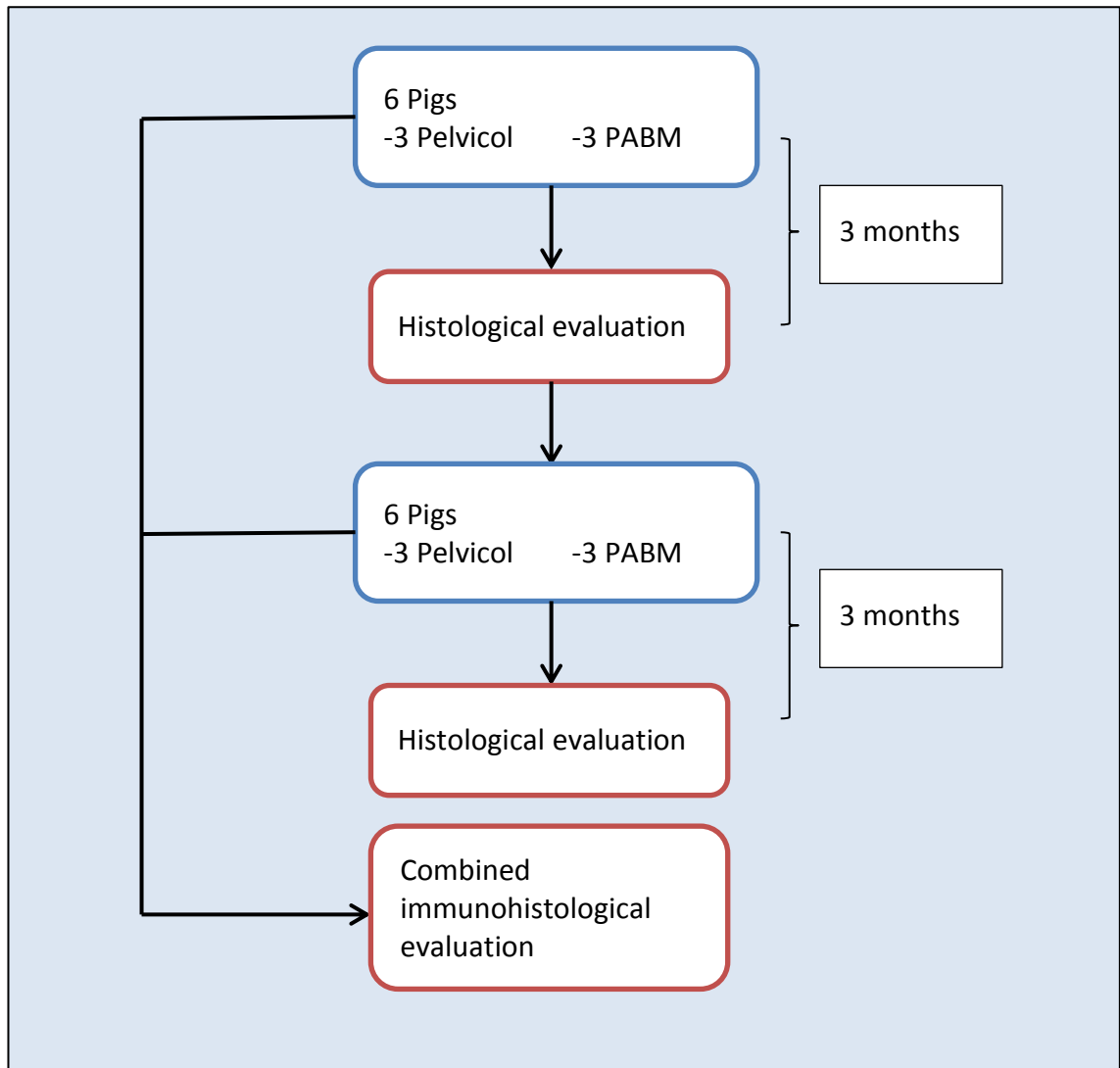
Figure 5-1: Flow scheme of porcine peri-urethral graft model
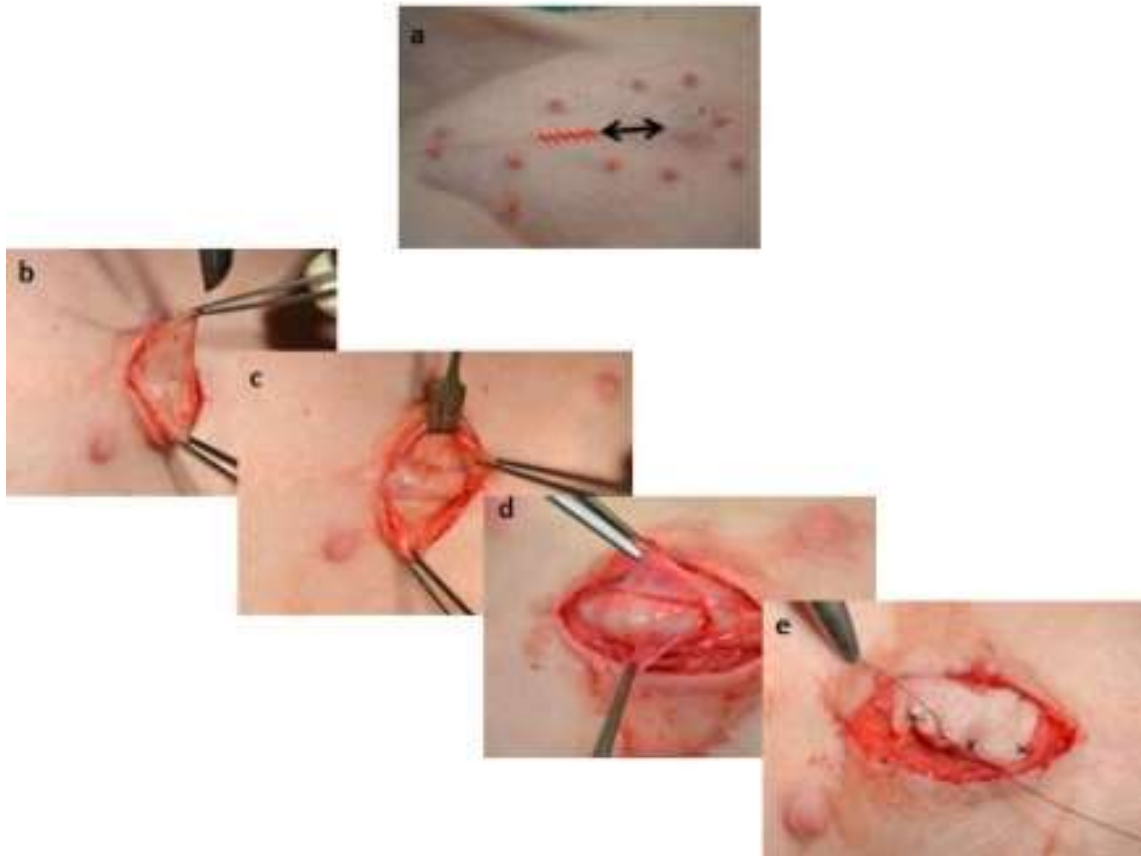
Figure 5-2: Initial steps of the peri-urethral graft procedure

*An incision (red hashed line in **a**) was made approximately 5cm caudally from the preputial sac (black arrow **a**). The superficial adipose tissue was dissected (**b**) to reveal the peri-urethral tissues and fascia (**c**). This fascia was opened (**d**) in order that either Pelvicol™ or PABM could be sutured within this space (**e**) with eight Vicryl™ sutures.*
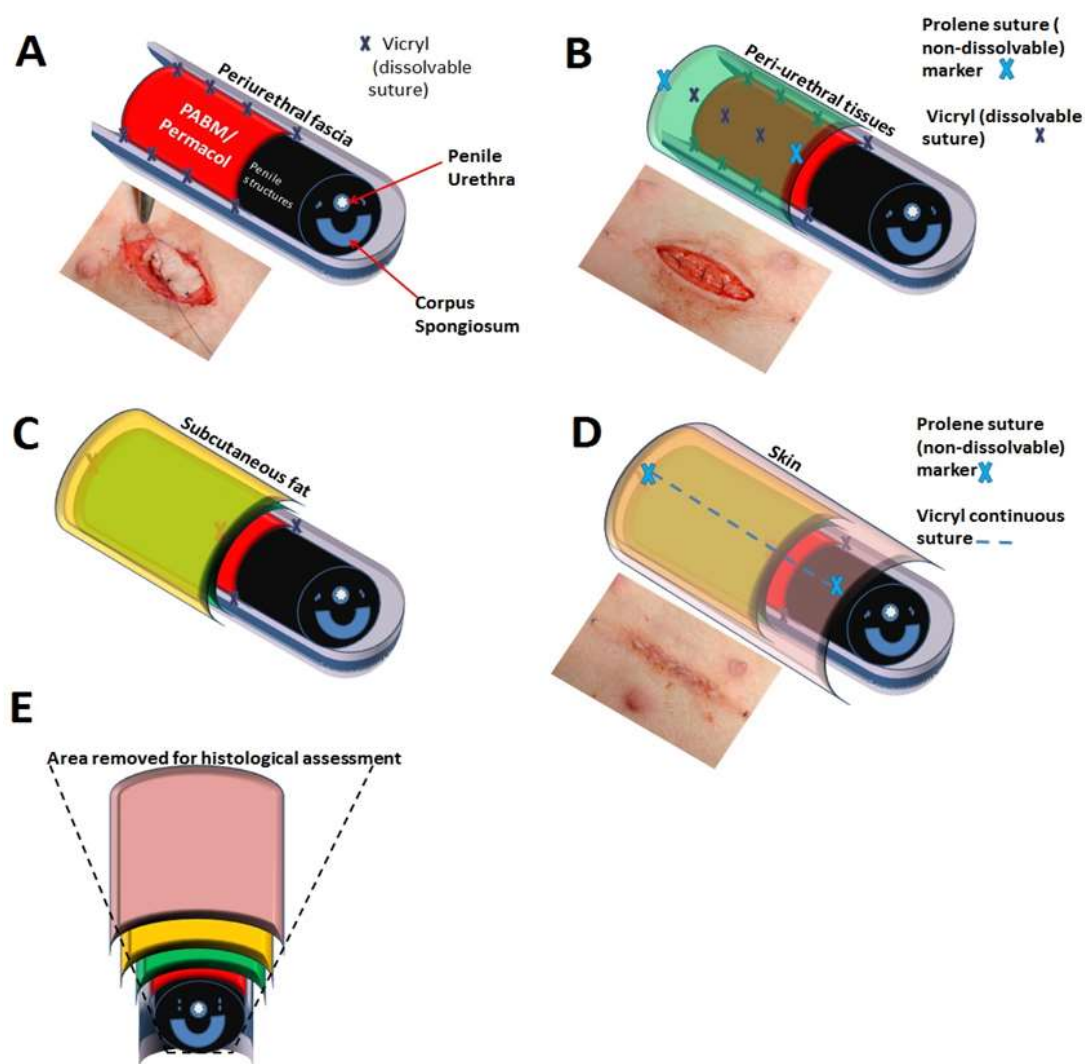
Figure 5-3: Closure of incision and area for histological evaluation

The PABM or Pelvicol™ was placed as a free graft within the peri-urethral fascia (A) and secured with interrupted 4'0 Vicryl™ sutures. Peri-urethral tissues superficial to the fascia were closed over the graft with two 3'0 Prolene® sutures used as markers at either end of the graft (B). Subcutaneous fat was then opposed (C) followed by skin closure achieved with 5'0 Monocryl® (copolymer of glycolide and epsilon-caprolactone) (Ethicon) or Vicryl™ continuous suture with two external Prolene® marker sutures externally at the caudal and cranial end of the incision (D). The area was removed "en-bloc" for histological analysis (E) using both sets of marker sutures as guides.

5.3.2 Histological evaluation of integration at 3 months

Standard H&E staining was performed to evaluate the location, position and general histological appearance of the grafts and peri-urethral tissues, with particular consideration of the extent of cellularisation and vascularisation. The former was also aided by staining with DAPI (4', 6-diamidino-2-phenylindole, Fluoroshield™), which intercalates with double-stranded DNA to identify nuclei. Immunohistochemistry of serial sections was performed to distinguish different cell and tissue elements, but was restricted by the availability of characterised antibodies reactive with porcine tissues (see *Tables 5-1 and 2-1*).

For every experiment a negative control (no primary antibody) was performed alongside a section labelled for CK7 as positive control, which utilised the same anti-mouse secondary antibody. All new antibodies were titrated and optimised to prevent background and non-specific labelling. Positive controls were used when new antibodies were being titrated and optimised to ensure specificity to the epitope of interest.

Table 5-1: Antigens detected by immunohistochemistry

Epitope	*Location of marker*	*Purpose for this study*
Smooth Muscle Actin	Vascular structures Myofibroblasts	To evaluate extent of vascularisation and infiltration by myofibroblasts (within graft)
CD45	Monocyte-derived cells	To identify cells of monocyte lineage
CD163	Reported as expressed exclusively by monocytes and macrophages of tissue-remodelling phenotype	Used ostensibly as a marker of tissue remodelling and integration
CD107a	Non-lineage restricted lysosome-associated membrane protein (LAMP-1) reported in a previous study as useful for identifying tissue-resident macrophages(Bullers et al., 2014)	Marker of macrophages

5.4 Results

5.4.1 Survival and health of surgical recipients

All pigs survived the immediate and long-term post-operative period with no complications relating to the graft implantation. One pig (#401), a PABM recipient, developed a lame right fore-limb immediately after surgery; the reasons for this were unclear, but the NVS did not believe this to be a direct consequence of the graft implantation. The lameness responded to anti-inflammatory medication and rest. Weight gain in #401 was initially delayed, however after the fore-limb had improved there was an increase in weight and the final weight, at the Schedule 1 procedure, was no different to the other animals.

5.4.2 Gross anatomy

Gross anatomy of explants, as visualised at harvest, was no different to that seen in the control animal with no significant scarring, fibrosis or encapsulation. Whereas the PABM grafts could not be identified macroscopically the Pelvicol™ explants could still be readily identified (*Figure 5-4*). In the first cohort of animals some difficulty was encountered, particularly in the PABM group with respect to orientation of the specimen in relation to penile structures. This was due to free movement of the penile structure within a surrounding sheath, which included the peri-urethral tissue and graft site and was a feature seen in the control pig (*Figure 5-5*). To prevent this loss of orientation from occurring in the second cohort, the penile shaft was clamped proximally to prevent movement and the distal end dissected down, guided by the Prolene™ marker sutures. The deep aspect of the penile shaft was cut flush with surrounding tissue but the superficial aspect was removed, complete with superficial fat to help orientate the specimen.
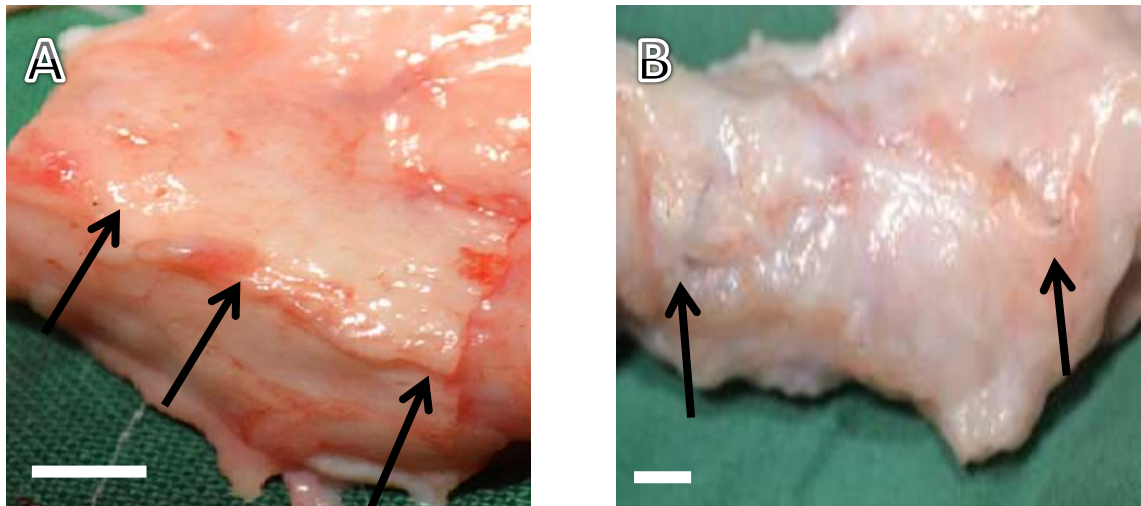
Figure 5-4: Macroscopic appearance of explants 3-months post-implantation

After three months the graft sites were harvested. In (A) the Pelvicol™ graft was visible (arrowed) and the dissolvable sutures were no longer present. The tissues superficial to the Pelvicol™ had been freely folded away from the graft (away from the arrows) with no adhesions or fibrosis evident. Image B represents a PABM explant and shows the deep marker sutures in the fascia just above the graft (arrowed). No PABM graft was visible at the time of removal and there was no defined separation between the graft site and surrounding tissues. However there was no evidence of fibrosis or scarring, the peri-urethral tissue, felt as if there was no graft present. This macroscopically improved integration proved an issue in the localisation of the PABM grafts in the first cohort of animals due to free movement of the peri-urethral tissues (and graft site) in relation to the penile structures and procedural changes were made in the second cohort to try and prevent this. Scale bar 1 cm.
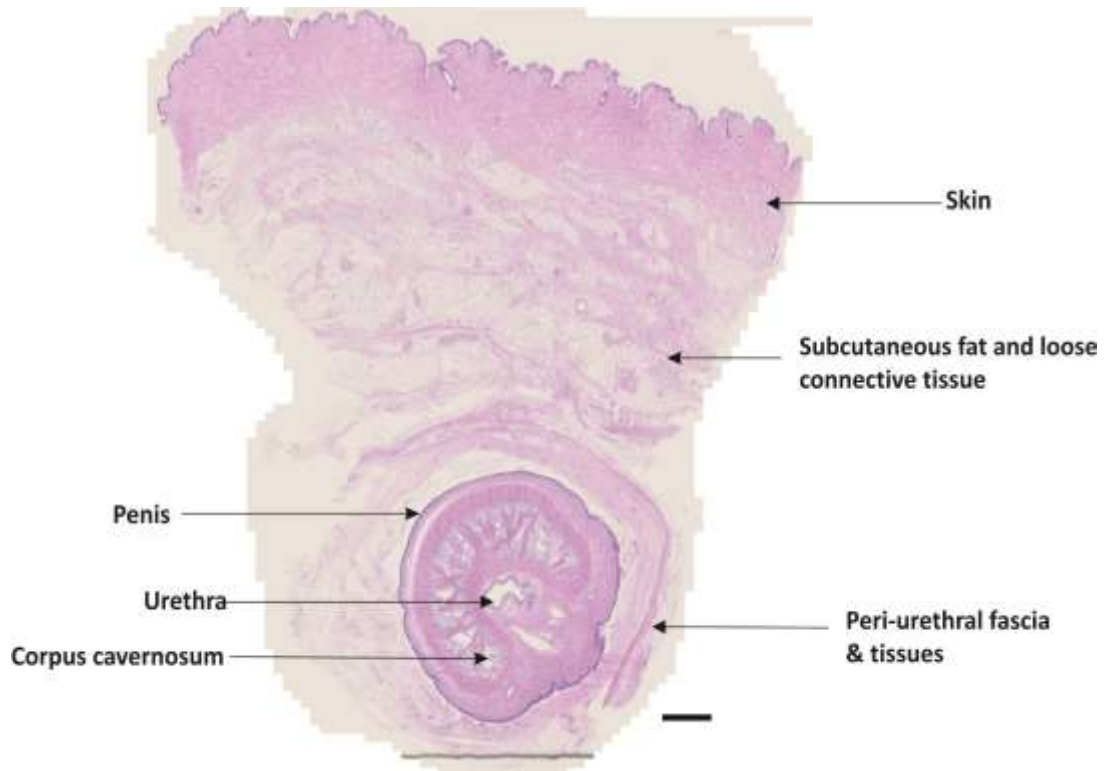
Figure 5-5: Gross anatomy of the porcine penis and peri-urethral region

H&E staining was performed using a section of peri-penile tissue from a control pig.

The gap seen between the penis and the peri-urethral fascia created a tunnel allowing

free movement of the porcine penile structures in relation to the peri-urethral tissues;

the so called "corkscrew penis" associated with boars.

5.4.3 Histology and immunohistology

Sections of Pelvicol™ and PABM that had been taken from grafts prior to implantation were evaluated using H&E and directly compared to sections of graft material 3-months post-implantation (***Figure 5-6)***. Images were evaluated at the same scale to aid graft identification. Eleven grafts from twelve were able to be located within the harvested sections using a combination of H&E staining and immunohistochemistry. No graft (PABM) could be located in one pig.

From the H&E there were no cells detected in sections of non-grafted PABM or Pelvicol™ (***Figure 5-6***, see also section **2.13.3**). Collagen bundles were however identified and these were multidirectional. By contrast cellularisation was apparent within the implanted ACM in sections analysed from all 11 grafts. The images from H&E and immunohistochemistry were evaluated in comparison to those obtained in the control pig ™ (***Figure 5-7***).

Within the control there was good cellularisation noted on DAPI, H&E, SMA and CD107a (***Figure 5-7***), which is homogenous throughout the tissue. The SMA localisation was predominantly related to the corpus spongiosum and vasculature. CD107a was also associated with vessel but also demonstrated widespread labelling throughout the tissue, with few cells present that appeared not to be stained.
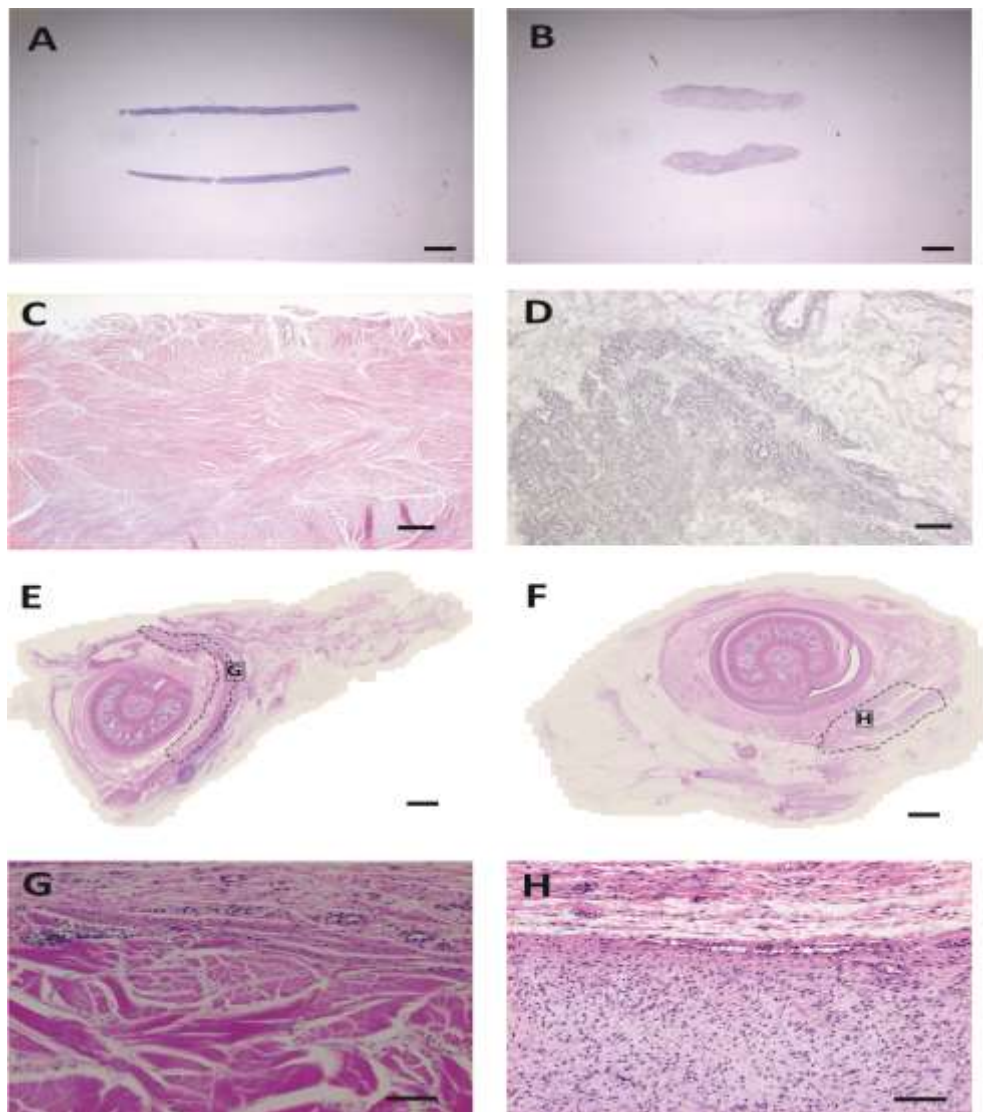
Figure 5-6: Location of Pelvicol and PABM using H&E

Control sections of non-implanted Pelvicol™ (A) and PABM (B) were stained using H&E. The generalised appearance varied between the two materials, with Pelvicol™ having a smaller width than PABM and recognisable by the multi-directional collagen bundles and natural fissures (C). PABM maintained the collagen scaffold of a full-thickness bladder and therefore the appearance was less uniform in comparison (D). After three months post-implantation the Pelvicol™ (study number#663) persisted (dashed line E) and was easily recognisable with vascularisation and cellularisation at the edges of the graft and some integration centrally (G) along the fissures. The PABM margins (F) appeared less distinct (study number#583) (dashed line F) with marked cellularisation see throughout the graft (H). Scale bar 200 μm X 4, 50 μm x40. Other experimental animal sections images are available in Appendix V.
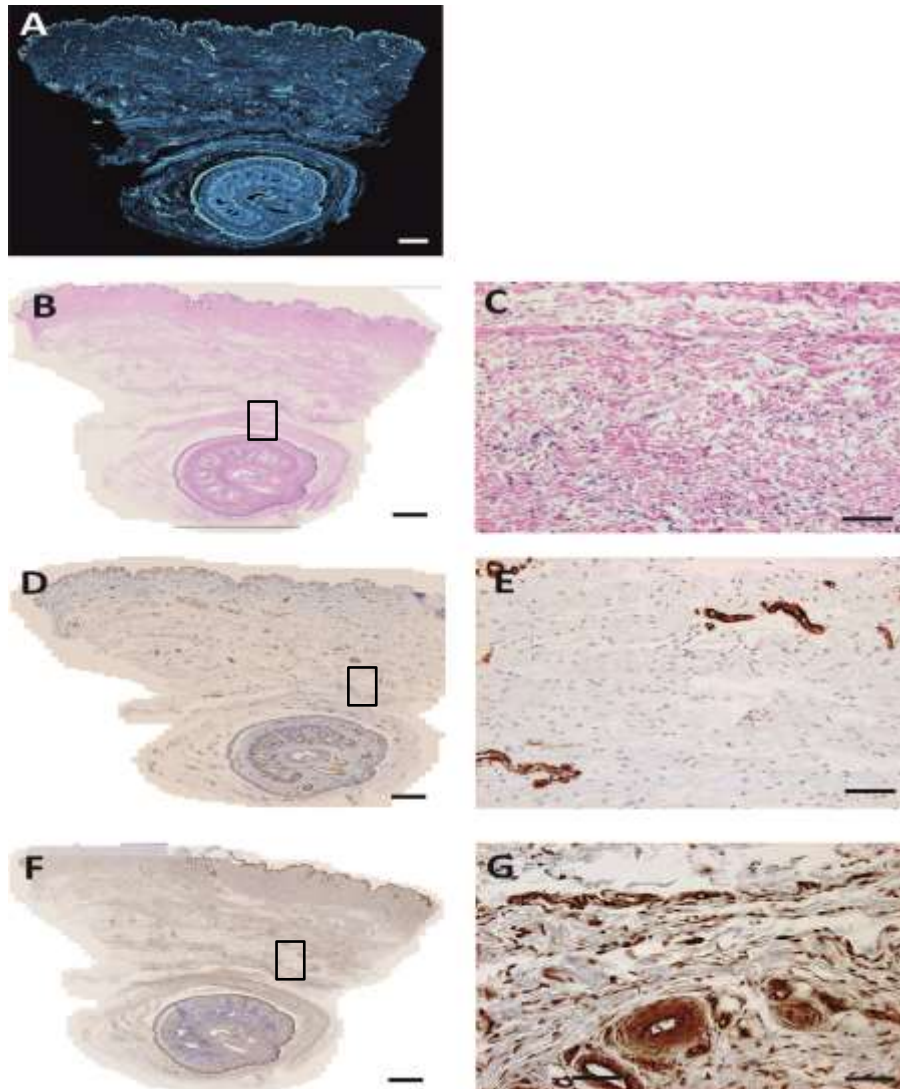
Figure 5-7: Sections from control pig

Fluorescent DAPI staining is shown in (A). H&E stain in (B) has a boxed region of interest which has been taken at higher magnification (C) and identifies well cellularised connective tissue and vasculature. (D) & (E) were labelled for SMA epitope at x4 and x40 magnification respectively. The area shown in (E) is represented by the boxed area in (D). There is sparse SMA labelling predominantly located around vasculature. Labelling for CD107a is shown in (F) and (G) with the latter being within the boxed area in (F). CD107a labelling is seen associated with vasculature but throughout the surrounding tissue, with a few cells not being labelled. Scale bar (A, B, D, F) = 200 μm, (C, E, G) =50 μm.

The Pelvicol™ grafts showed a sparsity of nuclei demonstrated by DAPI and H&E staining and supported further by SMA and CD107a labelling all found with very low frequency within the central region of the graft itself. Infiltration of cells tended to occur through natural pathways within the graft with very little infiltration into the collagen bundles (***Figure 5-8)***. The exception was related to discrete regions marked by a focal infiltration of inflammatory cells. This tended to be at the edges of the graft material, including the superficial edge, and in proximity to suture position (***Figures 5-8 and 5-9***).

SMA appeared to be associated with vessels that were also associated with the interface between Pelvicol™ and host tissues, with some evidence of SMA expression within the collagen bundles adjacent to the graft boundaries. In addition SMA was markedly increased in labelling in areas associated with inflammation, for example the suture site identified in (**Figure 5-9)**. SMA was also found in several explants to be associated with the superficial interface of graft and host, and appeared to be forming a fibrous band segregating the graft way from the native tissues. CD107a was grossly associated with all cells and again was found to have increased labelling in areas where there was a reaction to sutures (**Figure 5-8)**.
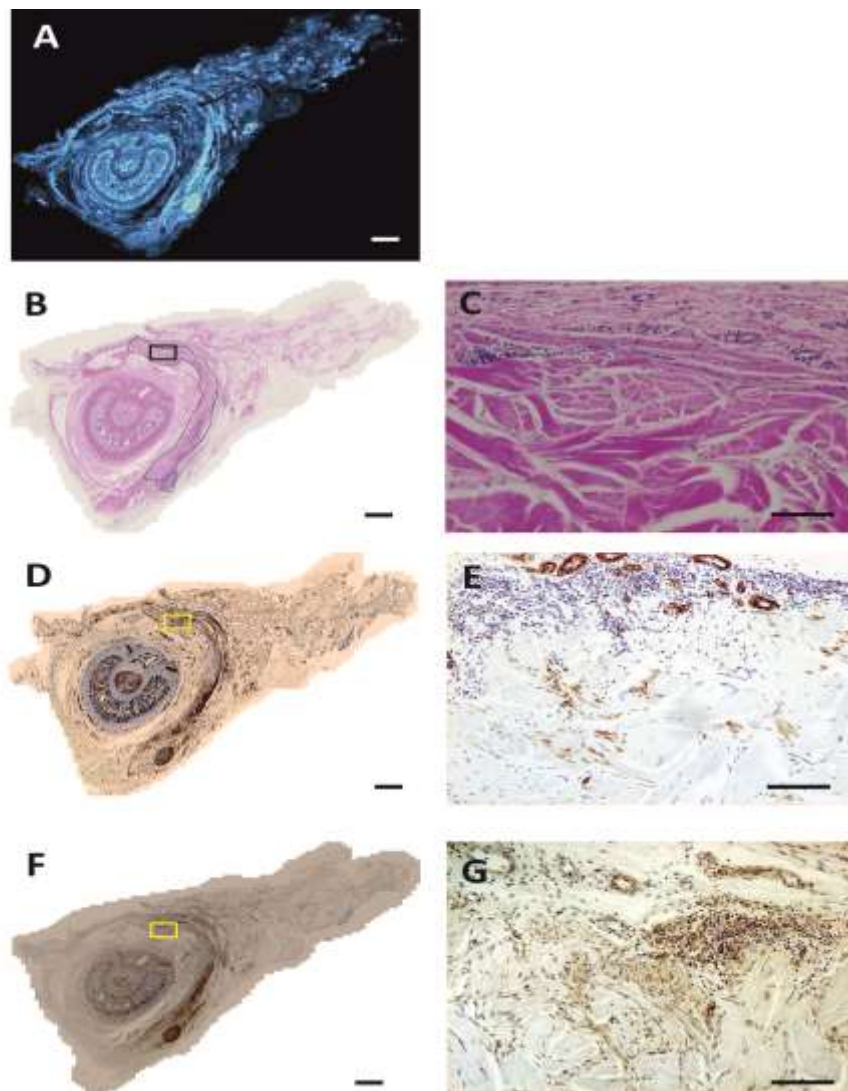
Figure 5-8: Cellularisation in the Pelvicol cohort

*Example shown is from animal #663 (Pelvicol™). DAPI staining of nuclei is shown in **A**. Note the densely packed area of nuclei in **A** (arrowed) likely to be associated with suture material. H&E staining is shown at x4 (**B**) and x40 magnification (**C**) illustrating a lack of cellularisation within the graft itself other than along natural pathways. The Pelvicol™ explants exhibit marked SMA labelling with surrounding vascularisation adjacent to the graft and in areas of inflammation but little within the graft itself (**D&E**). CD107a in **F** & **G** reflects these findings but the pan-macrophage marker also highlights the area of dense cellularisation associated with potential encapsulation (**G**). The rest of the cohort results are available in Appendix V.*
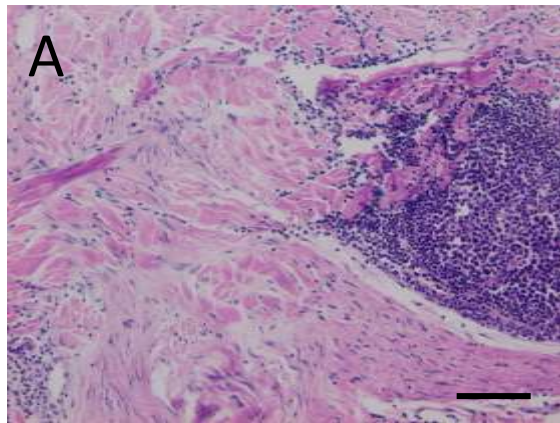
A Area of marked immunocyte infiltration at the edge of the Pelvicol™ graft. Scale bar 50 µm
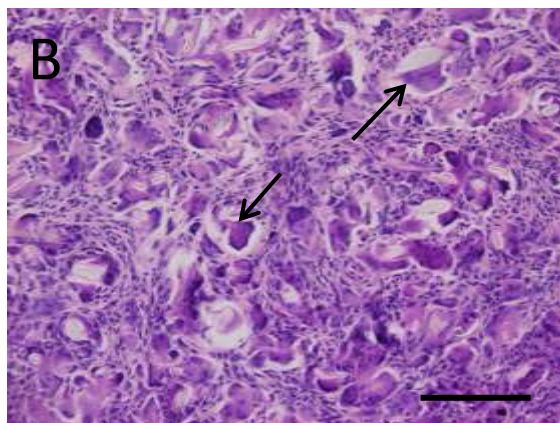
B High magnification of area of interest in **A**. Note infiltrating cells around synthetic fibres (arrowed) consistent with remnant suture material. Scale bar 50 µm.
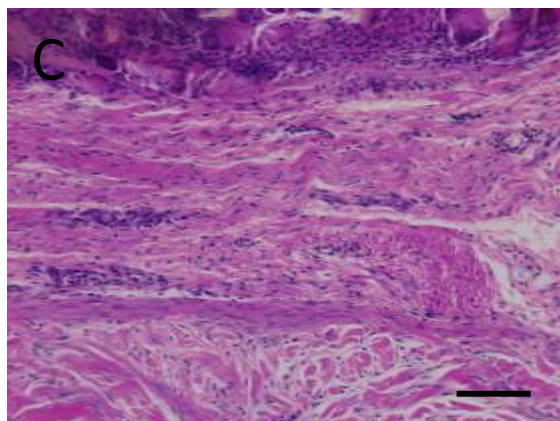
C Further area of increased cellularisation at the superficial border of the graft. Potentially consistent with a degree of encapsulation. Scale bar 50 µm.

Figure 5-9: Other areas of interest noted in Pelvicol explants

PABM in comparison to Pelvicol™ was identified by marked increased cellularity throughout its structure. DAPI staining demonstrated a stark contrast between the relatively acellular subcutaneous fat to the left of image **A**, ***Figure 5-10*** and the PABM to the right-hand side. The region was identified by H&E, although this was similar in structure to surrounding host tissues. On high magnification it is seen that the graft was extremely well cellularised and this is homogeneous throughout the graft.

As observed in the Pelvicol™, evidence of vasculature at the graft peripheries was also found. SMA labelling highlights these nicely in the adjacent host tissue. SMA was also found throughout the graft, with the vast majority of cells labelling positive within the graft itself. The pattern of SMA labelling also helped to identify the morphology of these cells which appeared to be predominantly spindle-shaped. CD107a was expressed by the vast majortiy of cells within the graft and again demonstrated peripheral vascularisation. Unlike Pelvicol™ the PABM grafts did not exhibit the focal areas of cellularisation associated with suture material.
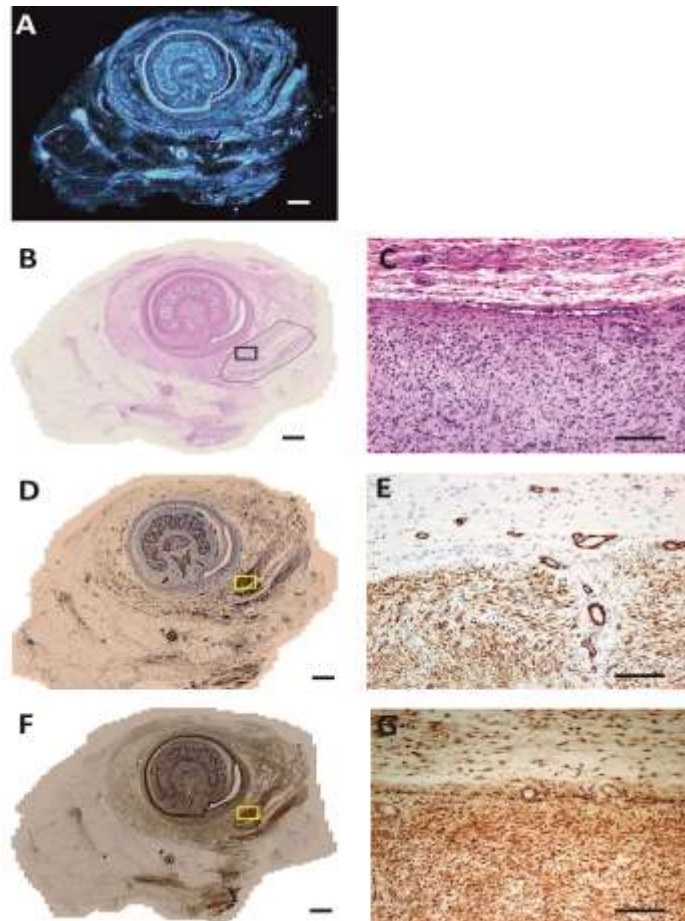
Figure 5-10: Cellularisation of a PABM explant

Example shown is from animal #583 (PABM). DAPI staining of nuclei is shown in (A) with no heterogeneous focal areas of high intensity staining seen. H&E staining is shown at x4 (B) and x40 magnification (C) illustrating complete cellularisation throughout the graft in comparison to adjacent stromal tissue. The PABM exhibited marked SMA labelling (D) by the majority of the cells seen in (C), these appear to be predominantly elongated and spindle-like in morphology. There was evidence of vascularisation along the boundary between graft and host but also encroaching into the graft itself (D&E). CD107a in F & G reflected these findings (G). The rest of the cohort results are available in Appendix V

Formal assessment of cell number using serial sections labelled for CD163 and CD45 was performed.(***Table 5-2***). Given the apparent increase in cellularity in ***Figure 5-7*** in the PABM than Pelvicol™ implants this data was used to assess whether the CD163+ population may , in part, accounted for this. The difference in the number of CD163+ cells in PABM (71.13 ± 33.65) compared to Pelvicol™ (33.61 ± 20.61) was found to be very significant (*p = 0.0011).* This difference in cell number however was not replicated in cells labelled for CD45 ; PABM explants (22.73 ± 24.98) and Pelvicol™ (30.28 ± 43.74) with *p=0.6205.*

As shown above, monocyte-derived cells were identified based on CD45 labelling and other immunohistochemical analysis also showed abundant labelling for CD163. The morphology of the cells labelling for CD163 in the control tissue (***Figure 5-11***) and infiltrating the both biomaterials (***Figures 5-12 and 5-13***) graft appeared predominantly spindle-like in appearance or round, depending on the section angle. The frequency of labelling for CD163 appeared subjectively more prevalent than that for CD45.

The variance between CD163 and CD45 in favour of CD163 was also supported by the serial section data summarised in ***Table 5-2***. This highlighted that all samples had more CD163$^+$ cells than CD45$^+$and that this difference was more apparent in the PABM than in Pelvicol™. The CD163:CD45 ratio, in favour of CD163, was also present in the control pig explant (***Figure 5-11***) which did not have a graft implanted (6.26:1 ± 0.82). Non-parametric statistical analysis (Mann-Whitney U) to compare the ratio values from each biomaterial cohort supported a significant difference between the CD163:CD45 ratios found in Pelvicol™ and PABM, with a two-tailed p-value <0.05.

Table 5-2: Mean total cell number and ratio of CD45+ and CD163+ labelled nuclei

Explant	Median no. CD45$^+$ nuclei (s.d)	Median no. CD163$^+$ nuclei (s.d)	Median Ratio CD163$^+$:CD45$^+$
Pelvicol™ (n=6)	46.33(27.77)	99.00 (35.56)	2.18:1
PABM (n=5)	42 (66.42)	193 (85.54)	4.60:1
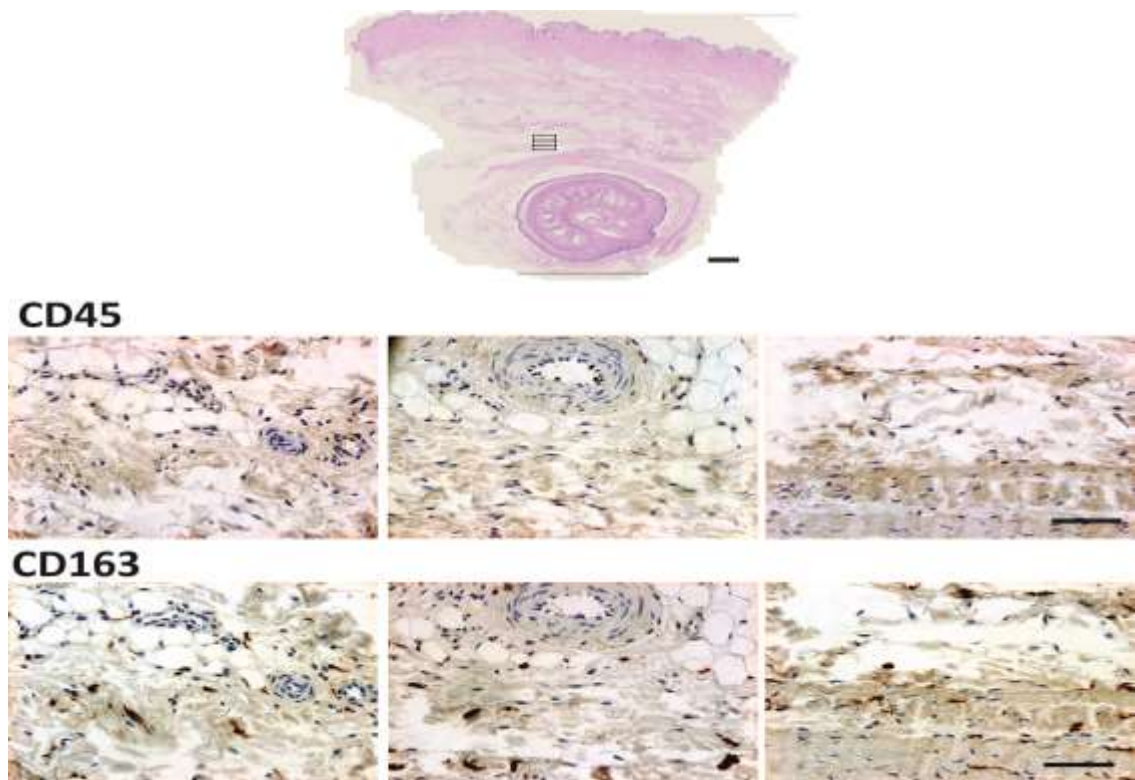
Figure 5-11: Matched images labelled for CD45 and CD163 in control tissue

Peri-urethral and penile tissue was taken en-bloc from a pig that had not had any surgical procedure performed. The tissue was taken from the same location as the grafts had been implanted in the experimental animals. CD45 and CD163 labelling was performed in serial 5 µm sections. Images were taken at x40 magnification at three adjacent areas (shown in H& E above), which have been merged in the above figure. The number of positive cells were counted in the matched images and converted to a ratio. Scale bar 50 µm (H&E 200 µm).
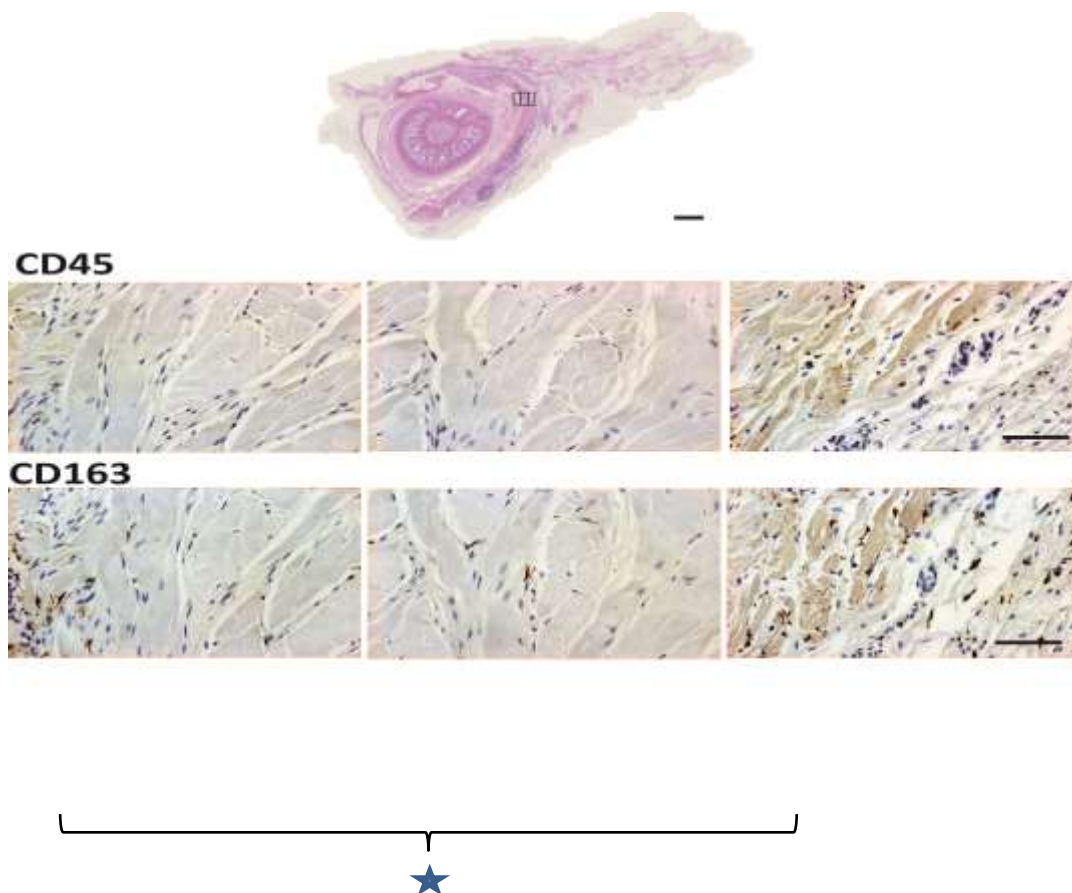
Figure 5-12: Matched images labelled for CD45 and CD163 in tissue implanted with Pelvicol

CD45 and CD163 labelling was performed in serial 5 μm sections of implanted Pelvicol™. Images were taken at x40 magnification at three adjacent areas, which are shown in the above image (see H&E at the top of the image to see origin of these areas). The numbers of cells were counted in the matched images and converted to a ratio. Pelvicol™ graft has been identified by starred bracket. Within the graft there were few CD45+ or CD163+ cells seen, those that were found were between the collagen bundles along natural "fissures". There were more abundant CD163+ cells than CD45+ cells and both were located predominantly at the edges of the graft and tissue immediately adjacent to it. Images for the rest of the Pelvicol™ cohort can be found in Appendix V. Scale bar 50 μm (H&E 200 μm).
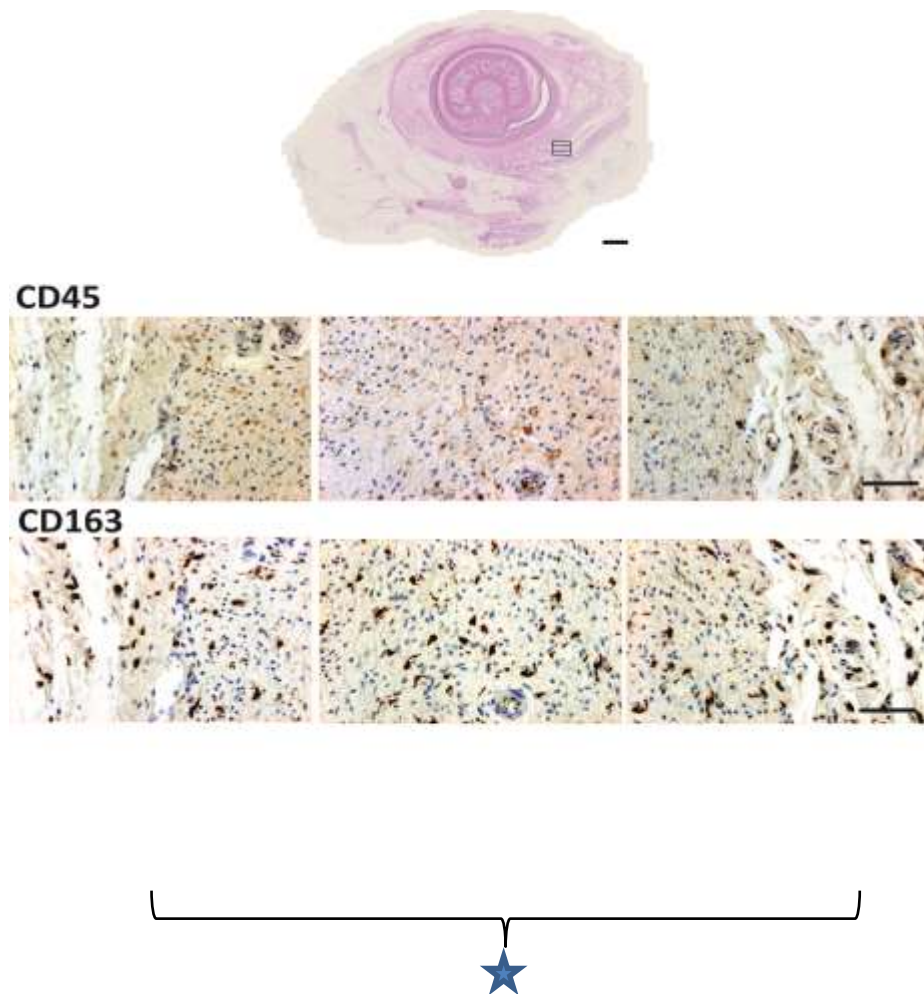
Figure 5-13: Matched images labelled for CD45 and CD163 in tissue implanted with PABM

CD45 and CD163 labelling was performed in serial 5 μm sections of implanted PABM. Images were taken at x40 magnification at three adjacent areas, which are shown in the above image (see H&E at top of image for origin of these areas). The numbers of positive cells were counted in the matched images and converted to a ratio. PABM graft has been identified by the starred bracket. Of note was the homogenous and abundant localisation of CD163^{+} cells throughout the images as opposed to CD45^{+} cells, which were sparse and located predominantly in association with vasculature. Images for the rest of the PABM cohort can be found in Appendix V. Scale bar 50 μm (H&E 200 μm).

5.5 Discussion

5.5.1 General considerations and characteristics of PABM

In 1976, at the inaugural Consensus Conference of the European Society for Biomaterials, a biomaterial was defined as 'a nonviable material used in a medical device, intended to interact with biological systems' (Gross U 2014). That definition has since been modified and the current definition is a 'material intended to interface with biological systems to evaluate, treat, augment or replace any tissue, organ or function of the body (O'Brien, 2011); demonstrating that the aim when designing biomaterials is no longer merely to interact with the body but also to potentially alter the biological processes that can lead to regeneration. Despite these growing complexities some basic characteristics are essential for any biomaterial to possess before being considered for translation into a clinical setting. These include biocompatibility, biodegradability, suitable mechanical properties and suitable architecture.

PABM had already demonstrated biocompatibility *in vitro (*Bolland et al., 2007*).* This chapter has also shown PABM to be well tolerated *in vivo* using a porcine peri-urethral onlay-graft model with none of the experimental subjects having any complications related to the implantation of the graft. In terms of biodegradability the PABM appeared well integrated at three-months, both macroscopically and microscopically with cellularisation shown throughout the grafts. In this respect PABM was superior to Pelvicol™, which persisted and could be visualised macroscopically at the time of tissue harvesting (***Figure 5-4***) and was easily identifiable by histology. The cellularisation of the Pelvicol™ was through the natural pathways (***Figure 5-7***) and tended to be

predominantly at the graft periphery and in areas where suture material had been located and an immunocyte reaction had been provoked.

The structure of Pelvicol™ is chemically cross-linked by hexamethylene diisocyanate (HMDI) (Khor, 1997), which produces stable urea groups by the interaction of amine groups isocyanate (Olde Damink LHH, 1995). The process of chemical cross-linking results in a product that remains flexible but is resistant to degradative processes and therefore maintains strength and 3D structure. This resilience was utilised by Springer *et al* (Springer and Subramaniam, 2012) where Pelvicol™ was ideal as an implant for support of a urethral repair. The rigidity provided by Permacol™ is potentially more important within the first few weeks post-urethral repair than at a later stage. Of importance was that the authors in the above study were unable to palpate any abnormality of the penile tissues at six months, which may suggest a degree of biodegradation by this time point. There is good evidence however from animal models, that cross-linking inhibits the ability for host cells to infiltrate into all such grafts, including Pelvicol™ (Mestak et al., 2014). In porcine ventral hernia models, this has been particularly noted in the first month (other time points in this study 6 and 12 months) with improvement over time (Cavallo et al., 2015).

PABM is not cross-linked and that may be why there was improved integration seen with diffuse labelling of SMA, CD107a, CD163 and CD45, unlike the Pelvicol™ which did have evidence of cellular infiltration but this was heterogeneous, with limited integration centrally. Another benefit of PABM is that in terms of mechanical properties and architecture it is homologous to the urinary tract and therefore should be superior in those respects if it were to be used in regenerative medicine strategies within urology. When similarly placed within the periurethral plane in this simple porcine urethroplasty model, PABM did not have the same "splinting"characteristics to perform a "splinting" role. However, it did provide a scaffold that was both strong and

supple. From its characteristics, it is predicted that in primary repairs, where insufficient native tissue is available, PABM may fulfil an unmet need as a scaffold for augmentation of the native tissue in order to prevent subsequent complications, such as UF.

5.5.2 Immunological response to Pelvicol™ and PABM

Biocompatibility and degradation is irrefutably related to the host's innate immunological response to a biomaterial (Badylak et al., 2009). Traditional thinking follows the restrictive polarisation of monocyte-derived macrophages to an M1 pro-inflammatory phenotype or an M2 anti-inflammatory, tissue remodelling phenotype (Mantovani et al., 2004). Scaffold integration has been assessed commonly by this macrophage dichotomy; with an M1 phenotype being associated with poor integration due to inflammation, whereas a more favourable response has been seen when the dominant phenotype has been M2, although there is a relationship between M2 sub-populations and encapsulation and fibrosis (Brown et al., 2012).

The pan macrophage marker CD107a in this study was not particularly useful other than as a general cellularisation marker due to expression by multiple cell types. CD45 was more discerning and identified a generally small number of cells within the grafts, predominantly perivascular in location and with little invasion into the Pelvicol™ explants. To attempt to differentiate between M1 and M2-type macrophages CD163 was used.

CD163, also known as M130, is a member of the scavenger receptor cysteine rich family (SRCR) and is associated with the M2 phenotype (Bullers et al., 2014). Expression of CD163 is reported to be M-CSF dependent; resulting in phagocytic

differentiation of human blood monocytes and associated with anti-inflammatory modulators such as IL-6 and IL-10. Monocytic cells treated with GM-CSF and interleukin-4 have reduced CD163 expression and follow the dendritic differentiation pathway (Mia et al., 2014). Expression of CD163 is also known to be downregulated by pro-inflammatory mediators such as LPS, interferon-γ and TNF-α (Onofre et al., 2009). Given CD163 is associated with macrophages, which belong to the monocyte lineage (van Furth, 1970), CD45 expression should have been present in an equal, if not more noticeable degree in the explants. This in fact was not supported by the results presented in this chapter; in fact the reverse was demonstrated finally.

The mononuclear phagocyte system suggested by Van Furth, has restricted the way that macrophages have been perceived as deriving only from a monocyte lineage. Such presumption has recently come into question, with the suggestion that tissue resident macrophages are capable of not only tissue surveillance and homeostasis but self –renewal and response to insult (Hashimoto et al., 2013). However, there are only limited reports of CD45$^-$ CD163$^+$ cell populations within the published literature.

Dermal resident macrophages were investigated by (Zaba et al., 2007) who reported CD163$^+$ macrophage-like cells, which had reduced expression of CD45 but expressed factor XIIIa. Factor XIIIa has also been recognised as expressed by macrophages in human and murine skin by a different group (Malissen et al., 2014) but this group did not assess CD45 or CD163. Similarly but in a rat model crosslinked PCL implanted subcutaneously demonstrated by immunohistochemistry a sub-population of stromal cell which were CD163$^+$ (Baker et al., 2011). CD163 has been noted to be expressed by macrophages, of presumed M2 phenotype, in infantile haemangiomas (Tan et al., 2015). These cells were hypothesised to be linked to a subtype of placental macrophages known as Hofbauer cells, which have a role in preventing vertical transmission between mother and fetus (Tang et al., 2013). Importantly work with the

PABM used in theis thesis has demonstrated ex vivo a similar population of cells (CD80$^-$ CD163$^+$) which was associated with an integrative response (Bullers et al., 2014).

Fibrocytes also express CD163 and CD107a with and without the presence of CD45, however if the latter is absent then CD34 is usually expressed (reviewed by Reilkoff et al., 2011). Other groups have suggested that the expression of CD45 and/ or CD34 diminishes after the initial insult (Bellini and Mattoli, 2007). The role of the fibrocyte in health and disease is still be elucidated and given the spindle-shaped cells seen predominantly in the CD163+ group this needs to be considered a possibility and labelling for fibrocytic markers such as CD34, CD204, CD206, CD90 (Pilling et al., 2009) may help may aid identification of this distinct population.

Given the lack of porcine antibodies available it may be that an antibody related anomaly may have given rise to the anomalous results with CD45:CD163 (Wong and Davis, 2013), however the labelling did appear clean and controls successful and agreed with the findings reported when co-culturing PABM with human ureteric tissue (Bullers et al., 2014) and cross-linked PCL subcutaneously in rats (Baker et al., 2011).

5.5.3 PABM and the compromised bladder

An alternative potential area where PABM may add to the paediatric urologist's toolkit would be the treatment of conditions where bladder morphology is altered by disease. An example of this would be in early or pre-end-stage bladder disease as an adjunct to detrusorotomy before end-stage fibrosis has occurred. As far as these patients are concerned, early intervention by detrusorotomy ("autoaugment") is a better option to prevent the unwanted serious clinical sequelae of augmentation using segments of bowel (Veenboer et al., 2013, Welk et al., 2012).

The bladder is a complex organ; with its filling and voiding cycle and waterproof urothelial lining it is not an easily reproducible entity. Many animal and human studies have resulted in fibrosis and contracture of the grafted area including with a cell-seeded, non-crosslinked patch (SIS) (Zhang et al., 2006) despite initial promising results (Zhang et al., 2004). Atala has also reported similar results in a phase II clinical trial, using both smooth muscle and urothelial cells grown *ex vivo* which were subsequently seeded onto a biodegradable scaffold (Atala et al., 2006). Despite the success in pre-clinical canine studies (Yoo et al., 1998) the phase II trial demonstrated no significant difference in bladder compliance nor bladder capacity and adverse events occurred in all 10 patients (Joseph et al., 2014). Four had serious adverse events which included bladder perforation and bowel obstruction. Urothelial cells from two patients with compromised bladders had poor cell growth at the *in vitro* expansion time-point, similar to the findings reported by Subramaniam *et al* (Subramaniam et al., 2011).

PABM offers a full-thickness biomaterial which due to its compliance and integration properties could be used in patients for auto-augmentation. It would be useful support and cover to the underlying mucosa that has been exposed during auto-augmentation, rather than as an "organ- replacement. Evidence reported here suggests that PABM is readily integrated and remodelled within three months in a porcine model. Regardless of this, given the propensity of biomaterials in the bladder to contract secondary to fibrosis (which would be counterproductive in these patients) combination with vascularisation, for example from an omental patch, might be a useful strategy. PABM may provide a useful adjunct to cover the bulging mucosa on an auto-augmented bladder to provide support to the fragile mucosa whilst tissue integration occurs and the expected/adequate bladder capacity and compliance is achieved.

6. Conclusion – a promise for the future and the application of new TERM therapies in paediatric urology.

The surgical "last-chance saloon" for end-stage bladder disease is augmentation cystoplasty, most commonly using bowel, with the associated side-effects described in section **1.5.3**. The "composite cystoplasty" model was proposed as an alternative whereby autologous urothelium, expanded *in vitro,* was placed on a demucosalised bowel segment and augmentation performed as usual. Success was reported in a healthy porcine model (Turner et al., 2008), however issues with propagating and differentiating human urothelium from end-stage diseased paediatric bladders were reported (Subramaniam et al., 2011). As the urothelium has not been implicated in the disease process, the reasons for such compromise were unknown.

In Chapter Three, a previously unreported significant increase in nuclear HIF-1α was found in the urothelium from neuropathic and other end stage bladders of high pressure. Indeed, the intensity of HIF-1α labelling in bladder tissue showed positive correlation with detrusor pressures recorded clinically. The hypoxia disease model demonstrated that exposure of NHU cells to persistent hypoxia in cell culture was associated with a detrimental effect on proliferation and differentiation. By switching cells from hypoxia into normoxia, the reduction in proliferative capacity was overcome supporting a reversible element and raised the possibility that hypoxia promoted a quiescent phenotype.

The negative effect of hypoxia on the differentiated phenotype however persisted, even following a return to normoxia of two weeks. It was also shown that NHU cells

differentiated in hypoxia or pre-exposed to hypoxia demonstrated localisation of dimethylation at histone 3, lysine 9 at the periphery of the nucleus– a finding that had been reported in the literature in non-urothelial HTC75 (clonal cell line derived from HT1080 fibrosarcoma cells) (Kind et al., 2013) and metazoan cells (Poleshko and Katz, 2014) as promoting gene silencing (Towbin et al., 2012) (Meister and Taddei, 2013).

In Chapter Four, the use of a specific inhibitor of histone methyl transferase enzymes G9a and its close relation GLP (UNC0646) was found to alleviate the hypoxia-induced inhibition of differentiation in terms of barrier formation, but only once cells were returned to normoxia. Organ cultures were able to demonstrate no adverse impact on urothelial phenotype by the application of the epigenetic modifying agent in either the control or compromised samples. Recovery from the persistent effects of hypoxia with UNC0646 was also characterised by improved urothelial health with urothelium becoming better organised and expressing markers of differentiation, lost with pre-exposed to hypoxia. The nuclear lamina localisation of H3K9Me2 also reverted to a normal pattern and hypothetically this may have promoted reexpression of genes important for barrier formation, function and differentiation.

Similarities were drawn between the persistent compromise seen post-hypoxia and that reported in urothelial cells from end-stage disease bladders. Of translational significance application of UNC0646 onto urothelial cells cultured from diseased bladders, resulted in an improvement in two cell lines out of three. The third had a normal barrier in the control arm and UNC0646 did not increase nor decrease the barrier in these cultures. Such patients suffer with abnormal bladders with normal or borderline detrusor pressures and urothelium that is able to maintain its phenotype.

Currently such patients may be offered auto-augmentation, which has complications associated with exposure of the mucosa. Chapter 5 compared the integrative

properties of Pelvicol™, a crosslinked dermal-derived acellular matrix, to that of the non-crossllinked PABM. Cellularisation was seen throughout the PABM graft as opposed to the Pelvicol™. The conclusions were that the non-crosslinked PABM had superior integrative properties compared to Pelvicol™ and is promising for assessment in future work as a free or pre-vascularised patch of PABM in auto-augmentation.

The potential role for regenerative medicine and tissue engineering in urology is vast and a realistic area for clinical translation. However, more information is required to ensure the correct approach is utilised in the right context for the right patient. For this reason further experimental investigation and clinical research is required, ideally on a multi-centre basis to obtain sufficient data on a range of patients and pathologies. Based on this thesis and the principles of patient stratification a proposed future "management" strategy incorporating these new approaches for the treatment of end-stage bladder disease is shown in **Figure 6-1**

Figure 6-1: Prospective TERMs therapy for bladder reconstruction

```
                    ┌──────────────────────────────────┐
 .                  │ Neuropathic bladder + other       │
                    │ bladder diseases e.g. ketamine-   │
                    │ induced cystitis, interstitial    │
                    │ cystitis                          │
                    └──────────────────────────────────┘
                         ┌──────────────────────────┐
                         │ Failed conservative therapy │
                         └──────────────────────────┘
              ↙                              ↘
 ┌─────────────────────────┐    ┌──────────────────────────┐
 │ Intermediate bladder    │    │ End-stage bladder disease. │
 │ disease.  Low detrusor  │    │ High detrusor pressures,   │
 │ pressures               │    │                            │
 └─────────────────────────┘    └──────────────────────────┘
              │                              ↑
              ↓                              │
 ┌─────────────────────────┐                │
 │ Auto-augmentation       │────────────────┘
 │ + vascularised PABM flap │    ┌──────────────────────────┐
 └─────────────────────────┘    │ Differentiation in vitro  │
              ┊                  │ of autologous urothelial  │
              ┊                  │ layer with UNC0646        │
              ┊                  └──────────────────────────┘
              ┊                              │
              ┊                              ↓
              ┊                  ┌──────────────────────────┐
              ┊                  │ Composite cystoplasty     │
              ┊                  └──────────────────────────┘
              ↓                              ↙
 ┌─────────────────────────┐
 │ Short course of post-   │
 │ augmentation, intra-    │
 │ vesical UNC0646 to      │
 │ improve health of       │
 │ urothelium in situ      │
 └─────────────────────────┘
```

Appendix I: Suppliers

3M United Kingdom PLC

3M Centre, Cain Road

Bracknell, RG12 8HT, UK

08705 360036

http://solutions.3m.co.uk/

Abcam

330 Cambridge Science Park

Cambridge, CB4 0FL, UK

+44 (0)1223 696000

www.abcam.com

Abnova

9th Fl., No.108, Jhouzih St

Neihu District, Taipei City

114 Taiwan

+886-2-87511888

www.abnova.com

Allergan (Actavis)

Estuary Banks

Estuary Commerce Park, Speke Road

Liverpool, L24 8RB, UK

+44 (0) 151 728 1750

http://www.allergan.com/

Ambion® Europe Ltd.

See Life Technologies

Ambu Ltd.

8 Burrel Road St Ives

Cambridgeshire PE27 3LE, UK

+44 1480 498403

www.ambu.co.uk

Anachem Ltd

Anachem House

1 & 2 Titan Court, Laporte Way

Luton, Bedfordshire, LU4 8EF, UK.

+44 (0)1582 693029

info@anachem.co.uk

Animalcare Ltd

10 Great North Way York Business Park

York YO26 6RB, UK

+44 (0) 1904 487687

www.animalcare.co.uk

AstraZeneca

2 Kingdom St, Paddington

London W2 6BD, UK

+44(0)207 604 8000

www.astrazeneca.com

Autogen Bioclear UK Ltd

Holly Ditch Farm, Mile Elm Calne

Wiltshire

+44 (0)1249 819008

www.autogen-bioclear.com

Bayer AG

51368 Leverkusen, Germany

+49 214 30-1

www.bayer.com

BD Biosciences Ltd

Edmund Halley Road - Oxford Science

Park

OX4 4DQ Oxford

+44 1865 781 66

www.bdbiosciences.com

Bio-Rad   Bio-Rad Laboratories Ltd. Maxted Road,

Hemel Hempstead, HP2 7DX. UK

0800 181134

support_uk@bio-rad.com

Cambridge Bioscience Ltd   Munro House

Trafalgar Way, Bar Hill

Cambridge, CB23 8SQ, UK

+44 (0)1223 316 855

www.bioscience.co.uk

Carl Zeiss Ltd   509 Coldhams Lane

Cambridge, CB1 3JS, UK

+44 1223 401 500

www.zeiss.com

Ceva Santé Animale   10 Avenue de la Ballastière

33500 Libourne- France

+33 5 57 55 40 40

www.ceva.com

Conmed   Linvatec Europe SPRL

W.A. Mozartlaan, 3

1620 Drogenbos, Belgium

www.conmed.com

Corning   One Riverfront Plaza

                                       Corning, NY 14831, USA

                                       +1 607-974-9000

                                       inquiries@corning.com

Dako UK Ltd.   Cambridge House

                                       St Thomas Place, Ely

                                       Cambridgeshire CB7 4EX

                                       +44 (0)1 353 66 99 11

                                       www.dako.com

Diagenode   Liege Science Park

                                       Rue Bois Saint-Jean, 3

                                       4102 Seraing (Ougrée) - Belgium

                                       +32 4 364 20 50

                                       www.diagenode.com

(Elanco) Eli Lilly and Company Ltd   Lilly House

                                       Priestley Road, Basingstoke

                                       Hampshire, RG24 9NL

                                       +44 1256 353131

                                       elancouk@elanco.com

Elga Veolia Water Technologies UK   Windsor Court

                                       Kingsmead Business Park

                                       High Wycombe, UK

                                       HP11 1JU.

                                       sales.watertech@veolia.com

Enzo Life Sciences (UK) Ltd.   1 Colleton Crescent

	Exeter
	EX2 4DG
	+44 1392 825900
	info-uk@enzolifesciences.com
Falcon	see Corning
Fisher Scientific UK Ltd	see Thermo-Fisher Scientific Ltd.
Gibco®	see Life Technologies
Graphpad	www.graphpad.com
Greiner Bio-One	Greiner Bio-One GmbH
	Bad Haller Str. 32
	4550 Kremsmünster, Austria
	+43 7583 6791-0
	office@at.gbo.com
Halyard UK	Abbey House - 25 Clarendon Road
	Redhill, Surrey RH1 1QZ
	+44 203 68 42 399
	www.halyardhealth.co.uk
Hawksley Scientific	Marlborough Road
	Lancing Business Park
	Lancing, Sussex, BN15 8TN
	+ 44 (0)1903 752815
	www.hawksley.co.uk

Hendley Ltd.   Oakwood Hill Industrial Estate

Loughton Essex, UK

IG10 3TZ

http://www.hendley-essex.com/

Invitrogen™   see Life Technologies

Instat™   www.graphpad.com

Jencons Scientific Ltd   Stanbridge Road

Leighton Buzzard, Bedfordshire, UK

LU7 4UA

https://uk.vwr.com

Leica   Larch House, Woodlands Business Park,

Breckland, Linford Wood

Milton Keynes, MK14 6FG, UK

http://www.leica-microsystems.com

LICOR Biosciences Ltd.   St John's Innovation Centre

Cowley Road;Cambridge, CB4 0WS,UK

http://www.licor.com

Life Technologies Ltd   3 Fountain Drive

Inchinnan Business Park

Paisley PA4 9RF, UK

http://www.ukorders@lifetech.com

Media Cybernetics   Media Cybernetics, Inc.

401 N. Washington Street, Suite 350

	Rockville, MD 20850 USA
	+1301-495-3305
	www.mediacy.com
Medical Air Technologies Ltd.	Unit 2 Mercury Way
	Trafford Park,Manchester
	M41 7LY. UK
	0844 871 2100
	www.medicalairtechnology.com
MSD Animal Health	Walton Manor
	Walton, Milton Keynes
	MK7 7AJ, UK
	+44 (0)37 060 3380
	www.msd-animal-health.co.uk
Millipore (U.K.) Ltd	Suite 21, Building 6, Croxley Green
	Watford, WD18 8YH, UK
	0870 900 4645
	www.merckmillipore.com
Molecular Probes®	see Life Technologies
Molnlycke Health Care Ltd	The Arenson Centre, Arenson Way
	Dunstable
	LU5 5UL, UK
	0800 917 4918
	www.molnlycke.co.uk
MWG Eurofins Operon	Anzinger Str. 7a 85560 Ebersberg

+49 8092 8289-0

www.eurofinsgenomics.com

Nalgene Labware   see Thermo-Fisher Scientific

New England Biolabs® Inc.   75-77 Knowl Piece, Wilbury Way

Hitchin, SG4 0T, UK

+44 800 318486

www.neb.uk.com

Nikon   Nikon House

380 Richmond Road

Kingston upon Thames

Surrey, KT2 5PR

0330 123 0932

www.europe-nikon.com

Nordic Pharma   Abbey House

1650 Arlington Business Park

Theale, Reading, RG7 4SA UK

http://www.nordicpharmagroup.com

Novocastra Laboratories Ltd   Leica Microsystems (UK) Ltd

Larch House, Woodlands Business Park,

Breckland, Linford Wood, Milton Keynes

MK14 6FG, UK

0800 298 2344

www.leicabiosystems.com

Olympus	KeyMed House, Stock Road
	Southend-on-Sea, Essex SS2 5QH, UK
	+44 170-261-6333
	www.olympus-lifescience.com
Pall Corporation	Pall Life Sciences
	5 Harbourgate Business Park
	Portsmouth, PO6 4BQ. UK
	02392 338210
	BiopharmUK@pall.com
Philip Harris Ltd.	Philip Harris Education
	2 Gregory Street
	Hyde, Cheshire, SK14 4TH, UK
	0345 120 4520
	www.philipharris.co.uk
Pierce	supplied by Thermo-Scientific Ltd.
Progen Biotechnik GmbH	Maaβstaβe 30
	69123 Heidelberg
	Germany
	+49 6221 8278 0
	info@progen.de
Promega UK Ltd.	Delta House, Southampton Science Park,
	Southampton, SO16 7NS, UK
	02380 760225

ukcustserve@promega.com

Roche Products Limited (Pharmaceuticals)   Hexagon Place

6 Falcon Way, Shire Park

Welwyn Garden City, AL7 1TW, UK

+44 (0)1707 366000

www.roche.co.uk

RS Biotech Laboratory Equipment Ltd   1 Drommond Crescent

Irvine, Ayrshire

Scotland, KA11 5AN, UK

galaxy@rsbiotech.com

Rockland Immunochemical Ltd.   Limerick, PA 19468

800.656.7625

www.rockland-inc.com

Santa Cruz Biotechnology, Inc.   Bergheimer Str. 89-2

69115 Heidelberg, Germany

+49 6221 4503 0

europe@scbt.com

Serotec (AbD Serotec®)   Endeavour House

Langford Lane, Kidlington

OX5 1GE, UK

+44 1865 852 700

www.abdserotec.com

Serolab   supplied by SLS

Seward Thackray	Maerdy Industrial Estate
	Rhymney, NP22 5PY, UK
	+44 1685 844983
	sales@sewardthackray.com
Shandon	see Thermo-Fisher
Sigma Aldrich	Sigma-Aldrich Co. Ltd
	The Old Brickyard
	New Road
	Gillingham, Dorset, UK
	SP8 4XT
	http://www.sigmaaldrich.com
SLS	Scientific Laboratory Supplies Ltd
	Wilford Industrial Estate
	Ruddington Lane, Wilford
	Nottingham, NG11 7EP. UK
Starlab	5 Tanners Drive
	Blakelands, Milton Keynes,
	MK14 5BU, UK
	+44 1908 283800
	infoline(@)starlab.co.uk
Starstedt	68 Boston Road
	Beaumont Leys
	Leicester, LE4 1AW
	+441162359023

info(@)sarstedt.co.uk

Sterilin   see Thermo-Fisher Scientific Ltd

Swann-Morton Ltd.   Owlerton Green, Sheffield

                                                S6 2BJ

                                                +44 (0)114 234 423

                                                www.swannmorton.co.uk

Syngene   Beacon House, Nuffield Road

                                                Cambridge, CB4 1TF

                                                +44 (0)1223 727123

                                                www.syngene.com

Thermo Fisher Scientific Ltd.   Bishop Meadow Road

                                                Loughborough, LE11 5RG, UK

                                                fsuk.sales@thermofisher.com

Tissue Gnostics GmbH   Taborstraβe 10/2/8

                                                1020 Vienna, Austria

                                                +43 1 216 11 90

                                                www.tissuegnostics.com

Tocris Bioscience   Tocris House, IO Centre

                                                Moorend Farm Avenue

                                                Bristol, BS11 0QL, UK

                                                info.tb@bio-techne.com

Traves & Son Ltd.   Main Street, Escrick

                                                North Yorkshire, YO19 6TP, UK

+441904 728246

atravesandson.co.uk

Ultrawave
Eastgate Business Park

Wentloog Avenue, Cardiff, CF3 2EY, UK

+44 (0) 845 330 4236

admin@ultrawave.co.uk

Vector Laboratories Ltd.
3, Accent Park

Bakewell Road, Orton Southgate

Peterborough, PE2 6XS, UK

+44 (0)1733 237999

www.vectorlabs.co.uk

VWR International Ltd.
Hunter Boulevard

Magna Park

Lutterworth, LE17 4XN, UK

01455 55 86 00

services@uk.vwr.com

World Precision Instruments
1 Hunting Gate

Hitchin, Hertfordshire SG4 0TJ, UK

wpiuk@wpi-europe.com

Zoetis
100 Campus Drive, Florham Park

New Jersey, NJ07932

+1 973 822 7000

www.zoetis.com

Zymed
see Thermo Fisher Scientific

Appendix IIa: Stock Solutions and Buffers

Histology Solutions

Scott's tap water

H_2O containing 2 % (w/v) $MgSO_4$ and 0.35 % (w/v) $NaHCO_3$

20 % $MgSO_4$ (200 g $MgSO_4$/ 1 L) H_2O

7 % $NaHCO_3$ (70 g $NaHCO_3$/ 1 L H_2O)

Mayer's Haematoxylin solution

Solution 1:

3 g haematoxylin powder in 20 ml absolute ethanol

Solution 2:

0.3 g sodium iodate

1 g citric acid

50 g chloral hydrate

50 g aluminium potassium sulphate

850 ml H_2O

Solution 1 was added to solution 2 and mixed well. 120 ml glycerol was added and solution stored in a darkened bottle and filtered prior to use.

Tris-buffered Saline (TBS) (pH 7.6)

50 mM Tris-HCl

150 mM NaCl

3M NaCl (175.32 g/L

2M Tris (242.28 g/L) pH 7.6 achieved with HCl

Citric Acid Buffer pH 6.0

2.4 g Citric acid

1050 ml H_2O

Sodium hydroxide pellets to achieve pH 6.0

0.1% Calcium Chloride

1 g $CaCl_2$

900 ml H_2O

Sodium hydroxide to achieve pH 6.0

Immunocytochemistry solutions

Tris-buffered Saline (TBS) (pH 7.6)

50 mM Tris-HCl

150 mM NaCl

10 % (w/v) NaN_3 solution

10 % (w/v/ BSA in TBS (Pierce #37520)

3M NaCl (175.32 g/L)   2M Tris (242.28 g/L) pH 7.6 achieved with HCl

Antifade Mountant

 5 % (w/v) N-propyl Gallate (Sigma 02370) in glycerol stored at –20 ºC

Methanol: Acetone
- 50 ml Methanol
- 50 ml Acetone

Immunoblotting

TBS (Tris buffered saline) pH 7.4

1.21 g (10 mM)Tris

8.18 g (140 mM) NaCl

Up to 1 L with H_2O

2x SDS Sample Buffer

10 ml glycerol (20 %v/v)

1 g SDS (2 %w/v)

6.25 ml 125 mM Tris-HCl (pH 6.8)

0.42 g sodium fluoride (NaF)

18.4 mg sodium orthovanadate (Na_3PO_4)

0.446 g tetra-sodium pyrophosphate

H_2O up to 50 ml

20 % (w/v)dithiothreitol (DTT) to final concentration of 0.2 % (v/v)*

0.2 % (v/v) Protease Inhibitor Cocktail (Sigma) *added immediately before use*

Transfer buffer (1x)

1.45 g (12 mM) Tris

7.2 g (96 mM) glycine and

200 ml (20% v/v) methanol

Up to 1 L with H_2O

Ponceau red (10x)

5 g Ponceau

10 ml glacial acetic acid

Up to 100 ml with H_2O

TBS-Tween 20

1.21 g (10 mM)Tris

8.18 g (140 mM) NaCl

Tween 1 ml (0.1 %)

Up to 1 L with H_2O

Nucleic Acid analysis solutions

TBE (Tris-borate-EDTA), 1 litre of 10x solution

108 g Tris (0.9 M)

55 g Boric acid (0.9 M)

9.1 g EDTA (25 mM)

Bladder Decellularisation solutions

Transport Medium

500 ml HBSS

5 ml 1 M Hepes

1 ml Aprotinin

Sodium Acetate (20mM) storage buffer (pH 6.5)

20 mM sodium acetate (pH 6.5)

5 mM $CaCl_2$

0.1 mM phenulmethylsulfonylfluoride (PMSF)

50 % v/v glycerol

Hypotonic buffer

5 ml 2 M Tris-HCl pH 8.0

1 ml Trasylol®

10 ml 10 % (w/v) EDTA

984 ml H_2O

Hypertonic buffer

87.66 g sodium chloride

6.057 g Tris

800 ml H_2O

Adjust pH to 7.5 with addition of 6 M HCl

Make up to 1 L with H_2O

Wash buffer (+ EDTA)

989 ml PBS

1 ml Trasylol®

$\pm$ 10 ml 10 % (w/v) EDTA (100 g EDTA in 900 ml H_2O)

SDS Buffer

974 ml H_2O

5 ml 2 M Tris-HCl (pH 7.5)   (242.38g Tris in 600 ml H_2O: pH 7.5 with HCl)

10 ml 10 % (w/v) EDTA solution

10 ml 10% (w/v) SDS   (10 % SDS = 100 g SDS in 900 ml H_2O, filter sterilise)

1 ml Trasylol®

Nuclease solution

 25 ml 2 M Tris-HCl (pH 7.5)

10 ml 1 M $MgCl_2$ (203.3 g magnesium chloride hexahydrate in 700 ml H_2O)

50 mg BSA

10 ml of 100 U/ml RNase A

5 ml of 10 000 U/ ml DNase I

950 ml H_2O

Appendix IIb: Ethical documentation

Parent information sheet:

Parental consent for discarded kidney pelvis and ureter tissue removed at operation to be used for research

We are inviting you to take part in the above research project, taking part <u>is completely voluntary.</u> Before you decide we would like you to understand why the research is being done and what it would involve for you and your child.

What is the purpose of the study?

Our aim is to understand diseases and conditions that affect the waterworks (kidneys, bladder, ureters) in children and adults. One purpose of the research is to develop a new way of treating severe bladder disorders in children using their own bladder tissue which has been grown outside the body in a laboratory -a technique known as 'tissue engineering'.

Why are you asking us?

 As part of your child's operation, tissue joining the kidney to the bladder (renal pelvis or ureter) will be removed. Some of this tissue removed during the operation may be sent for microscopic examination (histology). The remaining portion would normally be discarded. We would like your permission to use some of the tissue that would otherwise have been discarded for research purposes. The unwanted tissue removed at the time of your child's operation would be used to further this research. Cells grown from the tissue would be used to increase our understanding of diseases affecting the bladder, ureters and kidneys in adults as well as children. Genetic information (DNA/RNA) may be extracted from these cells for the purposes of research.

What will happen if we agree for our child to take part?

The operation itself will not be affected in any way by the subsequent use of discarded tissue for research. No treatment will be withheld. We may also, whilst your child is under anaesthesia, take a small sample of blood, which may be used for genetic studies, and urine for the research. These can be done as part of the normal operation and no additional interventions / procedures will be needed to obtain these. You will have no additional responsibilities related to this study should you agree to take part

What happens if we change our mind?

You are free to withdraw consent at any point.

What will happen if we refuse to take part?

You are under no obligation whatsoever to give permission for any unwanted tissue to be used for research. If for whatever reason you do not wish to give permission, this decision will be respected and the operation will proceed as planned (with the exception that no samples will be sent for research).

Is this tissue donation?

This is not tissue donation. No tissue from your child will be implanted into another patient. The tissue obtained at the time of your child's operation will be used purely for research in the laboratory

Are there any risks/ side effects?

There are not any additional risks, side effects, inconveniences or restrictions from taking part.

Are there any benefits?

There are no immediate benefits for your child directly. Occasionally the laboratory can identify infections and other problems and they will inform us, this may then benefit your childs' care. In addition we hope that this research will help children and adults with diseases of the urinary tract.

As this is part of a planned medical care, we cannot offer any additional expenses reimbursements.

Will my child taking part in the study be kept confidential?

Yes we follow ethical and legal guidance and all data relating to your child is treated as confidential.

> *If the information in Part 1 has interested you and you are considering participation, please read the additional information in Part 2 before making any decision.*

Part 2:

What happens if I change my mind and do not want my child to be part of the study?

If you remove consent prior to the specimen being used in the research any stored samples that can still be identified as your childs' will be destroyed. If you withdraw from the study and samples have been used we will destroy all your childs' identifiable samples, but we will need to use the data collected up to your childs' withdrawal.

Confidentiality - Data

All information which is collected about your child during the course of the research will be kept strictly confidential, and any information about your child which leaves the hospital will have your name and address removed so that your child cannot be recognised.

What happens to the samples?

After your childs' specimens have been collected in the operating theatre they will be stored in a fridge with the following details; their age, sex, diagnosis and study number. The allocated study number will only be kept in their medical notes. The research team from York University will collect the specimen where it will be kept under secure conditions and allocated a specimen number only. Only researchers at the unit at York will have access to the samples. Samples will not be transferred outside the UK. Disposal of samples, if appropriate, will be in accordance to licence by the Human Tissue Authority and legislation within the Human Tissue Act.

Will our General Practitioner/Family doctor (GP) be informed?
Your GP will not be involved directly in the study, however we will ask your permission, should you agree to take part, to inform them of your childs' participation if necessary, please indicate on the form whether you agree to this.

What will happen to the results of the research?
Important findings may be published in scientific journals and/or presented to the medical/scientific community at academic meetings, however your child will not be identified in any such document or forum.

Who is involved and organising this study?
The Department of Paediatric Urology/Nephrology, Leeds General Infirmary.
Jack Birch Unit, Department of Biology, University of York.
There is no financial incentive for the above organisations or individuals to include you in this study nor conflicts of interest.

What if there is a problem?

Any complaint about the way you have been dealt with during the study or any possible harm you might suffer will be addressed. Initially our researchers will do their best to deal with any problems:

Mr Ram Subramaniam, Department of Paediatric Urology, Tel: 0113 392 6251. E-mail: Ramnath.Subramaniam@leedsth.nhs.uk

If you feel that issues have still not been resolved then please contact the Patient Advice and Liaison Service (PALS) **Tel: (0113) 2066261/ 2067168 Fax: (0113) 2066146. E mail:** patient.relations@leedsth.nhs.uk

In the event that something does go wrong and you believe that you child is harmed during the research and this is due to someone's negligence then you may have grounds for a legal action for compensation against Leeds Teaching Hospitals NHS Trust but you may have to pay your legal costs. The normal National Health Service complaints mechanisms will still be available to you (if appropriate).

Who has reviewed this study?

Before any research goes ahead it has to be checked by a Research Ethics Committee. They make sure that the research is fair. This study has been reviewed by the Yorkshire and the Humber – Leeds West and South Yorkshire Research Ethics Committee.

What if I have more questions?

When I talk to you to obtain consent for the operation, I would be happy to provide any further information you require in reaching your decision. If you have already agreed to take part this does not stop you from being able to ask more questions or refusing to take part.

Thankyou for your time,

Patient Information Sheet (example for ages 6 -10 years):

Young persons' assent for small sample of tissue at the edge of bladder incision to be taken at the time of operation for the purpose of research

Enquiries to: Mr Ram Subramaniam, Department of Paediatric Urology, Tel: 0113 392 6251

Title of Study: How pipes that make, move and store pee change when they are sick

Research is a way to help us answer questions. We want to know how pee problems change our bodies and would like you to help if you would like to. Talk to your family, friends, doctor or nurse if you want to.

Why are you asking me?

You are having an operation as you have a problem with your pee. As part of your operation where you store your pee is being opened. We would like to take a small amount of tissue at the edge of this cut and we would like your permission for us to do this and give it to scientists to look at to help us understand problems with pee in adults and children.
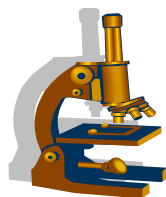
Did anyone check this study OK?

Before any research goes ahead it has to be checked by a Research Ethics Committee. They make sure that the research is fair.

Do I have to take part?

No. It is up to you. If you agree you can change your mind. You will always receive the same care.

What will happen if I agree to take part?

Nothing different, it is all part of the operation. No additional operation or things will need to be done. No surprises or anything new to upset you will happen,.

Will joining help me?

We cannot promise the study will help you but the information we get might help treat young people with pee problems in the future.

Will you tell anyone else?

We will only tell other people if we need too to help in your care.

What if I do not want to do research anymore?

If at any time you don't want to do the research anymore, just tell your parents, doctor or nurse. They will not be cross with you.

What happens if I have any questions?

When a doctor talks to you about the operation, they will be happy to provide any further information you require in reaching your decision. If you have already agreed to take part this does not stop you from being able to ask more questions or refusing to take part.

Thank you for your time,

Example of Consent Form (parental responsibility):

Patient Identification Number for this trial:

CONSENT FORM A: Parental consent

Consent for child up to 6 years of age

Title of Project: The role of the urothelium (lining of the urinary tract) in the development of conditions affecting paediatric populations attending urology and nephrology clinics.

Name and Contact of Researcher: Mr Ram Subramaniam, Department of Paediatric Urology

Tel: 0113 392 6251

Please initial all boxes

1. I confirm that I have read and understood the information sheet dated 25/10/2012 version 1A / 2A (DELETE AS APPROPRIATE) for the above study. I have had the opportunity to consider the information, discuss it with my child, ask questions and have had these answered satisfactorily.

2. I understand that my childs' participation is voluntary and that we are free to withdraw at any time without giving any reason, without my childs' medical care or legal rights being affected.

3. I understand that relevant sections of my childs' medical notes and data collected during the study may be looked at by individuals from regulatory authorities or from Leeds Teaching Hospitals NHS Trust, where it is relevant to my child taking part in this research. I give permission for these individuals to have access to my childs' records.

4. I agree to my GP being informed of my childs' participation in the study.

5. I agree to my child taking part in the above study.

Name of Parent/Guardian   Date   Signature

Relationship to child

Patient Assent Form (example for ages 6 – 10 years)

Young persons' assent for discarded kidney pelvis and ureter tissue removed at operation to be used for research

Title of Study: How pipes that make, move and store pee change when they are sick

(To be completed by the child and their parent/guardian) Child (or if unable, parent on their behalf) /young person to circle all they agree with:

Has somebody else explained this project to you?   Yes/No

Do you understand what this project is about?   Yes/No

Have you asked all the questions you want?   Yes/No

Have you had your questions answered in a way you understand?   Yes/No

Do you understand it's OK to stop taking part at any time?   Yes/No

Are you happy to take part   Yes/No

If any answers are "no" or you don't want to take part, don't sign your name!

If you do want to take part, you can write your name below

Your name

Date

The doctor who explained this project to you needs to sign too:

Print Name
Sign
Date

Thank you for your help.

Department of Paediatric Urology, Tel: 0113 392 625

III. Chapter 3 Additional results
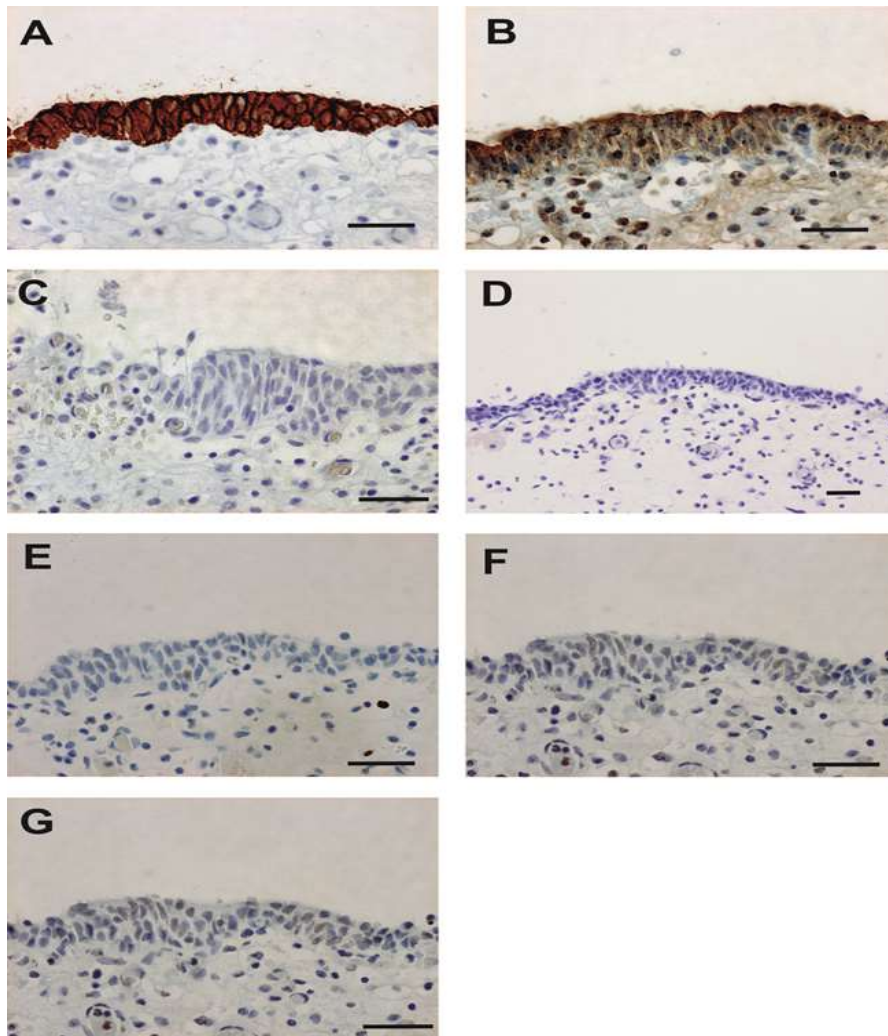
Figure III-I : Immunohistochemical analysis of a neuropathic bladder specimen (Y1427)

Sections from embedded human neuropathic bladders were evaluated using immunohistochemistry labelling for A - CK13, B-CK14, C- UPK3a D- CK20 E – Ki67 F- Cyclin-D3 and G – P63. An absence in markers of terminal differentiation was noted (UPK3a and CK20) Limited expression of P63, cyclin D3 and Ki67 was also seen. Scale bar 50 μm.
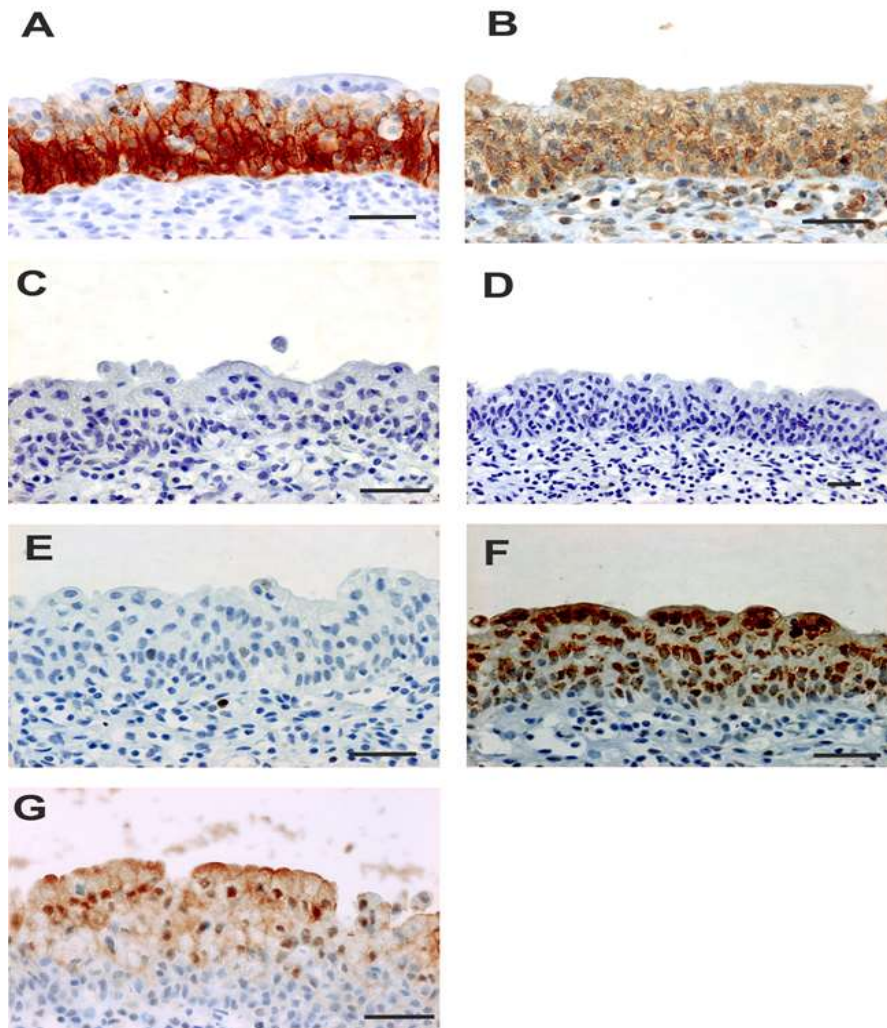
Figure III-II: Immunohistochemical analysis of a neuropathic bladder specimen (Y1180)

Sections from embedded human neuropathic bladders were evaluated using immunohistochemistry labelling for A - CK13, B-CK14, C- UPK3a D- CK20 E – Ki67 F-Cyclin-D3 and G – HIF-1α. An absence in markers of terminal differentiation was noted (UPK3a and CK20) Limited expression of Ki67 was also seen. Scale bar 50 μm
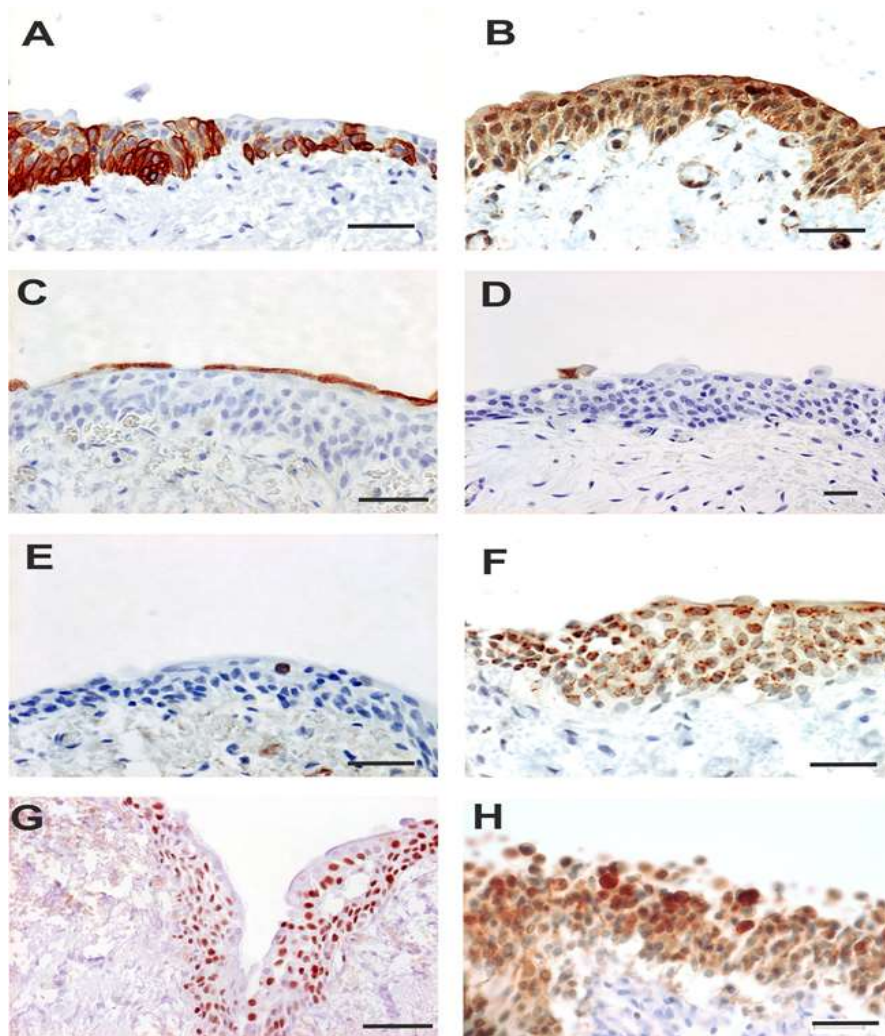
Figure III-III: Immunohistochemical analysis of a neuropathic bladder specimen (Y777)

Sections from embedded human neuropathic bladders were evaluated using immunohistochemistry labelling for A - CK13, B-CK14, C- UPK3a D- CK20 E – Ki67 F-Cyclin-D3, G p63 and H – HIF-1α. Both markers of terminal differentiation were present. Limited expression of Ki67 was also seen. Scale bar 50 µm
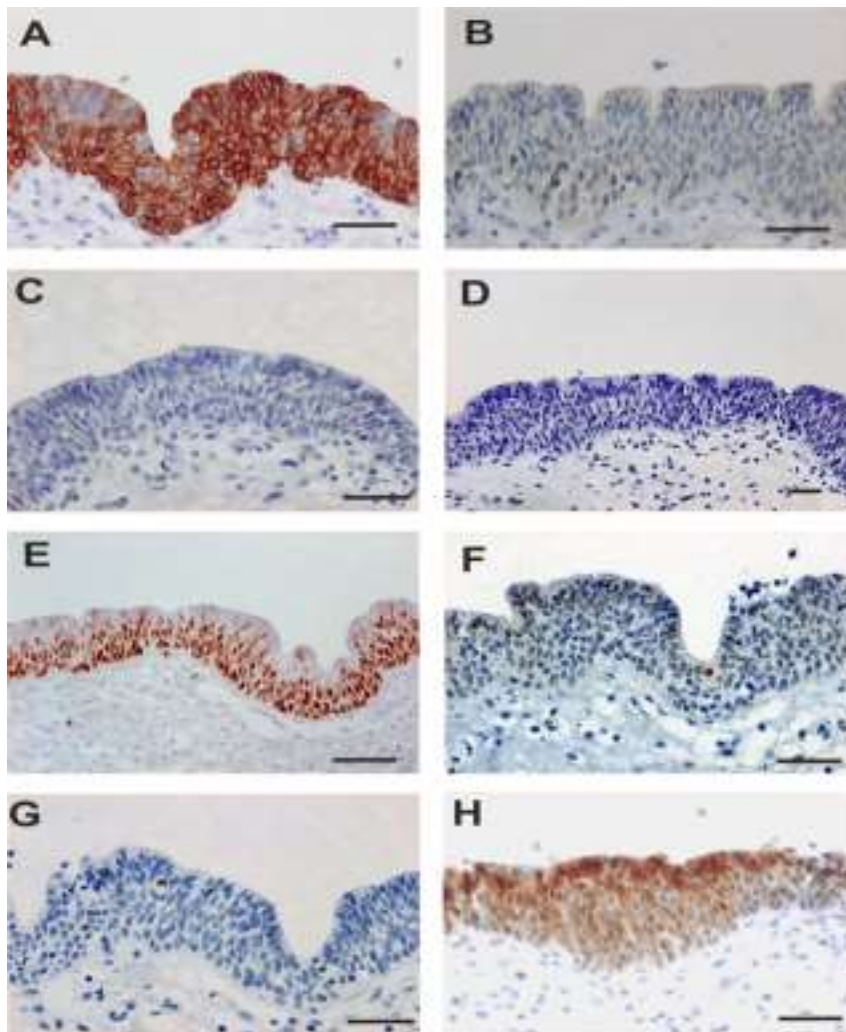
Figure III-IV: Immunohistochemical analysis of a neuropathic bladder specimen (Y1000)

Sections from embedded human neuropathic bladders were evaluated using immunohistochemistry labelling for A - CK13, B-CK14, C- UPK3a D- CK20 E – p63, F- Cyclin-D3, G – Ki67 and H– HIF-1α. An absence in markers of terminal differentiation was noted (UPK3a and CK20). Limited expression of Ki67 was also seen. Scale bar 50 µm
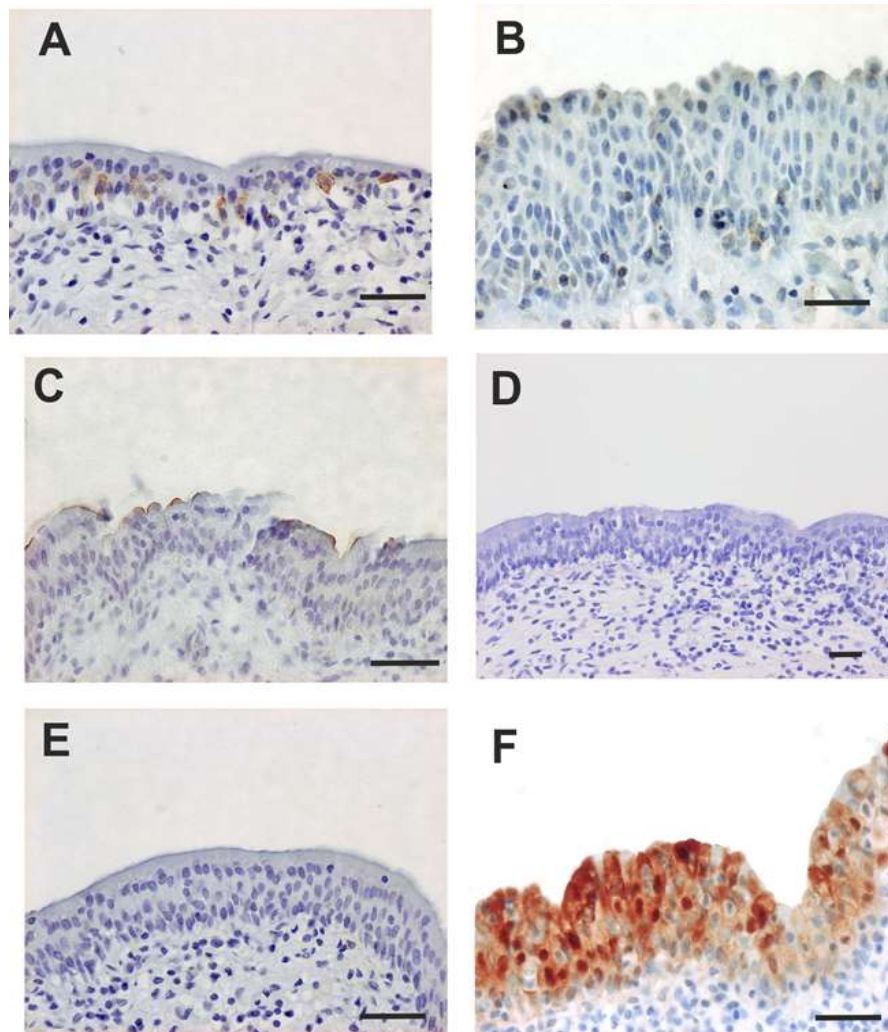
Figure III-V: Immunohistochemical analysis of a neuropathic bladder specimen (Y1107)

Sections from embedded human neuropathic bladders were evaluated using immunohistochemistry labelling for A - CK13, B-CK14, C- UPK3a D- CK20, E – p63 and F– HIF-1α. Limited CK13 and CK20 was noted with no p63 expression. Scale bar 50 µm
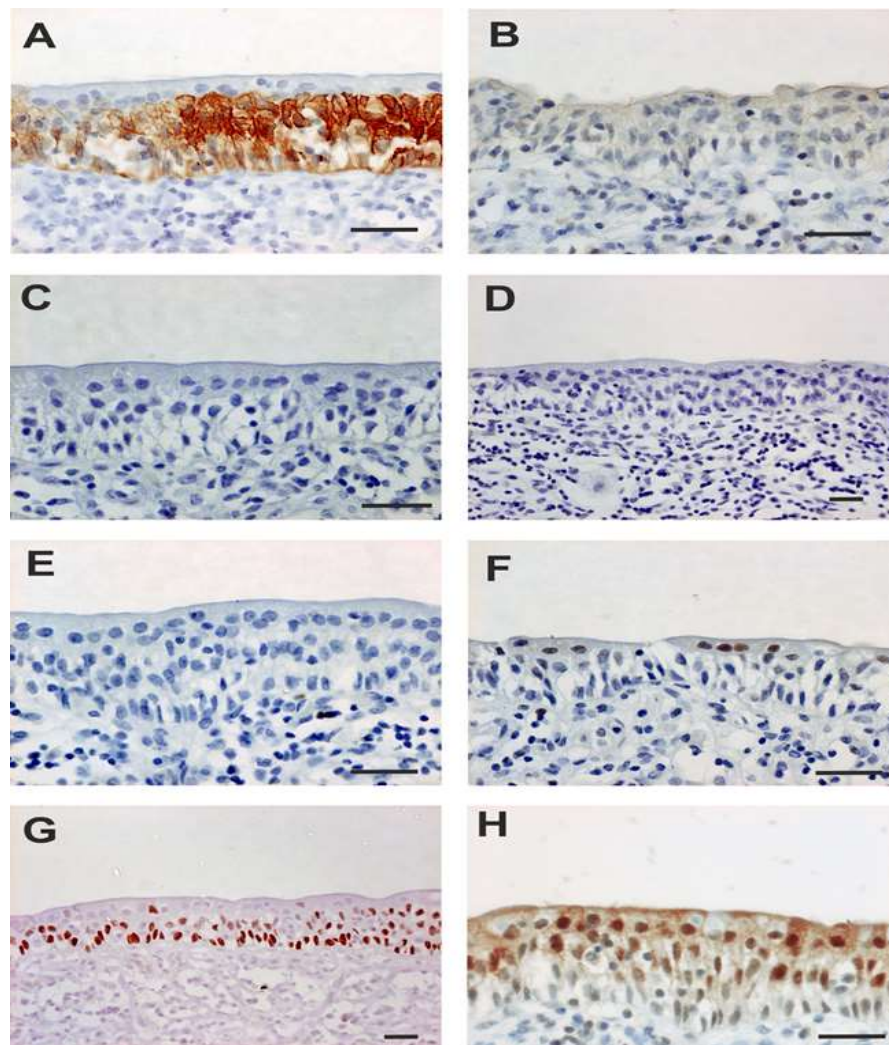
Figure III-VI: Immunohistochemical analysis of a neuropathic bladder specimen (Y1122)

Sections from embedded human neuropathic bladders were evaluated using immunohistochemistry labelling for A - CK13, B-CK14, C- UPK3a D- CK20 E – p63, F- Cyclin-D3, G – Ki67 and H– HIF-1α. An absence in markers of terminal differentiation was noted (UPK3a and CK20). Limited expression of Ki67 was also seen. Scale bar 50 µm
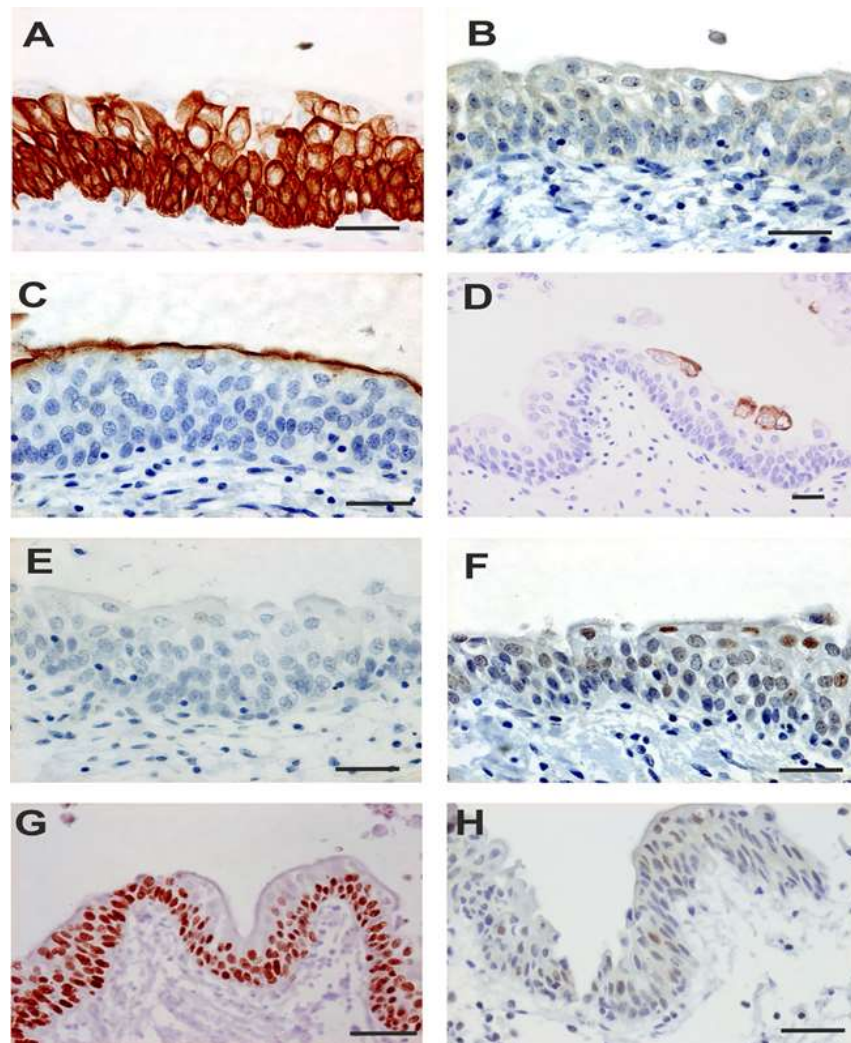
Figure III-VII: Immunohistological analysis of a normal bladder (Y1272B)

Sections from an embedded human control bladder (VUR) was evaluated using immunohistochemistry labelling for A - CK13, B-CK14, C- UPK3a D- CK20 E – p63, F- Cyclin-D3, G – Ki67 and H– HIF-1α. CK13 was significantly expressed whereas CK14 was not seen. The marked presence of UPK3a and scanty CK20 contrasts to most neuropathic bladders assessed.. Limited expression of Ki67 was also seen. Scale bar 50 µm
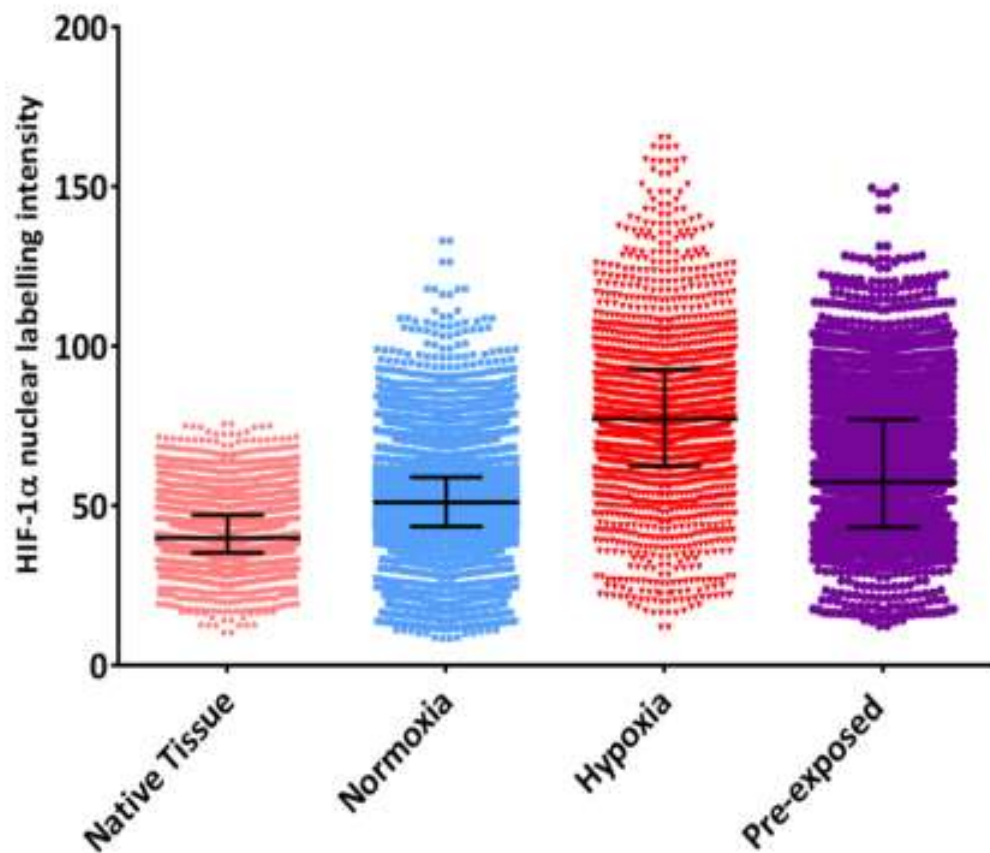
Figure III-VIII: Intensity of nuclear HIF-1α labelling in organ culture urothelium maintained in normoxia, hypoxia and pre-exposed to hypoxia.

Comparison was made between the median intensity of nuclear labelling for HIF-1α (DAB staining) of all nuclei of the urothelium within all organ culture (OC) conditions and native tissue that had not been exposed to organ culture. Total time in organ culture was 21 days. Each datum point represents a single urothelial nucleus, from a single donor (Y1593) across three organ culture sections. Native tissue n =2736, normoxia OC, n = 2121, hypoxia n= 1870, pre-exposed n=2724. The IQR is shown within the black range bars and the median the black horizontal line. Chart for other organ culture donor, Y1689 can be found in Chapter 3, section 3.4.6

IV) Chapter 4 additional results
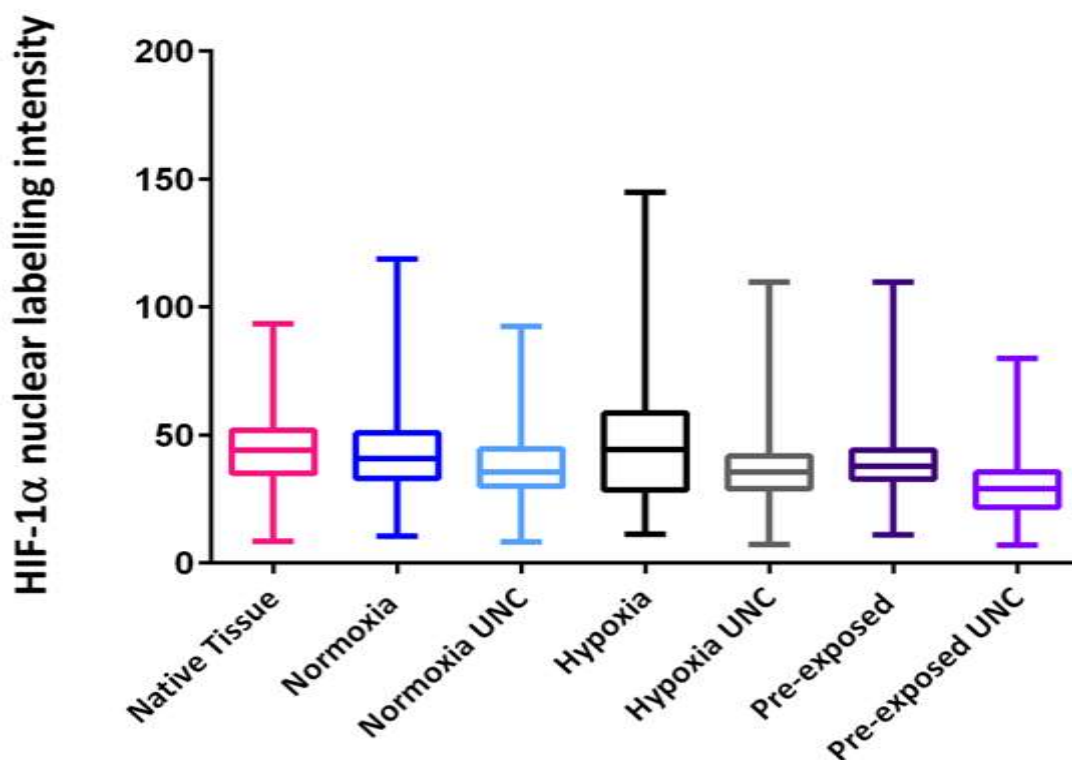
Figure IV-I: Box and whisker chart depicting nuclear HIF-1α labelling intensity in organ culture urothelium maintained in normoxia, hypoxia and pre-exposed to hypoxia ± UNC0646.

Comparison was made between the median HIF-1α intensity of urothelial nuclei within sections of all organ culture (OC) maintained in normoxia, hypoxia or pre-exposed conditions ± 500 nM UNC0646 and native tissue. All sections were maintained in organ culture for 21 days with three replicates in each condition. Each datum point analysed represented a single urothelial nucleus, from a single donor (Y1593) from all three replicates. Total number of nuclei analysed was: native tissue n = 2736, normoxia n = 10264 (+ UNC0646 = 780), hypoxia n= 1812 (+ UNC0646 = 486), pre-exposed n=3036(+ UNC0646 = 2254). IQR is shown within the boxes with the median represented by the horizontal line within. Whiskers illustrate the full range of labelling intensities.
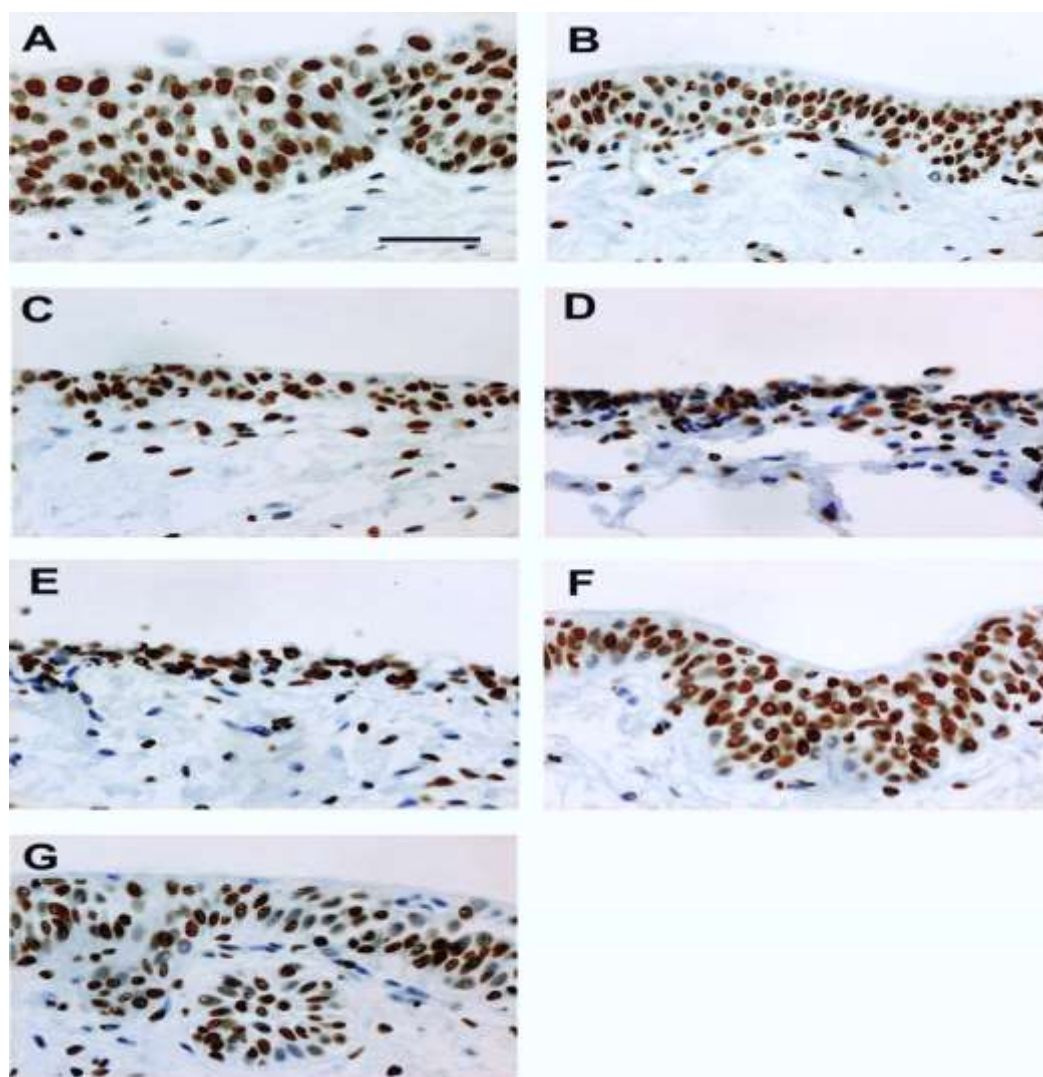
Figure IV-II: Immunoperoxidase labelling of H3K9Me2 expression and localisation in Y1593 organ cultures pre-exposed to hypoxia ±UNC0646

A: Normoxia, B: Normoxia +UNC0646, C: Hypoxia, D: Hypoxia + UNC0646, E: Pre-exposed, F: Pre-exposed + UNC0646 and G: In situ. All sections were maintained in organ culture for 21 days, 500 nM UNC0646 was added for seven days. H3K9Me2 was heterogeneously expressed throughout the urothelium in normoxia ± UNC0646, pre-exposed + UNC0646 and in situ. A more intense, uniform labelling is seen in the hypoxia ± UNC0646 and pre-exposed untreated samples. Treatment as compared to no treatment improved the thickness of the urothelium (E compared to F). Scale bar = 50 µm

Figure IV-III: RT negative control gel image (Figures 4-7)

Negative control reactions, with omission of reverse transcriptase (RT negatives) were included and are demonstrated here to confirm the absence of contaminating DNA.
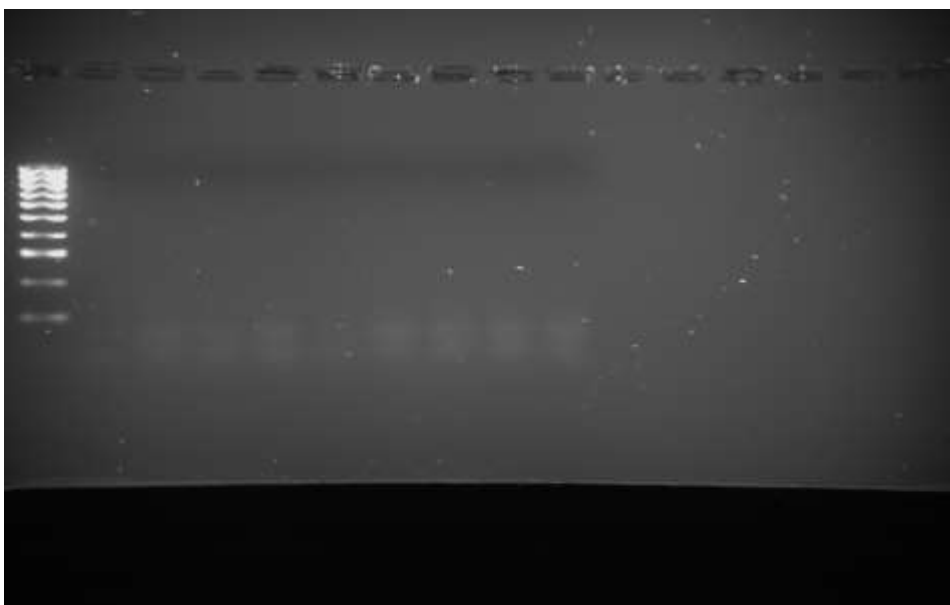
Figure IV-IV: RT negative control gel image (Figure 4-8)

Negative control reactions, with omission of reverse transcriptase (RT negatives) were included and are demonstrated here to confirm the absence of contaminating DNA.

Regenerative medicine applications in paediatric urology: barriers and solutions
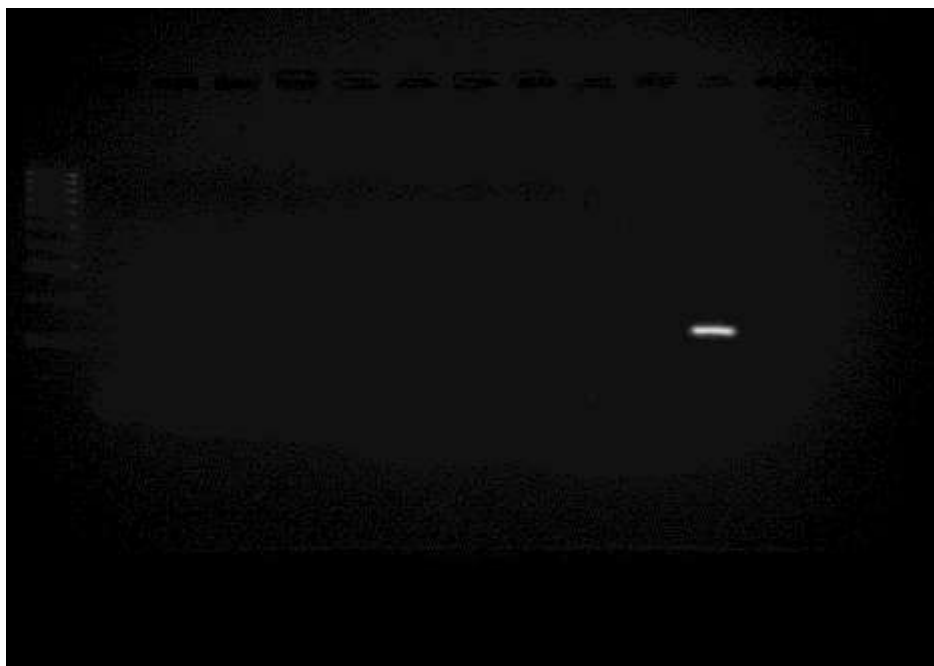
Figure IV-V: RT negative control for Figures 4-12 & 4-13

Negative control reactions, with omission of reverse transcriptase (RT negatives) were included and are demonstrated here to confirm the absence of contaminating DNA. Note the end lane is an RT (+) genomic DNA sample.

V.   Chapter 5 additional results

Example operation note constructed after implantation of graft:

DETAILS OF PROCEDURE:

No: 663   **Date:** 31/03/2014

Species: LWH   **Weight:** 17kg

Pre-operatively: iv antibiotics, pain relief and anaesthesia. No intubation.

Pig prepped with chlorhexidine and draped

Operation: Approximately 5cm from the preputial orifice, with urethra secured a 5cm longitudinal incision was made. Dissection with scalpel blade through subcutaneous tissues and fascia was performed. The tunica albuginea was opened approximately 2-3cm. Haemostasis.

3.0 x 1.5cm section of Permacol ™ (5033-50) Lot 13B08-9X, Exp. 12/09/2018 was placed over the tunica albuginea defect and secured with 4'0 vicryl using interrupted sutures. The overlying fascia and tissue was closed using interrupted 4'0 vicryl. Marker sutures of 5'0 prolene was placed at the caudal and cranial ends of the incision within the fascia. In addition prolene marker sutures were also placed 1cm above and below the incision in the skin.

Skin closure was achieved using continuous 5'0 monocryl subcuticularly. Opsite spray was applied. 3ml 0.5% Marcaine was infiltrated locally.

Post-operatively:

 Transfer to recovery pen with fresh water available, food once mobile and straw. Close monitoring until recovered. Able to socialise later today.

Regenerative medicine applications in paediatric urology: barriers and solutions
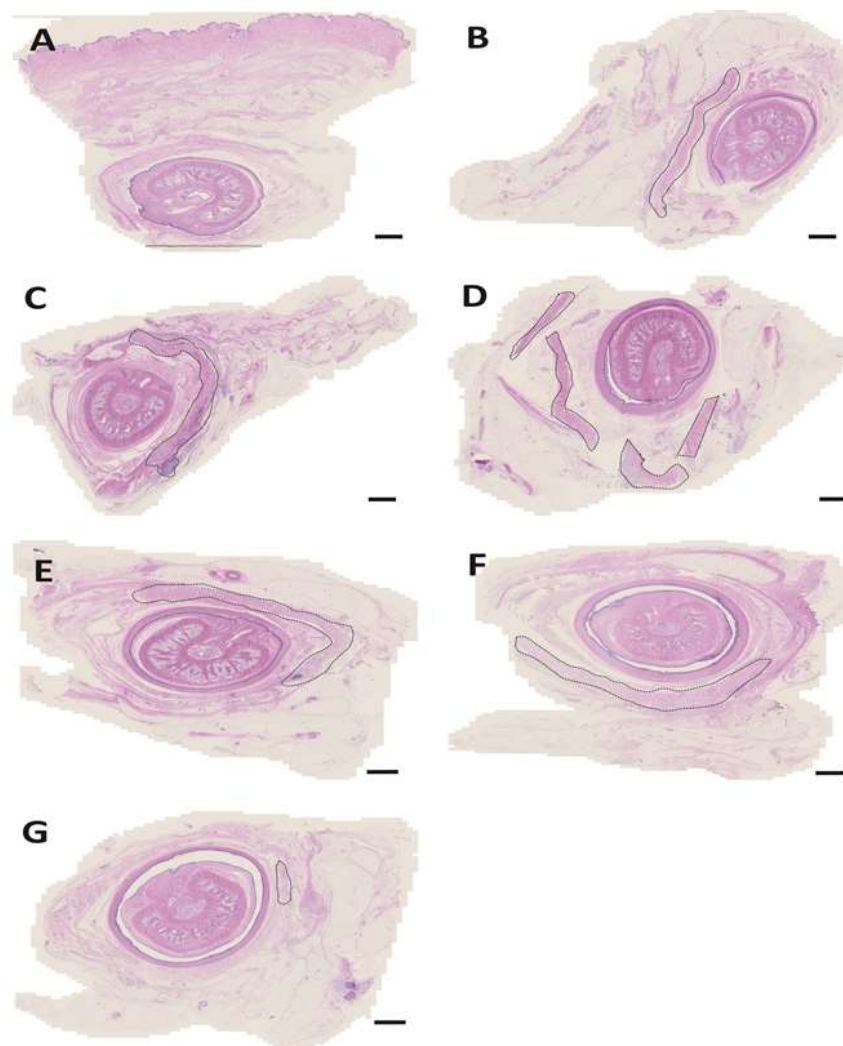
Figure V-1: H&E staining and identification of Pelvicol

(A) peri-urethral and penile tissue section from a control animal that had not been operated upon. Pelvicol™ was easily recognisable in all sections (circled) taken from the six study animals (B) #634, (C)#663), (D)#664, (E) #560, (F) #583, (G) #554. Scale bar 200µm.

Regenerative medicine applications in paediatric urology: barriers and solutions
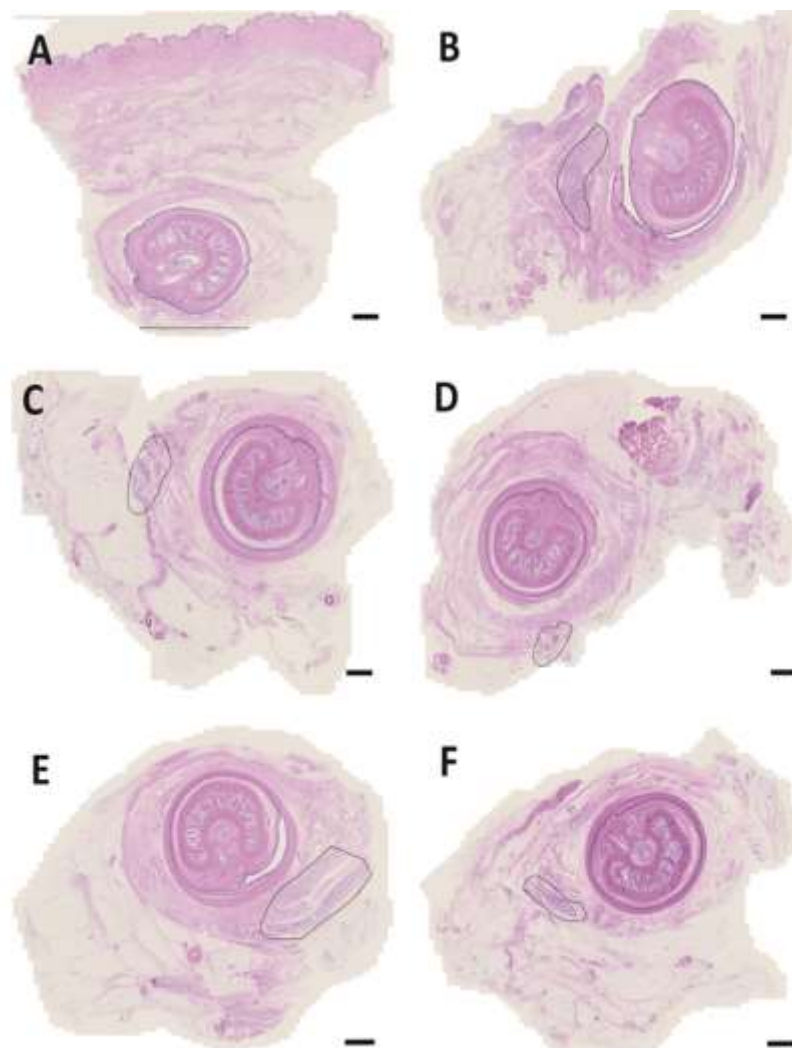
Figure V-2: H&E staining and identification of PABM

*(A) peri-urethral and penile tissue section from a control animal that had not been operated upon. PABM was not as evident (circled) as compared to Pelvicol™ (**Figure V-1**). However five out of six sections were identified (arrowed) taken from the five of the study animals (B) #631, (C)#633), (D)#635, (E) #583, (F) #563. Scale bar 200μm.*

Regenerative medicine applications in paediatric urology: barriers and solutions
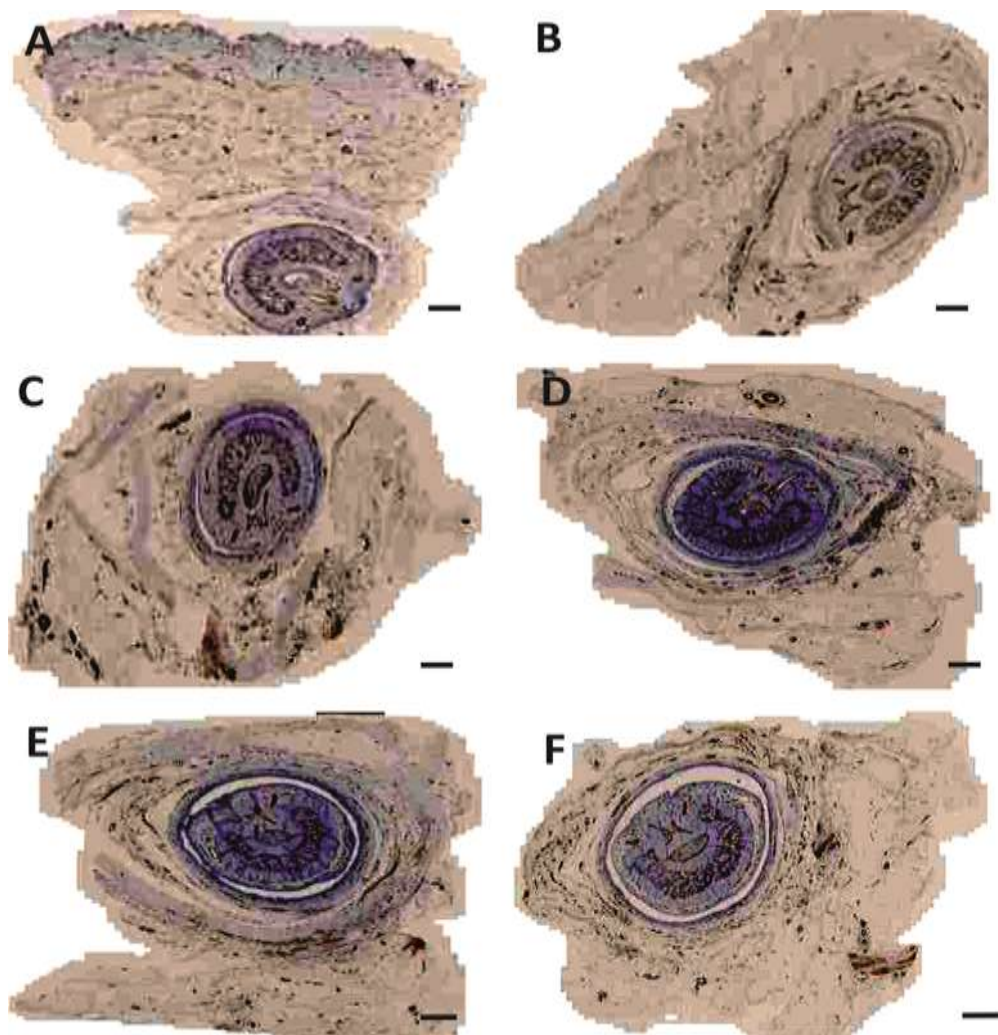
Figure V-3: SMA labelling in Pelvicol explants

A: Control pig, B: 1685D, C: 1705B, D: 2057, E 2058C, F: 2059C

Regenerative medicine applications in paediatric urology: barriers and solutions
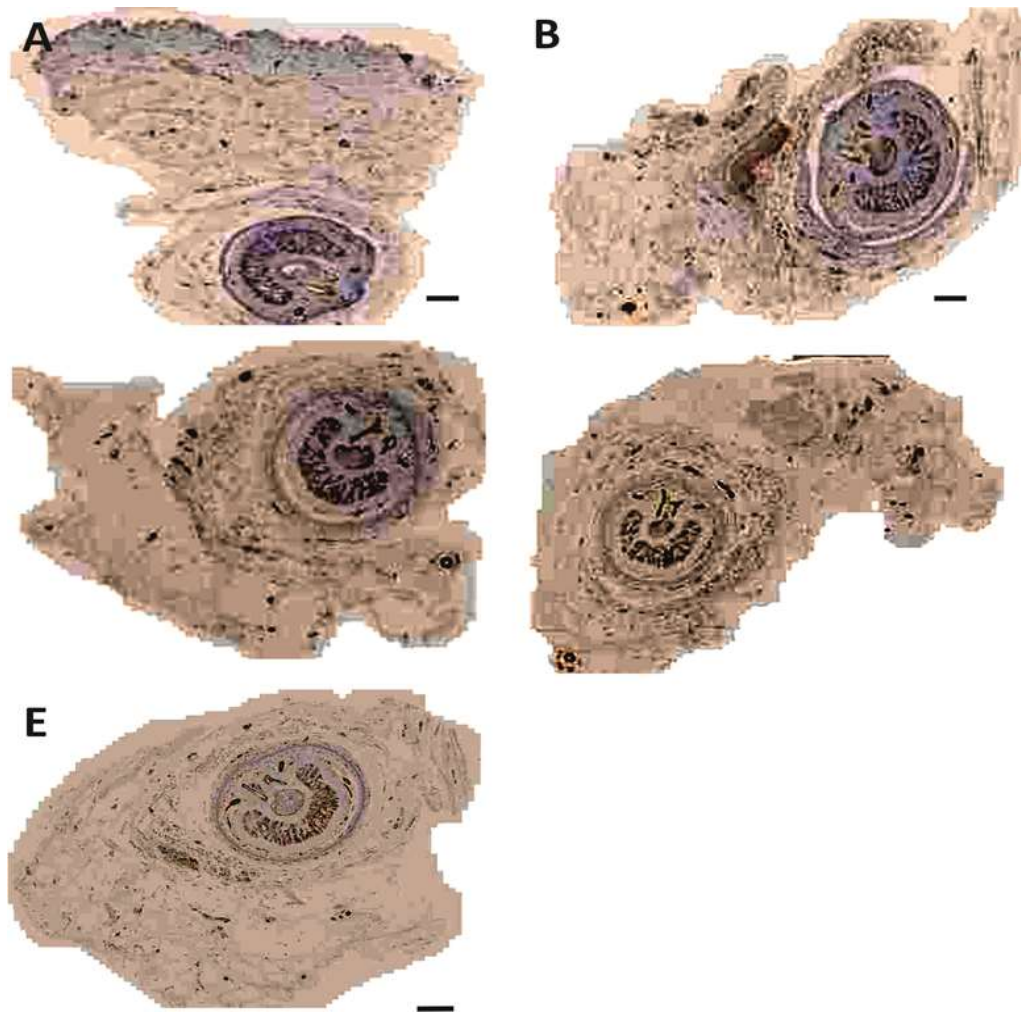
Figure V-4: SMA labelling PABM explants

A: Control pig, B: 1673D, C: 1679D, D: 1692D, E: 2065E

Regenerative medicine applications in paediatric urology: barriers and solutions
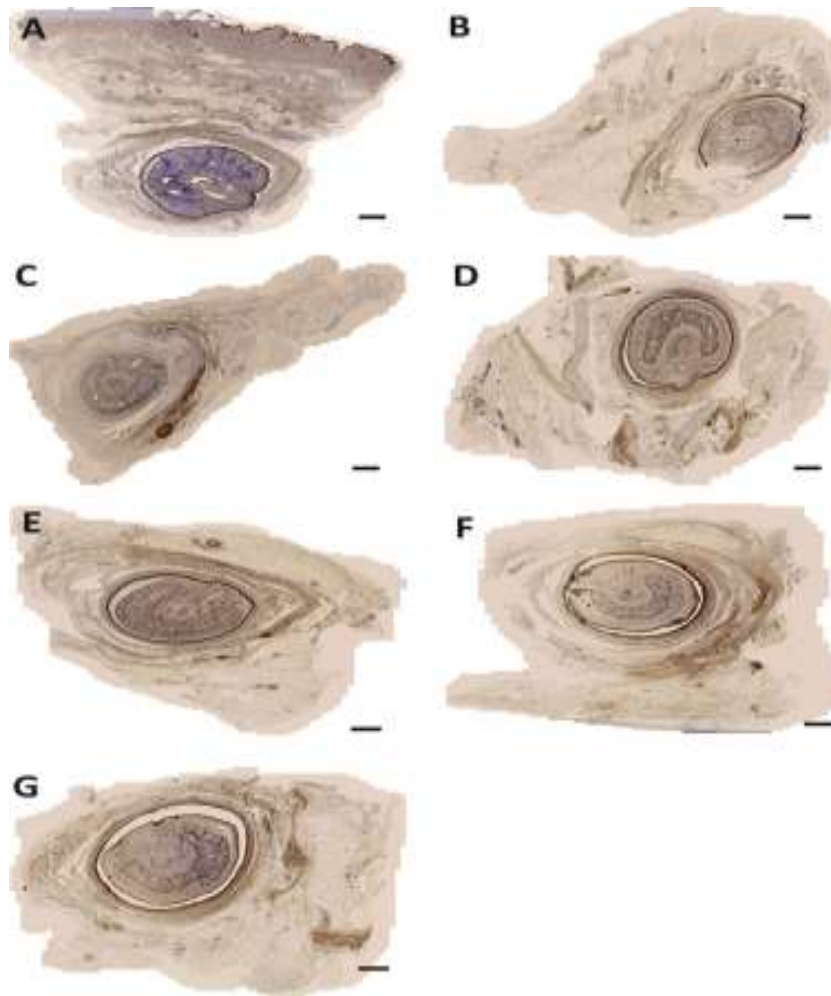
Figure V-5: CD107a labelling in Pelvicol explants

A: Control pig, B: 1685D, C: 1699C, D: 1705B, E: 2057, F: 2058C, G: 2059C

Regenerative medicine applications in paediatric urology: barriers and solutions
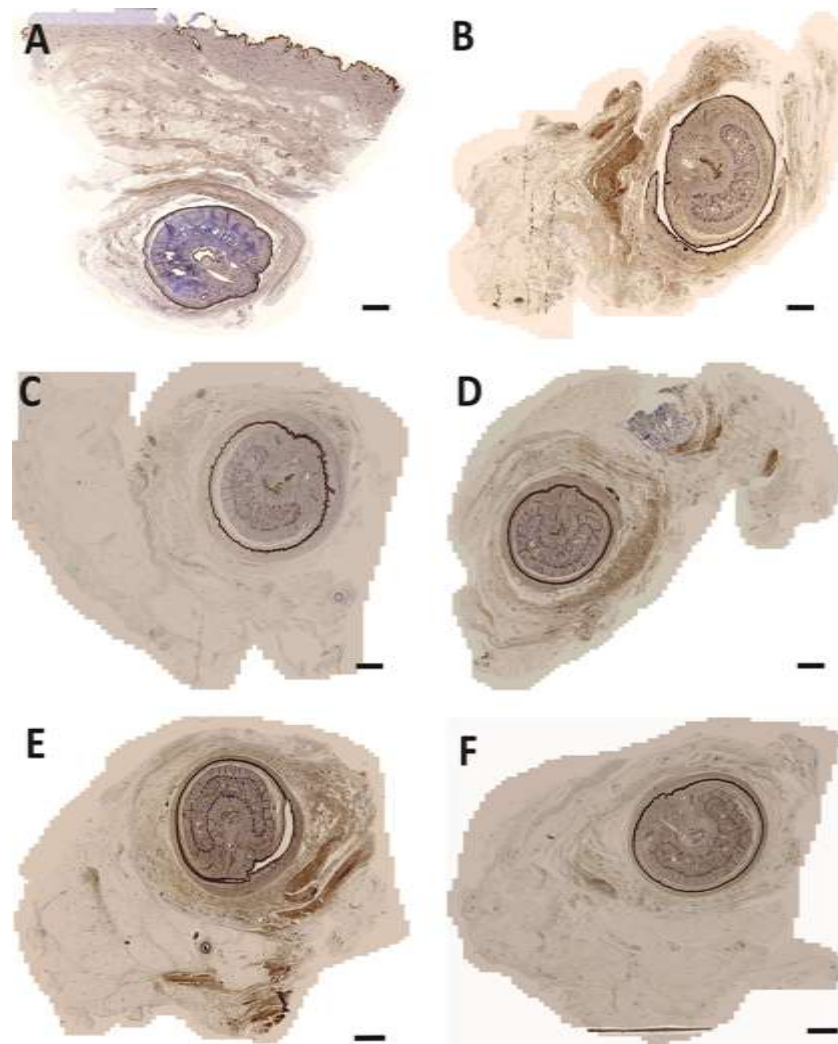
Figure V-6: CD107a labelling in PABM explants

A: Control pig, B: 1673D, C: 1679D, D: 1692D, E 2064C, F: 2065E
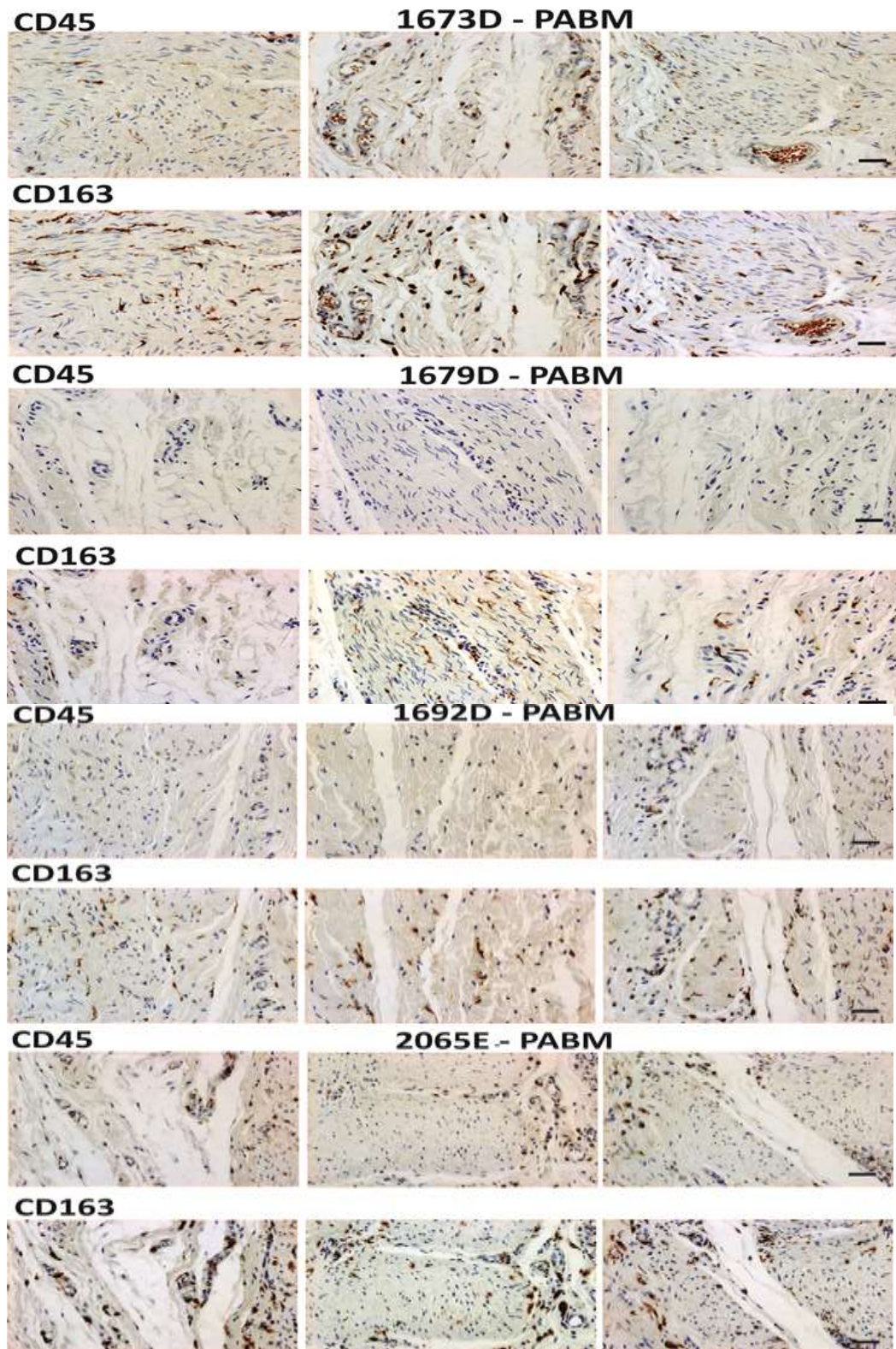
Figure V-7: Matched CD45 and CD163 labelled sections
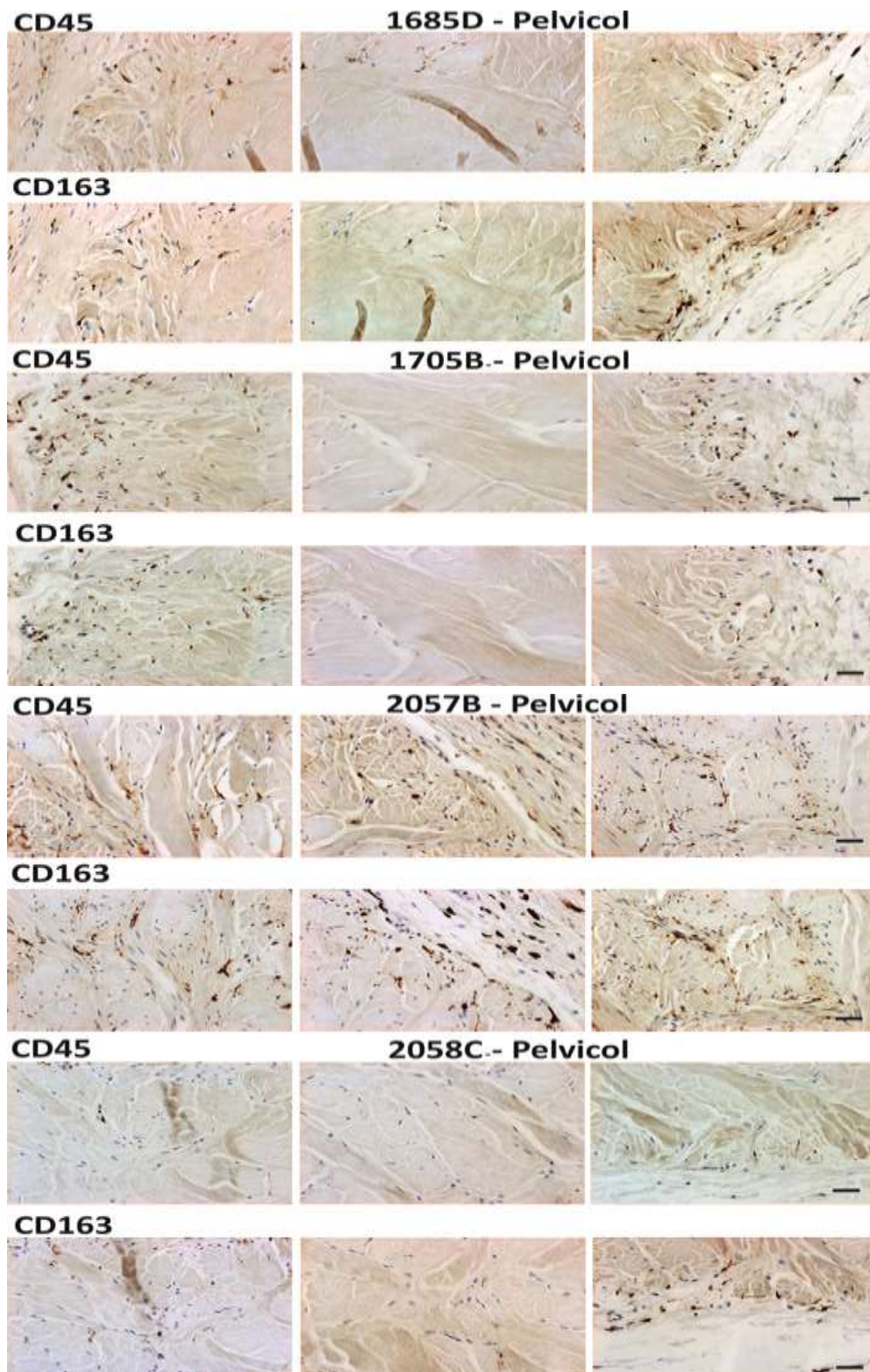
Figure V-8: Matched CD45 and CD163 labelled sections

Regenerative medicine applications in paediatric urology: barriers and solutions
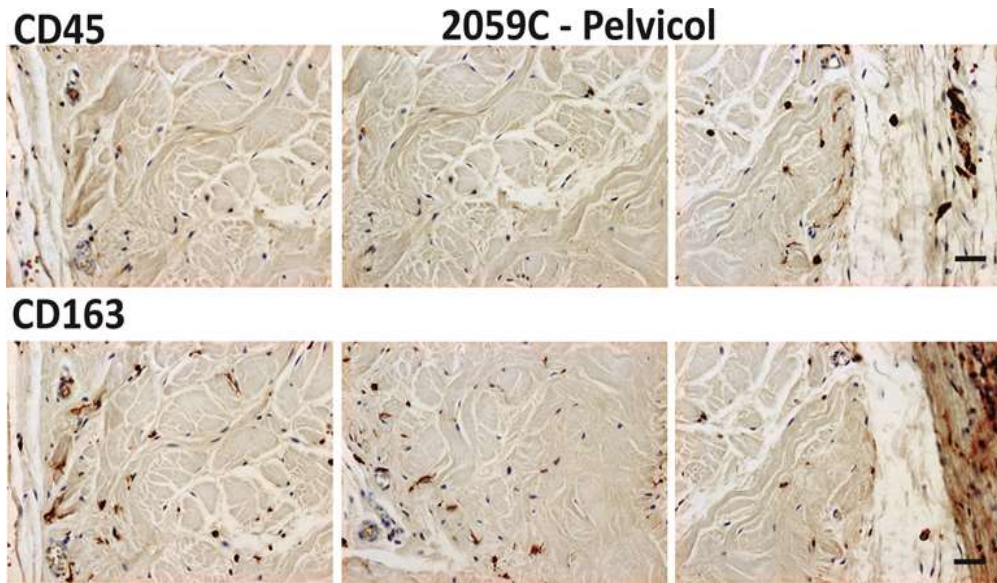
Figure V-9: Matched CD45 and CD163 labelled sections

Abbreviations

ABS	Adult Bovine Serum
BM	Basement membrane
BPH	Benign prostatic hypertrophy
CK	Cytokeratin
DFO	Deferoxamine mesylate
EGFR	Epithelial growth factor receptor
FBS	Fetal Bovine Serm
HIF-1α	Hypoxia-inducible factor -1α
IQR	Interquartile range
KSFM	Keratinocyte free medium
KSFMc	KSFM complete (with additives)
NGFR	Nerve Growth Factor Receptor
NHU	Normal human urothelium
OC	Organ culture
PBS	Phosphate-buffered saline
PUJO	Pelvi-ureteric junction obstruction
TEER/TER	Transepithelial electrical resistance
TBS	Tris-buffered saline
UC	Urothelial carcinoma
UF	Urethral fistula

UPK	Uroplakin
VUJO	Vesico-ureteric-junction obstruction
VUR	Vesico-ureteric reflux
ZO-1	Zona-occludens-

[Type text]